GEOLOGICAL SURVEY OF CANADA

OPEN FILE 3700

A multidisciplinary study of carbonate-hosted zinc-lead mineralization in the Mackenzie Platform (a.k.a. Blackwater and Lac de Bois platforms) Yukon and Northwest Territories, Canada

J.J. Carrière, D.F. Sangster

1999

Natural Resources Canada | Ressources naturelles Canada

Canada

GEOLOGICAL SURVEY OF CANADA

OPEN FILE 3700

A multidisciplinary study of carbonate-hosted zinc-lead mineralization in the Mackenzie Platform (a.k.a. Blackwater and Lac de Bois platforms) Yukon and Northwest Territories, Canada

J.J. Carrière, D.F. Sangster

1999

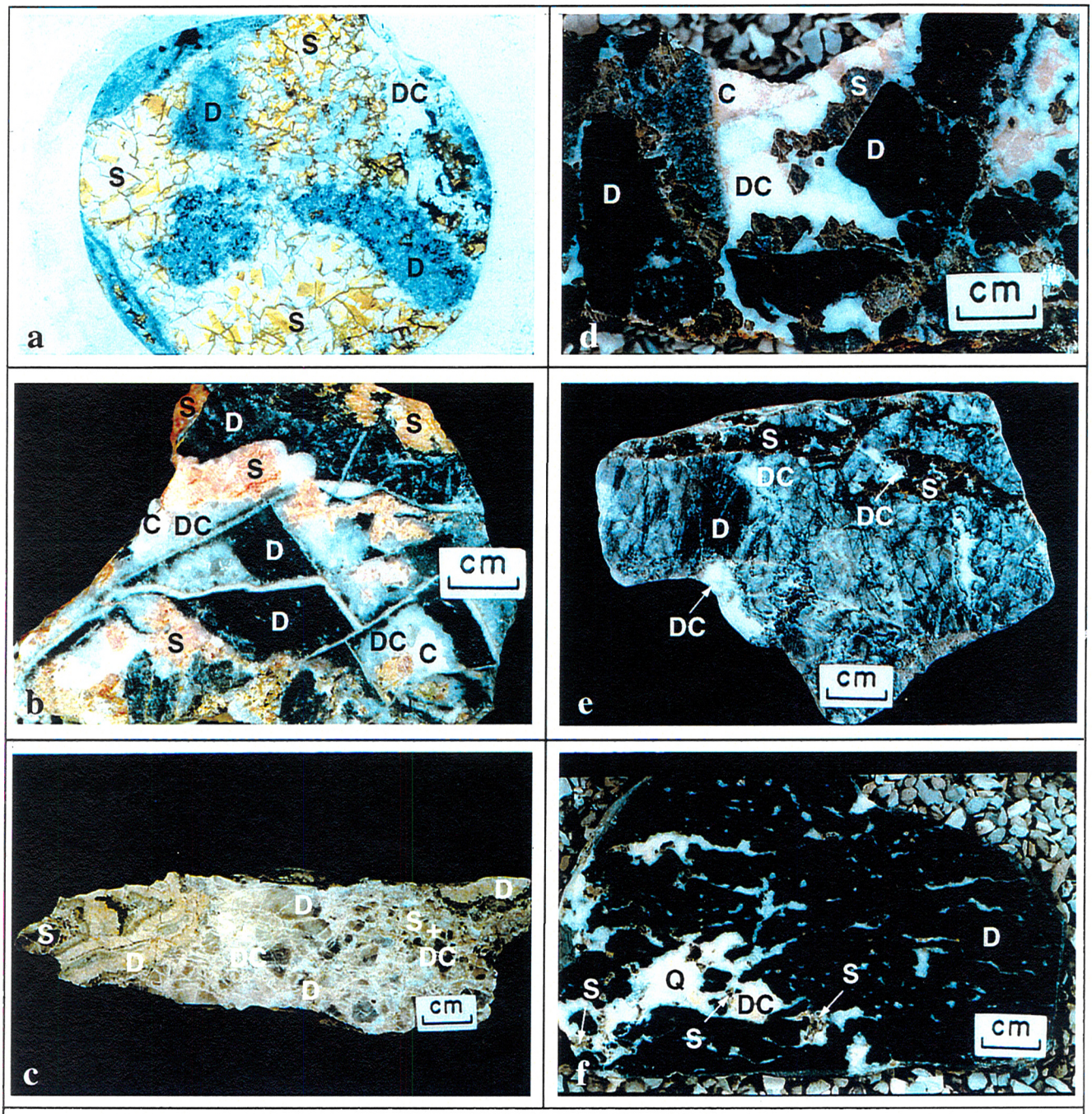

Frontispiece A. Selected hand samples and thin sections showing host dolomite fragments (D), cemented by dolomite (DC), sphalerite (S), quartz (Q) and calcite (C). Sphalerite colours are natural; samples have not been stained. a) Gayna River sample SP3408B, width of chip is 2.4 cm. b) Gayna River sample no. SP3409. c) Cypress sample no. SP3267. d) Econ sample Econ-1, open space filling. e) Econ SE Veins sample, vein-type mineralization. f) Palm Claims sample 1.

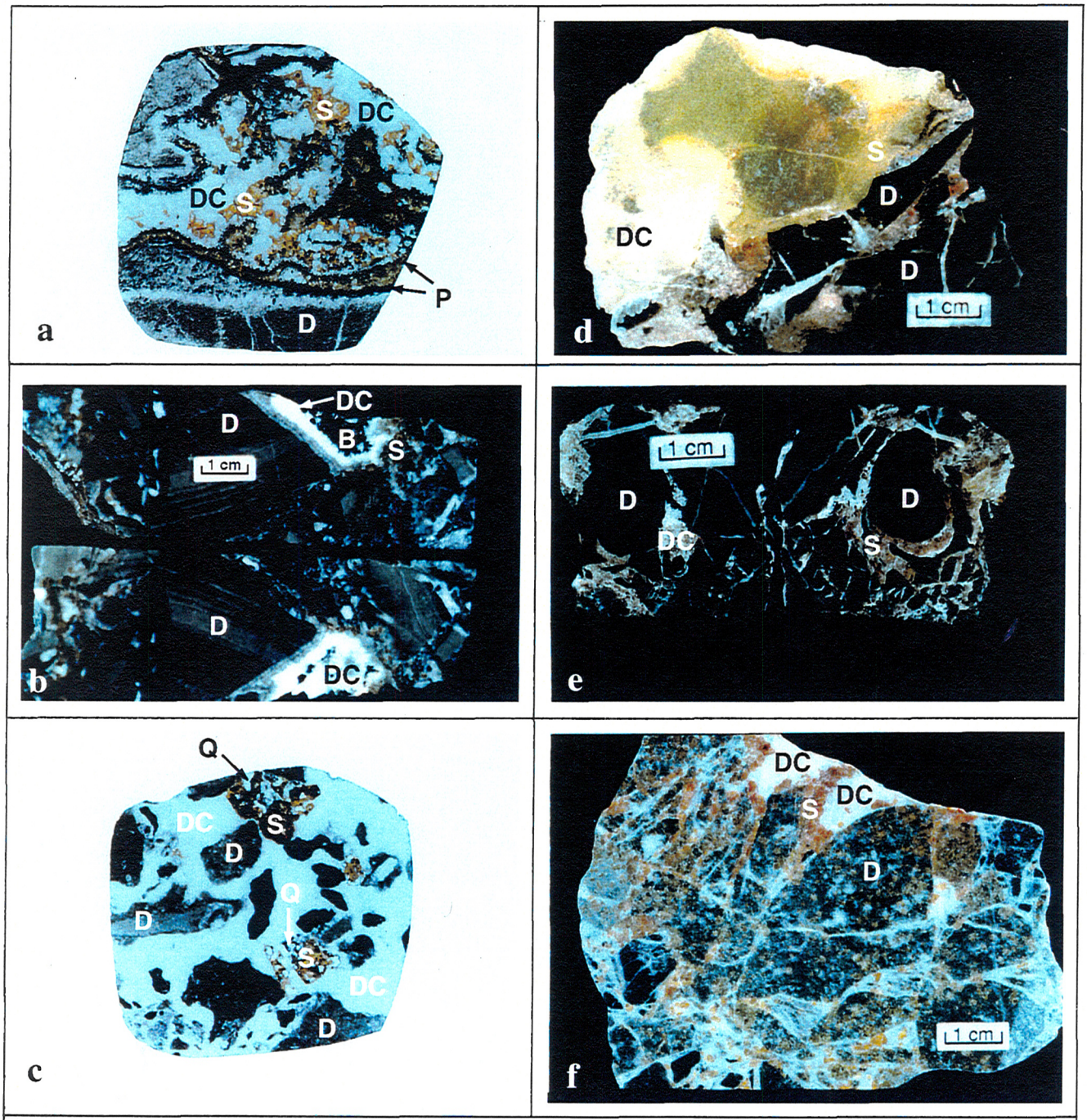

Frontispiece B. Additional selected hand samples and thin sections showing host dolomite fragment (D), cemented by dolomite (DC), sphalerite (S), quartz (Q), and pyrite (P). Sphalerite colours are natural; samples have not been stained. a) Bob sample no. SP5399(1), width of chip is 2.4 cm. Dark bands are pyrite. b) Bob sample no. SP5394. In top centre of photo note black bitumen (B) is later than the dolomite cement. c) Mawer sample no. SP5403, sparse sphalerite appears to replace host dolomite fragments. Width of chip is 2.4 cm. d) Joli Green sample 105I/16, open space filling. e) Bear sample no. SP5487. f) Rev sample SP5501.

ABSTRACT

Samples from 24 carbonate-hosted zinc-lead deposits in the Mackenzie Platform area of eastern Yukon and western Northwest Territories were subjected to a multidisciplinary study with the following objectives: i) to determine minimum temperatures and salinities of formation of the mineralization; ii) to evaluate the areal and stratigraphic extent of the mineralizing event; iii) to determine the paragenesis of the sulphides and cementing material using cathodoluminescence (CL) microscopy; and, iv) to propose a genetic model based on these and other data. Eight of the 24 deposits are hosted in limestone rather dolomite with little or no dolomite cement. These eight deposits have been studied using cathodoluminescence only. All deposits are located in strata older than Late Devonian, flank the eastern margin of the Selwyn Basin, and appear to be of Mississippi Valley-type.

Microthermometric data were collected from inclusions in sphalerite, dolomite, quartz, calcite, and barite. Five types of inclusions were identified although not all were present in every deposit: **Type 1**, two-phase H_2O (l) + H_2O (v); **Type 2**, three-phase H_2O (l) + H_2O (v) + solid (rounded or disc shaped - not halite); **Type 3**, three-phase H_2O (l) + CO_2 (l) + CO_2 (v); **Type 4a**, one-phase fluid CO_2/CH_4 (clear and colourless), **Type 4b**, one-phase fluid CH_4 (?) (clear and coloured - orange or yellow), **Type 4c**, two-phase fluid CH_4 (?) + solid; and **Type 5**, one-phase, dark-filled (organic-rich ?). Based on the analysis of the microthermometric data from **Type 1** inclusions, four distinct mineralizing fluids, with two sub-types, have been identified. Fluid Ia has mean characteristics of >20 eq. wt.% NaCl at T_{min} 175°C. Fluid Ib is less saline, ranging from 12.8-20.2 eq. wt.% NaCl and mean T_{min}153°C. **Fluid I** is the most common fluid and was found in primary and pseudosecondary Type 1 fluid inclusions from Gayna River, Cypress, Cab, Palm, Mawer, Joli Green, Bear-Twit, and Rev. **Fluid II** was found in primary and pseudosecondary Type 1 fluid inclusions from Econ, Ab, Cab, Palm, and Joli Green. Fluid IIa has a mean salinity >22 eq. wt.% NaCl and a T_{min} 104°C. Fluid IIb has mean salinity ranging between 15 and 20 eq. wt.% NaCl, and mean T_{min} 111°C. The mean salinity of **Fluid III** ranges from 3.5-6.8 eq. wt.% NaCl and mean T_{min} 177°C, and was found in either primary, pseudosecondary, or secondary Type 1 fluid inclusions from Cypress, Palm, Bear, and Rev. **Fluid IV** mean salinity ranges from 5-9.4 eq. wt.% NaCl and mean T_{min} 118°C, and was found in either primary, pseudosecondary, or secondary Type 1 fluid inclusions from Econ, Bob, and Bear. Relative to previously-published Conodont Alteration Index (CAI) data, microthermometric data revealed deposits fell into two groups, those with

homogenization temperatures equal to host rock temperatures and those with homogenization temperatures less than host rocks.

Minerals found in hand samples surrounding the host dolomite (sometimes limestone) fragments are identified in the study and included dolomite (cement), pyrite, sphalerite, galena, quartz, calcite, and barite. Minor amounts of bitumen, smithsonite, hydrozincite, and cerussite were also noted. Mineralization occurs in collapse breccias, open space filling of vugs, fractures, and veins, and as replacement of sedimentary structures and disseminations along bedding planes. The minerals were divided paragenetically into three groups: i) pre-"ore" (host dolomite and pyrite); ii) syn-"ore" (sphalerite1, dolomite cement1, pyrite, quartz, dolomite cement2, sphalerite2, and galena); and, iii) post-"ore" (calcite, barite, quartz, bitumen, cerussite, hydrozincite, and smithsonite). Post-mineralization deformation features in sphalerite, quartz, and dolomite were noted in several deposits.

Cathodoluminescence photomicrographs from all 24 deposits, revealed that, within each deposit the luminescent signatures were definitive and consistent, but no definitive correlations between deposits were possible. Cathodoluminescence, however, was very useful in other ways such as distinguishing between calcite and dolomite, revealing zonation in dolomite, identifying healed fractures, and illustrating paragenesis. The CL work showed that in all examples the saddle dolomite cement is paragenetically associated with sulphide mineralization. The dolomite cement, generally coarse-grained saddle dolomite and/or the finer grained dolomite cement is commonly intergrown with the sulphides and is either co-genetic or closely alternating with the sulphide minerals (in space and time).

Electron microprobe analyses of dolomite cement revealed higher Fe and slightly lower Mn content in deposits hosted in rocks older than Middle Cambrian. Ternary plots of analyses of carbonate minerals show end-member compositions for all dolomite types. Although both planar and non-planar dolomite textures are present, a majority of host dolomite and dolomite cements display nonplanar texture.

Both dolomite cement and sulphide minerals from all deposits except Econ appear to have been deposited, at depths exceeding 1 km, from warm, saline fluids, possibly expelled from the adjacent clastic-dominated Selwyn Basin. Fluids which formed Econ (Fluid IV) are significantly less saline and may have formed under somewhat different conditions. Age of mineralization is limited to the interval between Middle Devonian (age of the youngest host rocks) and Carboniferous (the presence of hydrocarbons in post-ore vugs).

ACKNOWLEDGEMENTS

The authors are indebted to many of their colleagues at the Geological Survey of Canada for logistic and technical assistance throughout this project: Gilles Lemieux for his patience and co-operation in producing all coloured photographs; Robert Kelly for photographing line drawings; Robert Laramée and Richard Burke for their unfailing help with solving the many word processing problems; Gordon Pringle for assistance with triangular plots; Beth Hillary for advice on CorelDraw; Richard Lancaster for selected computer graphics; and Dave Sinclair for technical help and advice. A special thanks to Michel Roy, a graduate student from University of Ottawa, who organized the vast array of electron microprobe data in Excel and created numerous spreadsheets and specified plots, using QuatroPro for data manipulation. The comments and suggestions of the following, who reviewed selected portions of earlier drafts, significantly contributed to improving the final product: John Stirling and Jean Dougherty (GSC), and Dan Marshall (Simon Fraser University). Suzanne Paradis bravely agreed to review the complete manuscript and to her we offer our heartfelt thanks and gratitude. Samples used in this study were from the collections of the second author, Ken Dawson and Rod Kirkham (GSC), and John Brock (Welcome North Mines).

CONTENTS

1. INTRODUCTION

BACKGROUND

The Mackenzie Platform area of eastern Yukon and western Northwest Territories (Fig. 1-1) witnessed an unprecedented level of exploration activity in the early- to mid-1970's. Exploration in this remote part of Canada was initiated, in part, by the discovery, in 1971, of significant carbonate-hosted deposits in the Robb Lake (Sangster and Carrière, 1991) area of northwestern British Columbia and, in 1972, the Howards Pass shale-hosted deposit in Selwyn Basin along the Yukon-NWT border. Although literally hundreds of carbonate-hosted Pb-Zn showings were discovered in a few short years, none warranted production and, by the mid-1980's, interest in the region had all but disappeared. The waning activity, the high cost of access (helicopter only), and the extreme remoteness of the region essentially precluded follow-up research on these deposits. Thus, little was known of these deposits other than brief notes in government assessment files and a few descriptive university theses. At the same time, research in the United States had suggested that carbonate-hosted Pb-Zn deposits could form essentially simultaneously over a large area as a result of regional-scale fluid flow (Leach and Rowan, 1986; Garven and Freeze, 1984 a ,b; Garven, 1985).

Thus, the decision was made to conduct a reconnaissance-level multidisciplinary study of a selected number of deposits in Mackenzie Platform using samples collected by the second author and his colleagues more than a decade previously. Objectives of this project were to: i) determine minimum temperatures and salinities of formation of the ore fluid(s); ii) evaluate the areal and stratigraphic extent of the mineralizing event; iii) determine the paragenesis of the sulphides and cementing material using cathodoluminescence microscopy; and iv) propose a genetic model based on these and other data. Attainment of these objectives will contribute to the understanding of carbonate-hosted Pb-Zn deposits and advance the understanding of the significance and genetic history of dolomitization relative to burial diagenesis and the mineralizing event(s) in this region. Although the interpretation and genetic model presented here may be regarded by some readers as overextending the available data, these provocative ideas may encourage further research.

REGIONAL SETTING

The "Mackenzie Platform" is a sub-district of the much larger Mackenzie Valley lead-zinc district proposed by Sangster and Lancaster (1976). The sub-district is located in the northern Canadian Cordillera, straddling the border between central Yukon Territory and western Northwest

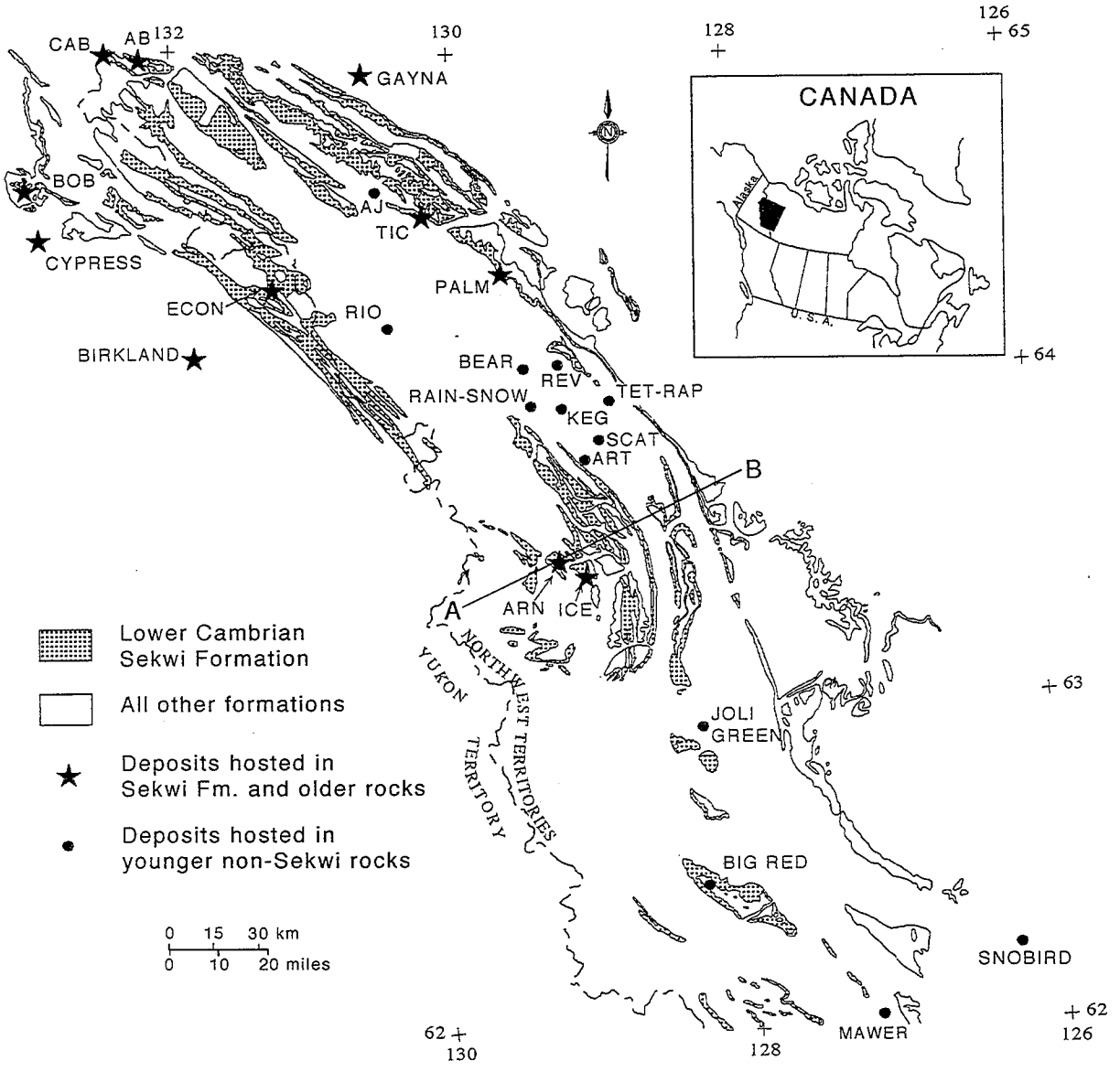

(after Krause, 1979)

Fig. 1-1. Map showing the area of the Mackenzie Platform covered in the study and the name and locations of the deposits discussed. Inset shows the location of the area within Canada. Line from A to B marks the location of the stratigraphic framework shown in Fig. 1-4.

Territories. Here, platform carbonates, containing dozens of lead-zinc deposits and occurrences, flank the eastern margin of Selwyn Basin. All lead-zinc deposits are located in strata older than Late Devonian; a majority occur in Lower Cambrian rocks or older, but there are a significant number in rocks of Late Cambrian to Middle Devonian age (Fritz et al., 1991). The deposits appear to be of classic Mississippi Valley-type (Dawson, 1975). Zinc commonly predominates over lead by at least 10:1 (Gibbins, 1983).

Many deposits occur in platform carbonates surrounding the Misty Creek Embayment (Fig. 1-2), an outlier of Selwyn Basin within the Mackenzie Platform area. The Selwyn Basin represents a large outer miogeoclinal basin and the Misty Creek Embayment is a distinct, north-northwest-trending, late Early Cambrian to Silurian, marine rift located between the Mackenzie Arch and the Selwyn Basin (Cecile et al., 1997). The embayment is a depositional feature defined by the change from Upper Cambrian-Lower Ordovician, and from Upper Ordovician-Lower Silurian platform carbonate, into correlative transition and deeper water limestone, shale and chert; and by Middle Cambrian and Middle Ordovician basin shale and transition units (Cecile,1982). The embayment is best defined by the transition from platform to basin facies because these strata are extensively preserved within and around the embayment.

The tectonic element originally referred to as the "Mackenzie Platform" (Gabrielse et al., 1991) has recently been divided into tectonic divisions, from south to north, the MacDonald Block, Blackwater Block, Mackenzie Block, and Franklinian Block (Fig. 1-2) along lineaments interpreted to reflect the position(s) of ancient transfer or strike-slip faults (Cecile et al., 1997). The Blackwater Block is located immediately north of the Liard Line and consists of several components including the Blackwater Platform, Meilleur River Embayment, Root Basin, and southern Selwyn Basin. The Mackenzie Block is located immediately north of the Fort Norman Line and includes Mackenzie Arch and Misty Creek Embayment. The Franklinian Block or southwestern Franklinian Miogeocline consists of Lac des Bois Platform, Peel Arch, Richardson Trough, Blackstone Trough and Porcupine Platform. The Lac des Bois Platform was a large area of mainly Cambrian clastic and Cambrian to Devonian shallow water carbonate deposition that thickens northwestward where it is transitional into basinal facies of the southwestern Franklinian Miogeocline. The Lac des Bois Platform represents the northern portion of the area formerly known as "Mackenzie Platform" and the Blackwater Platform covers the southern portion. The term "Mackenzie Platform" will be used in the text to describe the study area, and the reader will keep in mind the detail of the divisions described above.

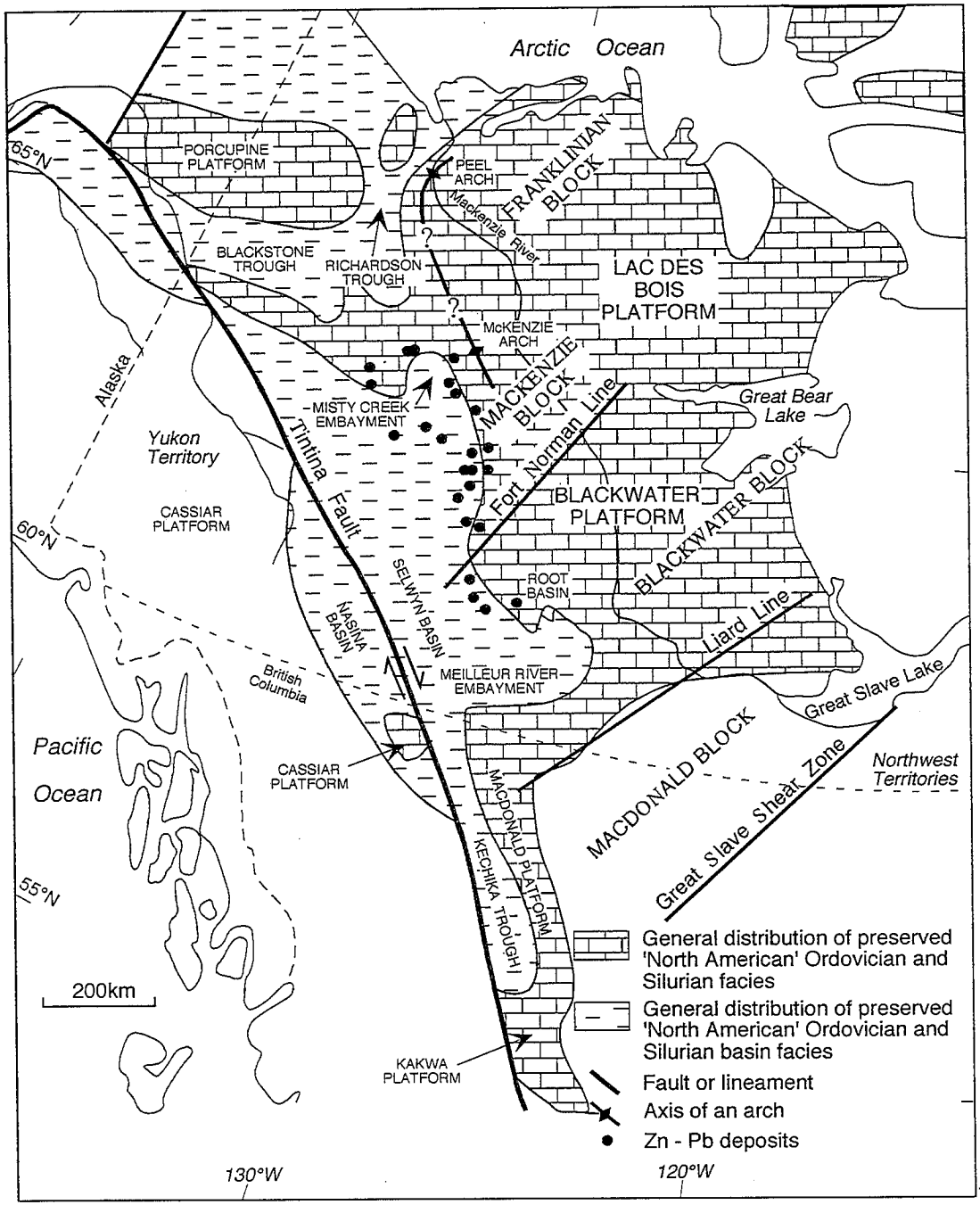

Fig. 1-2. Map showing 'structural' paleogeographic features and block divisions of the Lower Paleozoic Canadian Cordillera (after Cecile et al., 1997) and location of deposits.

Tectonic assemblages

The schematic stratigraphic section (Fig. 1-3) illustrates the stratigraphy found in the study area and, along with the stratigraphic framework (Fig. 1-4), show the positions of deposits discussed with respect to their host formations. The stratigraphic succession has been subdivided into assemblages of distinct tectonic affinity. Rifting in Late Proterozic (Neoproterozic) time resulted in the formation of a passive margin of Ancestral North America. Miogeoclinal sedimentation began with this latest Proterozoic rifting and deposition of the Windermere Supergroup along the North American continental margin. Sequences of Upper Proterozoic, dominantly clastic, sedimentary rocks of the Windermere Supergroup are commonly more than 2000 m thick and are exposed almost continously throughout the length of the eastern Cordillera. In the Mackenzie Mountains the supergroup unconformably overlies strata of the Mackenzie Mountains Supergroup (Gabrielse and Campbell, 1991).

Lower Cambrian to Middle Devonian miogeoclinal strata were deposited along this passive margin. The main characteristics of the Lower Cambrian to Middle Devonian rocks in the miogeocline are attributed to a complex interplay of continental rifting, attenuation, drifting, thermal subsidence and flexuring along the western margin of the continent (Fritz et al., 1991). The tectonic setting of the northern Canadian Cordillera is further summarized by Gordey and Anderson (1993) and the following has been paraphrased from that source. From the late Precambrian to Middle Devonian the area was segmented into two contrasting facies belts. The Mackenzie Platform, on the northeast, is defined by the deposition of shallow water sandstone, dolostone, and limestone. To the southwest, time-equivalent rocks comprise turbiditic sandstone, deep water limestone, shale, and chert of the Selwyn Basin (Fig. 1-2). The platform-basin boundary shifted with time and its formations of basin and platform are often interstratified. Important unconformities occur beneath the Upper Cambrian (i.e. Middle Cambrian unconformity, Fig. 1-4), middle Lower Devonian, and lowermost Middle Devonian. The aggregate thickness of Lower Cambrian to Middle Devonian platform and thick basinal near-platform strata is about 4200 m, while the equivalent outer basin strata is about 1600 m thick. Cecile et al., (1997) discuss evidence for three extensional events following initial rifting and breakup in parts of the Canadian Cordillera: 1) Early Cambrian; 2) Middle Ordovician; and 3) Late Silurian to Early Devonian. Middle Ordovician event was accompanied by widespread alkalic and potassic volcanism and igneous activity; the Late Silurian-Early Devonian event also resulted in alkalic volcanism (Goodfellow et. al., 1995).

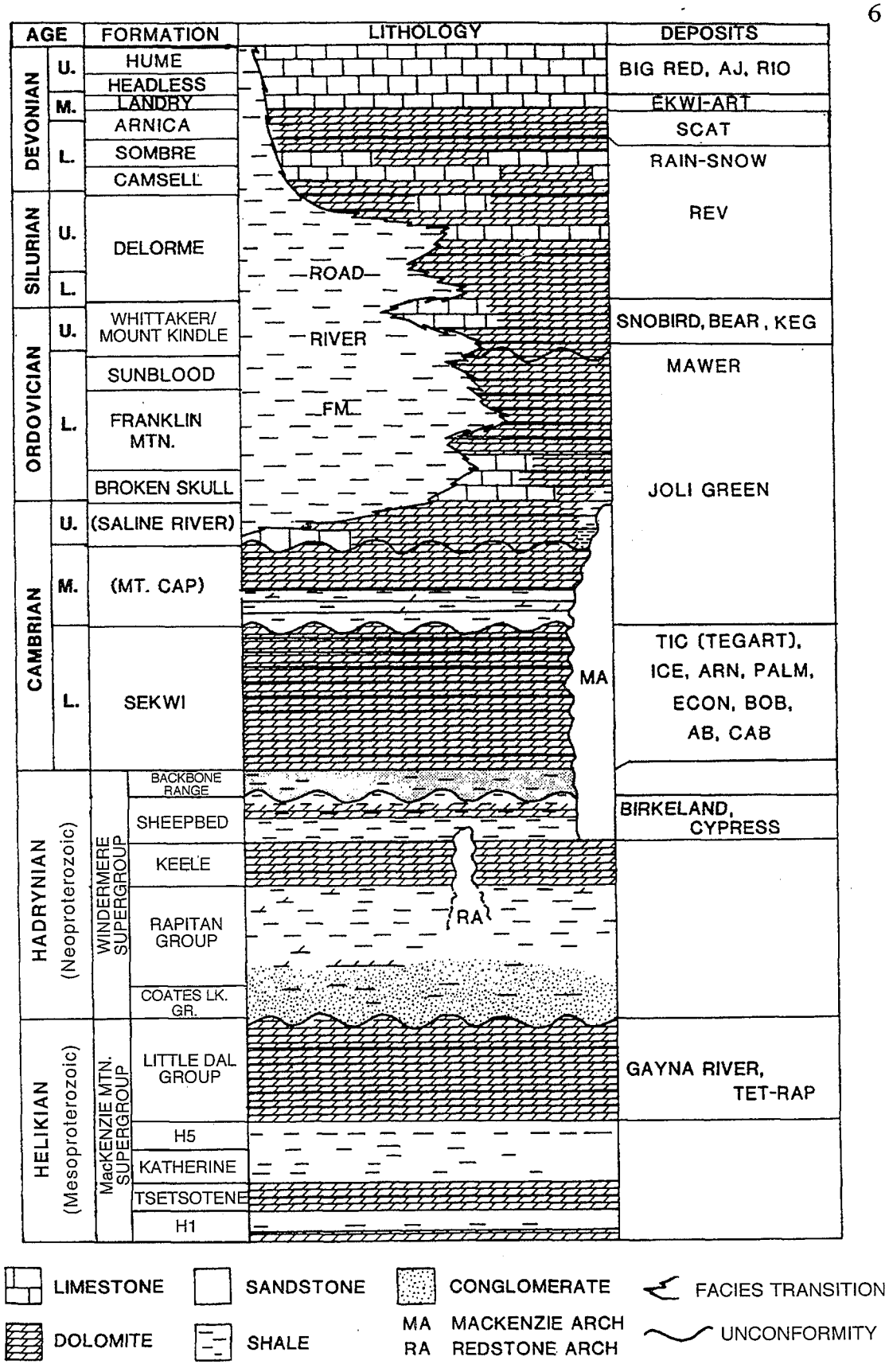

Fig. 1-3. Schematic stratigraphic section showing positions of deposits discussed in this study (after McLaren and Godwin, 1979a).

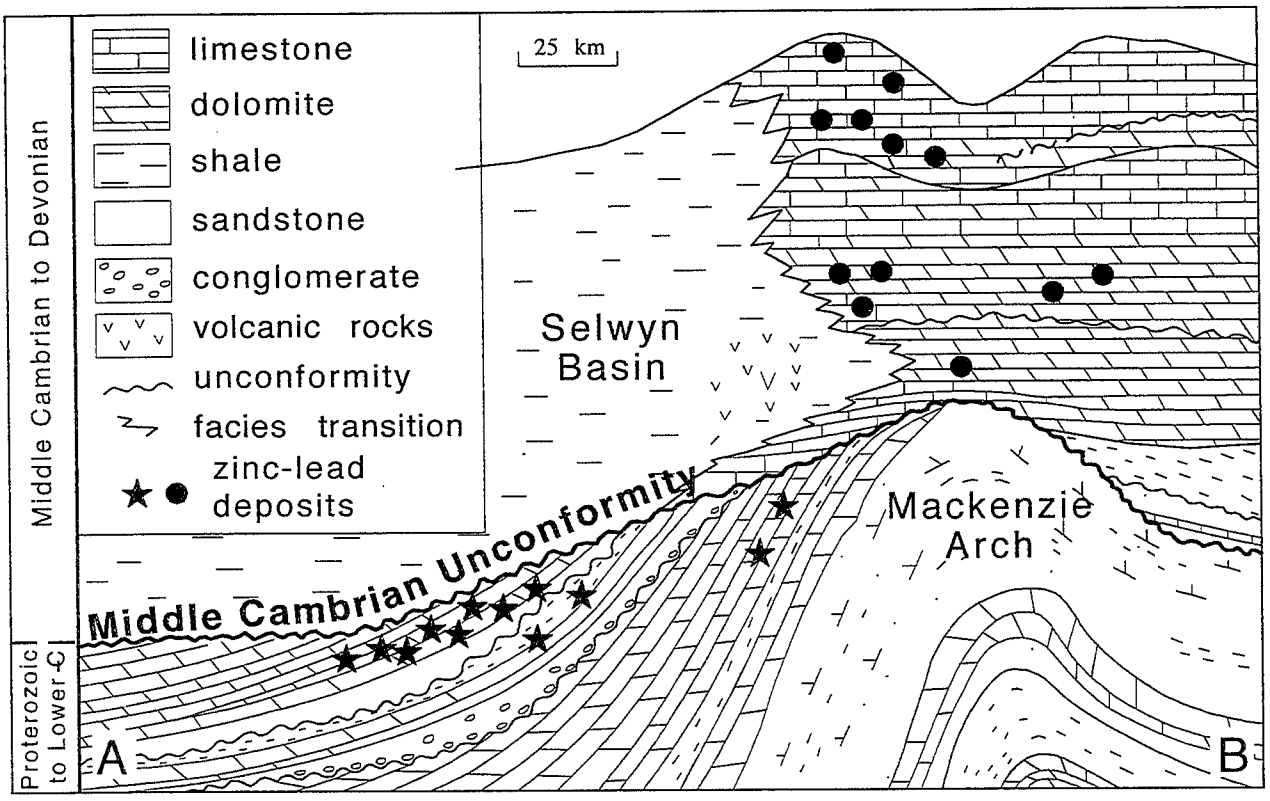

Fig. 1-4. Stratigraphic framework illustrating the relative positions of the zinc-lead deposits in the study (after McLaren and Godwin, 1979a). Location of A to B is shown in Fig. 1-1.

In late Devonian time there was an abrupt change in depositional regime. Shale was deposited across the older Mackenzie Platform to the northeast, while to the southwest turbiditic quartz-chert sandstone and chert-pebble conglomerate were deposited in a number of submarine fan complexes. Compressional deformation of Devono-Mississippian age is lacking. Regional unconformities occur beneath lower Upper Devonian and uppermost Devonian strata.

Mississippian to Triassic clastic shelf assemblage followed the turbiditic clastics. Shale, chert, minor sandstone, and siltstone compose strata of Early Permian and Triassic age. Regional unconformities occur beneath the Lower Mississippian, Lower Permian, and Lower Triassic. Aggregate thickness for this sequence is about 1700 m (Gordey and Anderson, 1993).

In the Early Cretaceous, the area was subject to northeast-southwest compression leading to the development of northwest-trending decollement style folds and minor thrust faults. Competent

carbonate strata defining Mackenzie Platform formed large-scale open folds. The largely incompetent strata of the Selwyn Basin area formed small- to large-scale, open to tight folds with pervasive axial-planar slaty cleavage (Gordey and Anderson, 1993).

PREVIOUS STUDIES

The stratigraphic framework (Fig. 1-4) presented by McLaren and Godwin (1979a) is used here to illustrate the relative positions of the zinc-lead deposits in this study. Two major groups of sedimentary rocks hosting zinc-lead deposits in the northern Canadian Cordillera can be identified on the basis of depositional tectonics. A Proterozoic to Lower Cambrian succession of carbonates and clastics is separated by a regional erosional hiatus from an Upper Cambrian to Devonian basinal shale and laterally equivalent platformal carbonate sequence. The grouping of zinc-lead deposits by host rock is reinforced by bimodal minor element distributions in sphalerite (McLaren and Godwin, 1979b). Sphalerite specimens were analyzed for silver, cadmium, cobalt, copper, iron, manganese, nickel, lead, and mercury. The deposit population with lower or 'depleted' minor element content in sphalerite is consistently centred on, and extends beyond the limits of, the Ordovician, Silurian and Devonian host rock distribution, whereas the 'enriched' population of minor elements in sphalerite exists mainly in the "older" group and rarely extends into the area of the younger hosts. This pattern suggested to McLaren and Godwin (1979a) that an event leading to mineralization in Ordovician to Devonian age rocks was concentrated in these units, but extended into adjacent Proterozoic and Lower Cambrian units. Conversely, a mineralizing episode affecting the Proterozoic and Lower Cambrian rocks was restricted to these older units, most probably because it occurred prior to deposition of the younger rocks. Continuing the research, Godwin et al. (1982) reported Pb-isotope data for 34 carbonate-hosted Pb-Zn deposits and demonstrated two groups of deposits, those with $^{206}Pb/^{204}Pb$ = 16.27 to 19.66 and another with $^{206}Pb/^{204}Pb$ = 18.17 to 20.26. Based on these two groupings, the authors proposed that two independent metallogenic events of different ages took place in the region, one at ~0.52 Ma (Early Cambrian) and another at ~ 0.37 Ma (Early Carboniferous). They suggest that a karstic model is supported for the older deposits and a (Selwyn) basin dewatering model for the younger deposits. Eight of the 34 deposits are included in the present study; one (Econ) falls in the "old" group of Godwin et al. (1982) whereas seven [Palm, Birkeland, Rev, Tegart (Tic), Backbone (Art), Weather (Rain-Snow), and Twitya (Bear-Twit)] are in the "younger" group.

GEOLOGIC DESCRIPTIONS OF ZINC-LEAD DEPOSITS

Following opening of the Pine Point district in 1965, several carbonate-hosted lead-zinc deposits were discovered in northern Rocky Mountains, the most significant of which was Robb Lake in 1971 with an estimated resource of 7.1 million tonnes at 4.7% Zn and 1.5% Pb (Paradis et al., 1999). Subsequent intense exploration resulted in hundreds of lead-zinc discoveries in the Mackenzie, Selwyn, Ogilvie, and Richardson Mountains. Overview descriptions of the deposits, their geological settings, and exploration histories were presented by Dawson (1975), Sangster and Lancaster (1976), Macqueen (1976), and Brock (1976).

Eight of the 24 deposits are hosted in limestone rather than dolomite with little or no dolomite cement. These eight deposits, which include Tet-Rap, Birkeland, Keg, Art, Scat, Rio, Aj, and Big Red, have been studied using petrography and cathodoluminescence only and are not described. General information, such as location and formations hosting these deposits can be found in Table 2-1. Additional details may be gleaned from the references provided.

Gayna River (64°56'N, 130°41'W)

Discovered in 1974, the Gayna River zinc-lead deposit occurs in platform carbonates of the Helikian (Mesoproterozoic) Little Dal Group exposed along a tributary to the Gayna River in the Mackenzie Mountains, western Northwest Territories. The deposit contains minimum reserves of 50 million tonnes of 4.7% zinc and 0.3% lead (Hewton, 1982).

Mineralization is found in the dolomitic Host Unit, made up of Lower Host, Upper Host and the intervening 15 m-thick Argillaceous Marker within the Little Dal Group. The Host Unit comprises brecciated stromatolitic and oolitic dolostone lying adjacent to large biohermal reefs having lateral dimensions of 6.5 x 1.6 km and heights of 500 m. The Little Dal Group has been truncated by a sub-Upper Cambrian unconformity that, in other areas of the region, has removed the entire Little Dal Group succession. Little Dal Group rocks in the Gayna River area have undergone more intense structural deformation compared to most Mississippi Valley-type districts. The Gayna River area has been subjected to large-scale, concentric and sinuous-type folds and numerous high-angle thrust faults.

More than 100 sulphide occurrences have been found both on surface and by drilling and are concentrated in secondary breccias in dolostones of the Host Unit. The breccias are interpreted to

have formed by a variety of processes including syn-sedimentary slumping and post-sedimentary faulting, solution-collapse, recrystallization, and dolomitization (Hewton, 1982). The breccias have been filled with and replaced mainly by sparry dolomite, sphalerite, and calcite; minor phases include barite, pyrite, galena, fluorite, pyrobitumen, and quartz. Sedimentary breccias are generally low-grade and characterized by sphalerite, galena, and pyrite. Best-grade intersections are found in secondary breccias characterized by vari-coloured sphalerite (red, green, yellow, orange, brown, purple, and white), pyrite, calcite, and dolomite with minor galena, barite, and quartz. Replacement mineralization is best developed along linear features with grades decreasing laterally away from these features, suggesting fault or fracture control. Sulphides consist of finely crystalline sphalerite with minor pyrite and even less galena.

Cypress (64°25'20"N, 132°52'00"W)

The Cypress claims are located 177 km northeast of Mayo, on the northeast side of the Bonnet Plume River, about 6 km to the west of the confluence of Goz Creek and the Bonnet Plume River. The deposit is underlain by a northwest-trending sequence of Hadrynian to Mississippian rocks which dip steeply to the northeast. Most of the lead-zinc mineralization occurs within a Hadrynian dolomite unit, immediately below a laminated brown-black shale and consists of sphalerite, pyrite and smithsonite. Accessory minerals are dolomite and quartz. Galena, minor barite and calcite have been reported in the literature (Sinclair et al., 1976), but were not observed in the present study. Sulphides are found in solution cavities and local collapse breccias, solution channel fillings, primary bedded material, and cross cutting structures. Crustiform textures are present in the dolomite. Mineralization occurs in two distinct textural forms: 1) replacement; and 2) open space fillings.

AB (64°59'N, 132°17'W)

The AB claim group lies 232 km northeast of Mayo, in the Mackenzie District, Northwest Territories. The deposit lies in lower Cambrian Sekwi Formation dolomitic limestone. The formation is repeatedly downfaulted to the north by a sequence of east-westerly trending faults which follow a major regional fault sequence. The Sekwi Formation is terminated in outcrop north of the claim group by a sequence of undifferentiated Ordovician to Devonian rocks.

On the AB property, the Sekwi Formation can be divided into at least four members. The

first member, lowest beds overlying the Backbone Formation, are interbedded quartzite, sandy dolomite and dolomite. The second member, overlying this member, is approximately 90 m of dark-grey bioturbated silty dolomite with interbedded oolitic and oncolitic dolomite. This member contains richly disseminated sphalerite, commonly containing 10-15% visible sphalerite (i.e. 9% zinc). The third member is a cliff-forming, light-grey, medium crystalline dolomite with minor dark-grey fenestral dolomite. The upper 90 m of Sekwi Formation is orange, thin-bedded, dolomitic quartz siltstone, quartzite, sandy dolomite and occasional beds of oncolitic dolomite. Small archeocyathid mounds and Salterella are found in this member. The uppermost beds of the Sekwi Formation form the forth member and are very fossiliferous containing brachiopods, archeocyathids, and trilobites of the Bonnia-Olenellus Zone (Fritz, 1972). Unconformably overlying the Sekwi Fm is a sequence of thick-bedded, coarse to fine crystalline, light to dark grey, resistant dolomites of the Cambrian-Ordovician Franklin Mountain Formation.

Mineralization consists of fine-grained dark grey patches of dolostone loaded with disseminated pyrite, replaced by a coarser-grained dolomite (sacchroidal or replacive dolomite) which is sparsely disseminated with pyrite and sphalerite. Cavities are filled with even coarser-grained hydrothermal dolomite which contains euhedral sphalerite grains but little or no pyrite. Perfect dolomite rhombs (from the replacive dolomite) are seen enclosed in massive sphalerite. Fine-grained disseminated sphalerite and quartz are sparsely disseminated throughout the replacive dolomite.

As in the Cab property, galena, associated with barite, is more abundant upsection in the mineralized unit which is almost sphalerite-free. Hydrozincite is a common oxidation product but smithsonite is only occasionally present (Brock, 1974).

Cab (64°59'N, 132°27'W)

The Cab claim group lies 225 km northeast of Mayo, and straddles the border between the Yukon and the Northwest Territories. The Cab deposit is located in an area of Paleozoic carbonate and clastic rocks representing miogeoclinal deltaic and platformal deposition of material eroded from the Mackenzie Arch to the northeast. These rocks are now exposed in an east-west set of fault blocks stepping down section to the north toward the Arch.

The mineralized unit, within the Sekwi Formation, underlies, and is part of, a dark-grey bioturbated limestone-dolomite with interbedded oolitic and oncolitic dolomite. This unit contains

richly disseminated sphalerite, commonly 10-15% visible sphalerite (i.e. 9% zinc). The mineralized unit is overlain and underlain by sequences of barren sandy dolomite, sandstone, quartzite and siltstone. Abundant late stage fracture and vug filling is controlled by fracturing and jointing related to regional tectonism (Welcome North Mines Ltd., Company Report, 1975). Unconformably overlying the Sekwi Formation is a sequence of thick-bedded, vuggy dolomites of the Cambrian-Ordovician Franklin Mountain Formation.

The main type of mineralization consists of thin interbands or beds of fine-grained, clear, pale-coloured, nearly transparent sphalerite with medium crystalline hydrothermal replacive dolomite. Fine-grained detrital quartz is sparsely disseminated throughout the replacive dolomite. These grains appear to be wind blown detrital grains because of their small size, sub-rounded to angular shape. Fine-grained dark grey patches of dolostone with disseminated pyrite are replaced by a medium-grained hydrothermal dolomite (saccharoidal dolomite) sparsely disseminated with pyrite and sphalerite. Fractures and vugs are filled with coarse-grained hydrothermal dolomite and authigenic quartz followed by euhedral sphalerite but little or no pyrite.

Typical specimens of this material assay in excess of 50% zinc. Mineralization selectively replaced the original dolostone and deposited zoned hydrothermal dolomite, quartz, pyrite, sphalerite, barite and minor galena. These minerals commonly occur as open space filling of vugs, in fractures and veins, and as replacement of sedimentary structures and disseminations along bedding planes. Channelways in the dolomite are controlled, in part, by jointing, fracturing and faulting within favourable units made up of bioturbated dolomite containing black, silty organic rich laminations. Upsection, the mineralized beds are almost sphalerite-free; galena, associated with barite, is more abundant. Hydrozincite and rare smithsonite have been reported as common oxidation products (McArthur and McArthur, 1976).

Bob (64°33'30"N, 132°56'W)

The Bob deposit, located approximately 180 km northeast of Mayo, is exposed along the west side of a north-flowing creek draining into Corn Creek. The property is underlain by dolomite, quartzite and siltstone of the Lower Cambrian Sekwi Formation which is overlain by carbonates of the Ordovician Mount Kindle Formation. The rocks strike easterly with a very gentle dip to the north. The host rock is stromatolitic, orange to buff weathering, fine-grained dolomite of the Sekwi Formation with narrow vugs localized within stromatolitic zones. Zebra structure is present. Coarse-grained galena, sphalerite, pyrite (marcasite?) and chalcopyrite constitute the mineralization.

Three colours of sphalerite are present; dark grey, red, and honey coloured. The mineralization is localized within vugs along the algal lamination planes of small moundlike bioherms, up to several feet in both length and width, and also along bedding planes in the dolomite. It occurs intermittently down dip for approximately 30 m and for 15 m along strike. Chip sampling of the main showing resulted in an average assay value of 23.66 g/t Ag, 5.86 % lead and 3.75 % zinc (Sinclair et al., 1976, p. 49).

Palm (64°24'N, 129°46'W)

On the Palm claims sphalerite and galena are hosted in dolomites of the Lower Cambrian Sekwi Formation. In hand specimen, the host is a medium grained crystalline dolomite with disseminated sphalerite grains throughout, and traces of pyrite are common. Vugs are lined with thin dolomite layers, followed by coarser saddle dolomite and coarse grained sphalerite. Quartz and small grains of hydrozincite occur in the centre of the vugs.

In thin section the host dolomite contains abundant disseminated euhedral to subhedral pyrite. Disseminated sphalerite occurs in the host and sometimes replaces the disseminated pyrite. Finer grained dolomite cement lines the vugs and is followed by coarse grained open space sphalerite. Quartz occurs associated with the coarse grained sphalerite near the centre of the voids. The coarse grained saddle dolomite is both syn- and post-ore. The hydrozincite that occurs in the centre of the vugs is post-ore.

Econ (Economic) (64°20'N, 131°13'W)

The ECON deposit is located at the headwaters of the North Stewart River, 7 km from the Yukon- N.W.T. boundary. Host rocks are the upper massive pale grey limestone of the lower Cambrian Sekwi Formation, which has been sporadically dolomitized. Two styles of mineralization were defined on the basis of mineralogical and textural differences: 1) breccia with dolomite, calcite, and minor barite; and 2) veins with dolomite, calcite, barite, and quartz. The breccia fragments are composed of fine-grained saccharoidal dolomite. Sphalerite, galena, pyrite and traces of chalcopyrite, occur with masses of ferroan-dolomite, coarse-grained saddle dolomite, and minor amounts of calcite, barite and quartz. According to Gibson (1975) the mineralization occuring in veins was emplaced along east-striking fractures related to a NW trending fault system cutting the top of the Lower Cambrian Sekwi Formation carbonates. The veins are steeply dipping and range from a few cm to 12 m wide and up to 300 m long. Galena is generally found concentrated in the

centre of the wider veins. Barite is restricted to the area east of the North Stewart River. Secondary alteration minerals include cerrusite, hydrozincite and limonite. Pyrobitumen was also identified.

Tic (Tegart) (64°33'N, 130°10'W)

The Tic Zn-(Pb) deposit is located north of Mountain River. The Tic C Zone was visited by the second author and K.M. Dawson in 1980. There are A, B, D and E zones but these were not visited. Zinc-lead mineralization is found within narrow veins in light grey to buff coloured fine to coarse crystalline dolomite of the Lower Cambrian Sekwi Formation. Mineralization appears to be fracture controlled near a fault zone. Two mineralized stratigraphic zones have been distinguished. The lower zone occurs in vuggy dolomite and dolomite breccia whereas the upper zone occurs in a porous dolomite. The C, D, and E zones are part of the lower mineralized zone.

In hand specimen medium to fine grained crystalline grey dolomite with arenaceous and vuggy parts comprise the host. Vugs and fractures are infilled with coarse crystalline dolomite followed by coarse, green sphalerite, and/or quartz, locally with pyrite, and often sphalerite is repeated with a final stage of euhedral quartz crystals. The quartz closely associated with the sphalerite contains solid inclusions of carbonate which suggests that this quartz likely grew at the same time as the carbonate. Some brecciated specimens show pyrite rimming the dolomite host fragments, which is then followed by saddle dolomite and coarse crystalline sphalerite and galena.

Ice (63°39'00"N, 129°03'15"W)

The Ice deposit adjoins the southeast side of the Emily deposit, and together form a northwest trending 136 claim block. The west part of the Emily block is underlain by Cambrian and earlier quartzite which has been brought against Sekwi Formation dolostone by a northwest striking, northeast dipping thrust fault. On the northeastern part of the claim block, northwest striking Sekwi Formation is unconformably overlain by Middle Cambrian and younger recessive black shale.

The Ice deposit is hosted in the porous, orange-weathering dolomite of the Lower Cambrian Sekwi Formation (Dawson, 1975). Fenestral fabrics in the host dolomite unit, adjacent to a northwest striking thrust fault, contains irregular patches and vugs of galena and sphalerite. Some sections of this host dolomite are highly mineralized and others barren. Minor amounts of pyrobitumen are disseminated throughout dolomites of the Sekwi Formation in the vicinity of the Ice deposit (Padgham et al., 1976, p. 164-165).

Arn (63°44'N, 129°15'W)

The Arn deposit is hosted in the porous, orange-weathering dolomite of the Lower Cambrian Sekwi Formation (Dawson, 1975). The 82 Arn and 77 Tee Claims form a contiguous northwest trending block 16 km long and as much as 3.2 km wide. The western part of the area covered by this claim block is underlain by northwest striking Cambrian orthoquartzite, argillaceous sandstone, and orange-weathering dolostone. These Lower Cambrian sequences have been thrust against Middle Cambrian black calcareous shales along a northwest striking fault. A facies change from shale to Whittaker Formation dolostone occurs in the northern and eastern part of the claims. The Ordovician to Silurian Whittaker Formation is overlain by the Silurian and Devonian Delorme dolostone and Middle Devonian Sombre Formation dolostone Bedrock exposure on Arn 6 is sparse. A 9x0.9x1.2 m trench did not encounter bedrock but a selected float sample from the trench assayed 4.75% Pb and 2.52% Zn. (Padgham et al., 1976, p. 165-166).

Joli Green (62°57'N, 128°20'W)

The Joli Green Zn-(Pb) deposit, consisting of a bedded zone of sphalerite mineralization up to 2 metres thick, occurs in Upper Cambrian to Lower Ordovician Broken Skull Formation.

Mawer (62°07'N, 127°10'W)

Sphalerite mineralization at the Mawer (Ma) Group occurs in the Sunblood Formation consisting of dolomite breccia, formed from host dolomite fragments cemented by dolomite. The sphalerite appears to replace the host dolomite fragments. Mineralization occurs just below an orange marker bed which marks the contact with the overlying Esbataottine Formation. This formation is in turn overlain by the Ordovician to Silurian Whittaker Formation followed by the Road River Formation. The Middle Ordovician Sunblood Formation is underlain, with possible disconformity, by the Late Cambrian-Early Ordovician Broken skull Formation.

Bear (Bear-Twit) (64° 02'50"N, 129°25'00"W)

The Bear lead-zinc deposit is hosted within breccias of Ordovician shale-carbonate transitional facies of the Mount Kindle Formation, and the overlying Delorme Formation. The Mount Kindle Formation occurs in the northern Mackenzie Mountains and is correlative with the Whittaker Formation to the south. The Mount Kindle Formation comprises up to 570 m of thick-

bedded massive dark grey dolostone and minor limestone that are often vuggy, medium to coarsely crystalline, locally silicified, and contain some chert nodules and beds. In the Misty Creek Embayment area (Fig. 1-2), and regionally, the Mount Kindle strata unconformably overlie the Franklin Mountain Formation and are unconformably overlain by Siluro-Devonian carbonate rocks. Mount Kindle transition facies host dolomite overlies the Duo Lake Formation. All macro fauna in the Mount Kindle Formation range in age from Late Ordovician to Early Silurian (Cecile, 1982). Brock (1976) noted that Lower and Middle Devonian carbonate strata are characterized by widespread evaporitic sequences, dolomite and limestone breccia.

The Bear deposit has two zones, a lead-rich one and a zinc-rich one. The lead-rich zone occurs as lenses of barite, with sphalerite, galena, quartz, calcite, and tetrahedrite in Delorme Formation breccia (K.M. Dawson, pers. comm., 1992); this zone, however, was not examined in the present study.

Samples used in this study came from the zinc-rich breccia zone that is hosted in the Mount Kindle Formation and composed of host dolomite, pyrite, quartz, dolomite cement, sphalerite, and calcite. Neither barite nor tetrahedrite was identified in this study. Reserves at the Bear deposit have been estimated at 18.14 million tonnes grading 7% to 8% combined lead-zinc and 17 to 34 g/t silver (Brock, 1976). The breccia hosting the mineralization was described as a tectonic breccia by Dawson et al. (1991), but as intra-formational breccia by Brock (1976). Dawson also noted the presence of stylolites. Stylolites at Bear are sutured and cut the dolomite cement. The deformation has overprinted ore-related minerals as suggested by the fact that veins of dolomite cement are offset by stylolites (Carrière and Sangster, 1996).

Snobird (62°14'50"N, 126°20'W)

The Snobird deposit is hosted in Ordovician-Silurian Whittaker Formation. Sphalerite fills vugs along with dolomite cement and calcite. The host dolomite contains significant quartz.

Rev (64°20'N, 129°08'W)

The REV Zn-(Pb) deposit location is taken from McLaren, (1978, M.Sc. Thesis). It is hosted within fault controlled breccias of Ordovician to Silurian dolomites of the Mount Kindle and Delorme Formations. These formations overlie the Cambrian to Ordovician Road River and transitional (to basin) Franklin Mountain Formations, on the northeastern edge of the lower

Palaeozoic Misty Creek Embayment (Cecile and Morrow, 1978, p. 472).

There are two generations of sphalerite at the REV deposit: 1) clear, pale sphalerite, occurs disseminated in the host rock. 2) Brownish-orange, coarse-grained sphalerite is later and fills open spaces replacing dolomite gangue. Sphalerite and galena occur in veins and as disseminations. In hand specimens from the Main showing, a fossiliferous host dolomite contains euhedral to subhedral grains of disseminated pyrite and veins of pyrite. Fine grained granular green sphalerite occurs disseminated in the host and appears to replace the host and in some cases the veins of pyrite. Dolomite cement follows the dolomite host rock in the paragenesis. Coarse grained, orange sphalerite, associated with and sometimes replacing the saddle dolomite, fills cavities followed by quartz. Calcite fills any remaining spaces and is twinned. In addition, coarse grains of brownish sphalerite cling to the host dolomite fragments and/or replace gangue dolomite which fills open spaces.

In thin section sample SP5506, from the Main showing, is made up mostly of spherical disseminated sphalerite. Some open-space coarser grained sphalerite does occur along with saddle dolomite. Small euhedral to subhedral grains of pyrite occur sparsely disseminated in the host dolomite and a few grains are also seen in the disseminated sphalerite.

Rain-Snow (63°59'N, 129°19'W)

The location for the Rain-Snow (Weather) deposit is taken from Godwin et al., (1982). Galena and sphalerite occur in narrow fractures and solution cavities within late Early Devonian Sombre and Arnica Formations near the fault. The sphalerite is either a distinctive red or, more commonly, a pale vitreous green. The northwest corner of the Rain-Snow deposit is underlain by Whittaker dolostone which is overlain to the southwest by a stratigraphic succession comprising Delorme limestone, Sombre dolostone, Arnica dolostone, Landry limestone and Headless limestone. The Sombre Formation forms the core of a northwest striking syncline with a parallel striking fault on its southwest side. This fault brings the Sombre Formation into contact with the overlying Arnica Formation. All Formations on the property, to the west of the fault, dip 45° to 75° to the southwest (Padgham et al., 1976).

2. GENERAL METHODOLOGY

The present study continues from those of earlier workers, such as McLaren and Godwin, and deposits from a number of stratigraphic positions have been selected; their locations are shown in Fig.1-3. The study involves the integration of petrography, microthermometry, cathodoluminescence microscopy, and electron microprobe analyses. Samples were collected, by various GSC staff during brief property visits, from outcrops, trenches and some drill core in an area covering 160,000 km^2 of the Mackenzie Platform. A total of 62 polished thin sections, representing 27 properties, were prepared and examined. The 24 deposits selected for study are listed in Table 2-1, along with their location, host formation, age of host, work done (this study), and references. Eight of the 24 deposits are hosted in limestone rather dolomite with little or no dolomite cement. These eight deposits, which include Tet-Rap, Birkeland, Keg, Art, Scat, Rio, Aj, and Big Red, have been studied using petrography and cathodoluminescence only.

Two sets of double-polished sections were prepared. One set of standard thin sections was used for cathodoluminescence microscopy (CL) and electron microprobe studies. Thin sections were also examined using transmitted and reflected light microscopy. Where present, at least two and as many as ten or more zoned saddle and/or hydrothermal/burial dolomite crystals in each thin section were photographed in plane polarized light, crossed polarized light, and CL. Detailed paragenetic analyses were made from projected 35 mm slides and colour prints. The second set, doubly polished sections (100-150 μm) prepared under temperatures not exceeding 80°C, was used for the fluid inclusion study, after which some selected chips were examined under CL or ultraviolet (UV) light.

Table 2-1. List of deposits studied, in order of age of host rock, oldest to youngest.

Deposit Name(s)/ N.T.S.	Location	Host Formation	Age of Host	Work Done: this Study*	Reference(s)
Tet-Rap 106A/1	64°03'N 128°17'W	Little Dal Group	Meso-proterozoic	P, CL	1.
Gayna (Gayna River) 106B/15	64°56'N 130°41'W	Little Dal Group	Meso-proterozoic	P, CL, FI, MP	2, 3, 4, 5, 7.
Birkeland 106B/4	64°09'N 131°55'W	Grit Unit	Neo-proterozoic	P, CL	7, 8.
Cypress (Mt. Tillicom) 106C/7	64°25'20"N 132°52'00"W	un-named dolomite	Neo-proterozoic	P, CL, FI, MP	1, 7, 9.
Ab	64°59'N 132°17'W	Sekwi Formation	Early Cambrian	P, CL, FI	3, 9.
Cab 106C/16	64°59'00"N 132°27'00"W	Sekwi Formation	Early Cambrian	P, CL, FI, MP	3, 6, 9.
Bob 106C/10	64°33'30"N 132°56'00"W	Sekwi Formation	Early Cambrian	P, CL, FI, MP	6, 9.
Palm 106A/5	64°24'N 129°46'W	Sekwi Formation	Early Cambrian	P, CL, MP	8, 14.
Econ (Economic) 106B/6	64°20'00"N 131°13'00"W	Sekwi Formation	Early Cambrian	P, CL, FI, MP	8, 9, 10.
Tic (Tegart) 106 B/9	64°33'N 130°10'W	atypical Sekwi Formation	Middle Ordovician-Silurian	P, CL, MP	3, 7, 8, 9.
Ice 105P/11	63°39'00"N 129°03'15"W	Sekwi Formation	Early Cambrian	P, CL, MP	1, 3, 9.
Arn 105P/11	63°44'N 129°15'W	Sekwi Formation	Early Cambrian	P, CL, MP	1, 3, 9.
Joli Green 105I/16	62°57'N 128°20'W	Broken Skull Fm.	Late Cambrian-Early Ordovician	P, CL, FI, MP	11.
Mawer (Ma) 95L/3	62°07'N 127°10'W	Upper Sunblood Fm.	Middle Ordovician	P, CL, FI, MP	12.

*P=Petrography,
CL=Cathodoluminescence,
FI=Microthermometry,
MP=Electron Microprobe

Table 2-1. (Con't.)

Property Name	Location	Host Formation	Age of Host	Work Done: this study*	Reference(s)
Keg 105P/14	63°59'50"N 129°14'50"W	Sunblood and Whittaker Formations	Middle Ordovician-Silurian	P, CL	1, 9.
Bear-Twit (Twitya) 106A/3	64°02'50"N 129°25'00"W	Mt. Kindle Formation	Ordovician	P, CL, FI, MP	1, 2, 3, 7, 8, 9, 13.
Snobird 95L/1	62°14'50"N 126°20'00"W	Whittaker Formation	Ordovician-Silurian	P, CL	3.
Rev	64°20'N 129°08'W	Mt. Kindle/ & Delorme Formations	Ordovician-Silurian	P, CL, FI, MP	7, 8.
Rain-Snow (Weather) 105P/14	63°59'00"N 129°19'00"W	Sombre and Arnica Formations	late Early Devonian	P, CL	1, 7, 8, 9.
Art (Backbone) 105P/14	63°51'15"N 129°10'25"W	Landry Formation	Middle Devonian	P, CL	1, 3, 7, 8, 9.
Scat 105P/14,15	63°54'15"N 129°02'15"W	Arnica, Landry, Formations	Middle Devonian	P, CL	1, 9.
Rio 106B/1	64°15'00"N 130°22'00"W	Nahanni Formation	Middle Devonian	P, CL	14.
Aj (Essau) 106B/15,16	64°45'N 130°32'W	Hume Formation	Middle Devonian	P, CL	1,7, 9.
Big Red 105I/8	62°25'N 128°21'W	Grizzly Bear & Haywire Formations	Middle Devonian	P, CL	11, 15.

References

1. Mineral Industry Report, 1973, Northwest Territories, Indian and Northern Affairs, Canada, EGS 1976-9, (1976)
2. Brock (1976)
3. Sangster and Lancaster (1976)
4. Hewton (1982).
5. Carrière and Sangster (1992).
6. Mineral Industry Report, 1975, Yukon Territory, Indian and Northern Affairs, Canada, EGS 1976-15, (1976)
7. McLaren and Godwin (1979b).
8. Godwin et al. (1982).
9. Dawson (1975)
10. Gibson (1975)
11. Gordey and Anderson (1993)
12. Dawson, pers. comm., 1996
13. Carrière and Sangster (1996)
14. Mineral Industry Report, 1975, Northwest Territories, Indian and Northern Affairs, Canada, EGS 1978-5, (1978)
15. Mineral Industry Report, 1979, Northwest Territories, Canadian Department of Indian Affairs and Northern Development, EGS 1983-9, (1983)

3. MINERALOGY, CATHODOLUMINESENCE, AND PARAGENESIS

MINERALOGY

The mineralogy of the sixteen deposits described in Section 1 is typical of carbonate-hosted Zn-Pb (MVT) deposits and includes dolomite cement, pyrite, sphalerite, galena, quartz, calcite, and occasionally barite. In addition there are a variety of secondary minerals such as bitumen, smithsonite, hydrozincite, and cerussite. Tetrahedrite, marcasite, and chert have been reported, but have not been identified in the samples used for this study. Mineralization commonly occurs in collapse breccias, as open space filling of vugs, fractures and veins, and as replacement of sedimentary structures and disseminations along bedding planes. Channelways in favourable host dolomite units are controlled, in part, by jointing, fracturing and faulting.

DOLOMITE TEXTURES

Introduction

The textures of host dolomite and dolomite cements from Mackenzie Platform Zn-Pb deposits were examined for clues to the genesis of the dolomite. Petrographic and cathodoluminescence evidence show that there are as many as three different dolomite textures present in the deposits studied. These consist of host dolomite, finer grained dolomite cement, and coarse-grained saddle dolomite cement. Finer grained dolomite cement is here defined as ranging in grain size from 60-2000 μm (mean 515 μm) and includes replacive saddle dolomite. Coarse-grained saddle dolomite ranges in grain size from 200-6600 μm (mean 1570 μm). Dolomite cement(1) is the finer grained cement (see Paragenesis) including replacive saddle dolomite. Dolomite cement(2) is coarse grained saddle dolomite. The average grain size of host dolomite ranges from 42 to 215 μm.

Definition of dolomite textures

Dolomite classification based on two types of diagenetic textures have been defined by Sibley and Gregg, (1987): (1) planar dolomite, which forms in both near-surface (<1 km) and burial diagenetic environments; and (2) nonplanar dolomite, which develops in excess of 50°C in the burial environment (1 km or greater) by dolomitization of limestone or neomorphic recrystallization of preexisting dolomite (Woody et al., 1996). The terms planar and nonplanar are equivalent to the terms idiotopic and xenotopic of Gregg and Sibley (1984). Planar dolomite crystals have straight boundaries and several variations exist: Planar-e dolomite is: i) mostly euhedral crystals with a crystal-supported structure and

inter-crystalline areas filled with another mineral; or ii) porous, such as in sucrosic texture. Planar-s dolomite has subhedral to anhedral crystals, low porosity and/or little intercrystalline matrix, with straight compromise boundaries common, and greater than 30% crystal face junctions. Planar-c dolomite occurs as euhedral crystals lining pores or surrounding patches of another mineral.

Nonplanar dolomite crystals have curved, lobate, serrated, indistinct, or otherwise irregular boundaries and they commonly have undulatory extinction. Crystals commonly show undulatory or sweeping extinction, commonly contain inclusions which gives a cloudy appearance, and are typically fabric-obliterative. Variations include non-planar-a dolomite or replacement saddle dolomite and nonplanar-c dolomite which is pore lining saddle dolomite cement, where cement is defined as passively precipitated crystals that grow attached to a free surface. Nonplanar-a dolomite is composed of tightly packed anhedral crystals with mostly irregular intercrystalline boundaries and less than 30% crystal face junctions.

Mackenzie Platform dolomite

Table 3-1a and 3-1b list the textural and genetic features of dolomites in the Mackenzie Platform. Although both planar and non-planar dolomite types are present, a majority of host dolomite and dolomite cement display nonplanar texture. Figure 3-1 and 3-2 show examples of nonplanar-a texture of the host dolomites from Tic, Ice, Cab, Mawer, Bear, Rev, Snobird, and Rain-Snow deposits. These dolomites, therefore, are considered burial dolomites that have formed at depths of approximately 1 km or greater.

Dolomite textures as clues to diagenetic history

The variations in dolomite texture are a result of the diagenetic history of the rock (Sibley and Gregg, 1987). Various lines of evidence including aqueous fluid inclusions, oxygen-isotope compositions and cement zonation demonstrate that "burial" cements can form over a substantial range of conditions. These include temperatures from 50°C to perhaps 200°C or higher, burial depth from a few hundred metres to kilometres, formation water compositions from brackish to highly saline, from acidic to strongly alkaline pH, and from moderately to strongly negative Eh values (Choquette and James, 1990). Dolomite displaying (planar-e) sucrosic texture, for example, is typical of dolomite that has not undergone extensive compaction (Table 3-1a).

Gregg and Sibley (1984) conclude that the petrographic recognition of nonplanar dolomite provides a quick and easy method of determining if the dolomite formed under epigenetic/diagenetic conditions above 50°C. Burial-stage dolomites are often characterized by coarsely crystalline sparry dolomite, in a "saddle" form. The dolomite cements of the Mackenzie Platform appear to be coarse

Table 3-1a. Textural and genetic classification of planar dolomites from the Mackenzie Platform (modified from Mazzullo, 1992).

PLANAR DOLOMITE:

A carbonate sedimentary rock containing more than 90% dolomite and less than 10% calcite, or one having a Ca/Mg ratio in the range of 1.5-1.7, or magnesium-carbonate equivalent of 41.0-45.4%. Dolomite occurs in crystalline and noncrystalline forms, is clearly associated and often interbedded with limestone, and usually represents a postdepositional replacement of limestone. Syn: dolostone

Formed at less than 50-60°C:

Host dolomite:

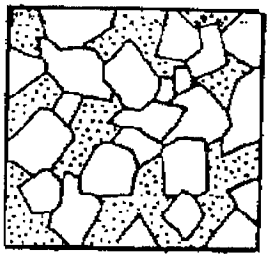

Planar-e: dolomite crystals mostly euhedral; crystal-supported with intercrystalline areas filled with another mineral or porous (as in sucrosic texture).

Deposits: BOB host dolomite (avg. grain size **100 μm**)

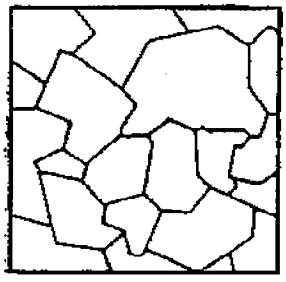

Planar-s: subhedral to anhedral crystals, low porosity and/or little intercrytalline matrix; straight compromise boudaries common, greater than 30% crystal face junctions.

Deposits: none observed

Finer-grained dolomite cement:
(as defined in Section 5.)

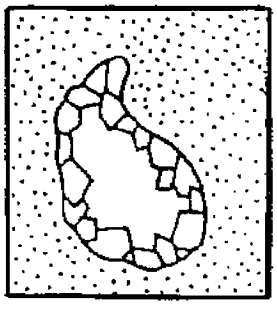

Planar-c: euhedral crystals lining pores or surrounding patches of another mineral. May also be replacive dolomite, where undolomitized interior of allochem was later dissolved.

Deposits: PALM(?) (avg. grain size **490 μm**),
SNOBIRD(?) (avg.grain size **540 μm**)

Table 3-1b. Textural and genetic classification of nonplanar dolomites from the Mackenzie Platform (modified from Mazzullo, 1992).

NONPLANAR DOLOMITE:

A variety of dolomite that has a warped crystal lattice, characterized by curved crystal faces and sweeping extinction. It is a common product of late-stage diagenesis and hydrothermal activity, and normally occurs as pore-filling cements or in veins. Also occurs as a replacement product.

Formed in burial diagenetic environment at greater than 50-60°C:
Host dolomite:

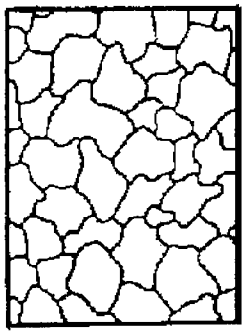

Nonplanar-a: anhedral crystals with mostly irregular intercrystalline boundaries (less than 30% crystal-face junctions); crystals commonly show undulatory or sweeping extinction, contain inclusions which gives a cloudy appearance; also includes replacement saddle dolomite.

Deposits: TIC (avg. grain size **215 μm**)
ICE (" **90 μm**)
GAYNA (" **50 μm**
CAB (" **90 μm**)
SNOBIRD (" **42 μm**)
REV (" **120 μm**)
BEAR (" **98 μm**)

Finer grained dolomite cement:
(as defined in Section 5.)

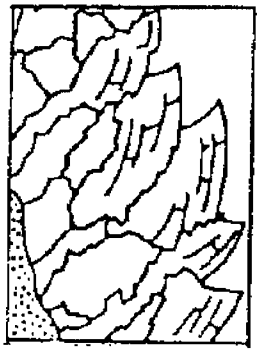

Nonplanar-c: pore lining saddle dolomite cement, where cement is defined as passively precipitated crystals that grow attached to a free surface.

Deposits: REV (avg. grain size **750 μm**),
JOLI GREEN (" **890μm**)

Coarse-grained saddle dolomite:

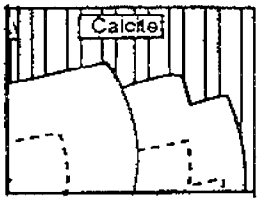

Deposits: ICE (avg. grain size **1200 μm**), TIC (" **1600 μm**),
PALM (" **1860 μm**), BOB (" **2090μm**),
CAB (" **2600μm**), ECON (" **1470 μm**),
GAYNA (" **1260 μm**)

burial cements. Figures 3-4 to 3-27 contain examples of dolomite as described from the sixteen deposits hosted in dolomite. Figures 3-28 to 3-37 show the contrast in mineralogy of the eight deposits hosted in limestone rather than dolomite containing little or no dolomite cement. Saddle dolomite (Fig. 3-4) is a variety of dolomite that shows a warped crystal lattice (Radke and Mathis, 1980). Such dolomite is turbid, coarsely crystalline with curved crystal faces, ranging from rhombohedra with slight facial curvature to classic saddle forms, and shows sweeping or undulatory extinction in cross-polarized light. The spearhead-shaped crystal (Fig. 3-12, 3-17) is typical and has curved terminal faces and peripheral zig-zag outlines. In crystals larger than a few millimetres the faces are usually a composite of subcrystals (Fig. 3-9, 3-23). The turbid or cloudy appearance results from an abundance of fluid inclusions (Fig. 3-11). Most crystals have growth bands which may be discerned by changes in fluid inclusion density. Saddle dolomite composition, slightly calcium-rich, range from 50 to 60 mole % $CaCO_3$, 31 to 49 mole % $MgCO_3$, and 1 to 33.5 mole % $FeCO_3$. It occurs as a void cement (Fig. 3-15) in all porosity types as well as a replacement mineral (Fig. 3-16). Hydrothermal dolomite is another term sometimes used for saddle dolomite, and its temperature of formation can be approximated from fluid inclusion data. Saddle dolomite shares an association with epigenetic sulphide mineralization, sulphate-bearing carbonates, and hydrocarbon accumulations (Radke and Mathis, 1980). According to Warren (1989), saddle dolomite is a burial indicator. A growing consensus is developing that saddle dolomite precipitated at temperatures between 60° and 150°C or greater from hydrothermal solutions carrying sulphides and hydrocarbons (Warren, 1989).

The burial-stage model as discussed by Warren (1989) states that burial-stage dolomites are a late-stage dolomitization event in deep subsurface carbonates and formed by the migration of hot magnesium-rich basinal fluids out of a basin. The deep-burial model of dolomite formation applicable to the interpretation of ancient dolomites first introduced by Zenger (1983) shows the minimum burial depth involved to be approximately 1 km.

The following characteristics of the Mackenzie Platform dolomite suggest burial dolomites: (i) a majority of the dolomite hosting Zn-Pb deposits is made up of nonplanar dolomite, (ii) all sixteen deposits hosted in dolomite contain saddle dolomite, (iii) fluid inclusion data for saddle dolomite from seven of these deposits indicate that the dolomite formed at temperatures greater than 150°C from highly saline, Na-Ca-Mg-Cl type, brines. In all examples the saddle dolomite cement is paragenetically associated with sulphide mineralization. The dolomite cement is commonly intergrown with the sulphides and is thought to be co-genetic or closely alternating with the sulphide minerals (in space and time).

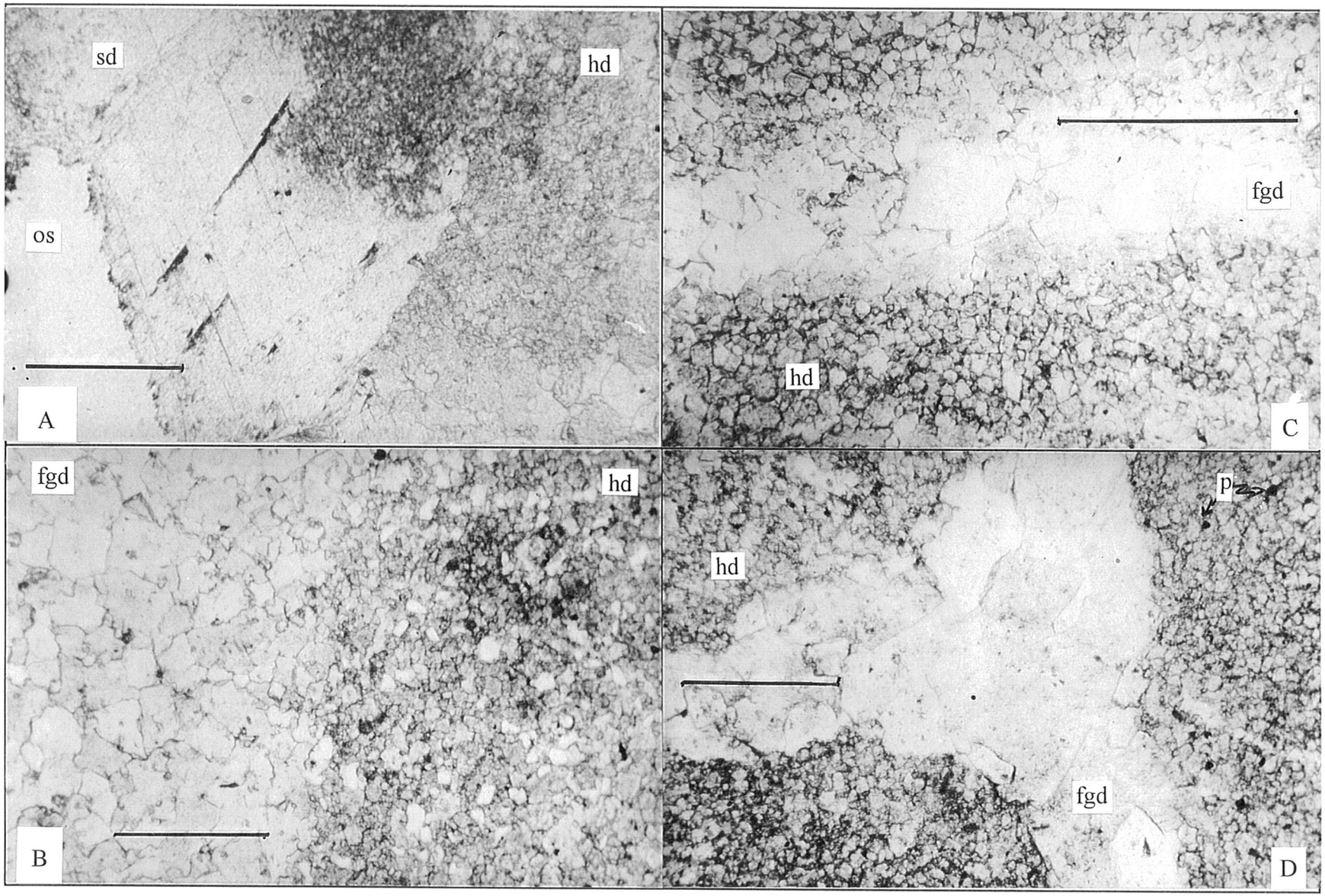

Fig. 3-1. Examples of host dolomite displaying non-planar-a texture. Plane-polarized light. All scale bars=0.5 mm. A) Tic sample SP4214B shows coarse grained saddle dolomite (sd) growing in open space (os) from host dolomite (hd). B) Ice sample SP5453 shows host dolomite (hd) on the right and finer grained dolomite cement (fgd) on the left. C) Cab sample SP3297 shows finer grained dolomite cement (fgd) filling cavity in host dolomite. D) Mawer sample SP5403 shows dolomite cement filling cavity in host dolomite (hd). Note the fine-grained pyrite (p) disseminated in the host rock.

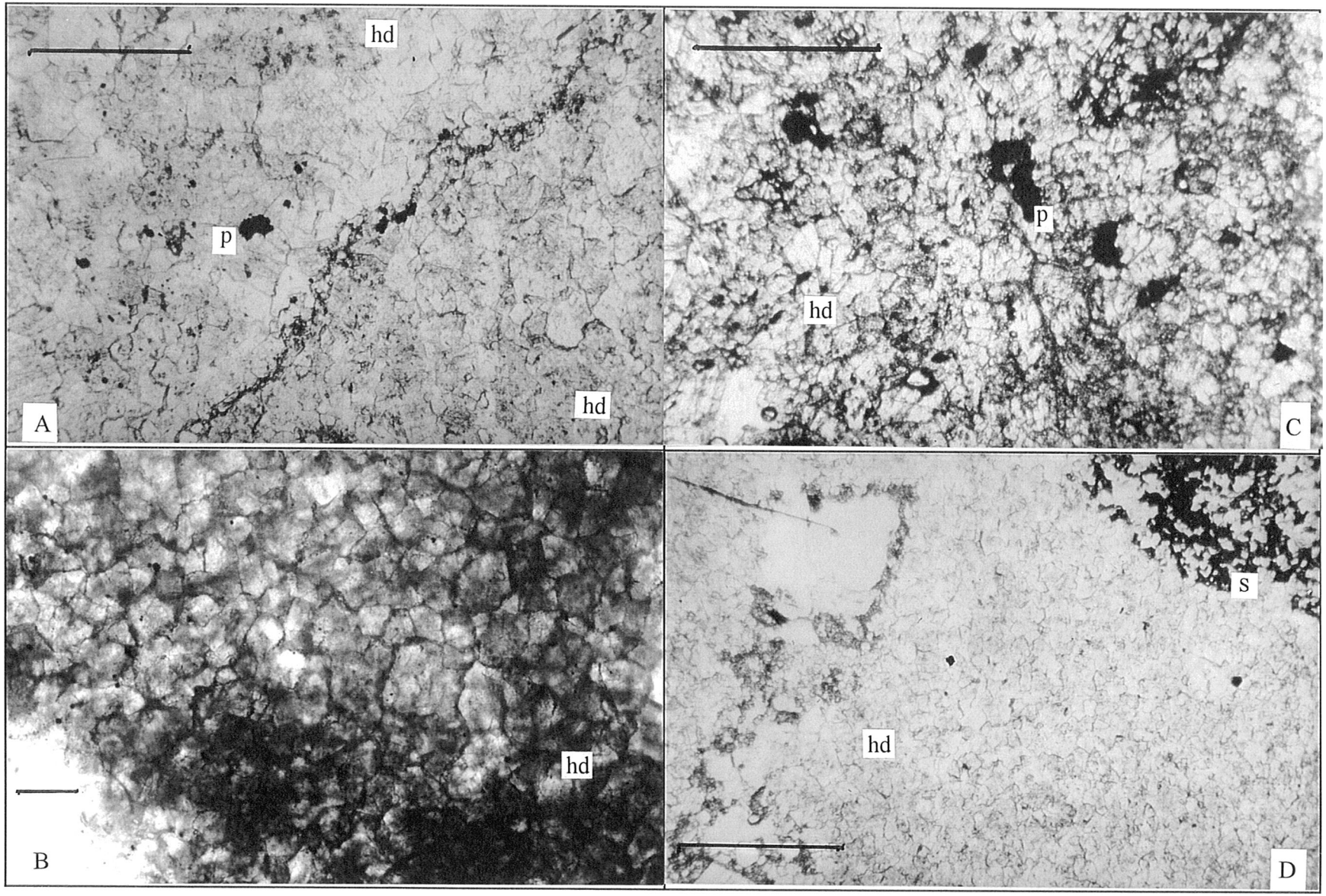

Fig. 3-2 . Examples of host dolomite (hd) displaying non-planar-a texture. Plane-polarized light. All scale bars=0.5mm. A) Bear sample SP5489 cut by stylolite, and contains disseminated pyrite (p). B) Rev sample SP5497 host dolomite. C) Snobird sample SP3415 with disseminated pyrite (p) in host dolomite (hd). D) Rain 3 sample with sphalerite (s) in upper right corner replacing host dolomite (hd).

CATHODOLUMINESCENCE

The cathodoluminescence technique has been used extensively in the study of sedimentary cements, including those associated with Mississippi Valley-type Pb-Zn deposits. Ebers and Kopp (1979) used cathodoluminescence to correlate carbonate gangue associated with sphalerite ores over a widespread area in the East Tennessee zinc district. Sequentially deposited ore and gangue minerals, resulting from the ore fluids changing as a function of time, may possess cathodoluminescent growth zones that are not visible using either transmitted or reflected light. These growth zones may be useful in sample-to-sample correlation and in the interpretation of paragenesis.

A similar correlation between carbonate gangue associated with sphalerite was attempted among deposits in the study area. "Luminescent signatures", referring to the patterns of alternating growth zones in ore-stage crystalline dolomite cement, were examined in more than 780 cathodoluminescence photomicrographs representing 24 deposits. Individual dolomite cement crystals were identified in 15 of these deposits and the cathodoluminescence zones were recognized on the basis of their texture, degree of crystal development, colour, presence or absence of banding, and intensity of luminescence. Microstratigraphic correlation of luminescent signatures between deposits must consider the relative thickness, colour, hue, and intensity of the zones. Although, within each deposit, the cathodoluminescent signatures were very distinctive and consistent, no definitive correlations of luminescent signatures between deposits could be made. After several attempts to correlate cement stratigraphy among deposits, this research was terminated although it was recognized that the difficulties could be due to experimental artifacts rather than natural causes. Experimental difficulties included: i) limitations of equipment (cold-cathode); ii) type of samples (grab samples); and iii) some variation in photographic, developing, and printing processes (see Table 3-2).

Table 3-2. Conditions under which the CL photomicrographs were taken which could affect the colour and/or intensity.

Microscope: Leitz Ortholux II
Instrument: Nuclide Luminoscope
Beam energy: avg. 14 KV
Spot diameter: 18-25 mm
Gun type: Cold cathode
Ambient gas: Air @ 30-40 millitor
Camera: Wild Leitz (Wild MPS52) with
Photoaumat (Wild MPS46)
Film type: Kodak Ektachrome
Film size and speed: 35mm, 200 ASA
Development: Normal to underexposed
Exposure: 10 seconds to 3 minutes

The value, however, in the cathodoluminescence (CL) work is in its ability to distinquish between minerals such as dolomite and calcite, document zonation, identify healed fissures, and illustrate paragenesis. A general caption (Fig. 3-3) explains the set-up of the colour photomicrographs. Figures 3-4 to 3-37 are triplet microphotographs of selected minerals in plane-polarized light, crossed-polarized light, and the CL from each deposit. In all examples the saddle dolomite cement is paragenetically associated with sulphide mineralization. The dolomite cement, generally coarse-grained saddle dolomite and/or the finer grained dolomite cement, which can be replacive saddle dolomite, is commonly intergrown with the sulphides and is thought to be co-genetic or closely alternating with the sulphide minerals (in space and time). The photomicrographs selected represent typical examples from each deposit and readily illustrate the close association between dolomite cement and sulphides. The eight deposits in which no significant dolomite cement was observed include Tet-Rap, Birkland, Keg, Scat, Art, Aj, Rio, and Big Red, and are shown in Fig. 3-28 to 3-37.

Fig. 3-3. General caption for Figures 3-4 to 3-37.

(a) Photomicrograph in plane-polarized light	(d) Photomicrograph in plane-polarized light
(b) Photomicrograph in crossed polarized light	(e) Photomicrograph in crossed polarized light
(c) Photomicrograph of cathodoluminescence view	(f) Photomicrograph of cathodoluminescence view
Bar Scale	Bar Scale
Name of deposit, Sample No., Description of view in (c). Views in (a) and (b) are shown for comparison and clarification.	Name of deposit, Sample No., Description of view in (f). Views in (d) and (e) are shown for comparison and clarification.

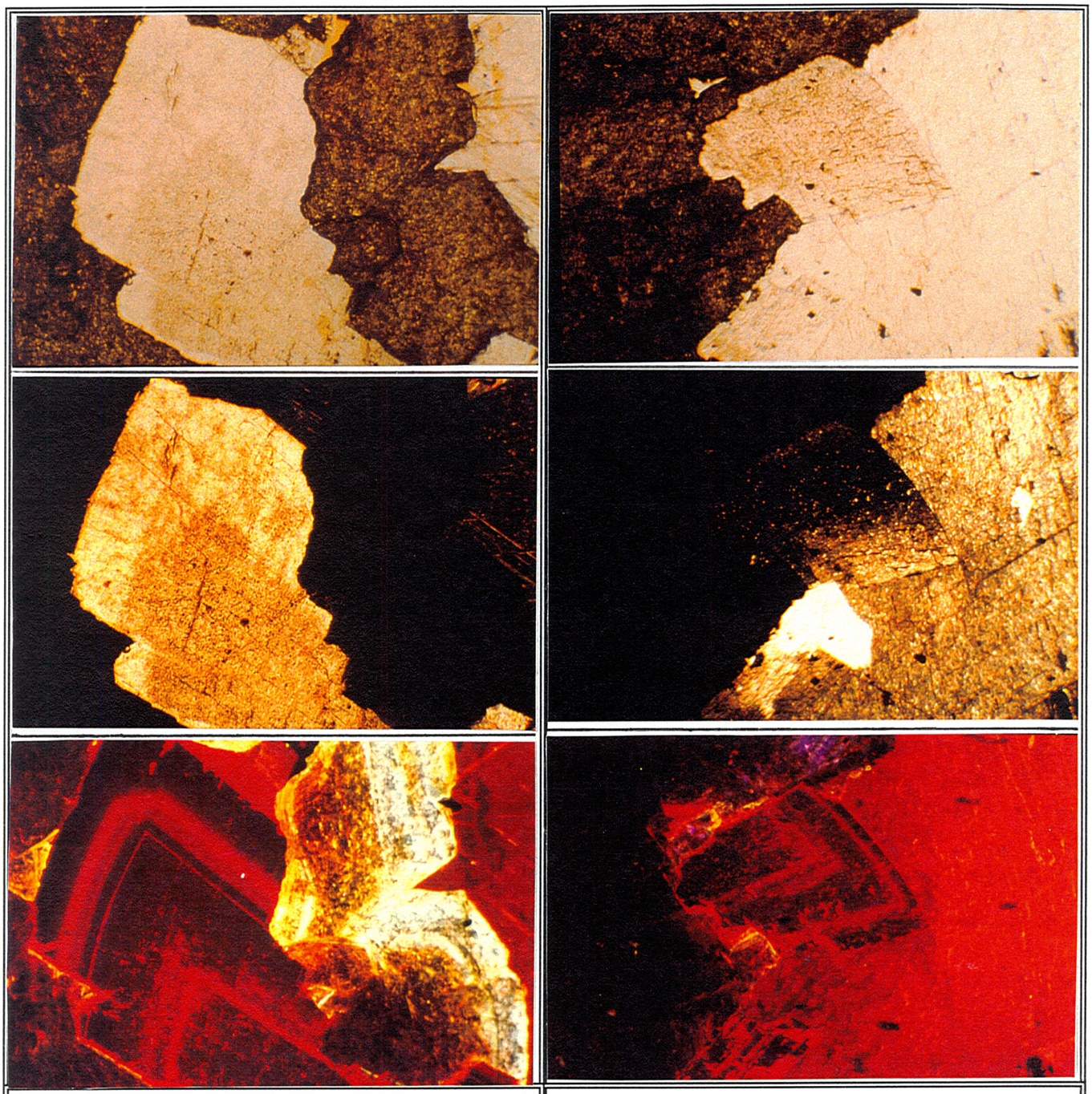

Fig. 3-4 . Gayna deposit, sample no. SP3400. Saddle dolomite (zoned red and black, centre), associated with sphalerite (luminescent, bluish, yellow, brown), shows typical shape, undulatory extinction, and compositional zoning. The dolomite was partially dissolved prior to deposition of sphalerite. Luminescent orange calcite (extreme right) filled remaining cavities. GSC photo 1995-215.

Fig. 3-4. Gayna deposit, sample no. SP3400. Saddle dolomite (centre) associated with sphalerite (luminescent, brownish-black, and purple) shows typical shape, undulatory extinction, and compositional zoning (red and black). The position of the saddle dolomite here is between the sphalerite and the late luminescent orange calcite (right).

1 mm

Fig. 3-5. Gayna deposit, sample no. SP3408A. Host dolomite (bottom, non-luminescent) followed by dolomite cement (zoned, red and black), quartz (non-luminescent) and sphalerite (luminescent yellow, dark cores and bright rims). In black and white copy of plain light photo (a), S=sphalerite, D=dolomite cement, d=host dolomite and q=quartz.

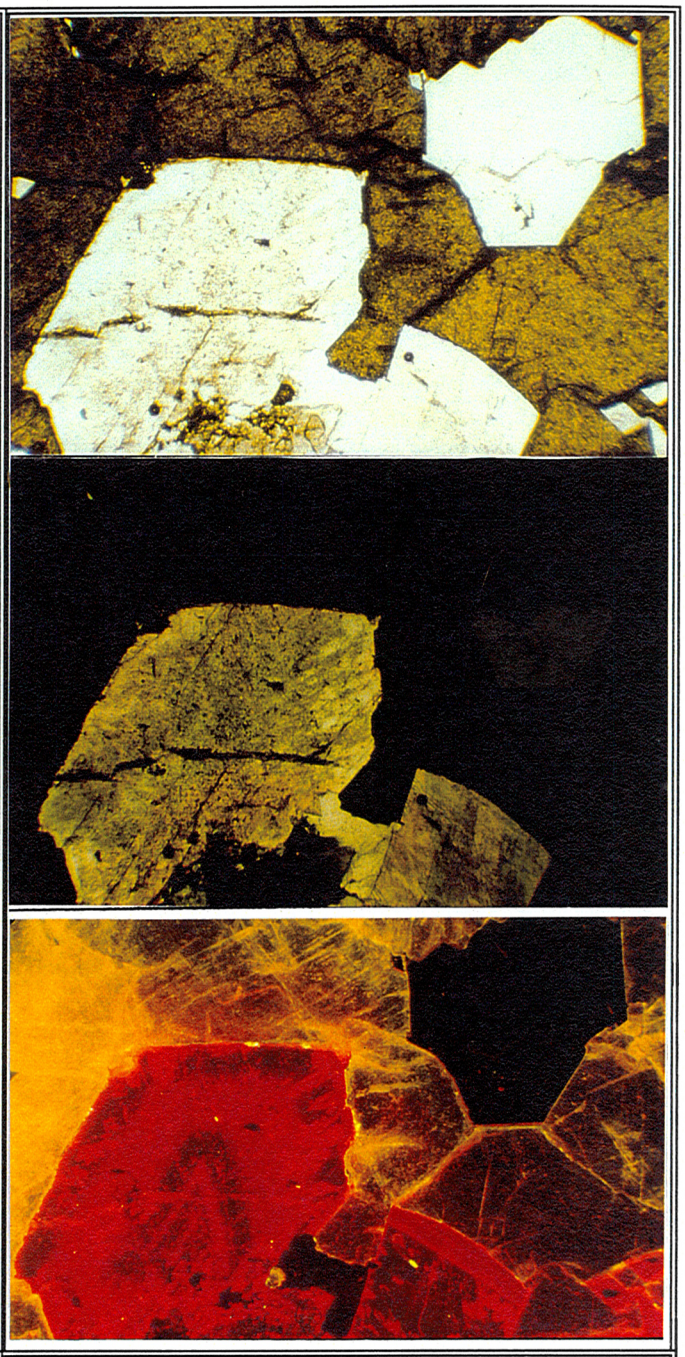

1 mm

Fig. 3-5. Gayna deposit, sample no. SP3409A. Sphalerite (luminescent, yellow) shown associated with saddle dolomite (centre, zoned, red and black) and quartz (top right, non-luminescent).

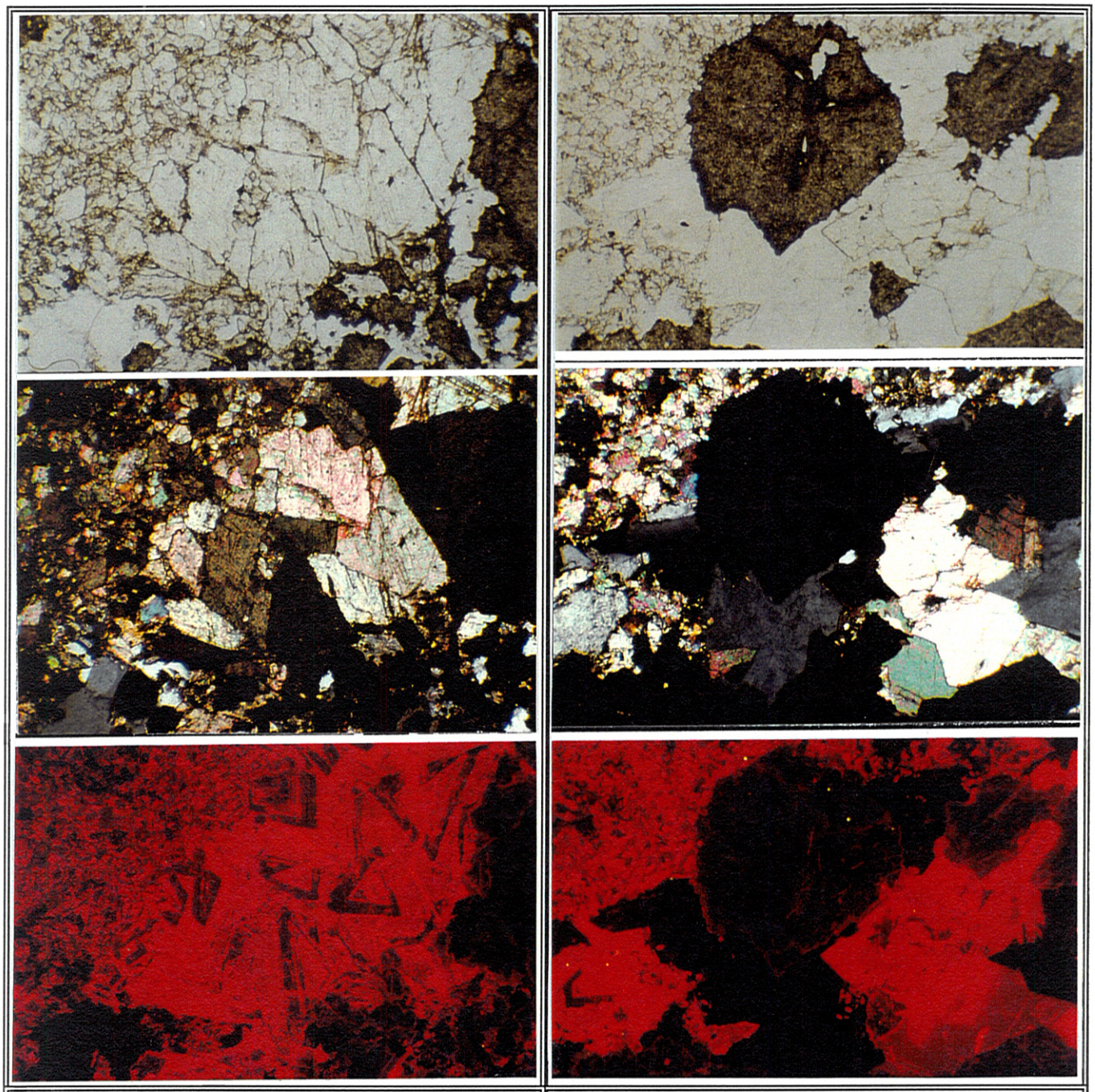

1 mm

Fig. 3-6. Cypress deposit, sample no. SP3264. Host dolomite (top left corner, mottled, dull red) followed by saddle dolomite (zoned red and black) associated with sphalerite (dull brownish-black).
Quartz (non-luminescent) occurs after host dolomite in the lower left corner.

1 mm

Fig. 3-6. Cypress deposit, sample no. SP3264. Host dolomite (top left corner, mottled, dull red) followed by saddle dolomite (zoned red and black) and/or sphalerite (dull brown). Quartz (non-luminescent) displays an interlocking contact with large sphalerite grain in the centre of the photomicrograph.

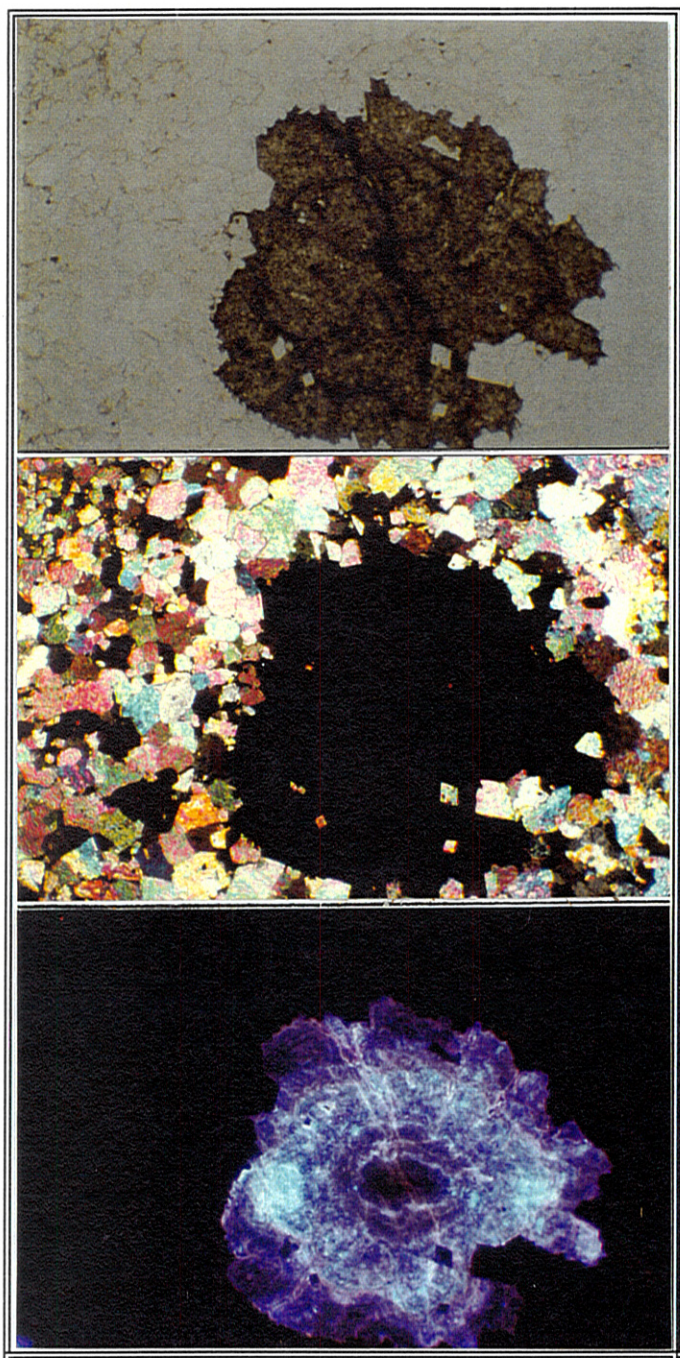

1 mm

Fig. 3-7. Cab deposit, sample no. SP3297. Sphalerite sphere (zoned, purple) replaces host dolomite (non-luminescent).

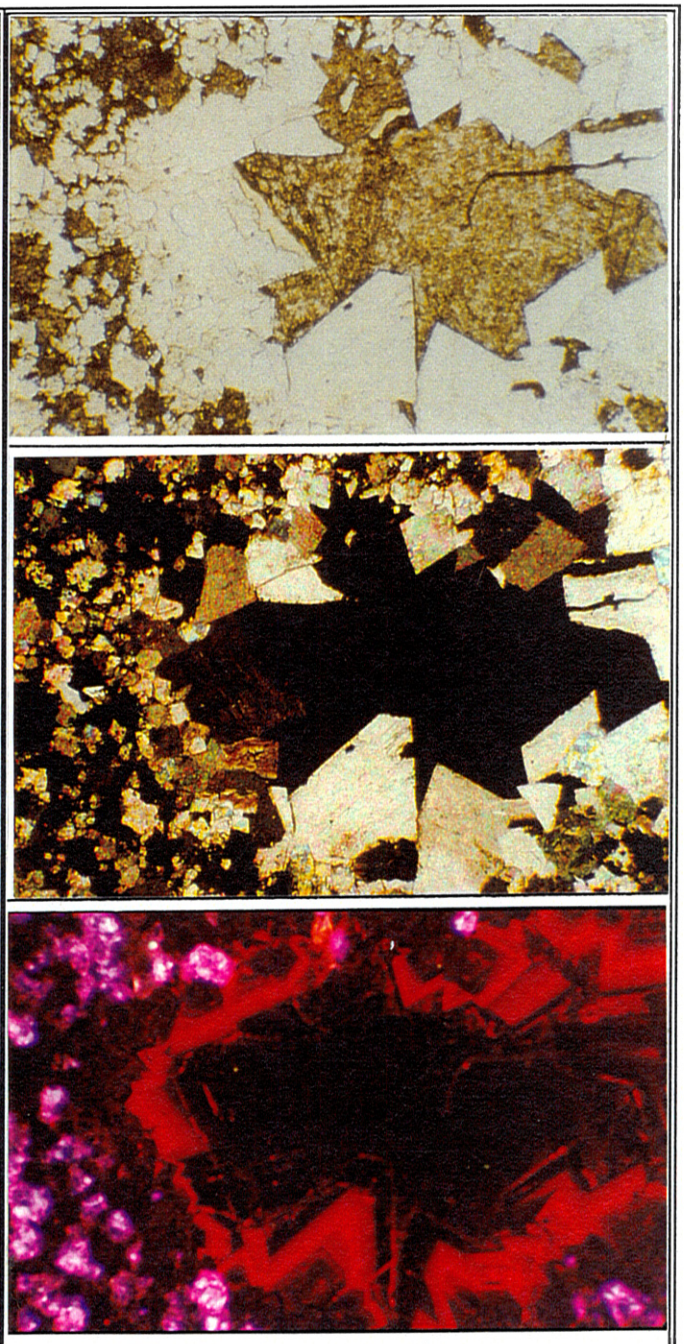

1 mm

Fig. 3-7. Cab deposit, sample no. SP3300. Sphalerite(2) (centre, non-luminesecent) fills cavity lined with dolomite cement (zoned, red and black) within host dolomite (non-luminescent) which contains disseminated sphalerite(1) (luminescent, purple).

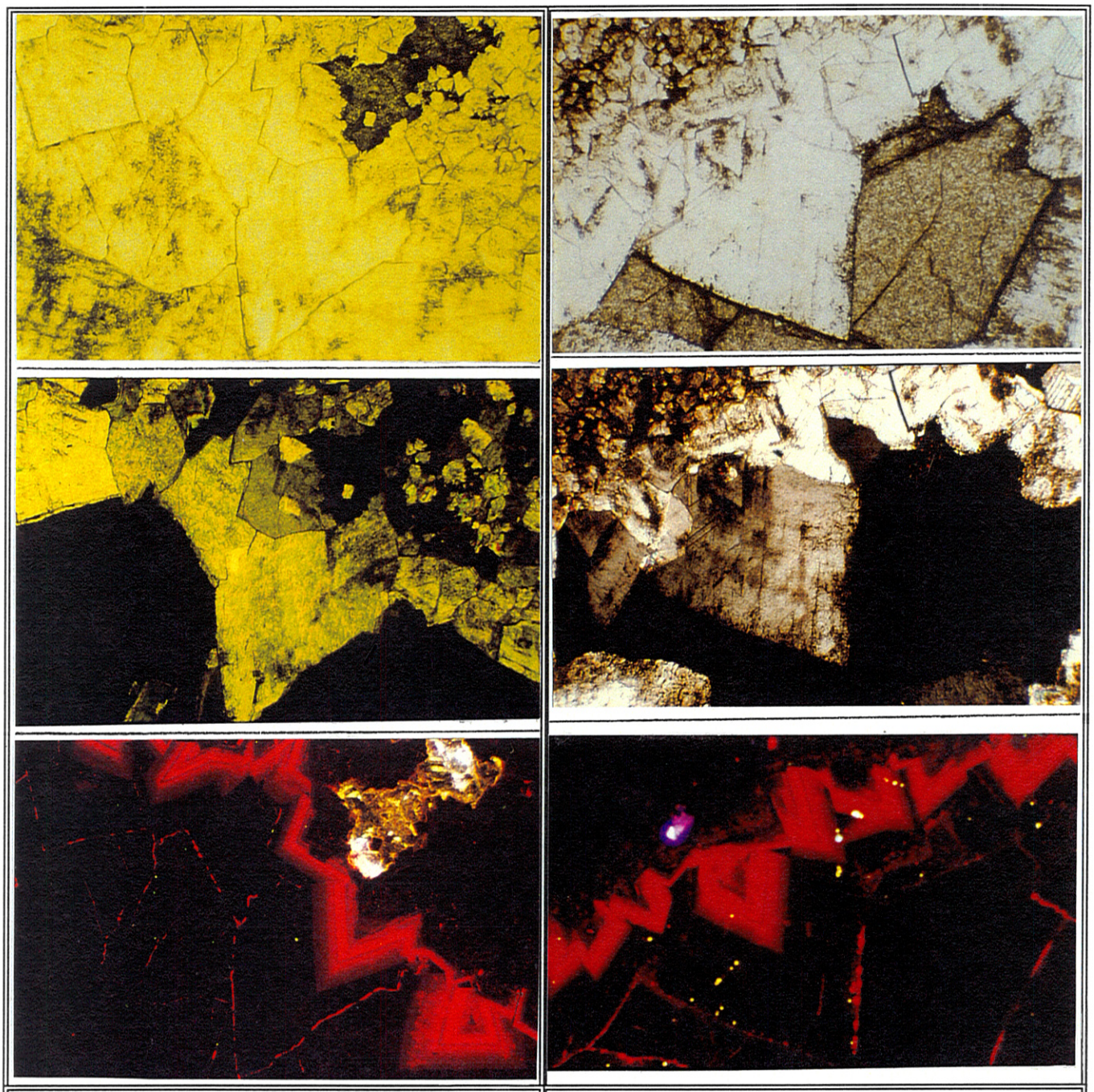

1 mm

Fig. 3-8. Cab deposit, sample no. SP5463. Host dolomite (top right corner, non-luminescent) with disseminated sphalerite(1) (luminescent, brown, yellow, purple) which contains remnant grains of the host dolomite. Saddle dolomite (centre, zoned, red and black) grows out from the host and is followed by quartz (non-luminesecent).

1 mm

Fig. 3-8. Cab deposit, sample no. SP3301. Host dolomite (top left corner, non-luminescent) contains one grain of sphalerite(1) (luminescent, purple) and disseminated pyrite (non-luminescent) followed by saddle dolomite (centre, zoned, red and black) and coarse-grained open space sphalerite(2) (non-luminescent).

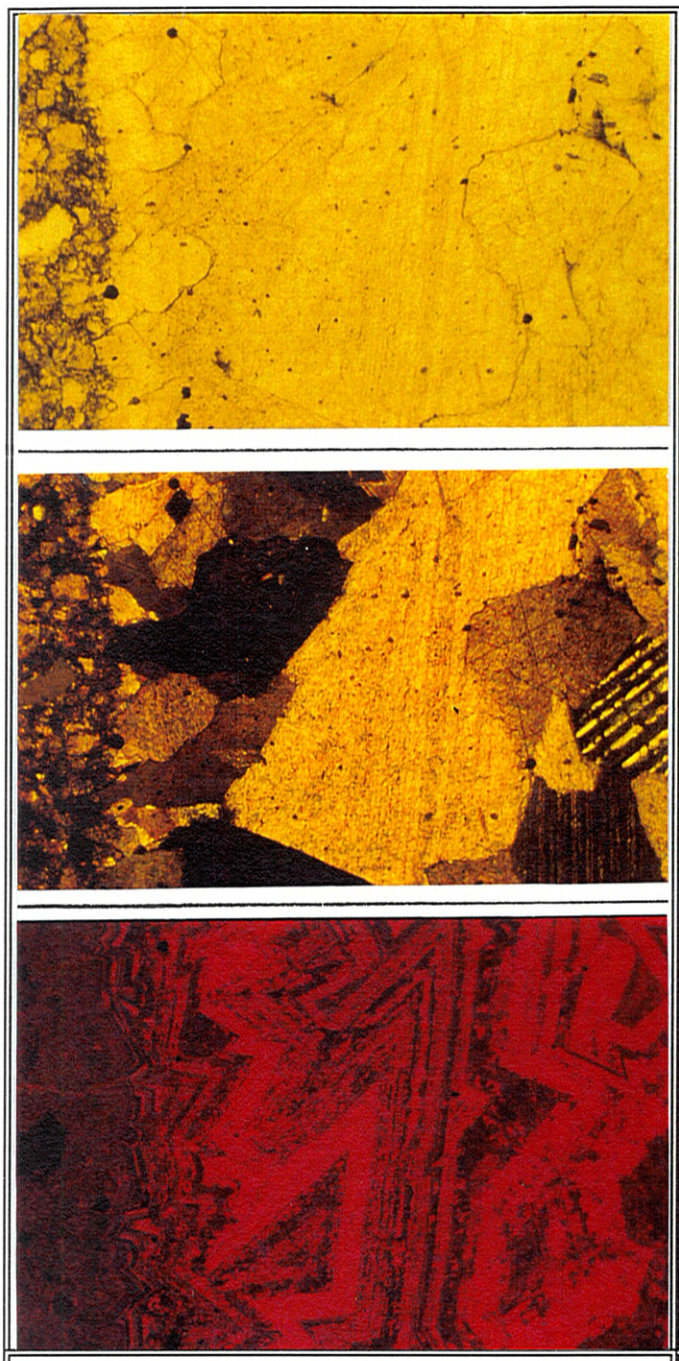

1 mm

Fig. 3-9. Bob deposit, sample no. SP5394. Finer-grained dolomite cement (zoned, red and black) grows out from host dolomite (extreme left, dull red).

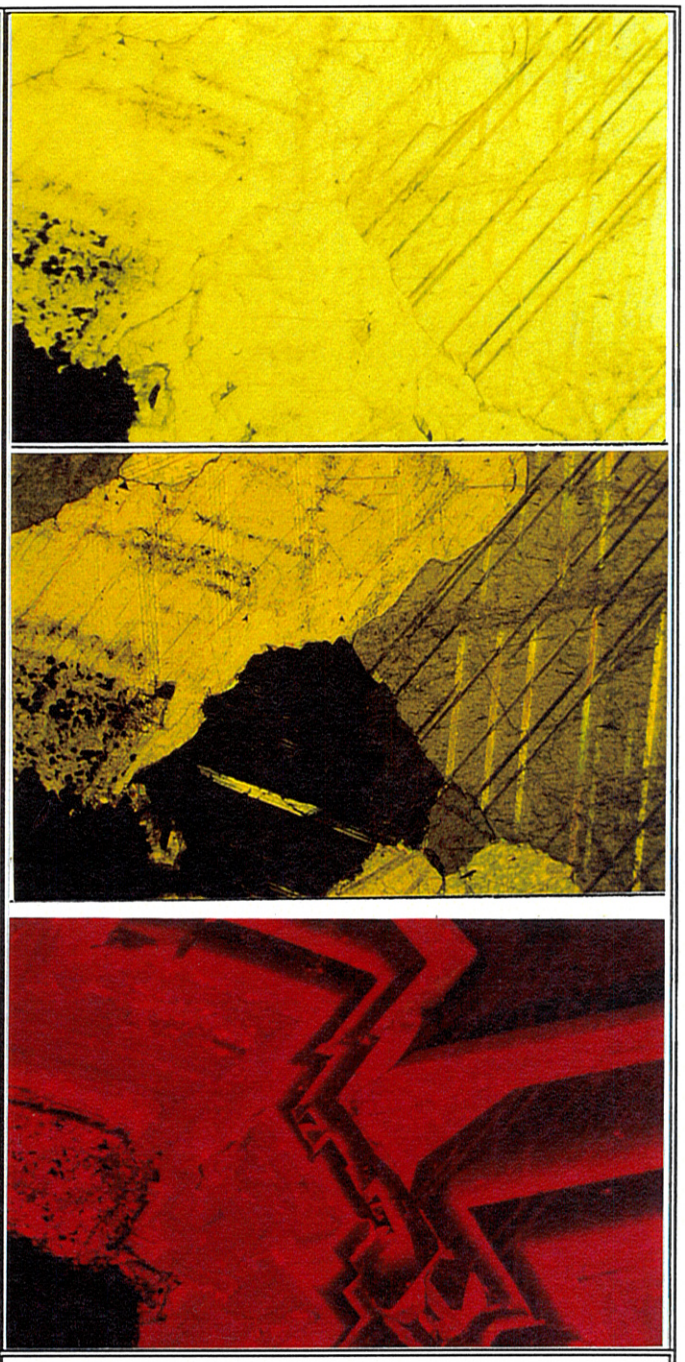

1 mm

Fig. 3-9. Bob deposit, sample no. SP5396. Coarse-grained pyrite (bottom left, non-luminescent) and very coarse-grained saddle dolomite fill cavities. Grain size of dolomite cement tends to increase towards the centre of the cavities. Note twinning in dolomite.

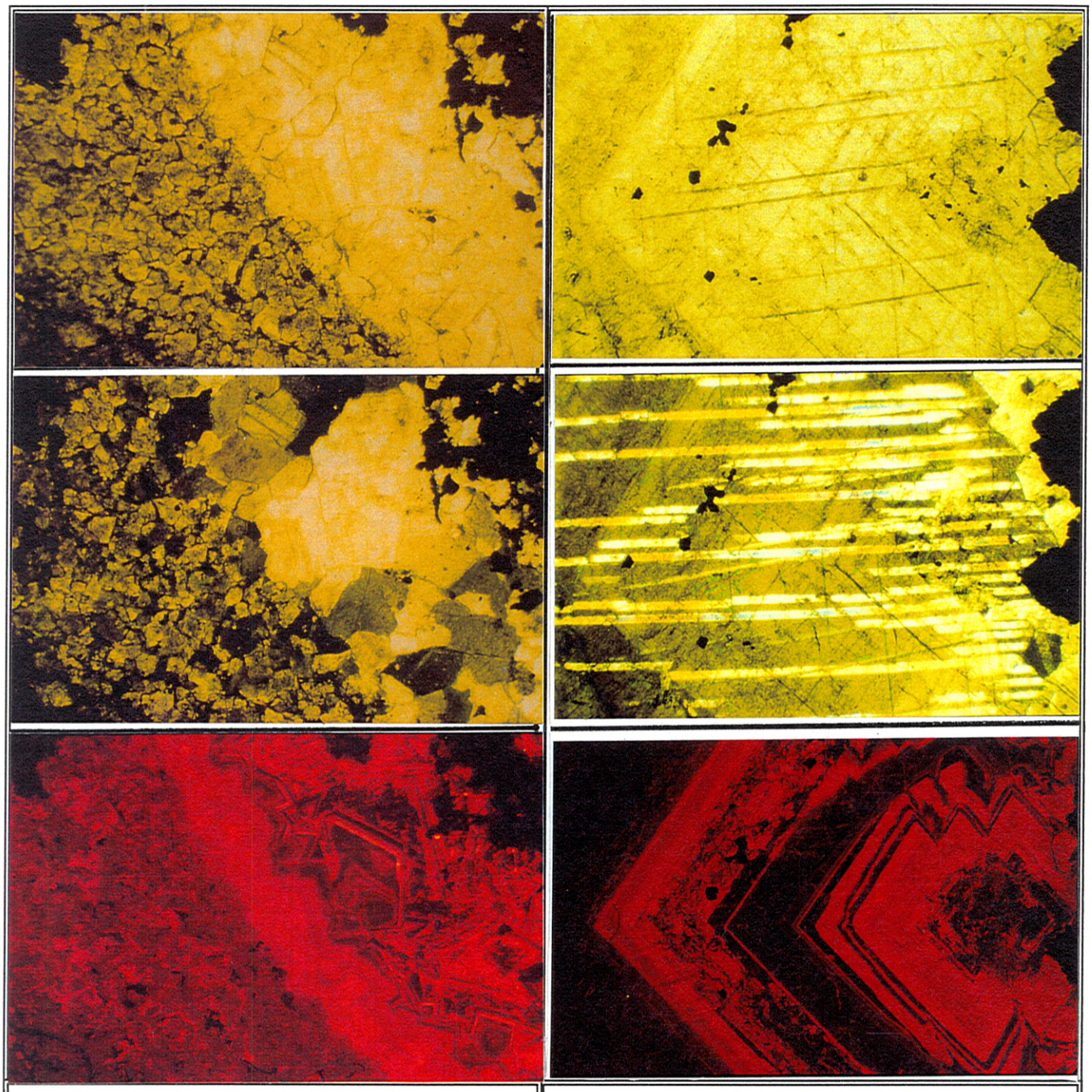

1 mm

Fig. 3-10. Bob deposit, sample no. SP5395. Host dolomite (left, mottled, dull red) followed by finer-grained dolomite cement (zoned, red and black) with pyrite (top right, non-luminescent).

1 mm

Fig. 3-10. Bob deposit, sample no. SP5395. Saddle dolomite filling centre of cavity, growing out from a layer of pyrite (extreme right, non-luminescent). Twinning in dolomite is particularly obvious under crossed polarized light (e). Pyrite is also concentrated in the "mottled" band nearer the rim of the grain. GSC photo A-9450088.

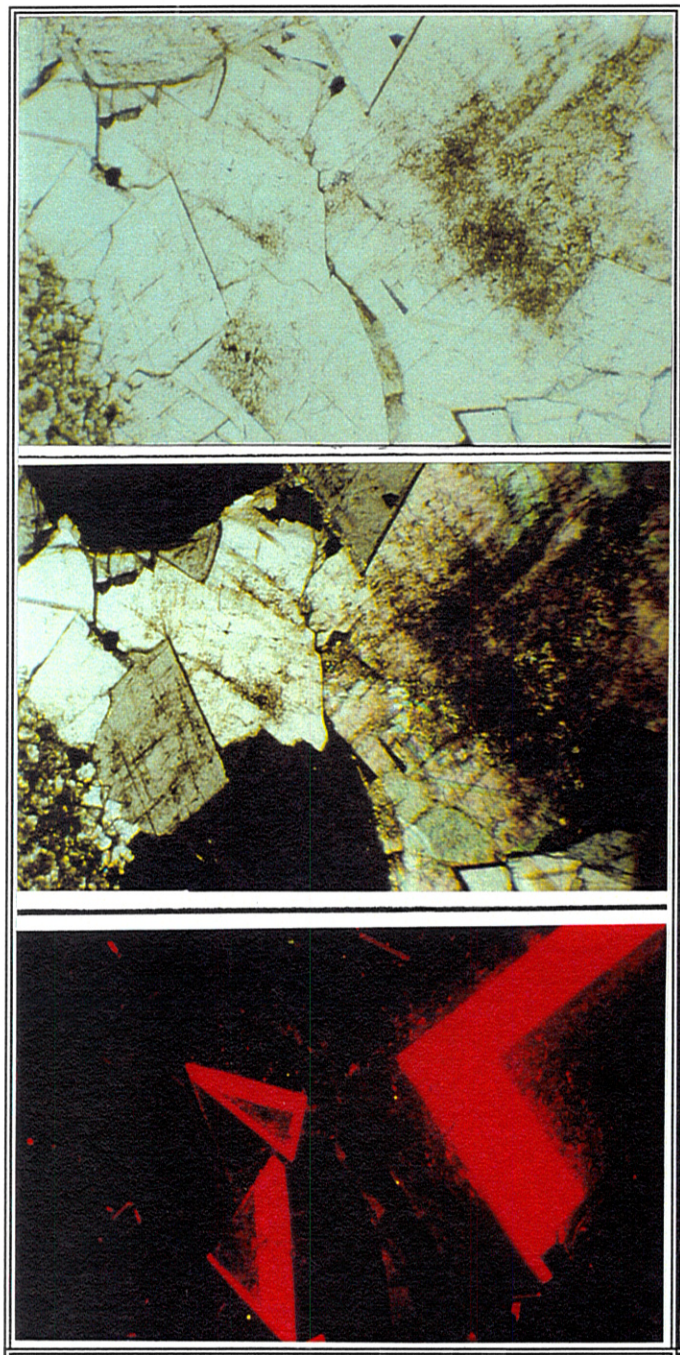

1 mm

Fig. 3-11. Palm deposit, sample no. Palm Claims (1). Host dolomite (bottom left corner, non-luminescent) followed by coarse-grained saddle dolomite (zoned, red and black). Note cloudy cores and clear rims.

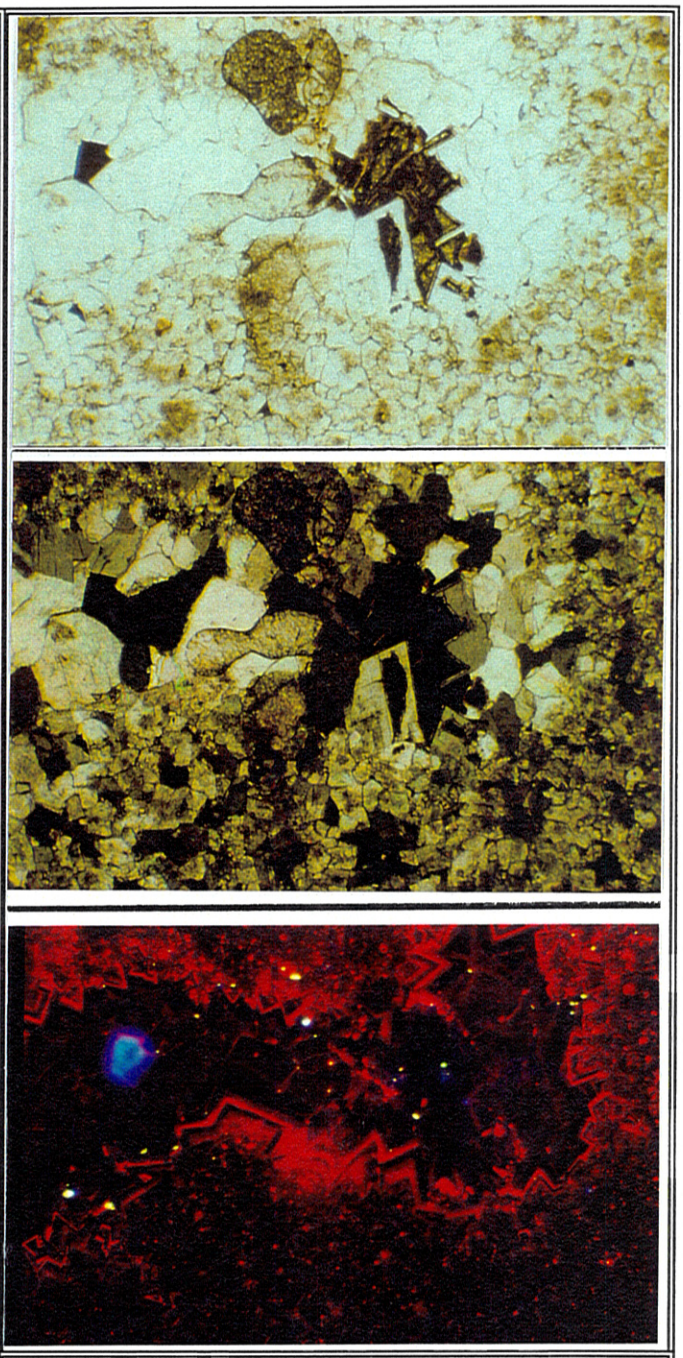

1 mm

Fig. 3-11. Palm deposit, sample no. Palm Claims (2). A void, in host dolomite containing sparse disseminated pyrite (dull to non-luminescent), is filled with finer-grained dolomite cement, followed by sphalerite (non-luminescent) and hydrozincite (left centre of cavity, blue).

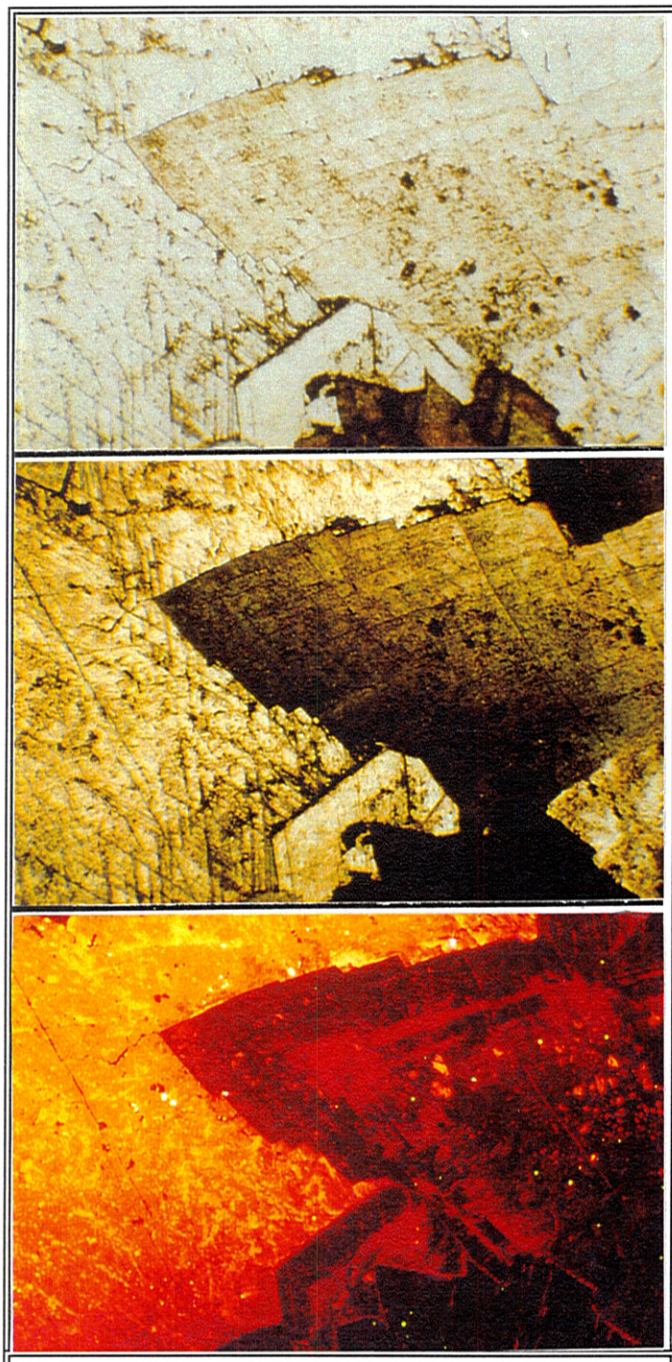

1 mm

Fig. 3-12. Econ deposit, sample no. 8002A. Classic saddle dolomite, associated with sphalerite (bottom right, non-luminescent), shows typical shape, undulatory extinction, and compositional zoning (red and black). Calcite (left, luminescent orange) fills remaining space.

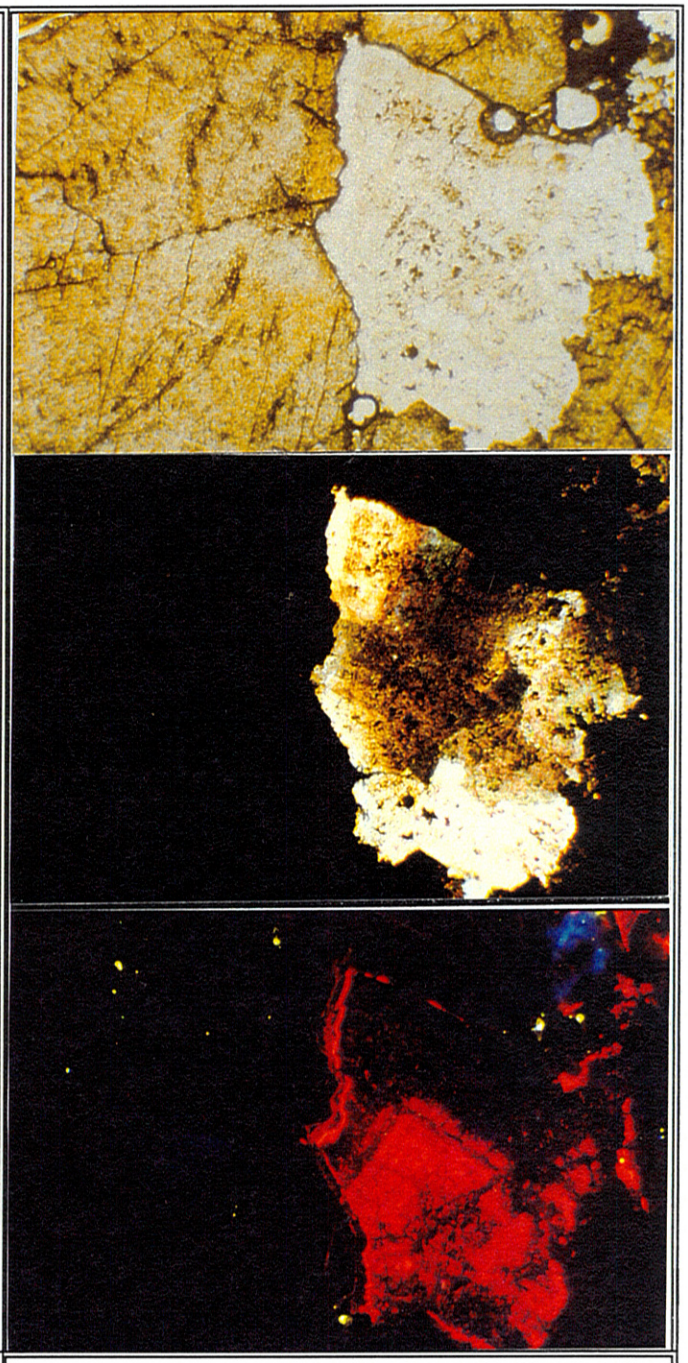

1 mm

Fig. 3-12. Econ deposit, sample no. SE- Veins. Sphalerite (non-luminescent) has invaded the fringes of saddle dolomite (right centre), which shows typical shape, undulatory extinction, and compositional zoning (red and black).

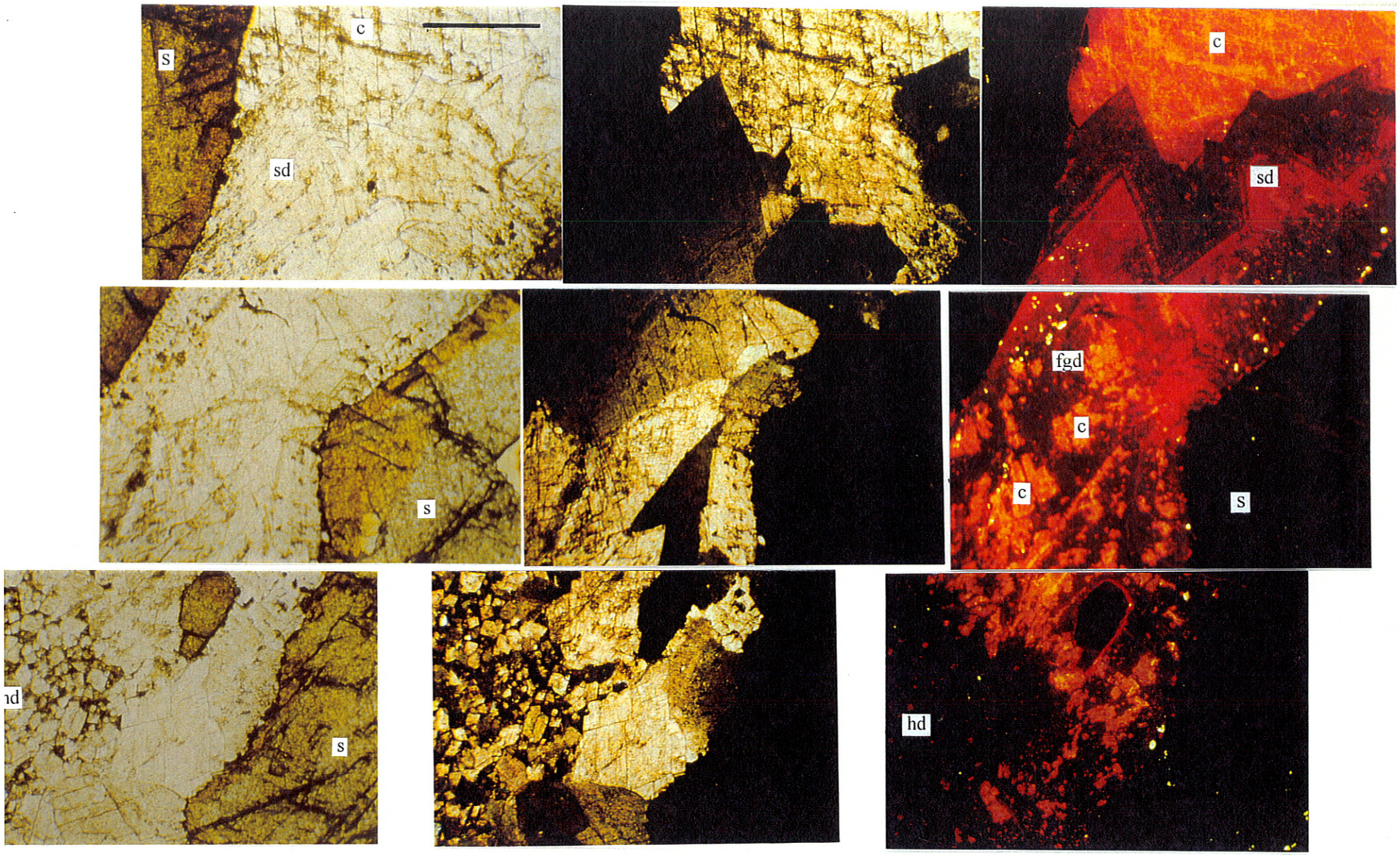

Fig. 3-13. Econ deposit, sample no. Econ-1. Three sets of photomicrographs joined top to bottom show host dolomite (hd, non-luminescent to dull red) followed by dolomite cement (fgd), mixed with calcite (c, mottled, red, black, orange) associated with sphalerite (s, non-luminescent). Saddle dolomite (sd, zoned, red and black) followed by calcite (luminescent, orange) fills remaining void. Scale bar is 0.5 mm.

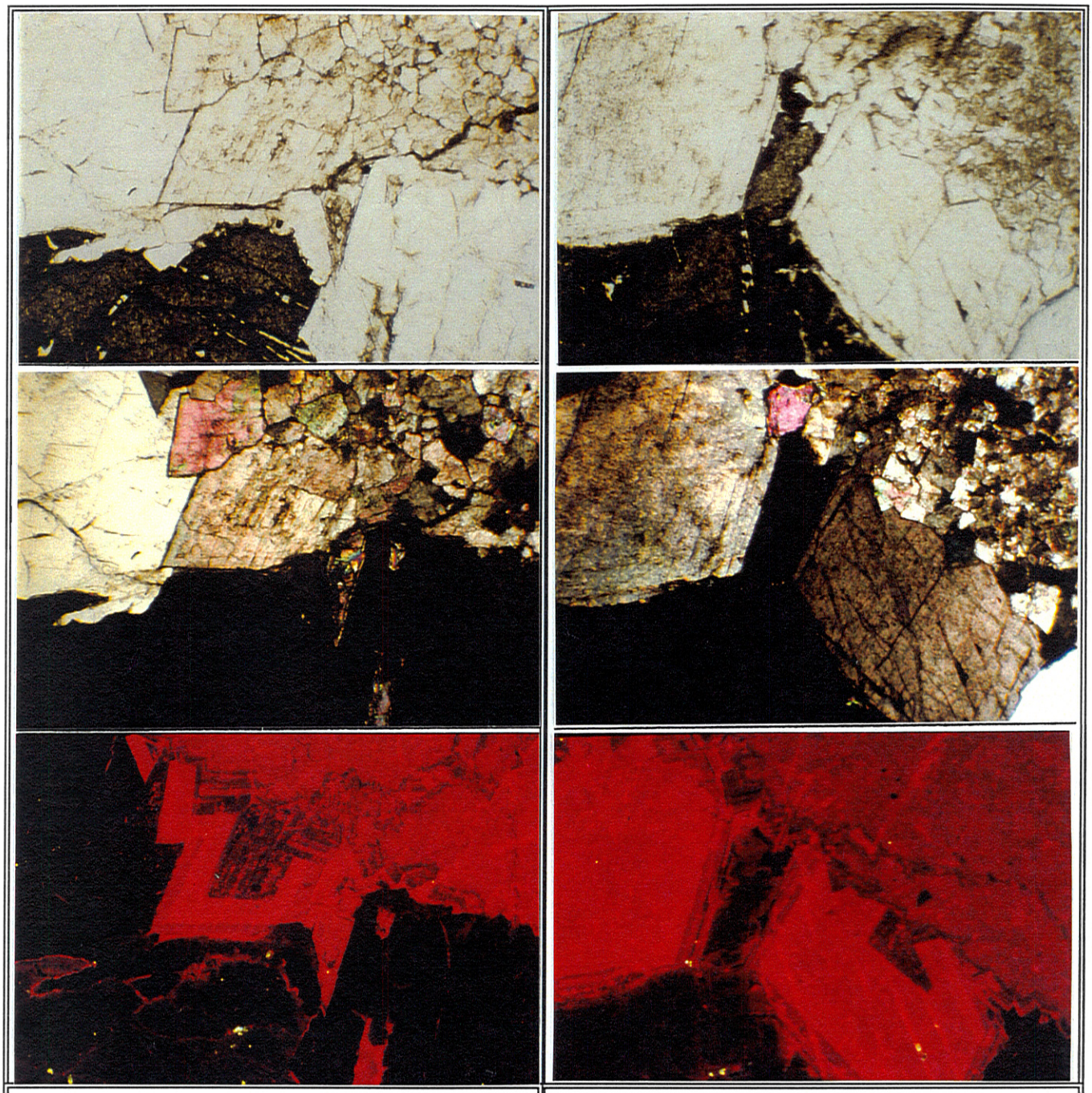

1 mm

Fig. 3-14. Tic deposit, sample no. SP4213. Host dolomite (top right, dull red) followed by saddle dolomite (zoned, red and black), quartz (non-luminescent), and sphalerite (bottom left, dull brown).

1 mm

Fig. 3-14. Tic deposit, sample no. SP4213. Host dolomite (top right, dull red) followed by saddle dolomite (zoned, red and black) and/or sphalerite (dull brown). Quartz (non-luminescent) is visible in the bottom right corner.

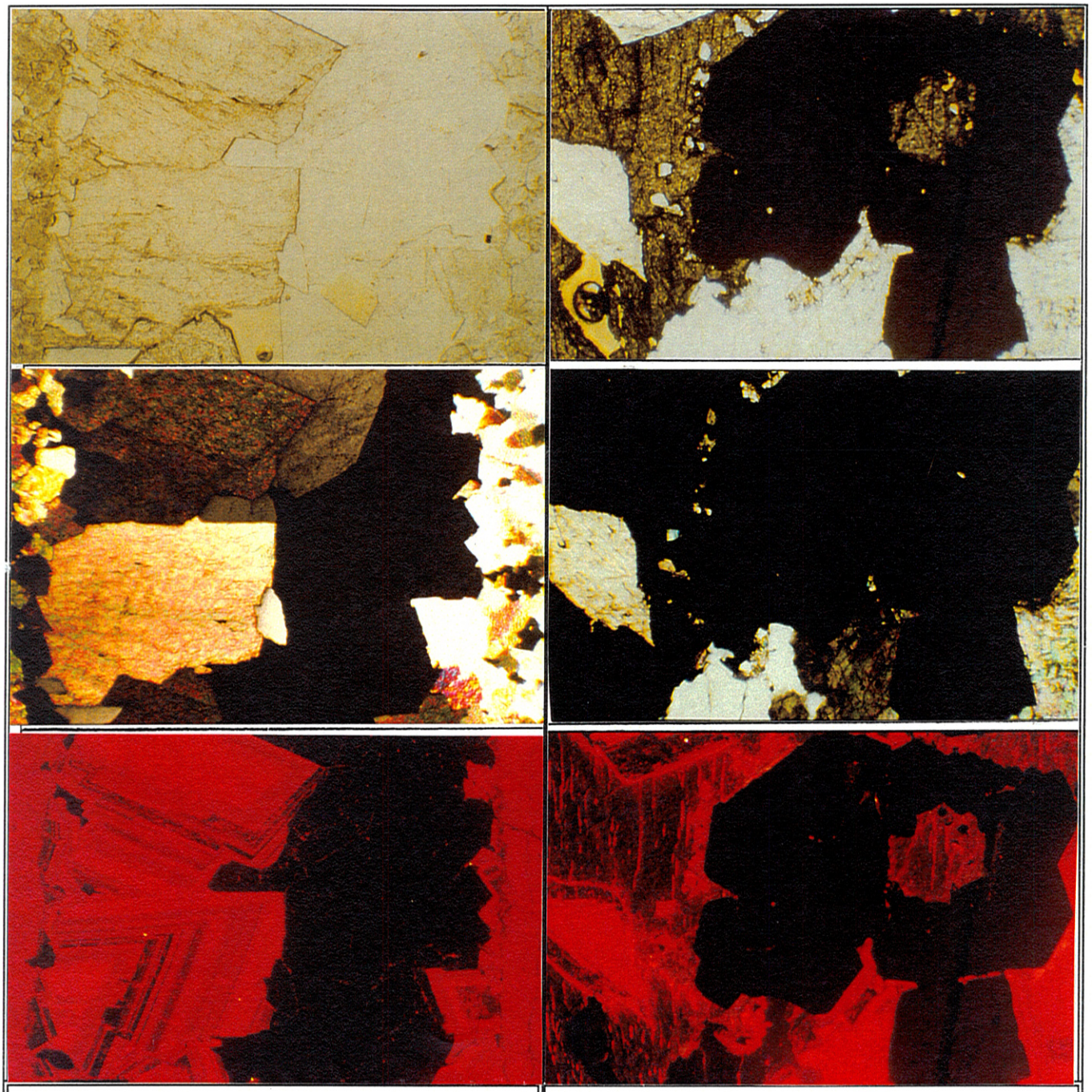

1 mm

Fig. 3-15. Tic deposit, sample no. SP4215. Host dolomite (extreme left and right, mottled, dull red) contains a cavity lined with saddle dolomite (zoned, red and black) and the remaining void filled with quartz (non-luminescent).

1 mm

Fig. 3-15. Tic deposit, sample no. SP4216. Saddle dolomite (zoned, red and black) associated with sphalerite (left: top and bottom and in centre of galena, dull brown) and galena (non-luminescent).

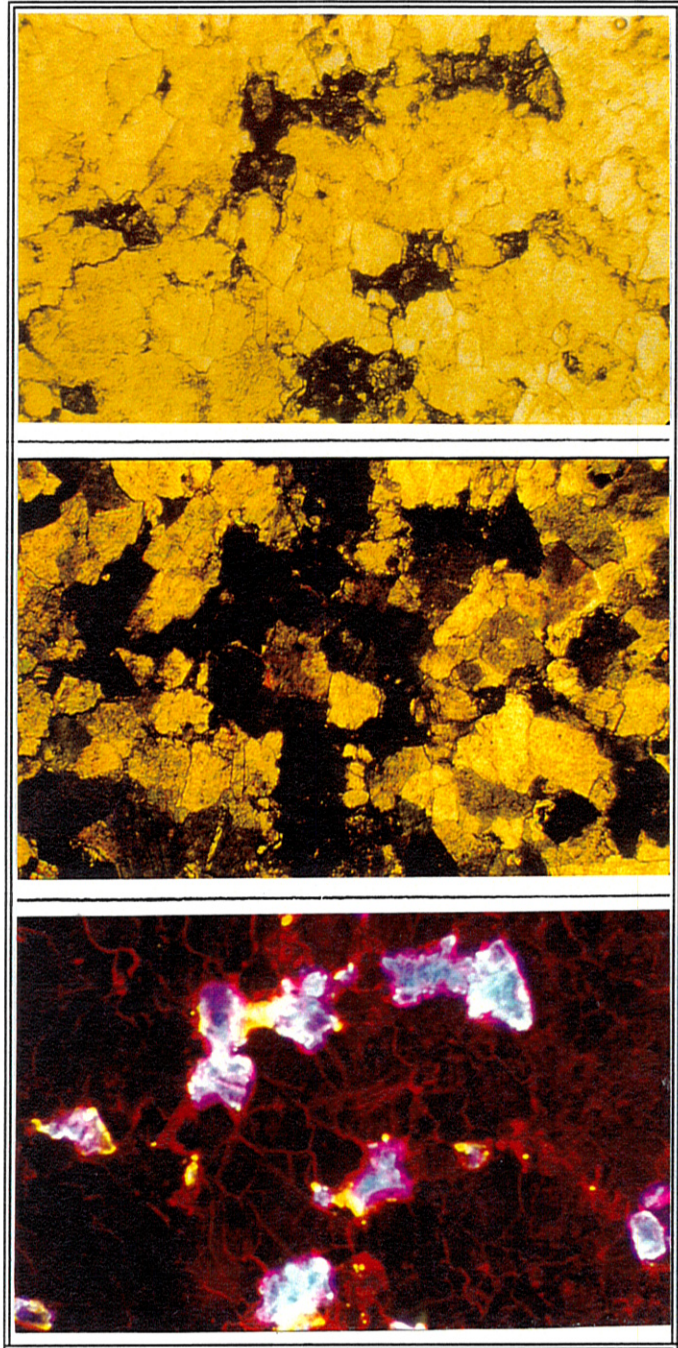

1 mm

Fig. 3-16. Ice deposit, sample no. KQ-73-285. Sphalerite (luminescent, purple, yellow) disseminated in host dolomite (dull red).

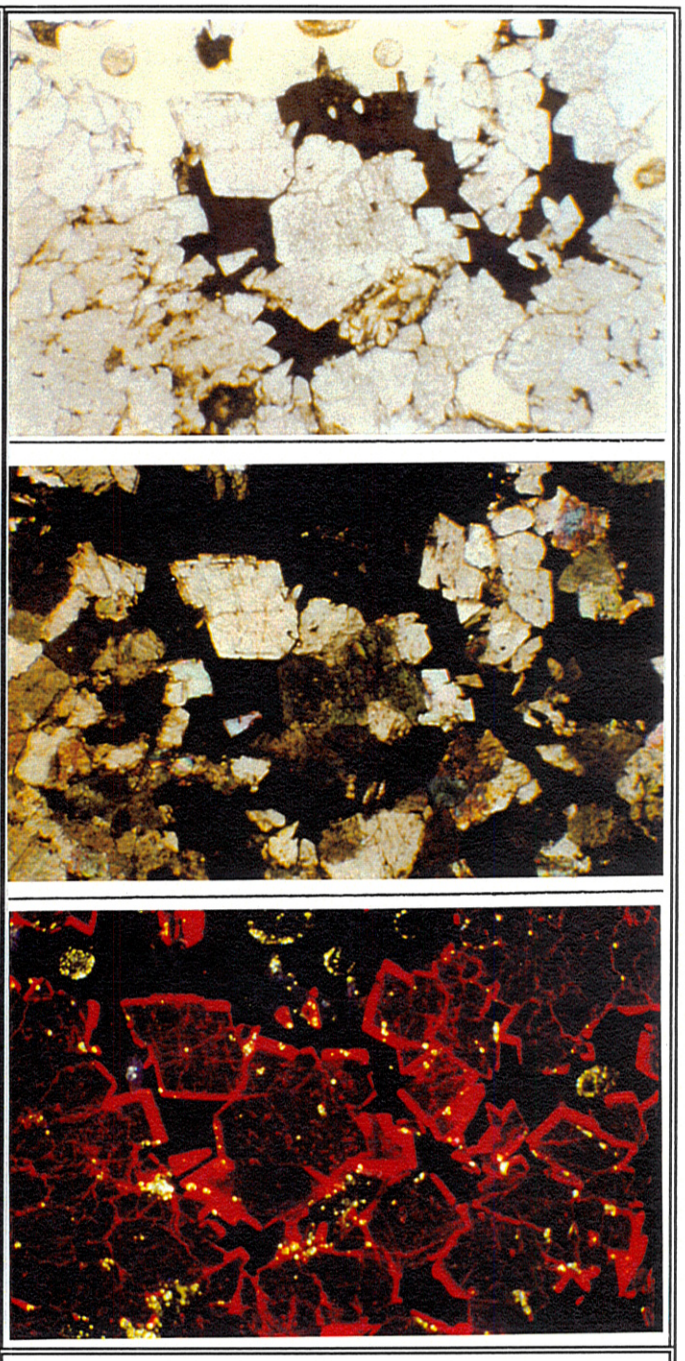

1 mm

Fig. 3-16. Ice deposit, sample no. SP4242. Galena (non-luminescent) fills cavities within replacive saddle dolomite (zoned, red and black, with dark cores and bright rims).

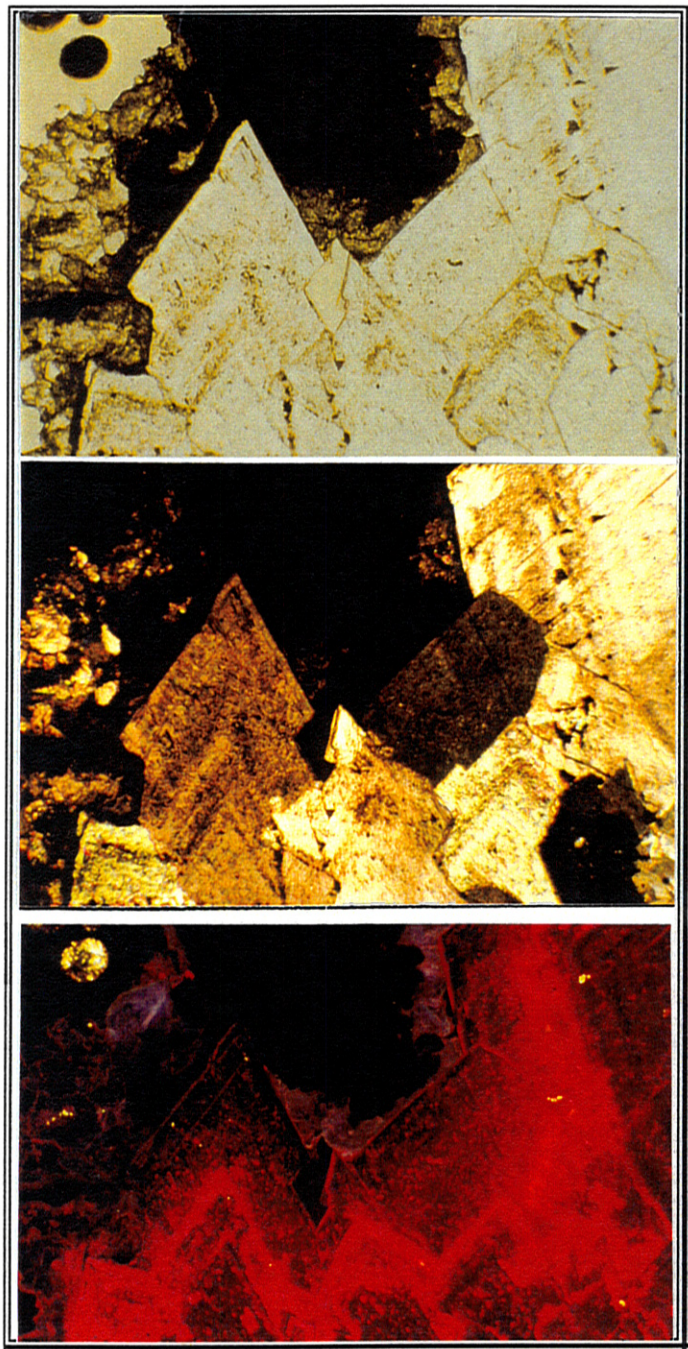

Fig. 3-17. Arn deposit, sample no. SP4237. Classic spearhead-shaped saddle dolomite (zoned, red and black) grew into cavity surrounded by host dolomite (bottom, just outside field of view). Sphalerite (purplish-pink) followed by galena (top centre, non-luminescent) filled remainder of void.

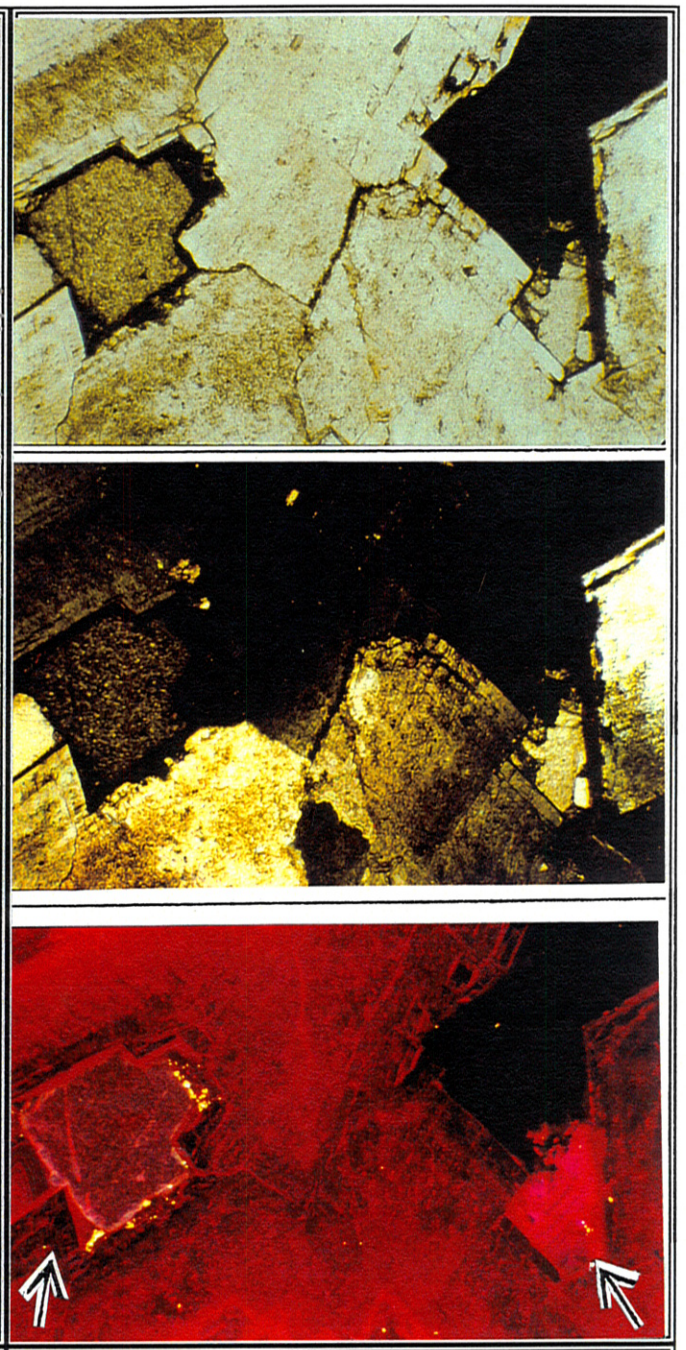

Fig. 3-17. Arn deposit, sample no. SP4237. Sphalerite (left centre, purplish-pink), associated with saddle dolomite grew into a cavity surrounded by host dolomite. Galena (right top corner, non-luminescent) partially fills remainder of cavity, while smithsonite (zoned, pink) fills last remaining voids (see arrows).

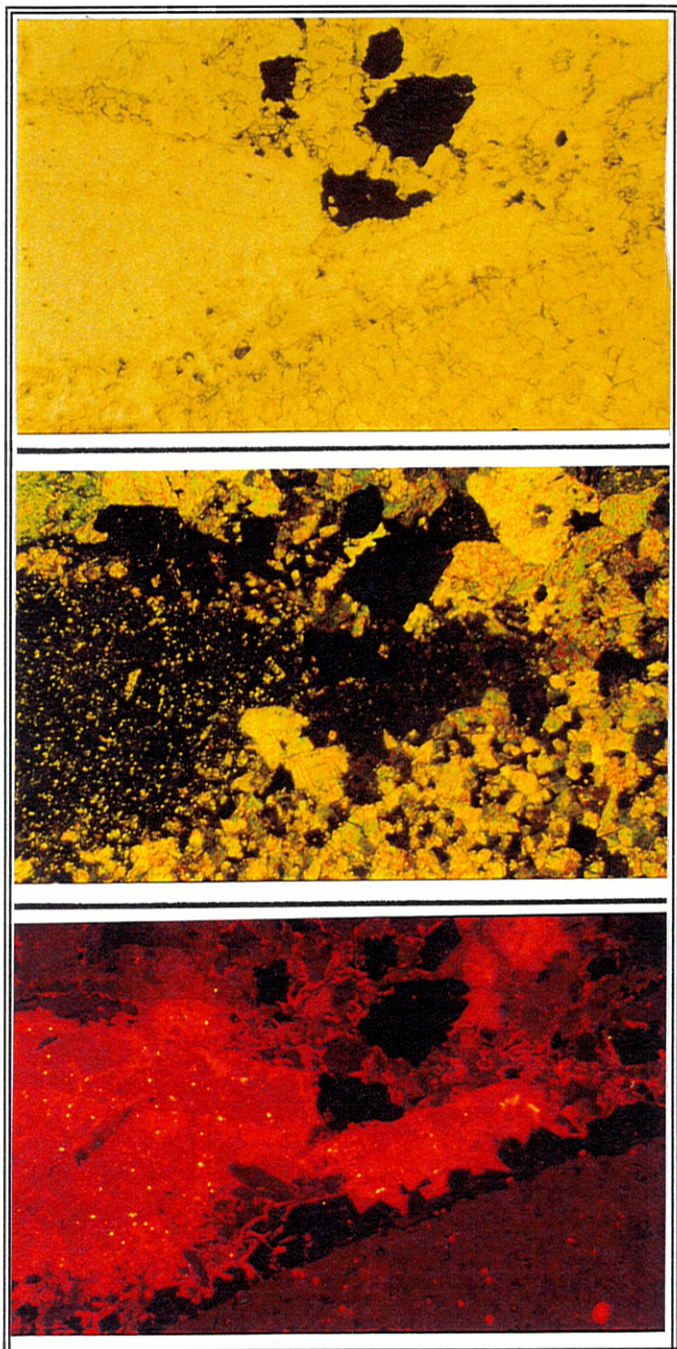

1 mm

Fig. 3-18. Arn deposit, sample no. SP5431. Dolomite cement (zoned, black with thin red rim) grows directly on host dolomite fragment (bottom right corner, dull red). Pyrite (non-luminescent) and calcite (luminescent, orange) fill remaining void.

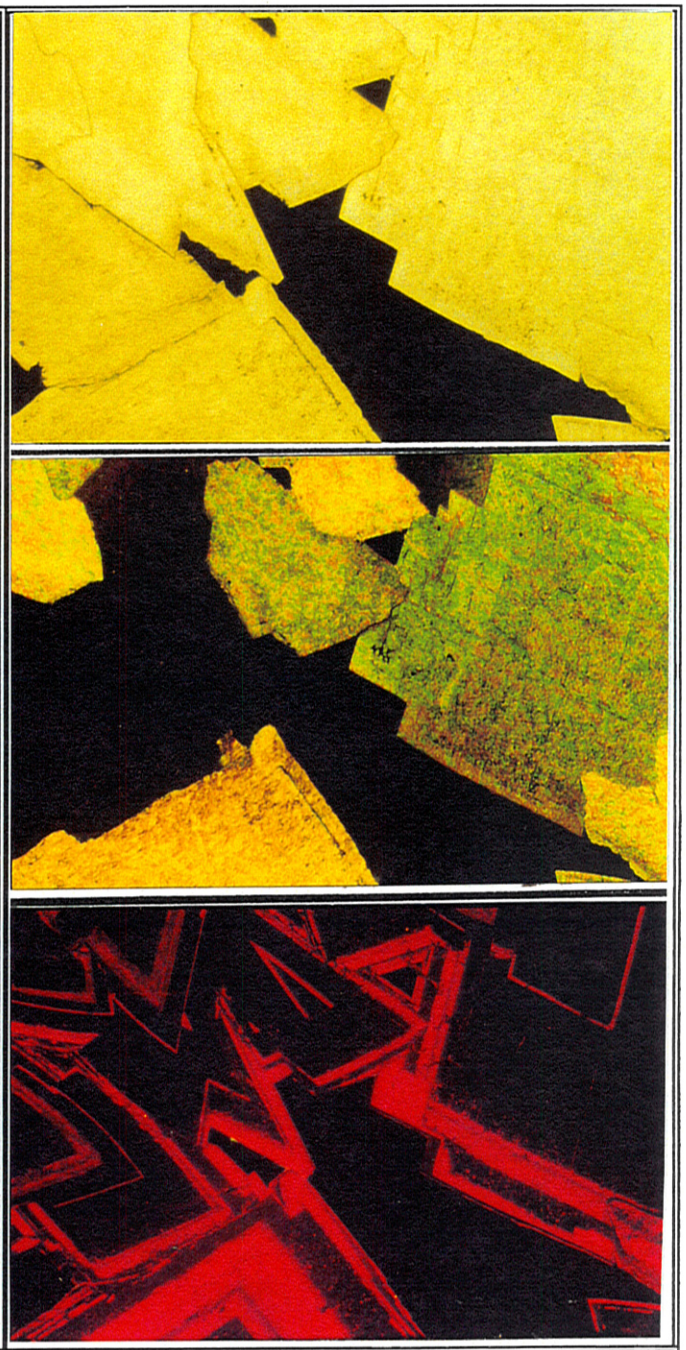

1 mm

Fig. 3-18. Arn deposit, sample no. SP5430. Coarse-grained saddle dolomite (zoned, red and black) grows into cavities within host dolomite (out of view). Grains are coarser closer to the centre of the cavities and galena (non-luminescent) fills last remaining voids.

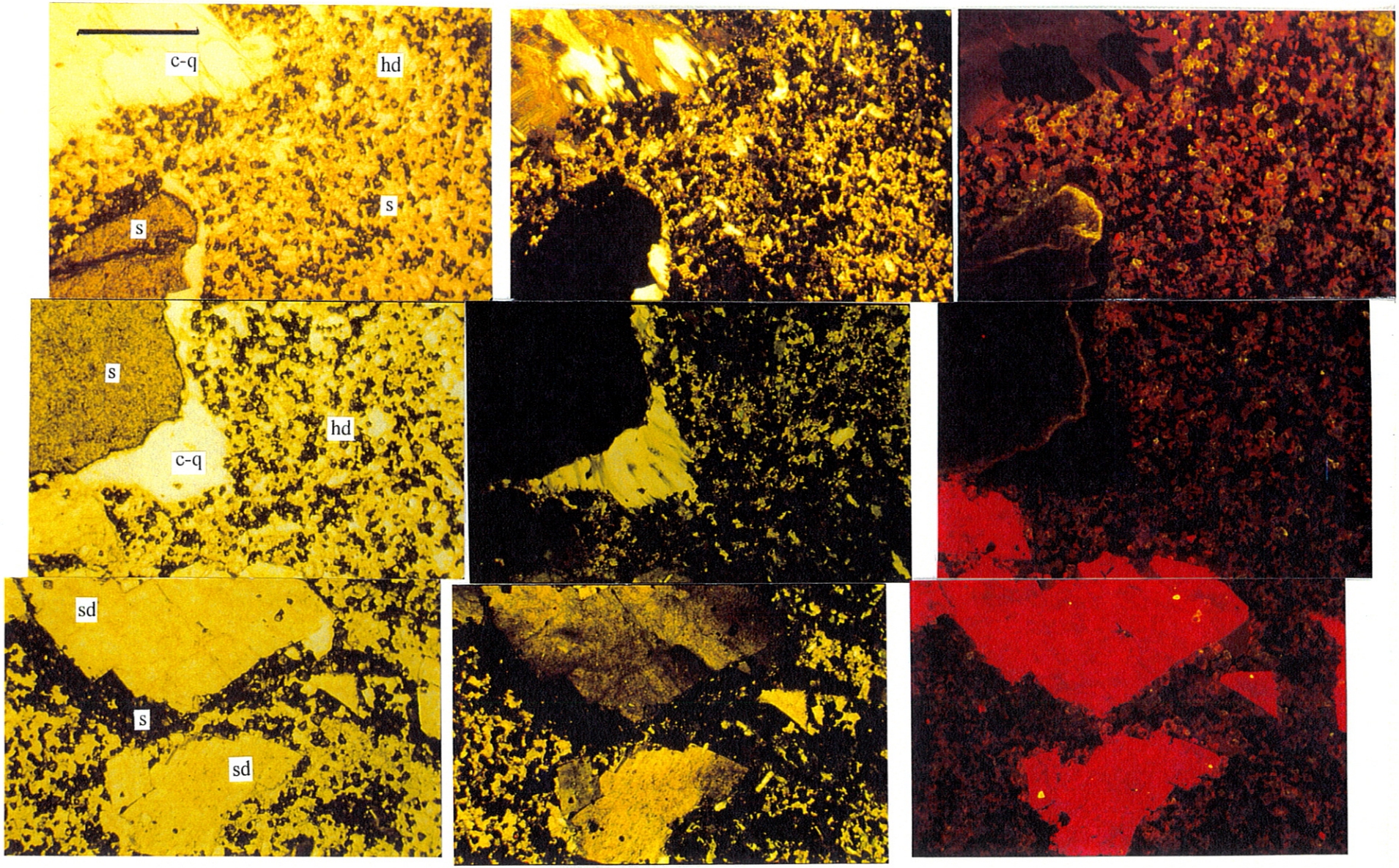

Fig. 3-19. Joli Green deposit, sample no. SP5413. Three sets of photomicrographs joined top to bottom show host dolomite (hd, dull red) peppered with disseminated sphalerite (s, luminescent dull brown, yellow) followed by calcite-quartz mélange (c-q, non-luminescent) showing pressure solution effects, followed by coarse-grained sphalerite (s, luminescent, dull brown with thin yellow rim). Replacive saddle dolomite (sd, luminescent red) forms rhombs within the host dolomite (hd). Sphalerite grains occur within the dolomite rhombs and are concentrated along the rhomb margins. Scale bar is 0.5 mm.

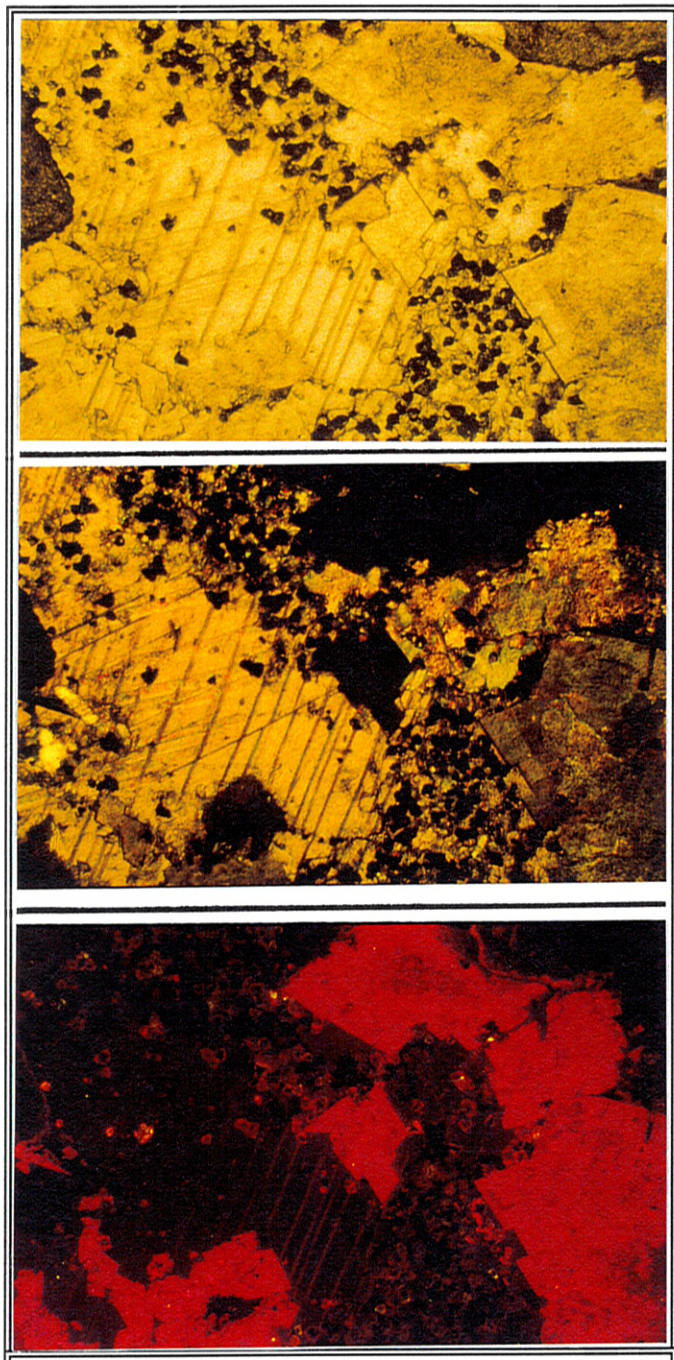

1 mm

Fig. 3-20. Joli Green deposit, sample no. SP5413. Host dolomite (dull red), peppered with disseminated sphalerite (luminescent dull brown, yellow), contains cavity filled with twinned calcite (luminescent, dull brown). Replacive saddle dolomite (mottled, red, black) and coarse-grained sphalerite (top right and extreme left centre, non-luminescent except for thin rim) are associated with host dolomite.

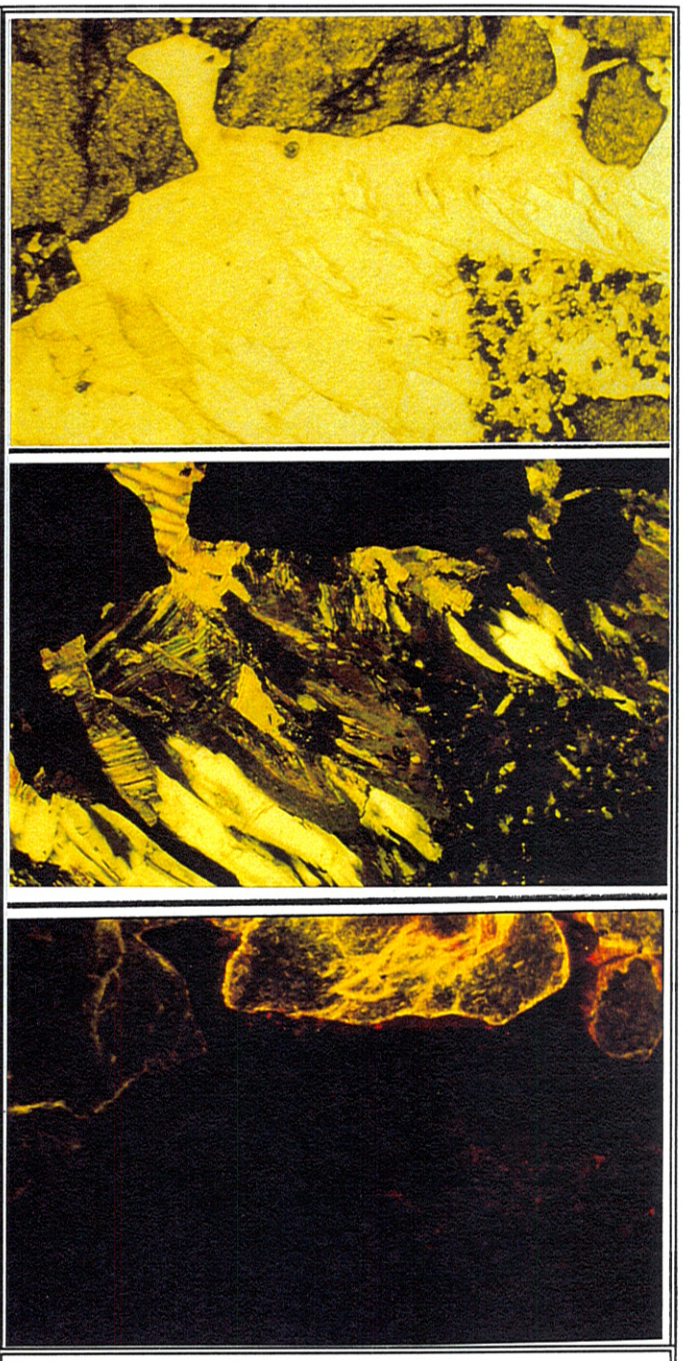

1 mm

Fig. 3-20. Joli Green deposit, sample no. SP5413. Host dolomite (bottom right, dull red), peppered with disseminated sphalerite (luminescent dull brown, yellow), is followed by calcite-quartz mélange (non-luminescent) showing pressure solution effects, followed by coarse-grained sphalerite (top, luminescent, dull brown and yellow).

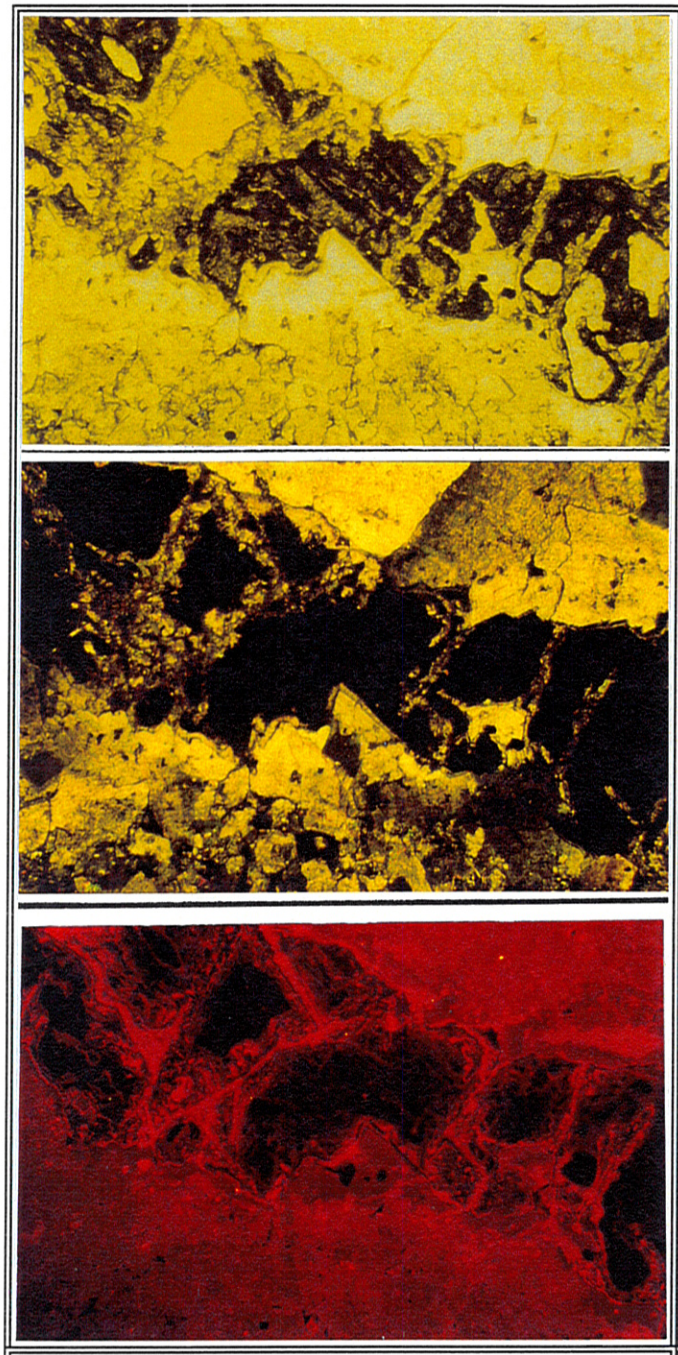

1 mm

Fig. 3-21. Mawer deposit, sample no. SP5403. Sphalerite (centre, non-luminescent) occurs adjacent to host dolomite (bottom, mottled, red) and is associated with finer-grained dolomite cement (top right, red) filling open space.

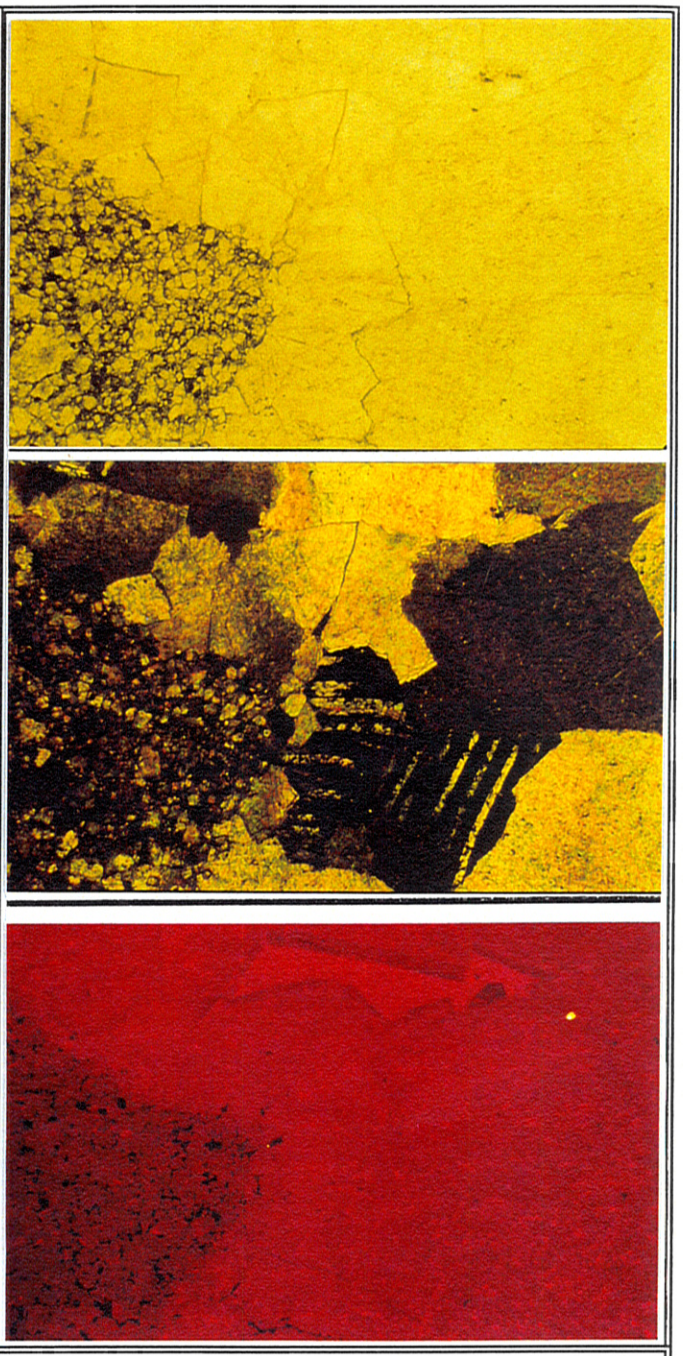

1 mm

Fig. 3-21. Mawer deposit, sample no. SP5403. Host dolomite (left, mottled, dull red), containing fine-grained disseminated pyrite, followed by coarse-grained saddle dolomite (red). Note twinning in dolomite is visible under crossed polarized light (e).

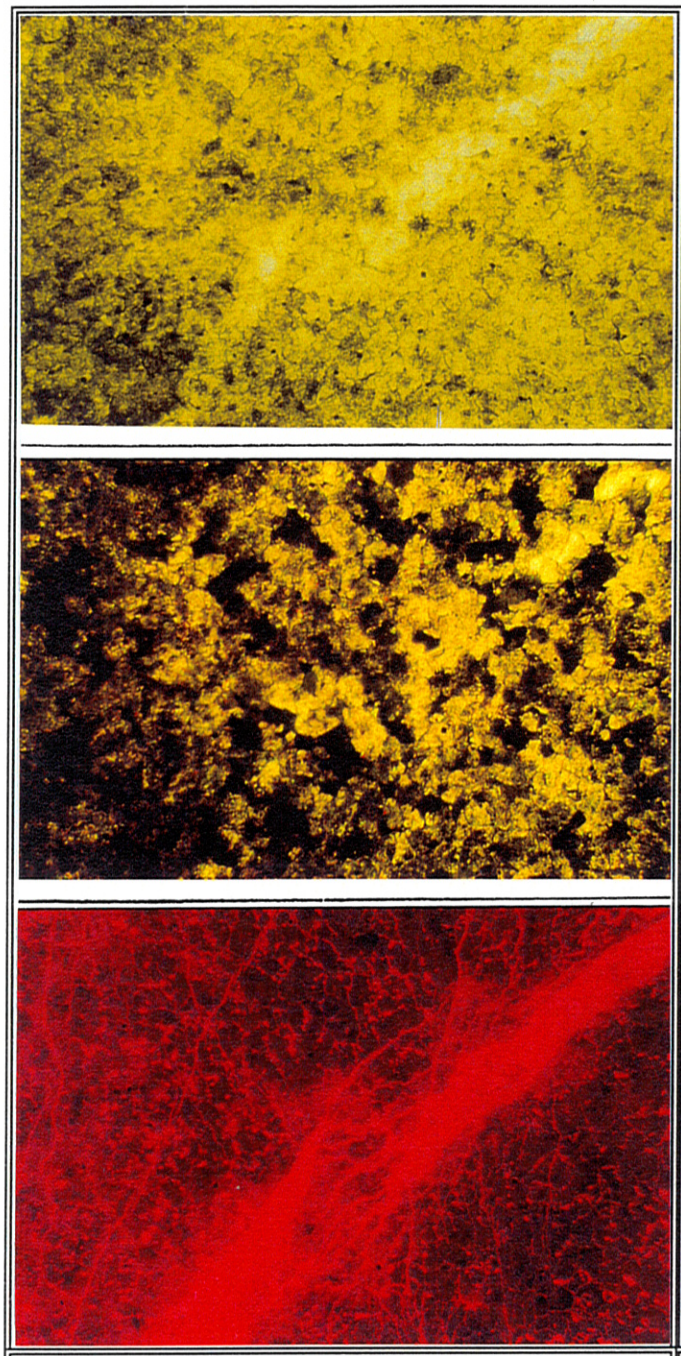

1 mm

Fig. 3-22. Bear deposit, sample no. SP5487. Host dolomite (mottled, red and black), containing fine-grained disseminated pyrite, cut by dolomite vein cement (centre, bright red).

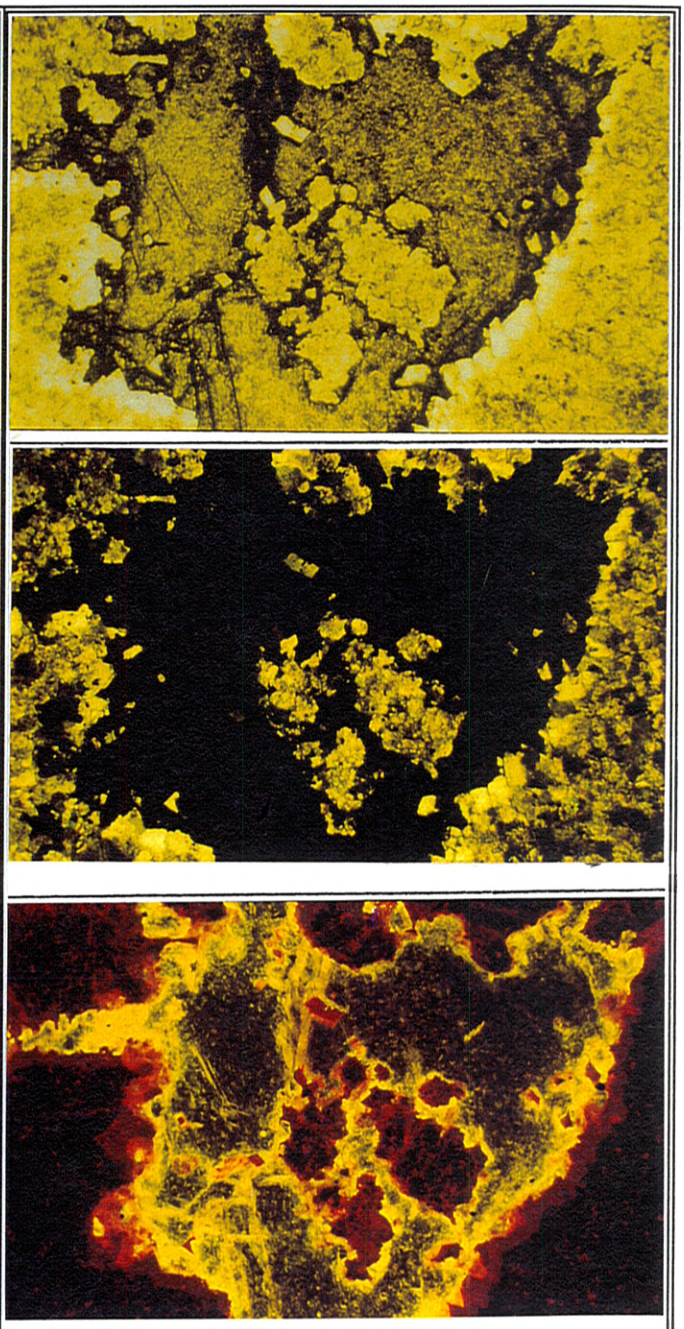

1 mm

Fig. 3-22. Bear deposit, sample no. SP5487. Host dolomite (dull red) contains sphalerite (centre, luminescent, dark cores, yellow rims) associated with dolomite cement (thin red band, located between host dolomite and sphalerite).

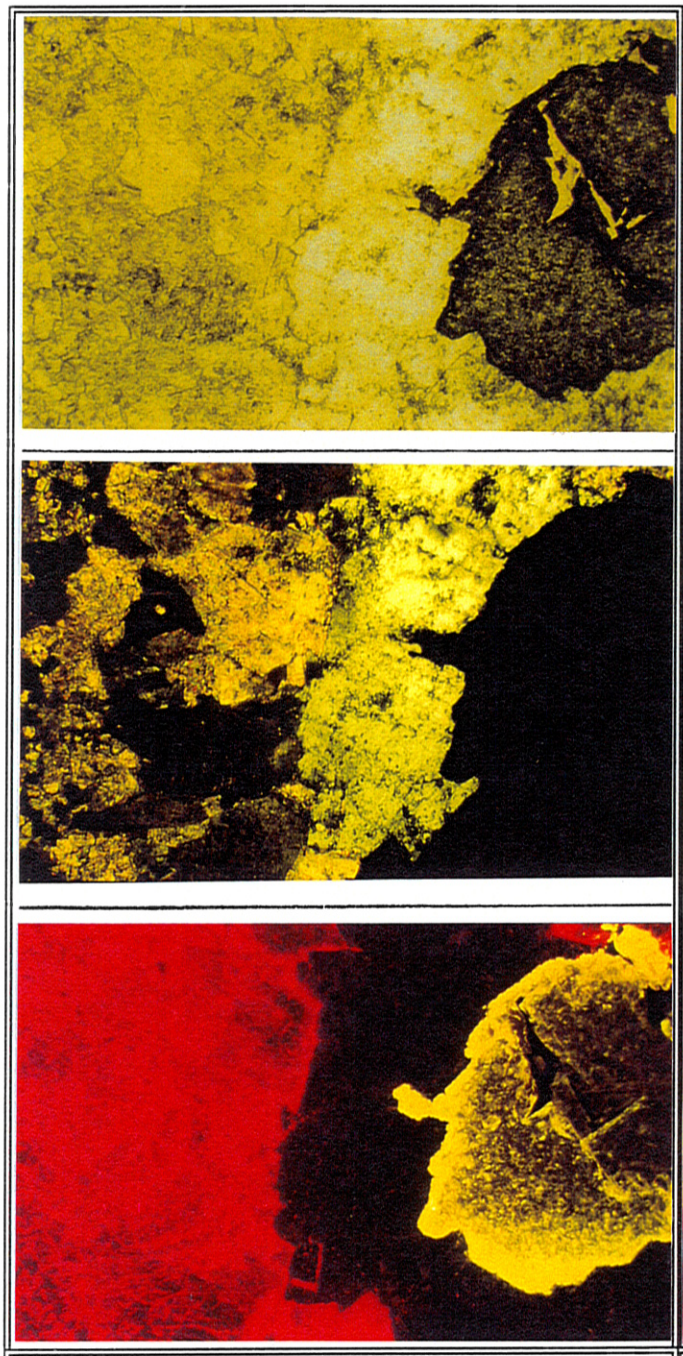

1 mm

Fig. 3-23. Bear deposit, sample no. SP5489. Sphalerite (luminescent, dark cores, yellow rims) followed by quartz (non-luminescent) and dolomite cement (left half, red).

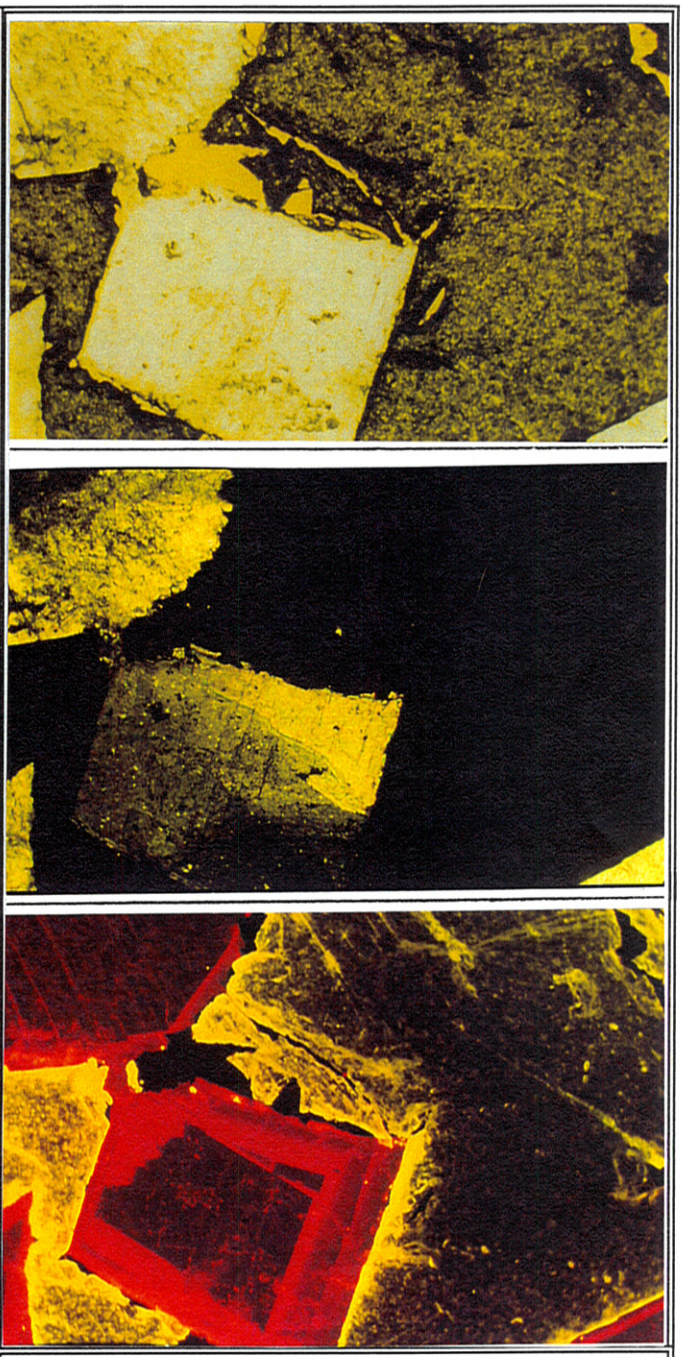

1 mm

Fig. 3-23. Bear deposit, sample no. SP5489. Saddle dolomite (left centre, zoned, red and black) associated with sphalerite (luminescent, dark cores, yellow rims) filled cavity.

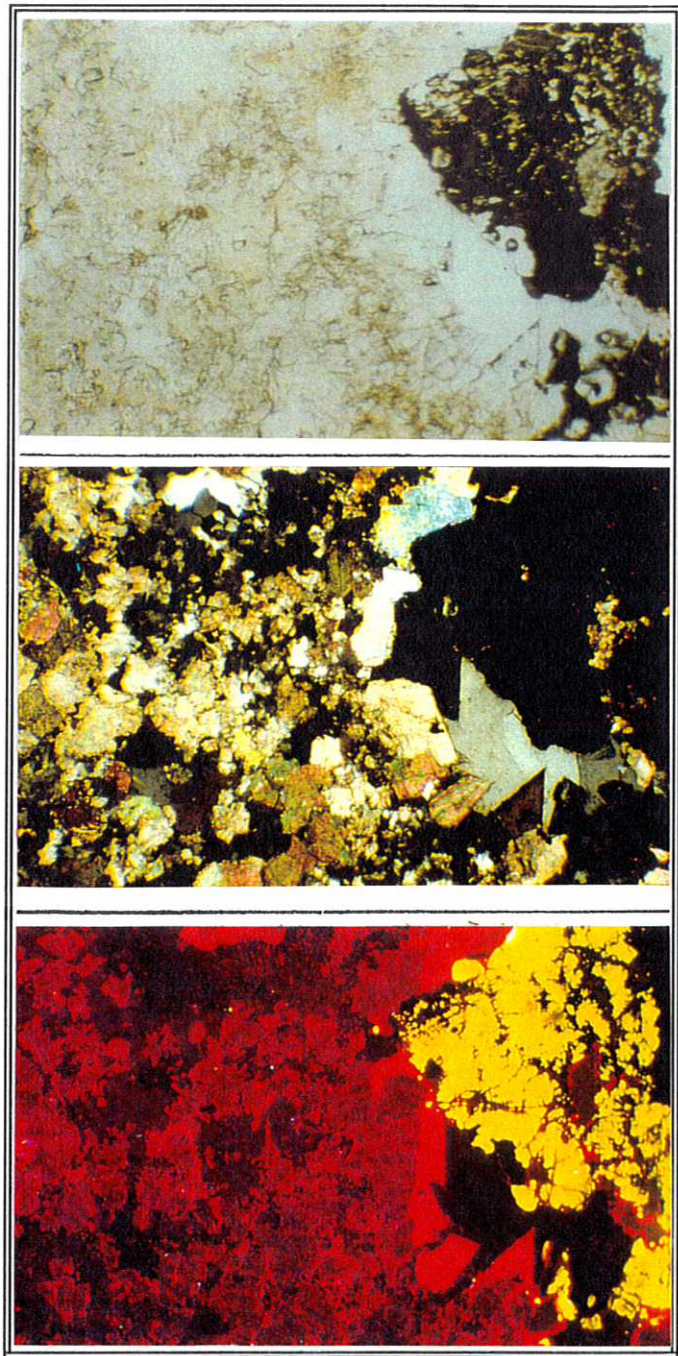

1 mm

Fig. 3-24. Snobird deposit, sample no. SP3417A. Host dolomite (left, dull red) mixed with quartz (non-luminescent) is bordered by finer-grained replacive saddle dolomite associated with sphalerite (top right, yellow) and open space quartz (non-luminescent).

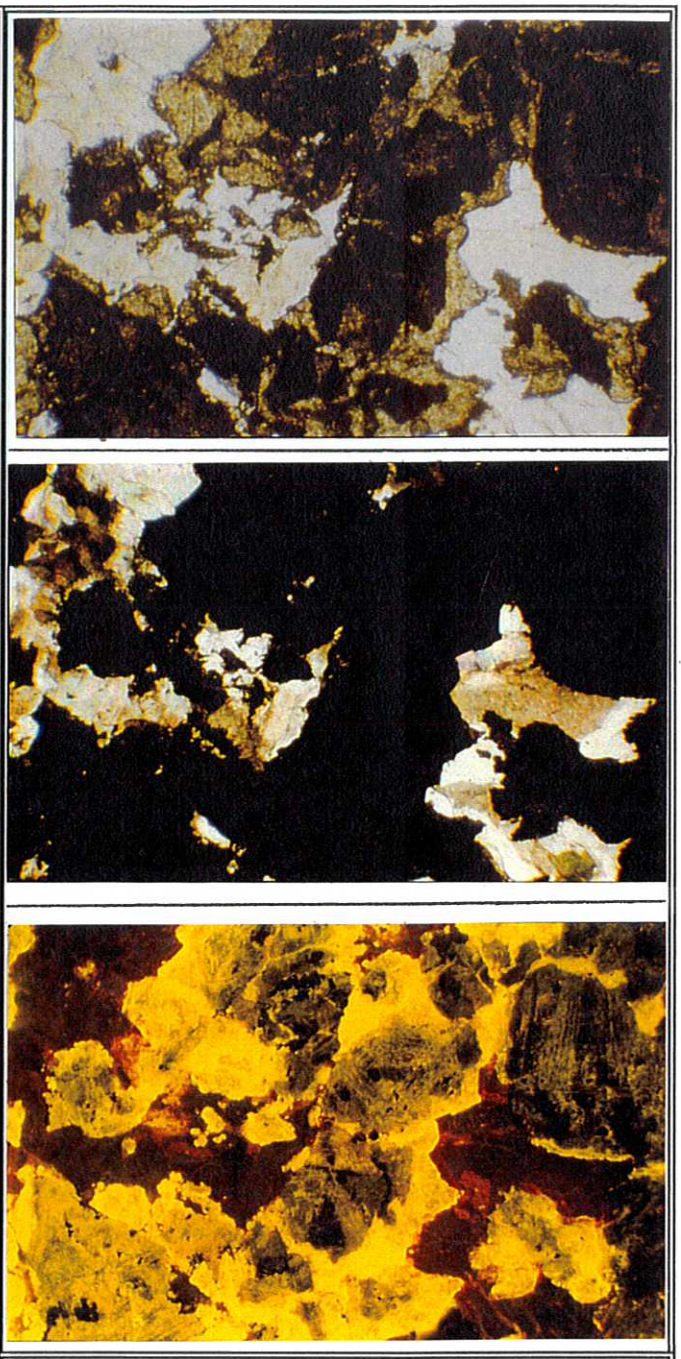

1 mm

Fig. 3-24. Snobird deposit, Sample no. SP3417B. Two phases of sphalerite (top centre and right, centre, and botton left and centre), one (dark yellow) and a second later phase (bright yellow) are associated with dolomite cement (dull red).

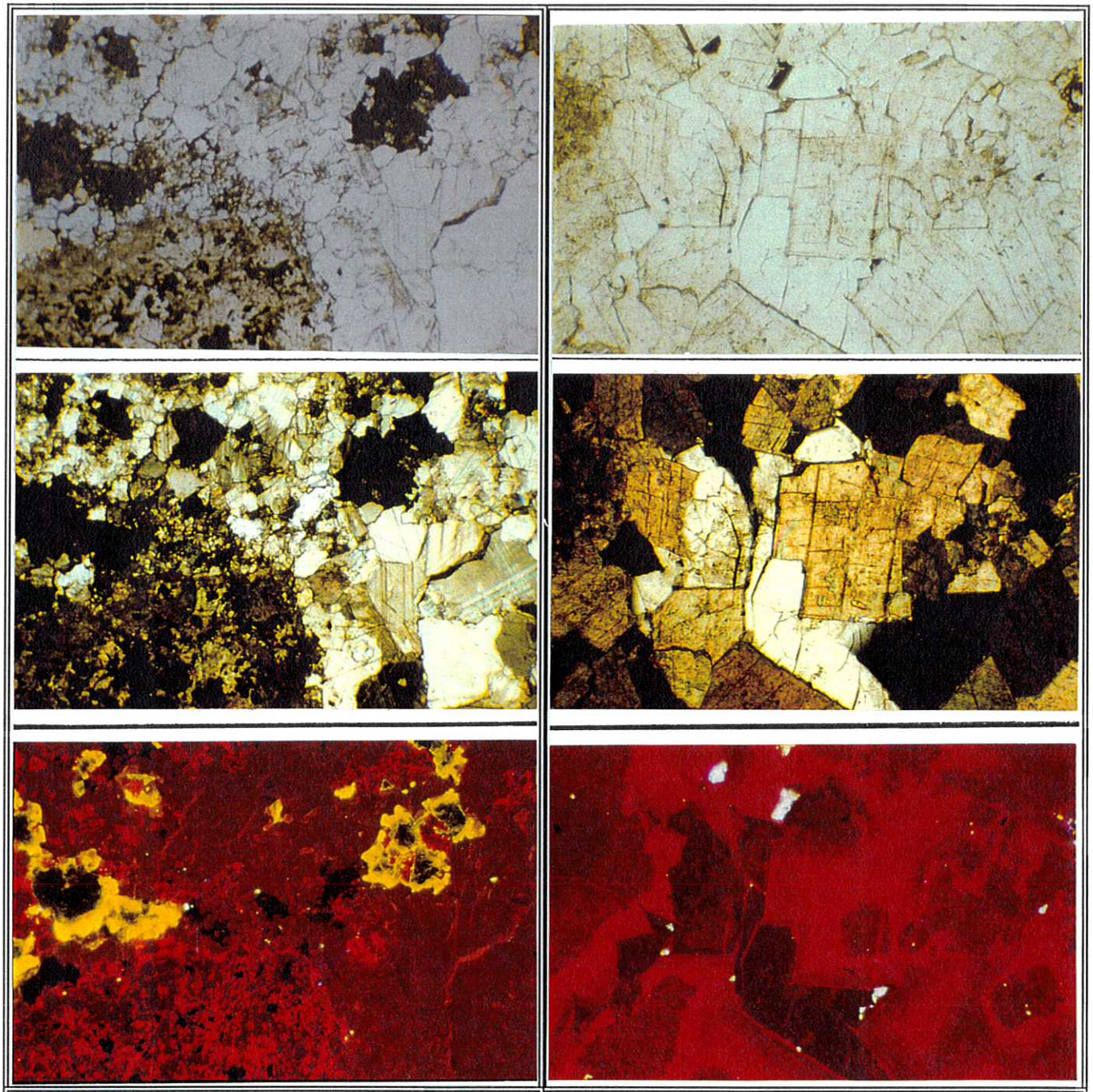

Fig. 3-25. Snobird deposit, sample no. SP3422. Host dolomite (mottled red, bottom left) containing disseminated pyrite, is followed by finer-grained dolomite cement (dull red) associated with sphalerite (dark cores, yellow rims) and quartz (non-luminescent).

Fig. 3-25. Snobird deposit, sample no. SP3417A. The corner of host dolomite fragment (dull red) is visible upper left side, and is surrounded by coarse-grained saddle dolomite (zoned, red and black) and quartz (non-luminescent).

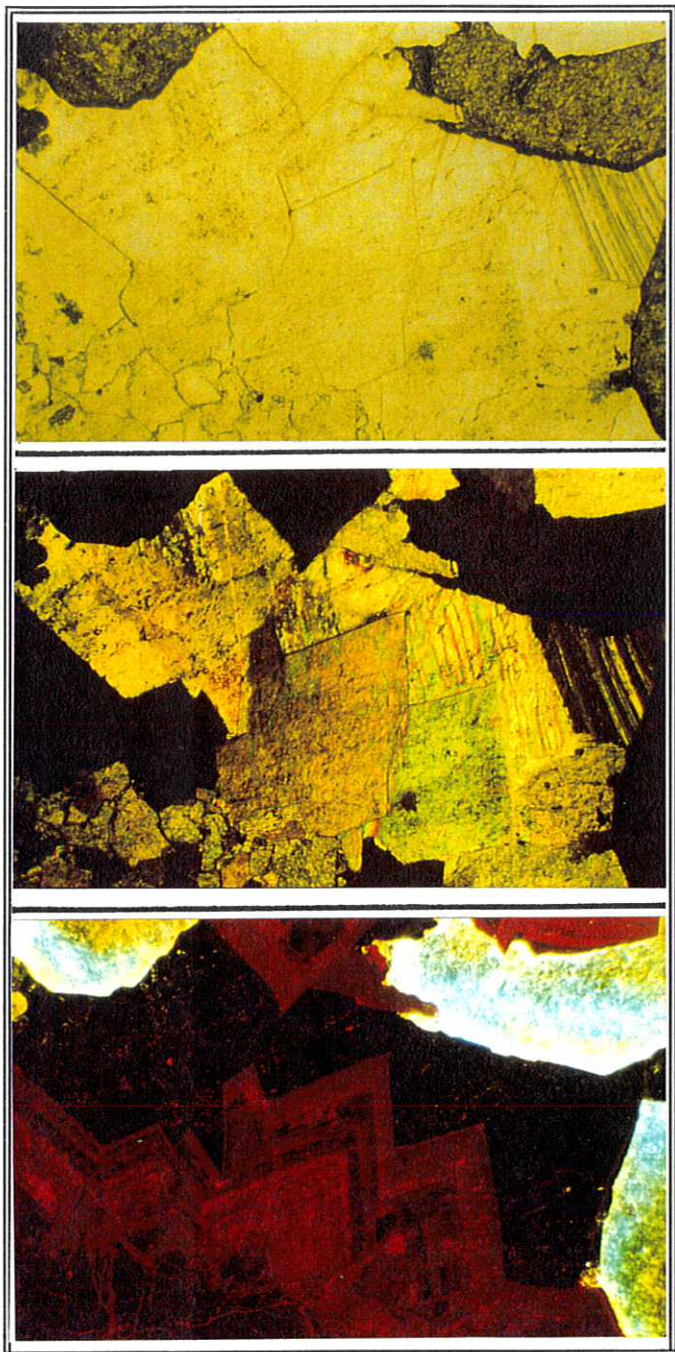

1 mm

Fig. 3-26. Rev deposit, sample no. SP5501. Host dolomite (bottom left corner, dull red to non-luminescent) followed by finer-grained dolomite cement (zoned, red and black) associated with sphalerite (luminescent, pale blue, green, yellow). Remaining void filled with calcite (non-luminescent). Note twinning in calcite is visible under crossed polarized light (b).

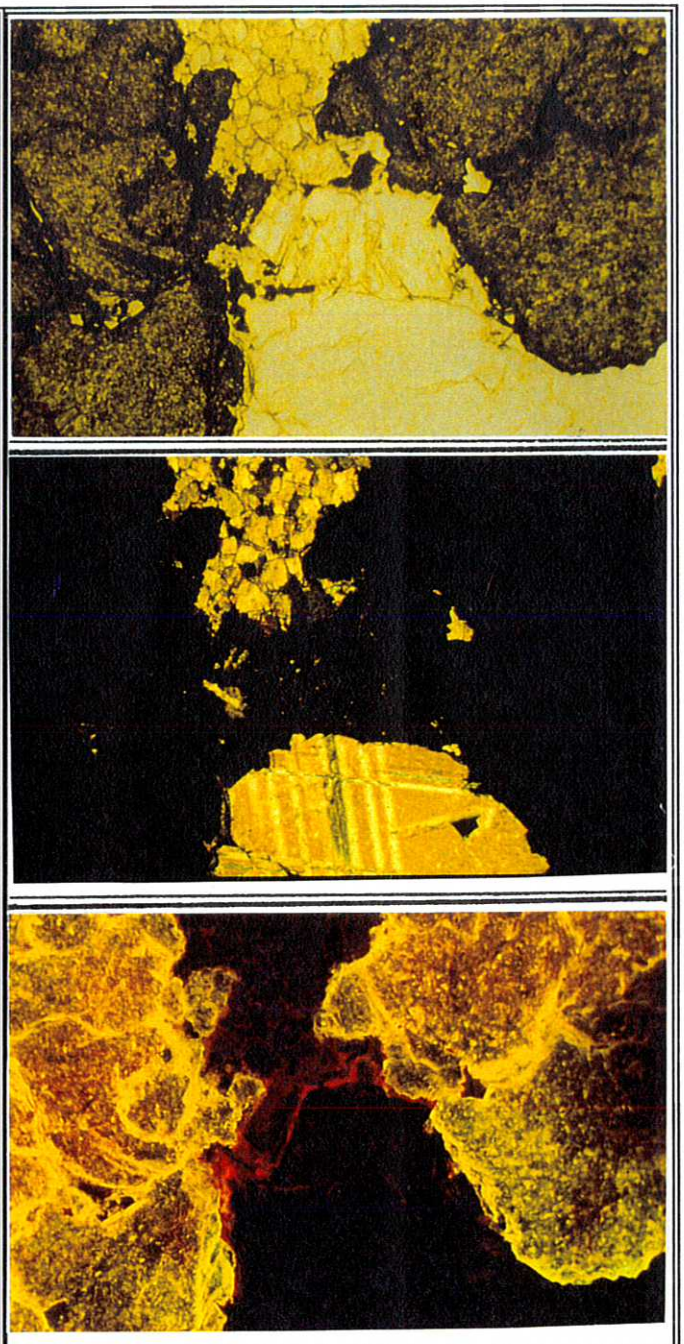

1 mm

Fig. 3-26. Rev deposit, sample no. SP5506. Host dolomite (top centre, dull red to non-luminescent) followed by sphalerite (luminesecent, mottled yellow), with quartz (centre, non-luminescent) and calcite (bottom centre, non-luminescent) filling remaining void. Note twinning in calcite is visible under crossed polarized light (e).

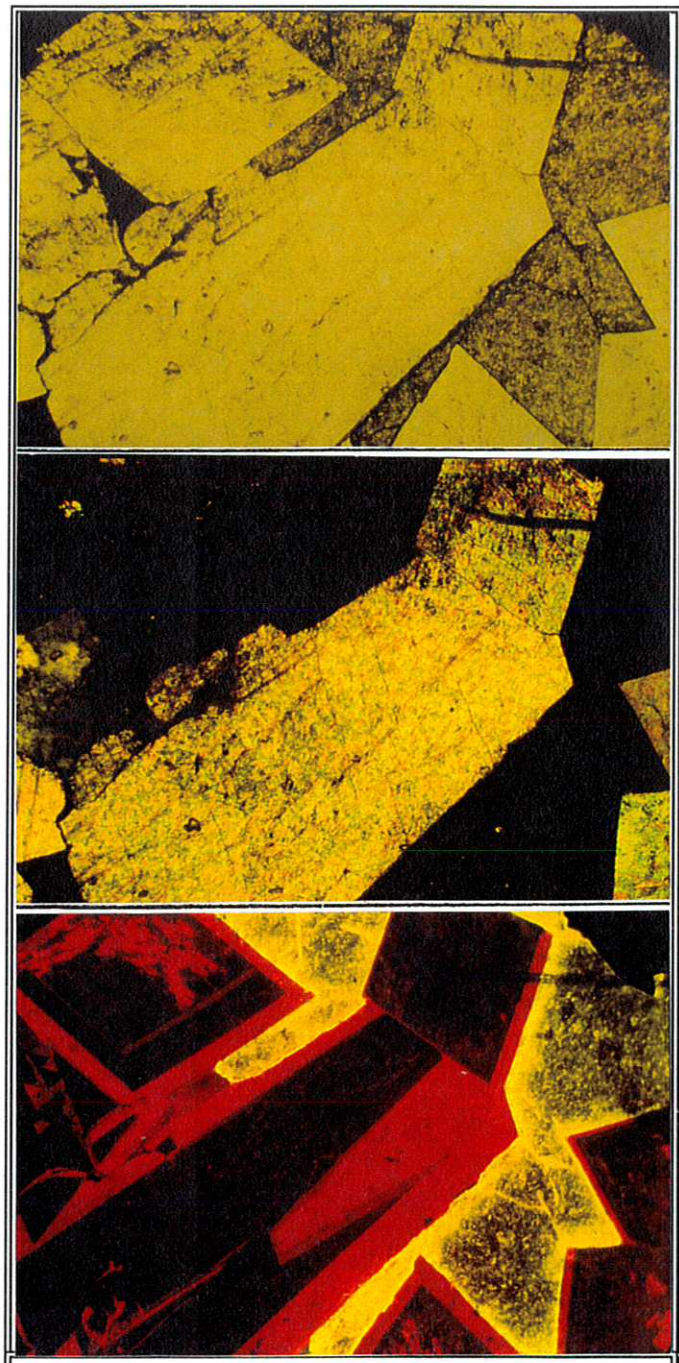

1 mm

Fig. 3-27. Rain deposit, sample no. Rain 3. Coarse-grained dolomite cement (zoned, red and black) associated with sphalerite (luminescent, yellow, dark cores and bright rims). This dolomite cement is not classic saddle dolomite but displays some of its features.

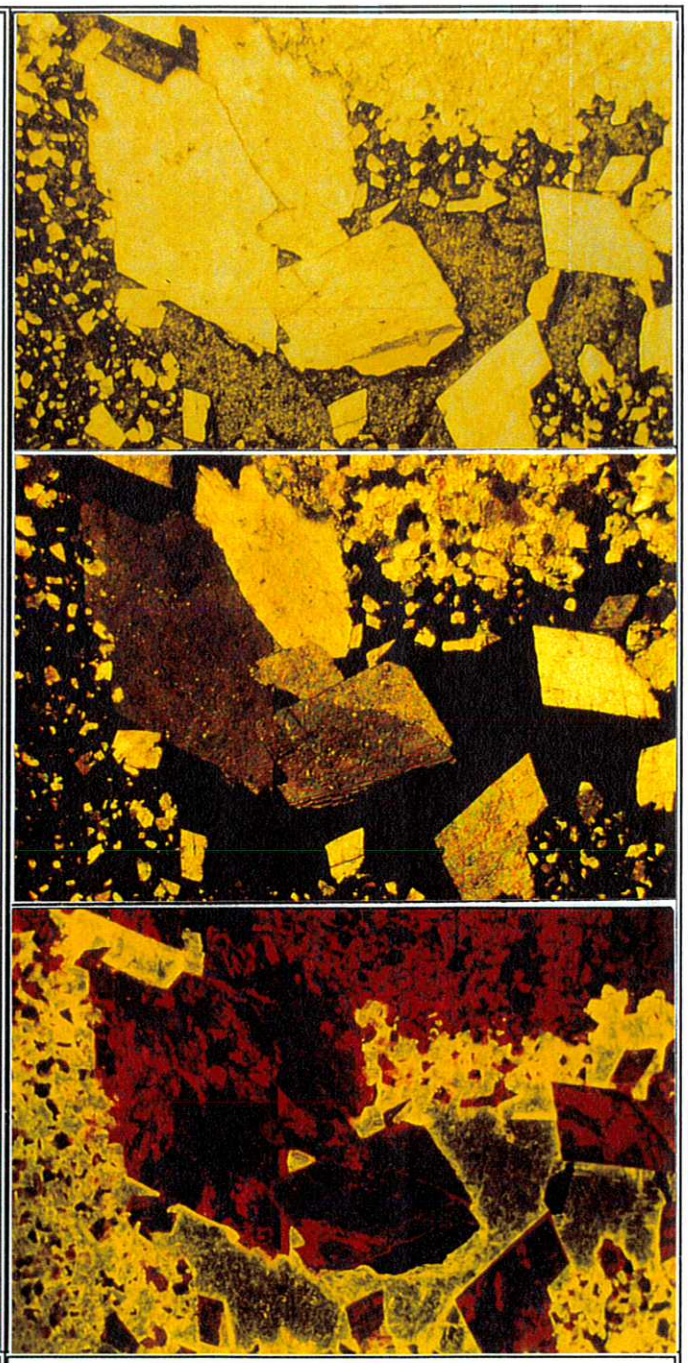

1 mm

Fig. 3-27. Rain deposit, sample no. Rain 3. Host dolomite (top right, mottled, red and black) followed by saddle dolomite (zoned, red and black) associated with sphalerite (luminescent, yellow, dark cores and bright rims).

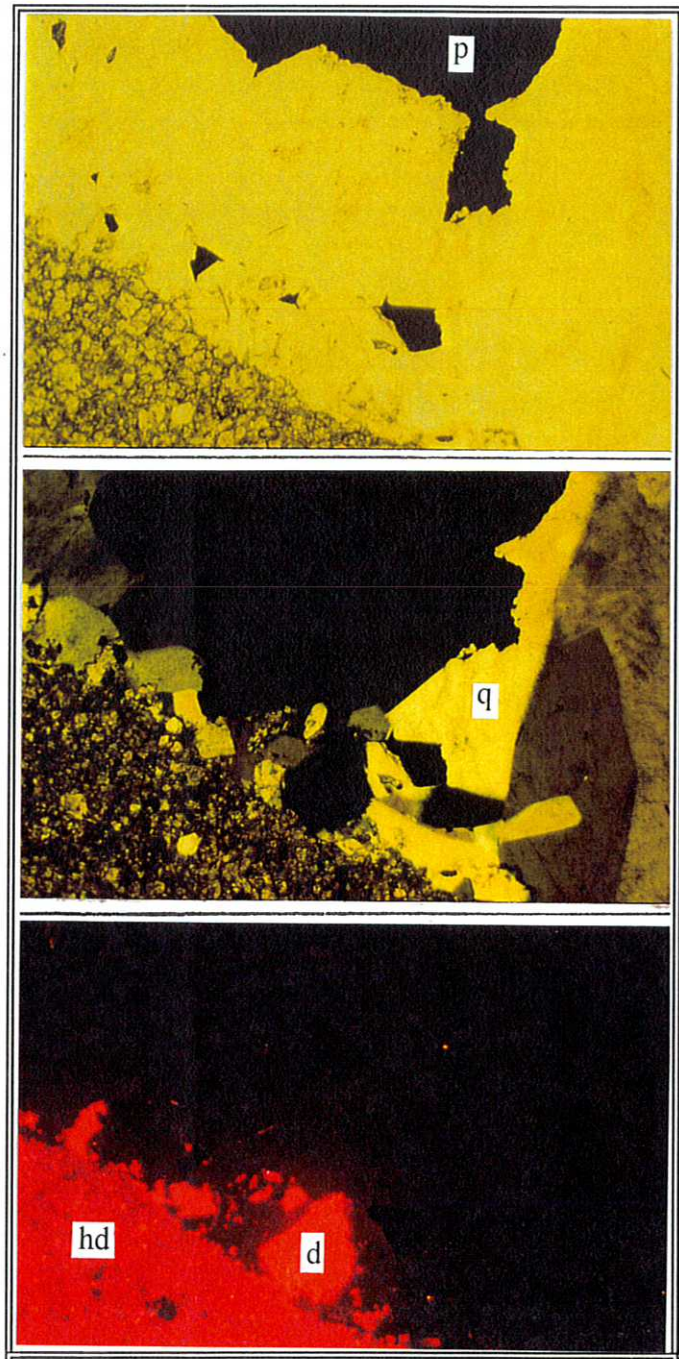

Fig. 3-28. Tet-Rap deposit, sample no. KQ-73-283. A few grains of dolomite cement (d, red) are attached to host dolomite (hd, bottom left corner, dark red) followed by quartz (q, non-luminescent) and pyrite (p).

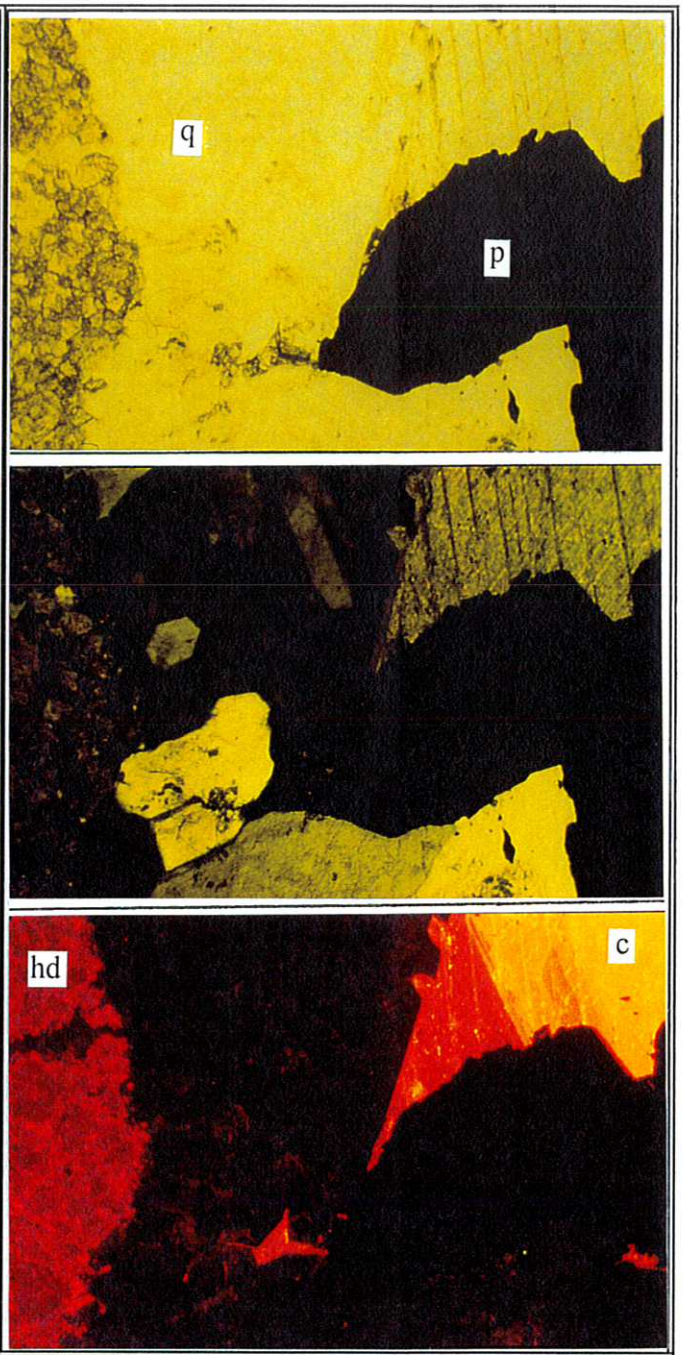

Fig. 3-28. Tet-Rap deposit, sample no. KQ-73-283. Host dolomite (hd, mottled, dull red) followed by quartz (q, non-luminescent), pyrite (p), and calcite (c, top right, dark orange and yellow). Note calcite is twinned.

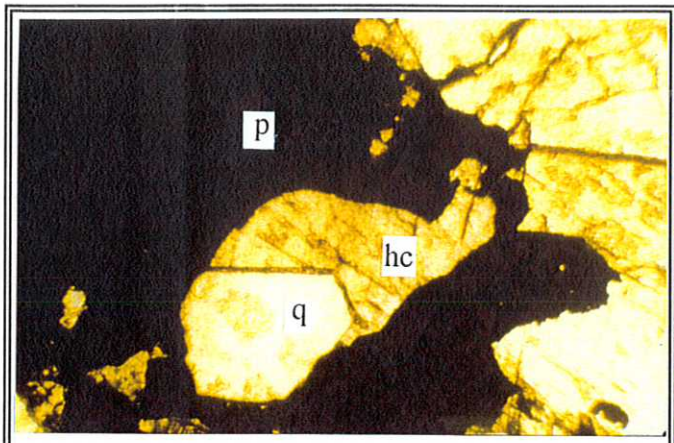

All minerals
non-luminescent

1 mm

Fig.3-29. Birkeland deposit, sample no. SP5485. Terminated quartz grains (q) in contact with host carbonate (hc, non-luminescent) and pyrite (p).

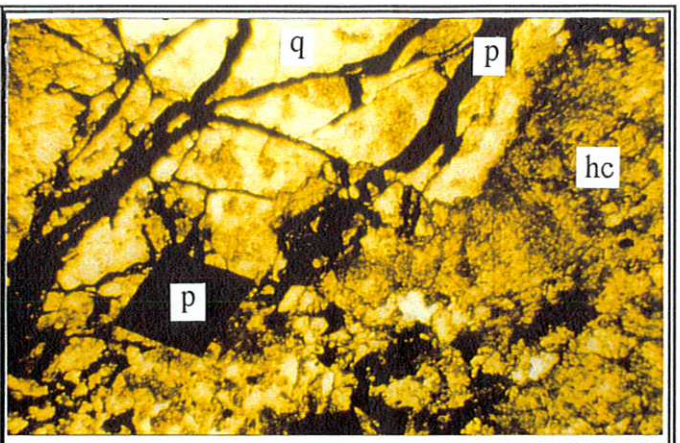

All minerals
non-luminescent

1 mm

Fig. 3-29. Birkeland deposit, sample no. SP5485. Euhedral pyrite (p) occurs in carbonate host (hc, non-luminescent), and veinlets of pyrite cut carbonate host in contact with quartz (q, top centre, non-luminescent).

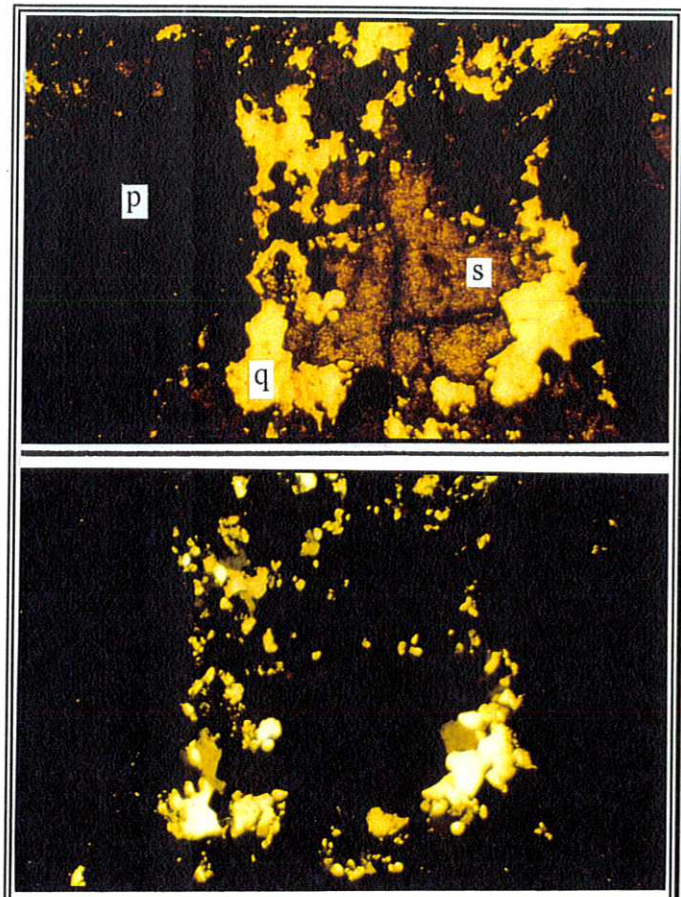

1 mm

Fig.3-30. Keg deposit, sample no. KQ-73-273. Sphalerite (s, centre, non-luminescent), quartz (q, non-luminescent), and pyrite fill cavity in quartz-rich carbonate breccia.

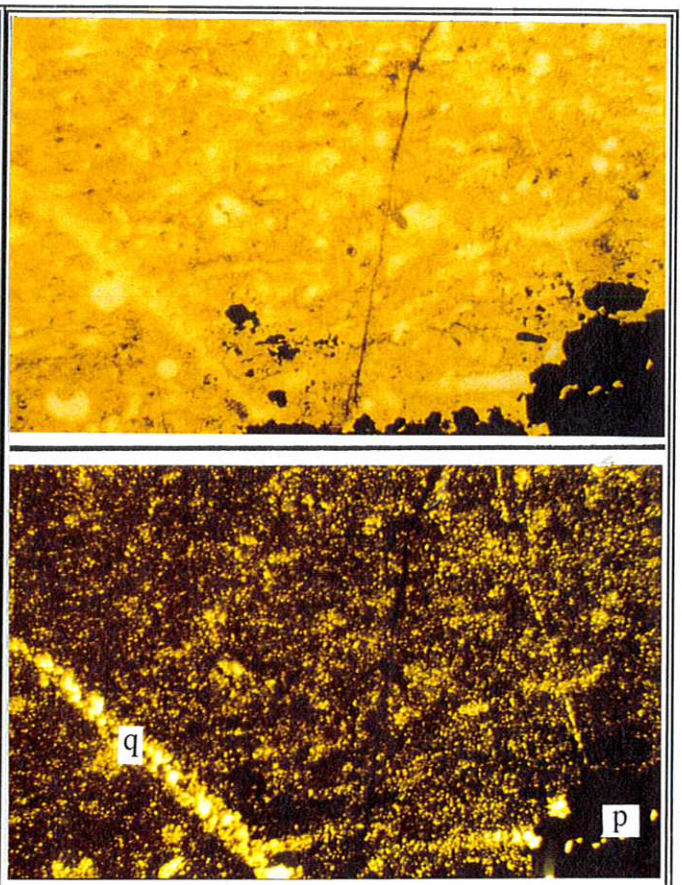

1 mm

Fig. 3-30. Keg deposit, sample no. KQ-73-273. Breccia fragment of very fine-grained quartz-dolomite(?) cut by quartz vein (q). Pyrite (p, bottom right) forms large part of mineralization cementing breccia fragments.

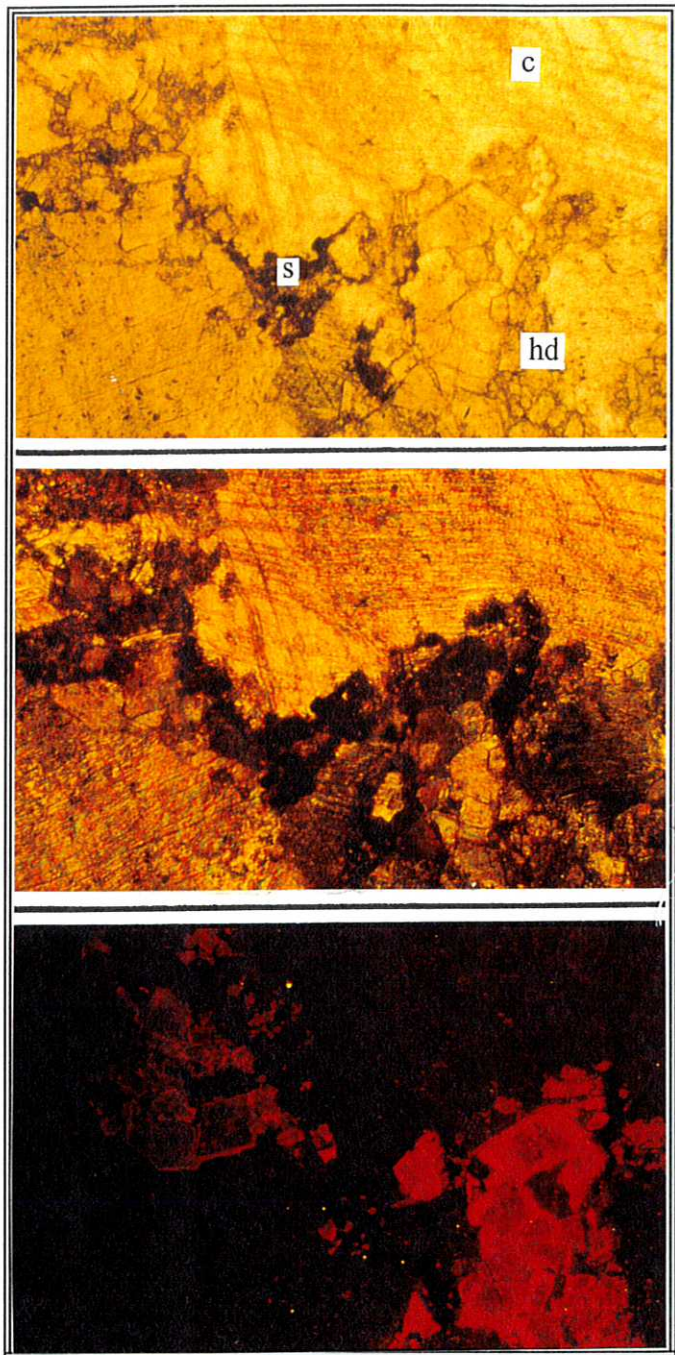

1 mm

Fig. 3-31. Art deposit, sample no. SP5482. Minor sphalerite (s, centre, non-luminescent) associated with host dolomite (hd, zoned, red, dark cores, bright rims) followed by twinned and strained calcite (c, top, non-luminescent).

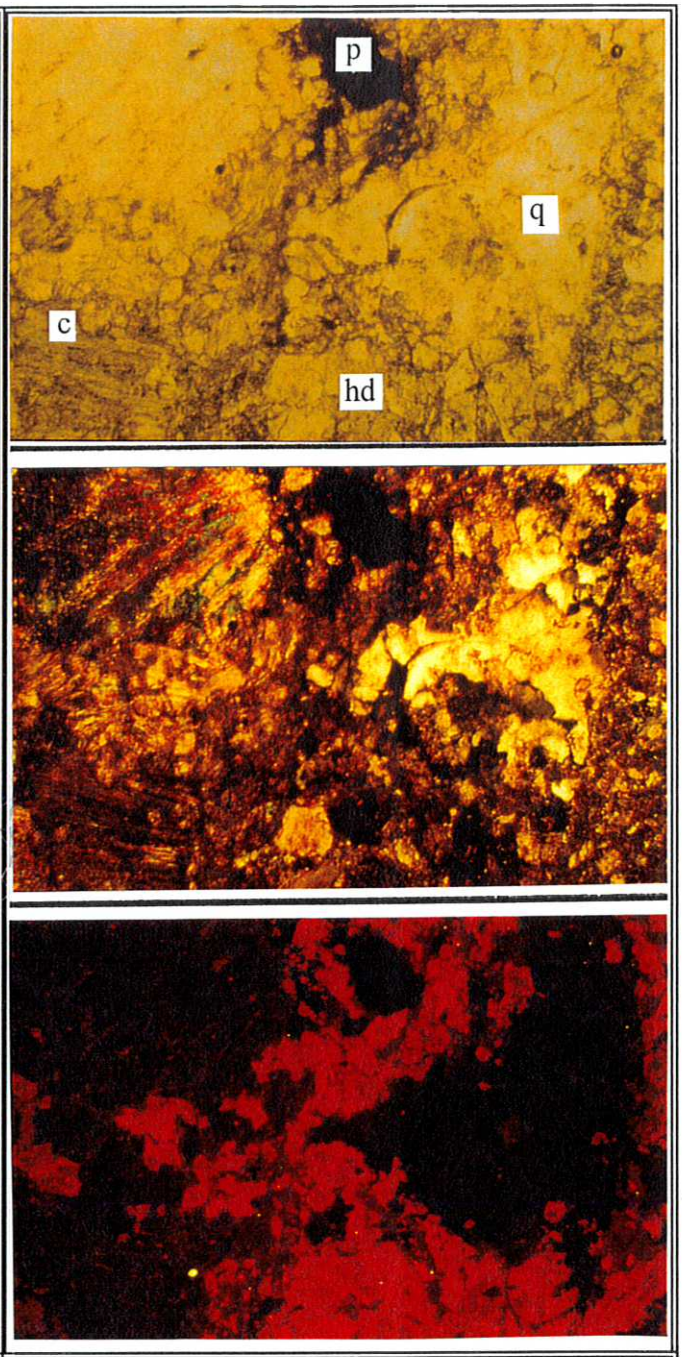

1 mm

Fig. 3-31. Art deposit, sample no. SP5482. Host dolomite (hd, red) and pyrite (p, top centre) asociated with quartz (q, right centre, non-luminescent) and strained calcite (c, left, dull orange to non-luminescent).

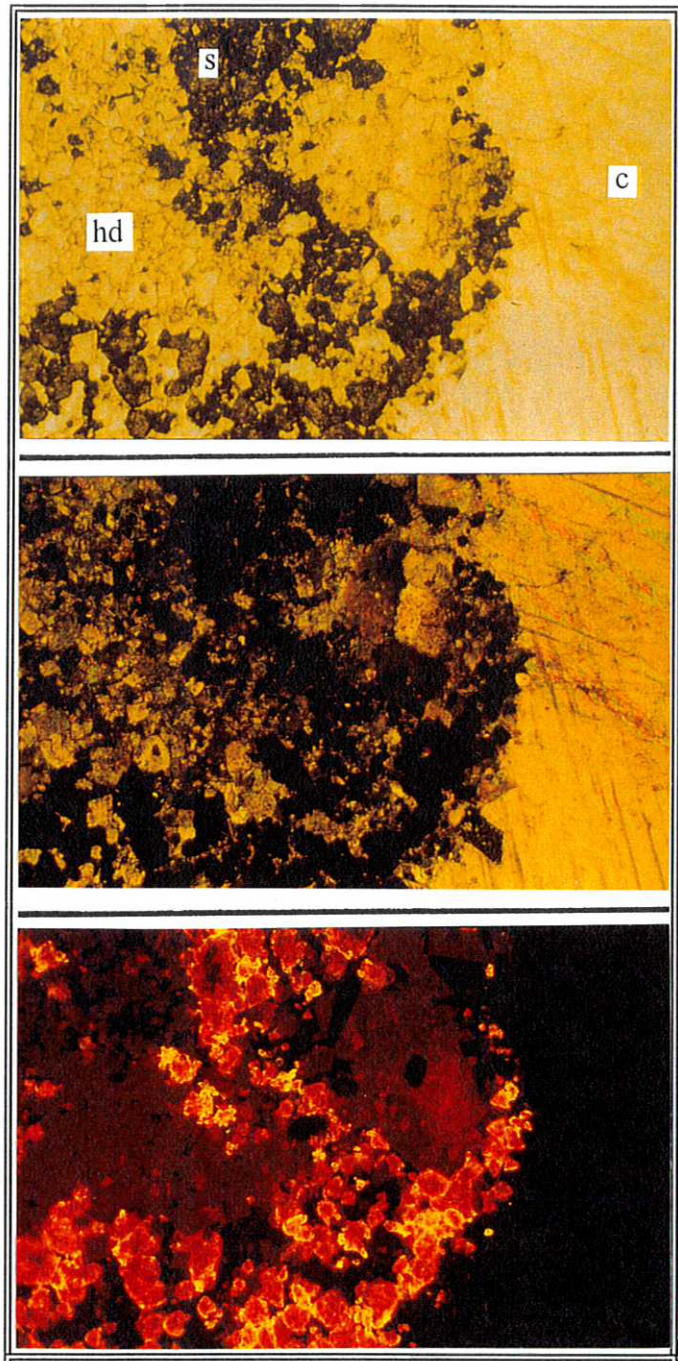

1 mm

Fig. 3-32. Scat deposit, no sample number. Disseminated sphalerite (s, luminescent, red cores, yellow rims) occurs in host dolomite (hd, dull red) followed by calcite (c, right, non-luminescent).

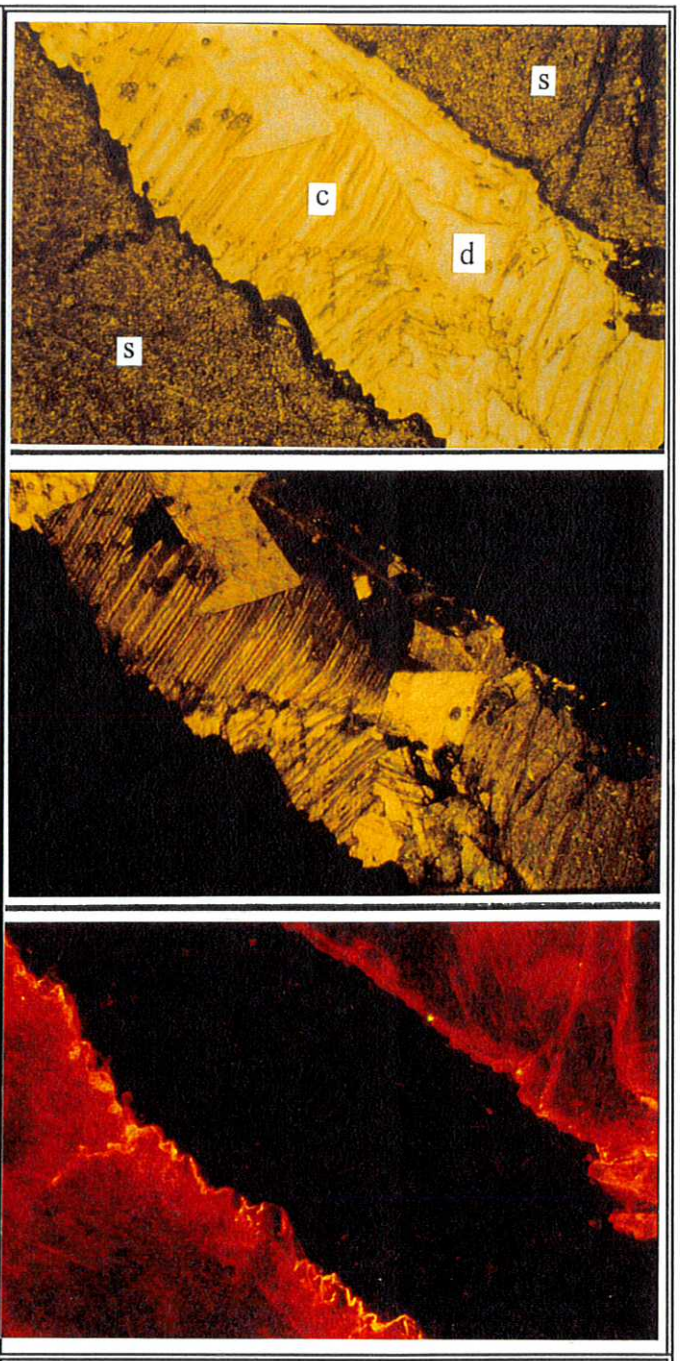

1 mm

Fig. 3-32. Scat deposit, no sample number. Coarse-grained sphalerite (s, luminescent, dull red, yellow rims) and calcite (c, centre, non-luminescent), along with minor dolomite (d, rhombs, non-luminescent) fill void in host dolomite. Note calcite is both twinned and strained.

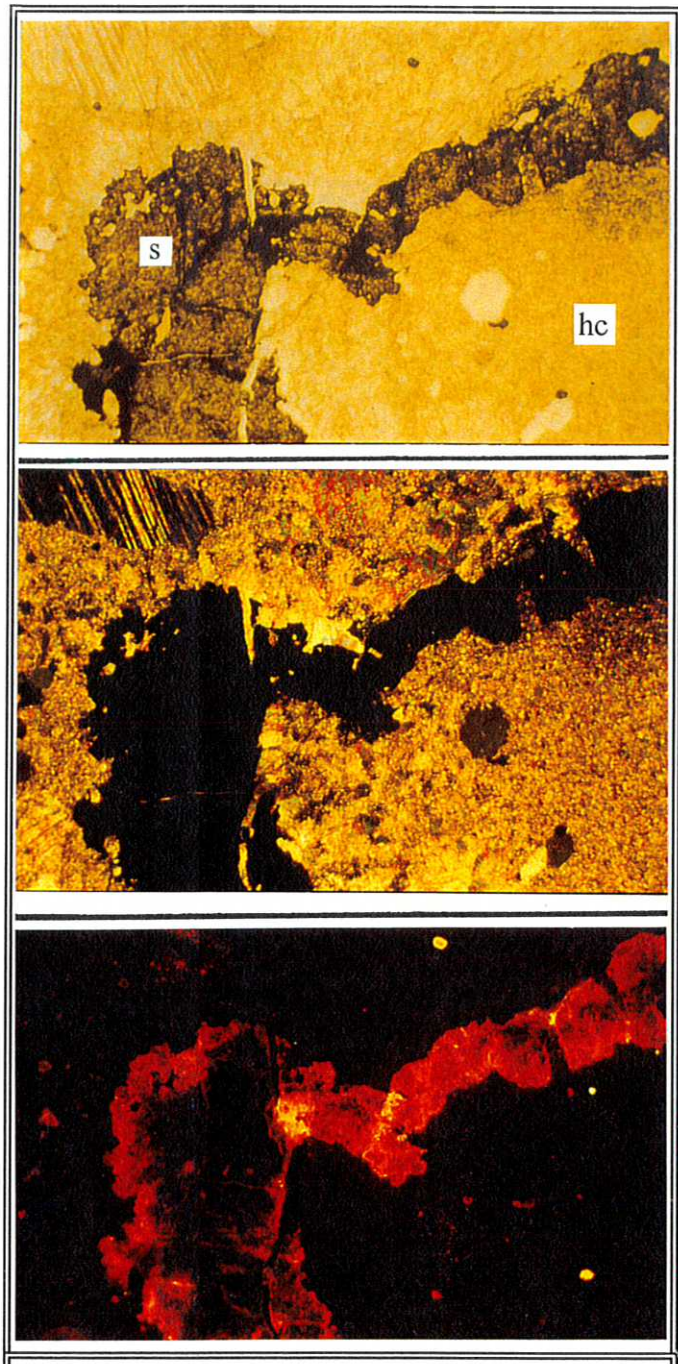

1 mm

Fig. 3-33. Rio deposit, sample no. SP5477. Sphalerite veinlet (s, centre, luminescent, dark cores, red rims tinged with yellow) cut through carbonate host rock (hc, dull red to non-luminescent).

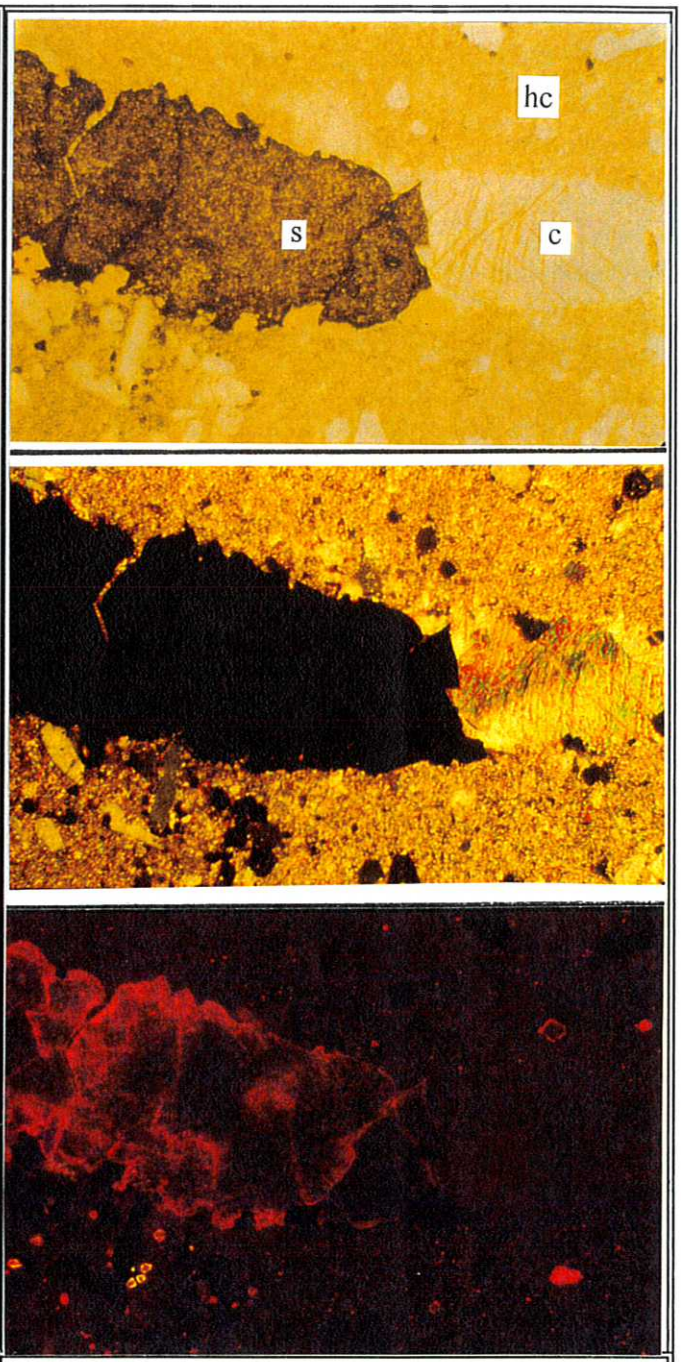

1 mm

Fig. 3-33. Rio deposit, sample no. SP5477. Sphalerite veinlet (s, left centre, luminescent, dark cores, red rims tinged with yellow) cut through carbonate host rock (hc, dull red to non-luminescent). Twinned and strained calcite (c, right centre, non-luminescent) fills remaining void.

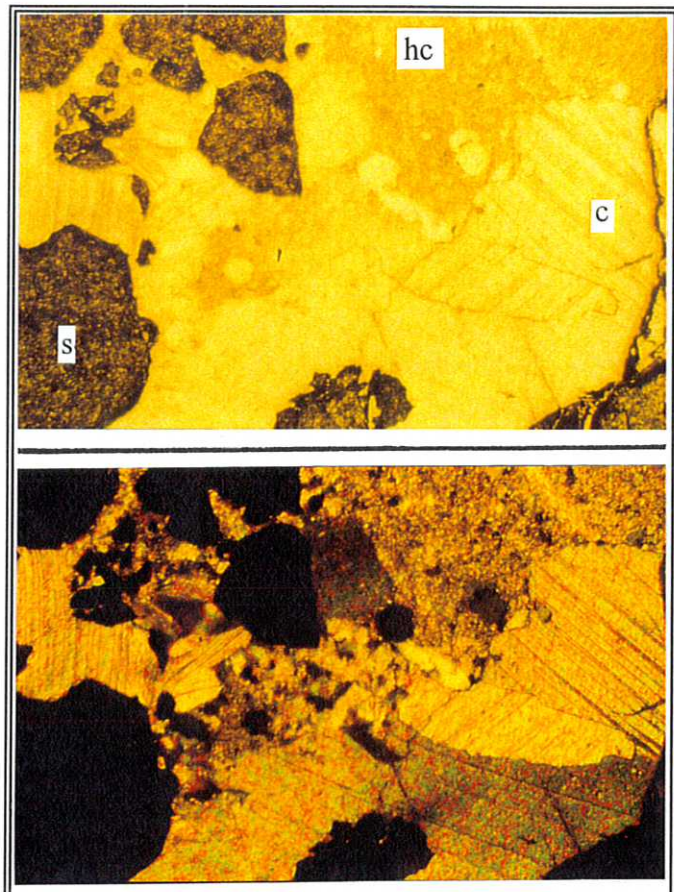

All minerals
non-luminescent

1 mm

Fig. 3-34. Rio deposit, sample no. SP5477. Sphalerite (s, non-luminescent) associated with calcite (c, non-luminescent) in carbonate host rock (hc, top right, non-luminescent).

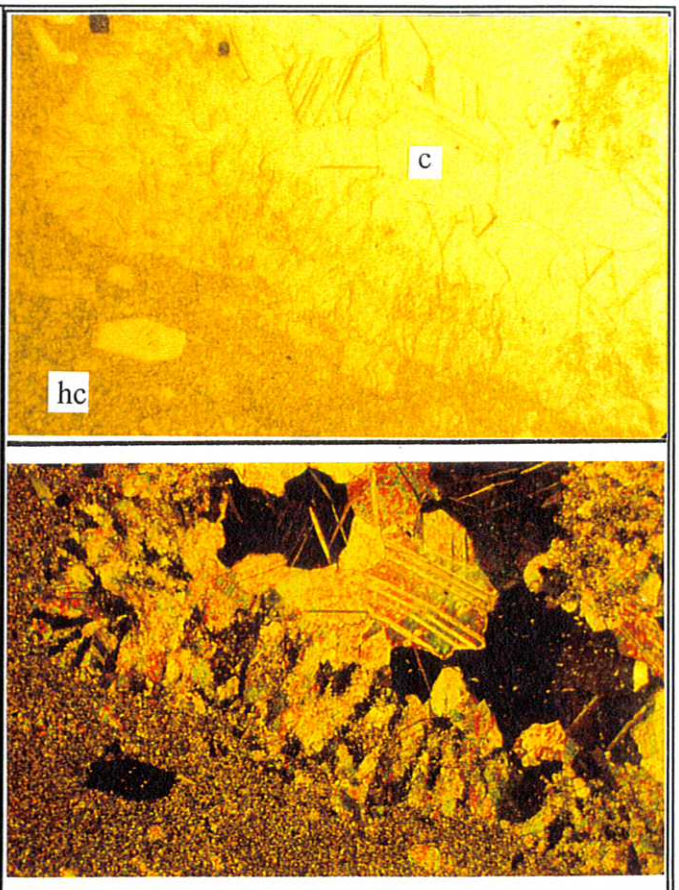

All minerals
non-luminescent

1 mm

Fig. 3-34. Rio deposit, sample no. SP5477. Cavity in host carbonate rock (hc, left bottom, non-luminescent) filled with calcite (c, non-luminescent). Note grain size becomes larger near the centre of the cavity. Calcite is twinned.

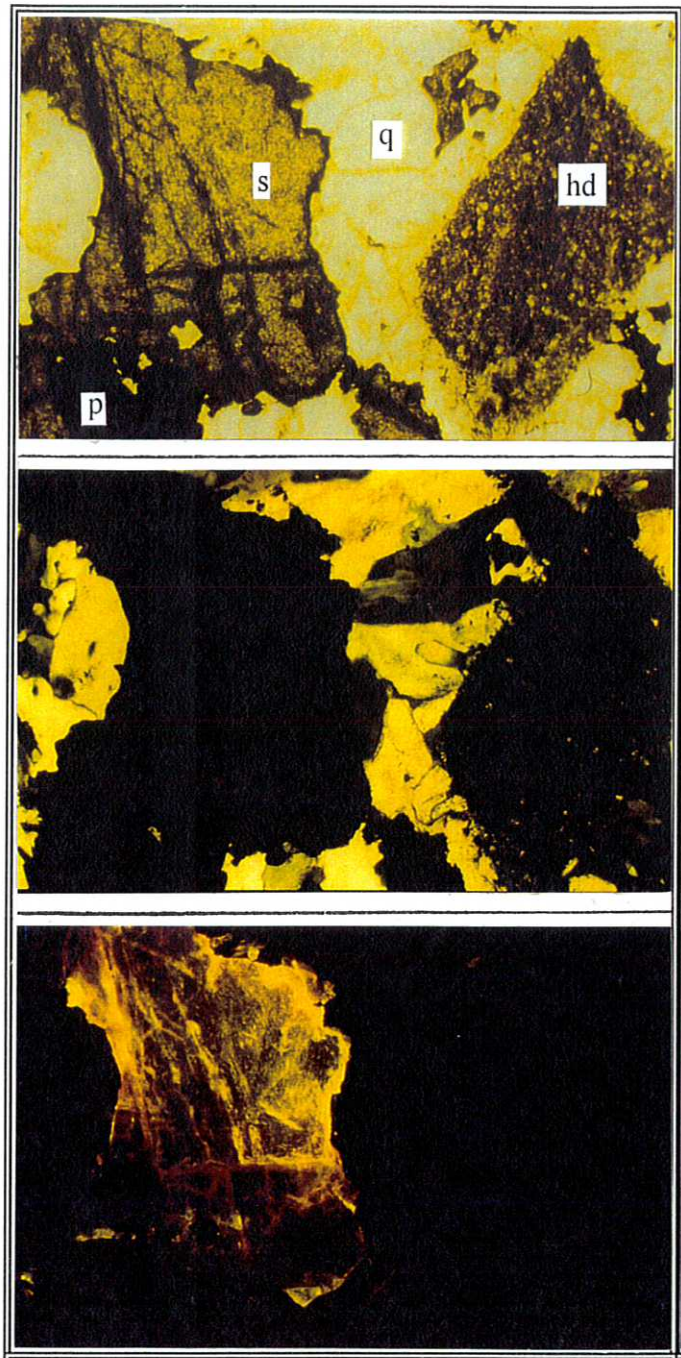

1 mm

Fig. 3-35. Aj deposit, sample no. SP5420. Host dolomite breccia fragment (hd, right centre, non-luminescent) cemented by quartz (q, non-luminescent), sphalerite (s, left centre, luminescent, yellow) and pyrite (p, bottom left and bottom right corner).

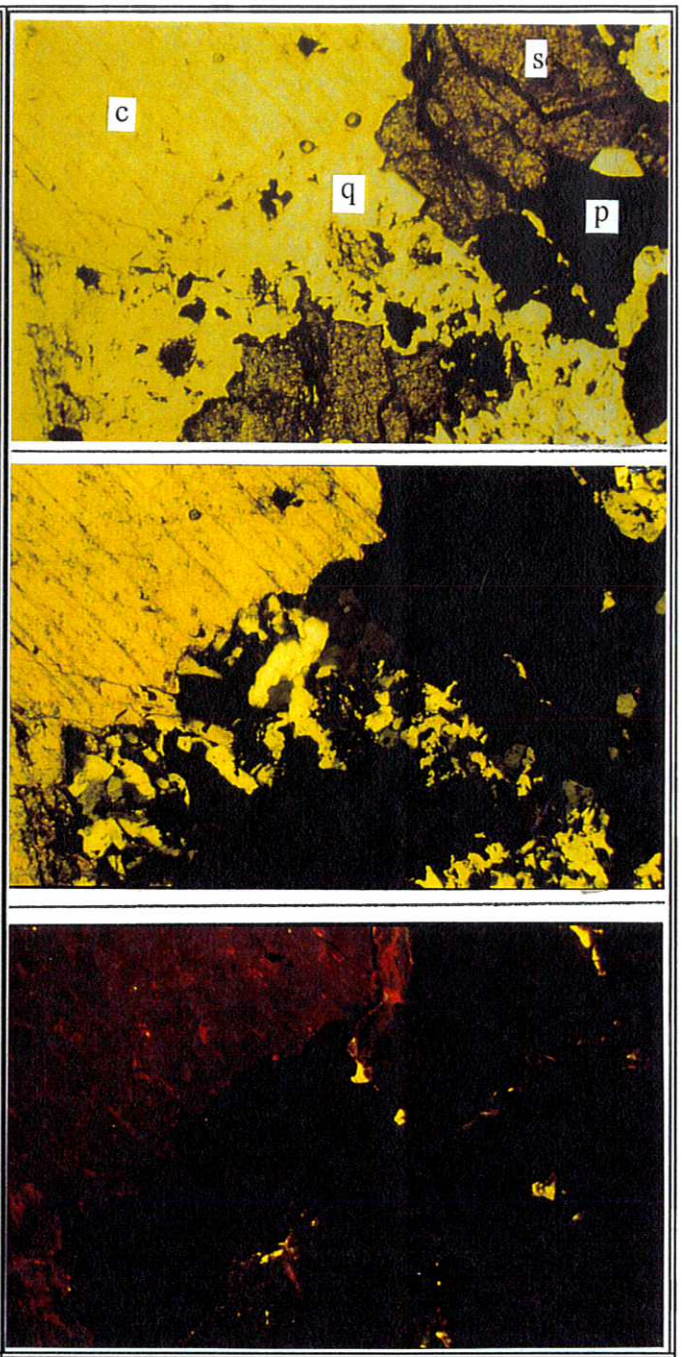

1 mm

Fig. 3-35. Aj deposit, sample no. SP5420. Sphalerite (s, top right and bottom centre, non-luminescent except for yellow rim) is associated with pyrite (p, right centre), quartz (q, non-luminescent) and calcite (c, top left corner, dull orange-red).

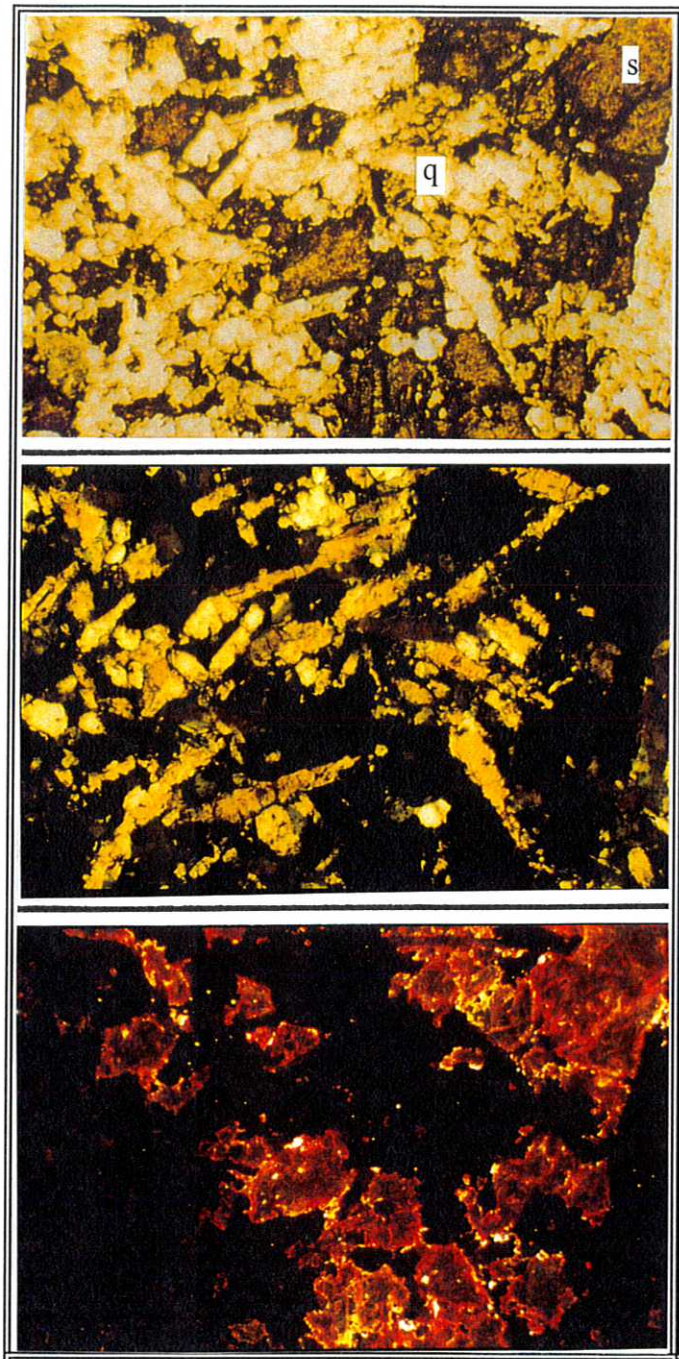

1 mm

Fig. 3-36 Big Red deposit, sample no. SP5443. Sphalerite (s, luminescent, red with yellow tinge) associated with elongated grains of quartz (q, non-luminescent).

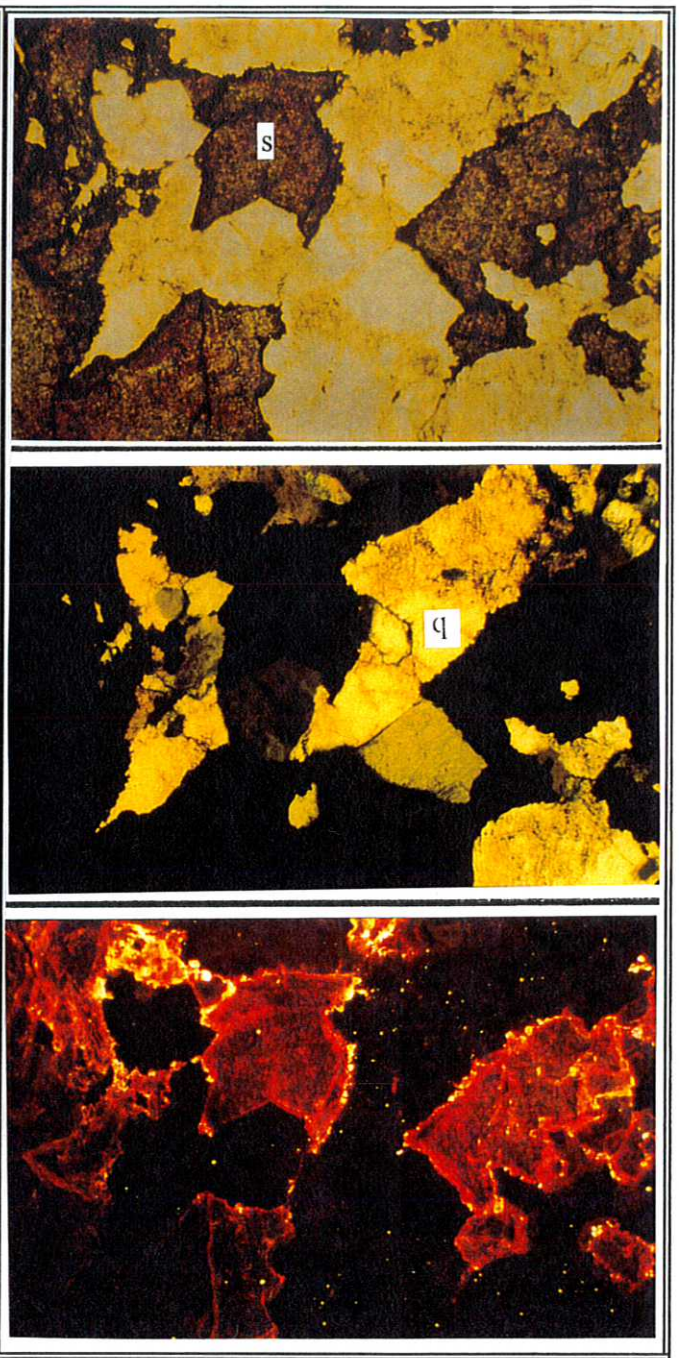

1 mm

Fig. 3-36. Big Red deposit, sample no. SP5443. Sphalerite (s, luminescent, red with yellow tinge) occurs with coarse-grained quartz (q, non-luminescent).

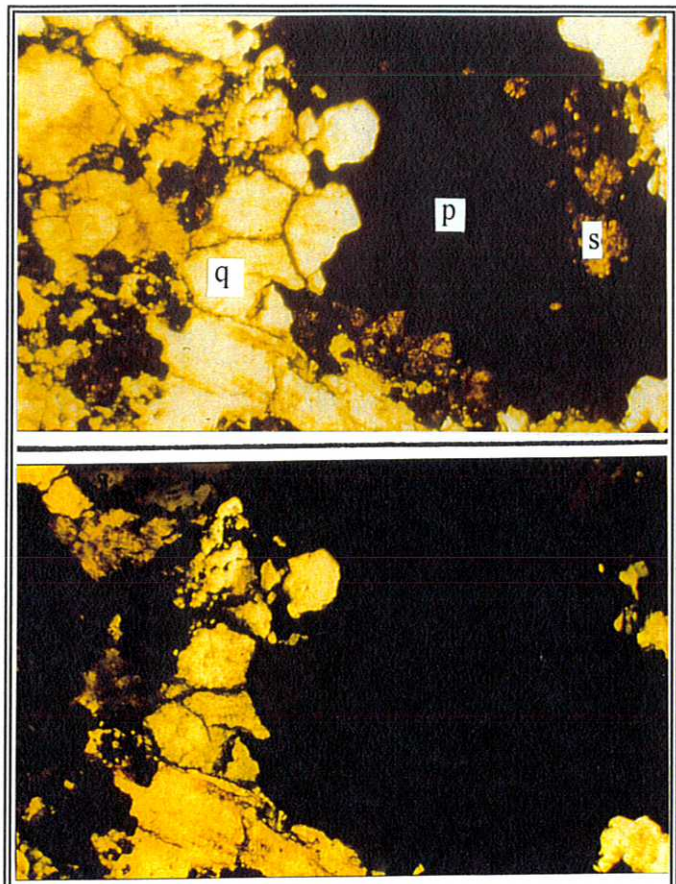

All minerals
non-luminescent

1 mm

Fig. 3-37. Big Red deposit, sample no. SP5441. Pyrite (p) and sphalerite (s, non-luminescent) occur with quartz (q, non-luminescent).

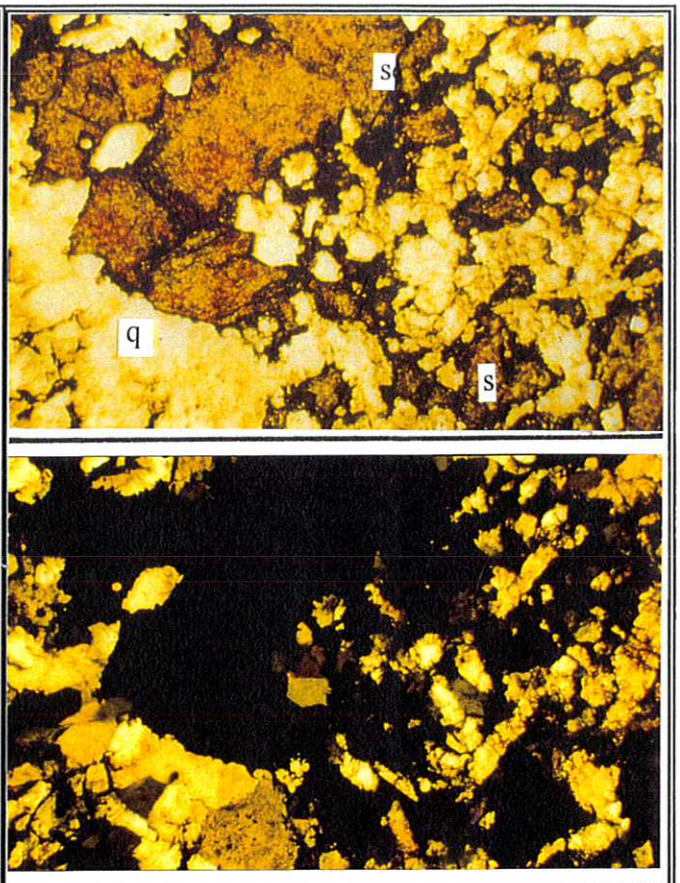

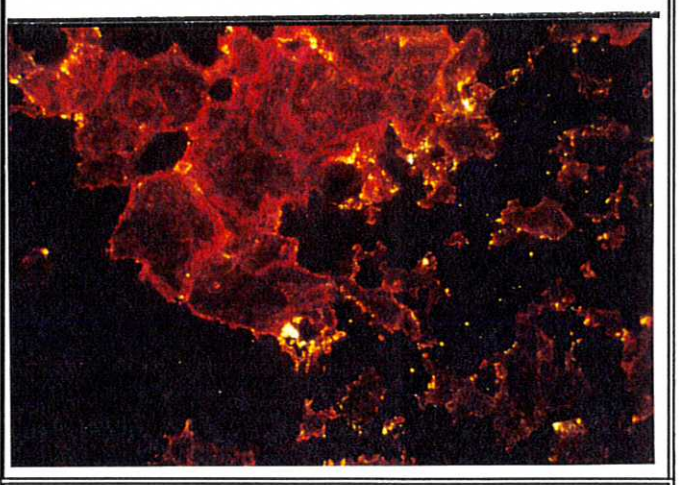

1 mm

Fig. 3-37. Big Red deposit, sample no. SP5443. Disseminated sphalerite (s, luminescent, dull red, yellow rims) occurs in quartzitic host rock composed of both rounded and elongated grains of quartz (q, non-luminescent). Coarser-grained sphalerite occurs with coarser-grained quartz (left bottom, non-luminescent).

PARAGENESIS

The observed paragenenetic sequence (Fig. 3-38) is generally similar in all sixteen deposits studied which have prodominent dolomite cement. The most obvious difference between the sixteen deposits is in the host dolomite which, in some cases, contains disseminated pyrite. The host dolomite is, for the most part, nonplanar dolomite, which develops in excess of 50°C in the burial environment (1km or greater) by dolomitization of limestone or neomorphic recrystallization of preexisting dolomite (Woody et al., 1996). The average grain size of host dolomite ranges from 42 to 215 μm. Dolomite cement(1) is finer grained dolomite cement defined as ranging in grain size from 60-2000 μm (mean 515 μm) and includes replacive saddle dolomite. Dolomite cement(2) is coarse-grained saddle dolomite and ranges in grain size from 200-6600 μm (mean 1570 μm). In most cases carbonate geochemistry suggested dolomite cements(1) and (2) formed from the same fluid. Possible exceptions could be Palm, Cypress, Bob, and Econ. One of the factors determining grain size was possibly the size of the cavity in which the cement grew.

Stage	Mineral	Early → Late
PRE ORE	Host dolomite	
	Pyrite	
ORE STAGE	Sphalerite(1)	
	Dolomite cement(1)	
	Pyrite	
	Quartz*	
	dolomite cement(2)	
	Sphalerite(2)	
	Galena	
POST ORE	Calcite	
	Barite	
	Quartz	
	Bitumen	
	Cerussite	
	Hydrozincite	
	Smithsonite	

Fig. 3-38. Generalized paragenesis of minerals in Mackenzie Platform MVT deposits. Sphalerite(1), where present, is disseminated in the host dolomite and commonly replaces the disseminated pyrite. Sphalerite(2) is coarse grained and fills open spaces. Dolomite cement(1) is the finer grained cement and includes replacive saddle dolomite. Dolomite(2) is coarse grained saddle dolomite. * In Joli Green deposit the ore stage quartz is a mélange of quartz and calcite (Fig. 3-19, 3-20).

Ab, Cab (Fig. 3-8), Bob (Fig. 3-10), Palm (Fig. 3-11), Mawer (Fig. 3-21), Bear (Fig. 3-22), Snobird (Fig. 3-25), and Rev have host dolomite which contains sparse to abundant euhedral to subhedral disseminated pyrite (Fig. 3-39). Deposits in which host dolomite does not contain pyrite include Econ, Ice, Arn, Rain, Cypress, Tic, and Joli Green. Pyrite occurs as an ore stage mineral in deposits Tic (Fig 3-15), Ice (Fig. 3-16), Arn (Fig. 3-17, 3-18), Tet-Rap (Fig. 3-28), Birkeland (Fig. 3-29), Keg (Fig. 3-30), Aj (Fig. 3-35), and Big Red (Fig. 3-37), and is particularly abundant at Bob deposit (Fig. 3-9, 3-10).

Sphalerite(1), where present, is disseminated in the host dolomite (Fig. 3-7, 3-8) and commonly replaces the disseminated pyrite. Sphalerite(2) is coarse-grained and fills open spaces (Fig. 3-7, 3-14, 3-23).

Quartz is another variable worth noting. It occurs as detrital grains in some host dolomite such as Cab, and in varying amounts as authigenic quartz in ore- and post-ore stages of the paragenesis. Ab, Cab (Fig. 3-8), Cypress (Fig. 3-6), Tic (Fig. 3-14), Palm, Mawer, Bear (Fig. 3-23), and Snobird (Fig. 3-25) contain quartz as an ore stage mineral. Econ, Ice, Arn, and Rain have no ore stage quartz. In the Joli Green deposit the ore stage quartz is a mélange of quartz and calcite (Fig. 3-19, 3-20).

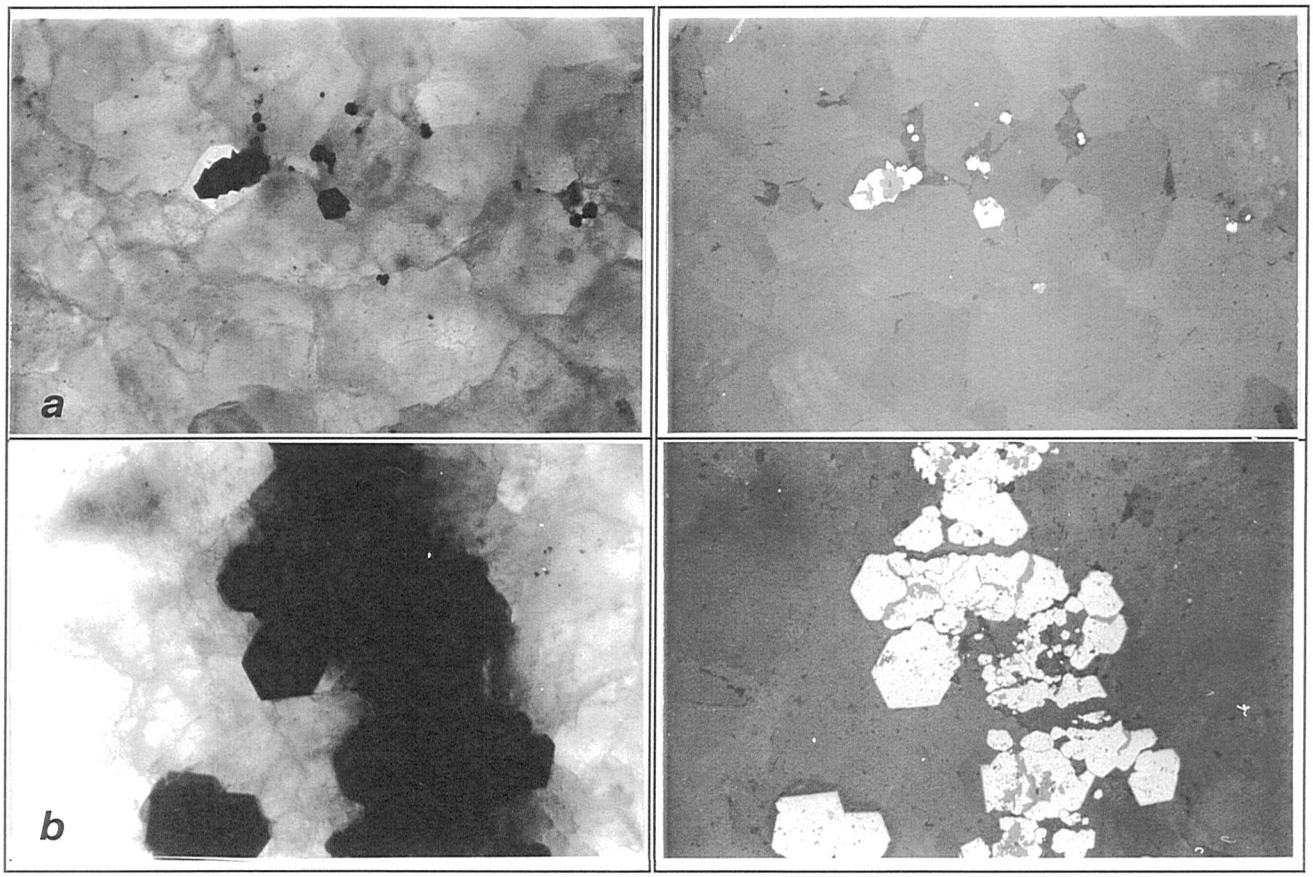

Fig. 3-39. Photomicrographs showing euhedral pyrite (light grey, reflected light) and Fe oxide mineral (darker grey within the pyrite, reflected light) disseminated in host dolomite. Both a) and b) from sample SP5489(2), Bear deposit, transmitted light, uncrossed polars on the left, and reflected light on right. Width of view equals 0.7 mm.

Galena is not abundant in the samples examined, with these exceptions: Arn deposit (Fig. 3-17) filling cavities lined with saddle dolomite, Tic deposit (Fig. 3-15) associated with sphalerite, and Ice deposit (Fig. 3-16) filling cavities within replacive saddle dolomite.

Post ore minerals include calcite which was observed as a later cavity filling (Fig. 3-4, 3-12). Some calcite grains are twinned (Fig. 3-26). Barite was found associated with calcite at Econ deposit. Quartz as coarse crystalline cavity fill was observed. Bitumen, in particular, at Bob deposit (Frontispiece B-b) fills cavity after saddle dolomite. Cerussite was confirmed at Arn deposit by x-ray diffraction. Hydrozincite was confirmed at Palm deposit (Fig. 3-11), and smithsonite at Arn deposit (Fig. 3-17) by electron microprobe analysis.

Table 3-3 summarizes the distinguishing characteristics of Mackenzie Platform carbonate-hosted Zn-Pb deposits with respect to host dolomite containing pyrite, whether dolomite cements (1) and (2) were formed from the same fluid, and presence or absence of ore-stage quartz.

Table 3-3. Summary of distinguishing characteristics of Mackenzie Platform carbonate-hosted Zn-Pb deposits. (* In Joli Green deposit the ore stage quartz occurs as a mélange with calcite.)

Deposit Name	Host contains pyrite	Dolomite cements (1) & (2) formed from same fluid	Ore-stage quartz
Ab-Cab	yes	likely	yes
Palm	yes	unlikely	yes
Bob	yes	unlikely	no
Mawer	yes	likely	yes
Bear	yes	likely	yes
Snobird	yes	likely	yes
Rev	yes	likely	no
Econ	no	unlikely	no
Ice	no	likely	no
Arn	no	likely	no
Rain	no	likely	no
Cypress	no	unlikely	yes
Tic	no	likely	yes
Joli Green	no	likely	yes*

POST-MINERALIZATION EFFECTS

Textures indicative of post-mineralization events have been observed in sphalerite, dolomite, quartz, and calcite and are listed in Table 3-4 and illustrated in Fig. 3-40 and 3-41. Evidence presented later (Chap. 7) constrain mineralization to the interval between Middle Devonian and Carboniferous. Post-mineralization effects, therefore, might be attributed to intrusion of Cretaceous granitic stocks and associated deformation (Anderson, 1988).

Table 3-4. Post-mineralization effects.

Deposit	Mineral	Feature	Example
Gayna	1) sphalerite	1-a) deformation twins 1-b) inclusions aligned along former cleavage fractures	1-a) Fig. 3-40 (a) 1-b) Fig. 3-40 (b)
	2) quartz	2) wispy texture	
	3) calcite	3) deformation twins	
Cypress	1) sphalerite	1) decrepitated inclusions	1) Fig. 3-40 (c)
	2) quartz	2) wispy texture	
Palm	1) dolomite	1) deformation twins	
Bob	1) sphalerite	1) decrepitated fluid inclusions and bent cleavage planes	1) Fig. 3-40 (d) and (e)
	2) quartz	2) undulatory extinction	2) Fig. 3-40 (f)
	3) dolomite	3) deformation twins	3) Fig. 3-9 (e), 3-10 (e)
Econ	1) sphalerite	1) bent cleavage planes	
	2) quartz	2) wispy texture	
	3) calcite	3) deformation twins	3) Fig. 3-12 (b)
Joli Green	1) quartz and calcite melange	1) pressure solution effect	1) Fig. 3-19 and 3-20 (e)
	2) calcite	2) deformation twins	2) Fig. 3-20 (b)
Mawer	1) dolomite	1) deformation twins	1) Fig. 3-21 (e)
Bear	1) sphalerite	1) fractured	1) Fig. 3-41 (a)
	2) quartz	2) wispy texture	2) Fig. 3-41 (b)
	3) dolomite	3) stylolites	3) Fig. 3-41 (c,d)
Rev	1) sphalerite	1) bent cleavage planes and disrupted extinction	1) Fig. 3-41 (e)
	2) calcite	2) deformation twins	2) Fig 3-26

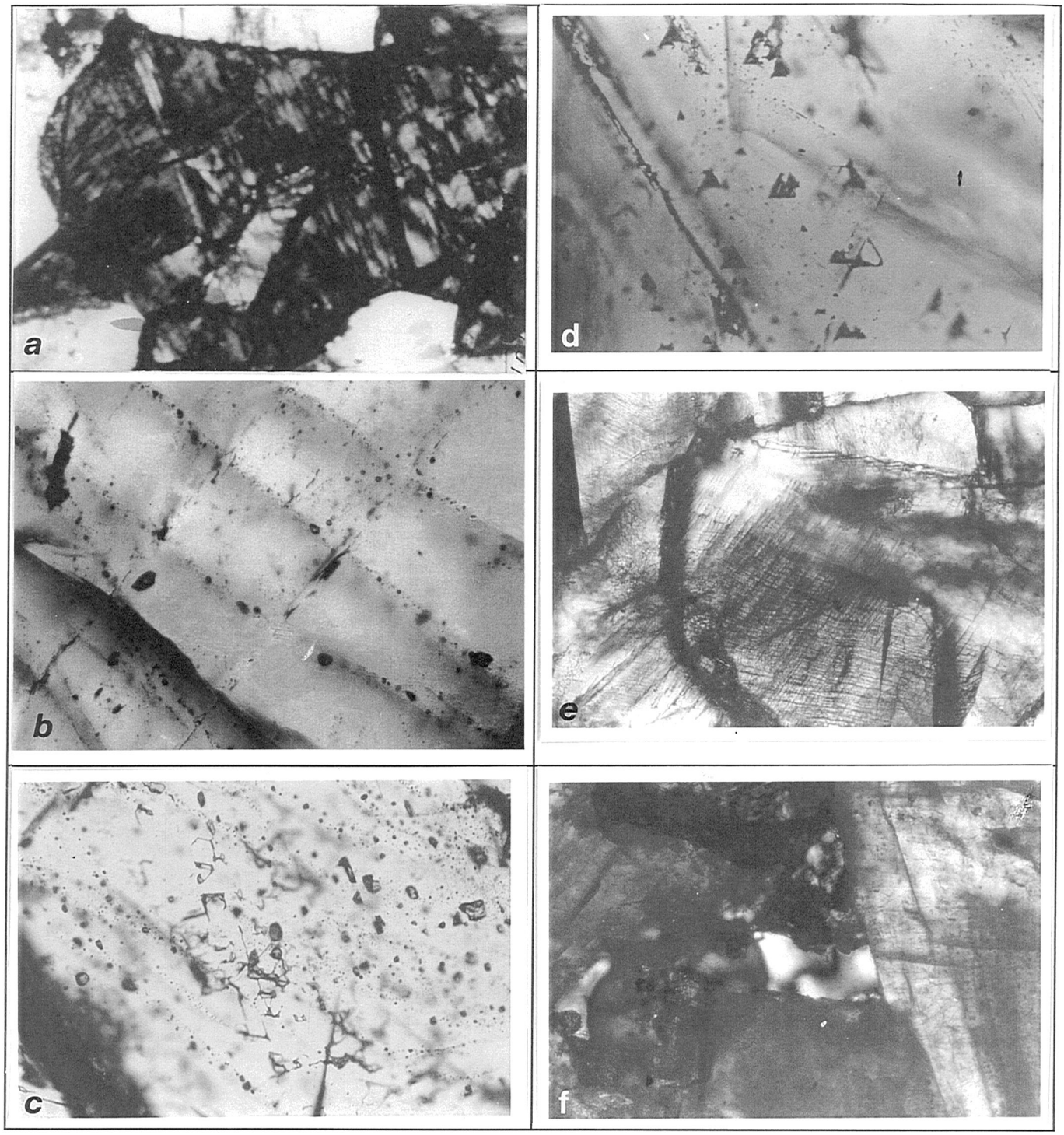

Fig. 3-40. Photomicrographs showing post-mineralization effects in deposits hosted in rocks older than Middle Cambrian (all photos taken in plane-polarized light unless stated otherwise). a) Gayna deposit, sample no. SP3409 showing twinned sphalerite grain. Photo taken in crossed-polarized light. Width of view equals 1.2 mm. b) Gayna deposit, sample no. SP3389A showing fluid inclusions aligned along former cleavage fractures. Width of view equals 1 mm. c) Cypress deposit, sample no. SP3266(2), showing decrepitated inclusions. Width of view equals 0.1 mm. d) Bob deposit, sample no. SP5399(1), showing decrepitated inclusions. Width of view equals 0.02 mm. e) Bob deposit, sample no. SP5399(1) showing bent cleavage planes in sphalerite. Width of view equals 0.13 mm. f) Bob deposit, sample no. SP5399(1) showing undulatory extinction in quartz (centre). Photo taken in cross-polarized light. Width of view equals 0.13 mm.

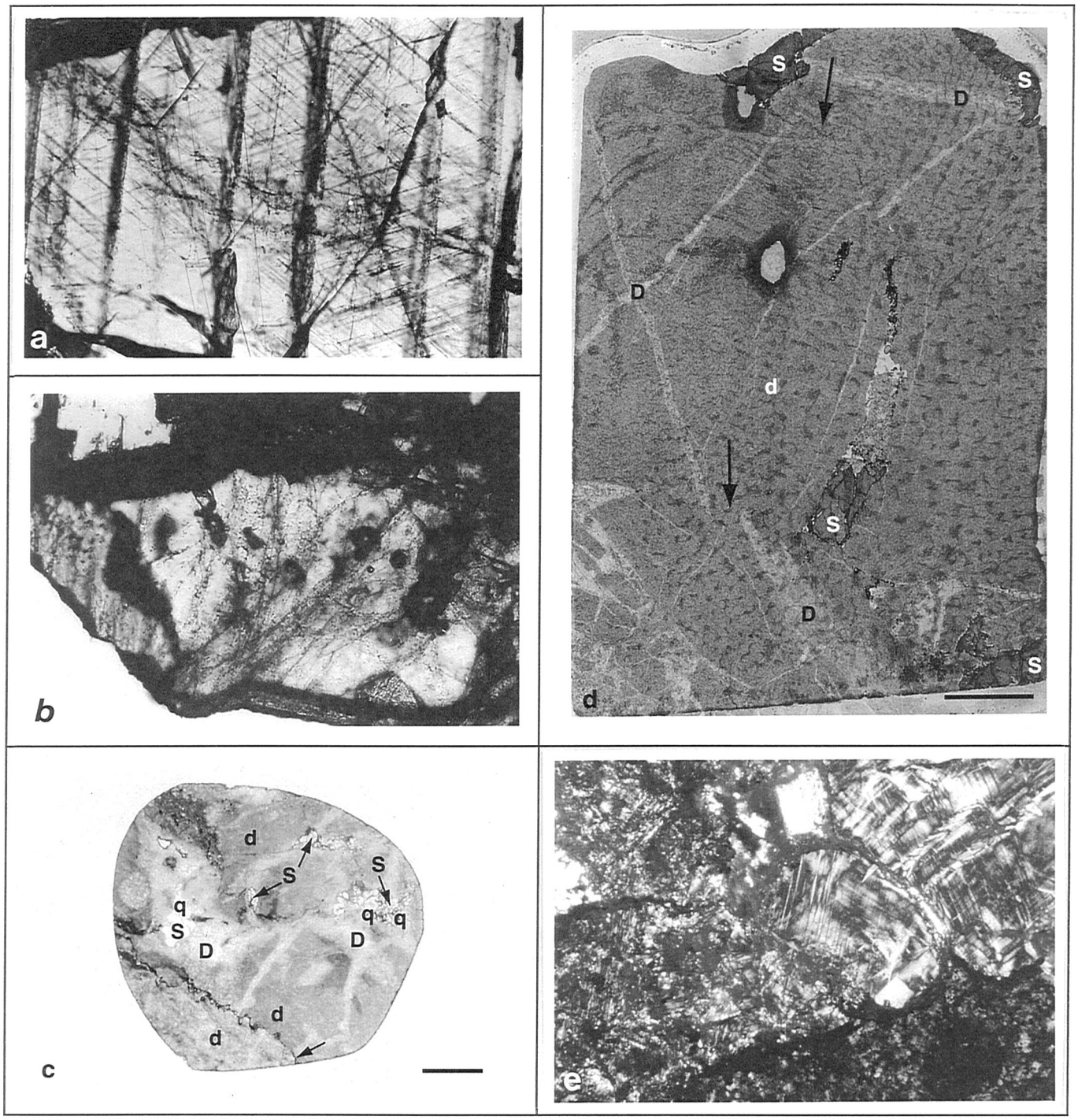

Fig. 3-41. Photomicrographs showing post-mineralization effects in deposits hosted in rocks younger than Middle Cambrian (all photos taken in plane-polarized light unless stated otherwise). a) Bear deposit, BEAR sample, showing healed fractures in sphalerite. Width of view equals 1.4 mm. b) Bear deposit, sample no. SP5489(2) displaying wispy texture created by many fluid inclusions trails criss-crossing the quartz grain. Width of view equals 1.4 mm. c) Bear deposit, sample no. SP5489(1), showing dolomite host rock (d) cut by stylolite (unlabelled arrow), saddle dolomite (D), followed by quartz (q) and sphalerite (S). Scale bar represents 0.5 cm. d) Bear deposit, sample no. SP5487, showing dolomite vein cement (D) cutting dolomite host rock (d), with sphalerite (S) in cavities. Stylolites are indicated by unlabelled arrows. Scale bar represents 0.5 cm. e) Rev deposit, sample no. SP5502(2) showing bent cleavage planes and disrupted extinction in sphalerite. Photo taken in crossed-polarized light. Width of view equals 1.4 mm.

4. MICROTHERMOMETRY

ANALYTICAL METHODS AND RESULTS

One thousand, seven hundred and thirty-two microthermometric determinations [homogenization temperature (Th)=1034 and melting temperature (Tm)=698] were carried out on inclusions in sphalerite, dolomite, quartz, calcite, and barite in doubly polished sections (100-150 μm thick) using a Linkam heating/freezing stage. The stage was calibrated both before and after measurements using SYNFLINC Synthetic Standards and an additional four compounds of known melting points ranging from -56.6° to 200°C. A calibration curve was constructed from the results and all Th and Tm temperatures were corrected accordingly. Criteria used to identify the fluid inclusions as primary, pseudosecondary, or secondary were based on those of Roedder (1984).

To limit the possibility of unknowingly measuring inclusions deformed by overheating in the lab, doubly polished sections were prepared carefully at temperatures not exceeding 80°C. In addition, only inclusions from one field of view per chip were measured during a heating/freezing run. Attempts were made to isolate Fluid Inclusion Assemblages (FIA). An FIA is a group of petrographically associated fluid inclusions that resulted from the same, most finely discernable event of fluid inclusion entrapment. Data have been collected from primary inclusions in individual growth zones or pseudosecondary inclusions, of different sizes and shapes, in individual planes. Heating runs were conducted before freezing runs to reduce the possibility of inclusion stretching by freezing (Lawler and Crawford, 1983). All homogenization runs were repeated and results were replicated within 4°C; those exceeding this error limit were not recorded. Replication is a repetition of temperature measurements collected under the same experimental conditions, e.g. sample is not removed from the stage between measurements (Goldstein and Reynolds, 1994). Freezing runs were also repeated and results were replicated within 0.5°C. Poor optical characteristics of many inclusions and their small size combined to give an average estimated accuracy of ±2°C on readings above, and ±0.5°C on readings below 0°C.

INCLUSION TYPES

Fluid inclusions were studied using optical, ultraviolet (UV), and cathodoluminescence microscopy, and microthermometry. Five types of fluid inclusions were identified although not all five were present in any one deposit. They are shown in Fig. 3-1, and are defined as follows: **Type 1**, two-phase H_2O (l) + H_2O (v); **Type 2**, three-phase H_2O (l) + H_2O (v) + solid (rounded or disc shaped - not

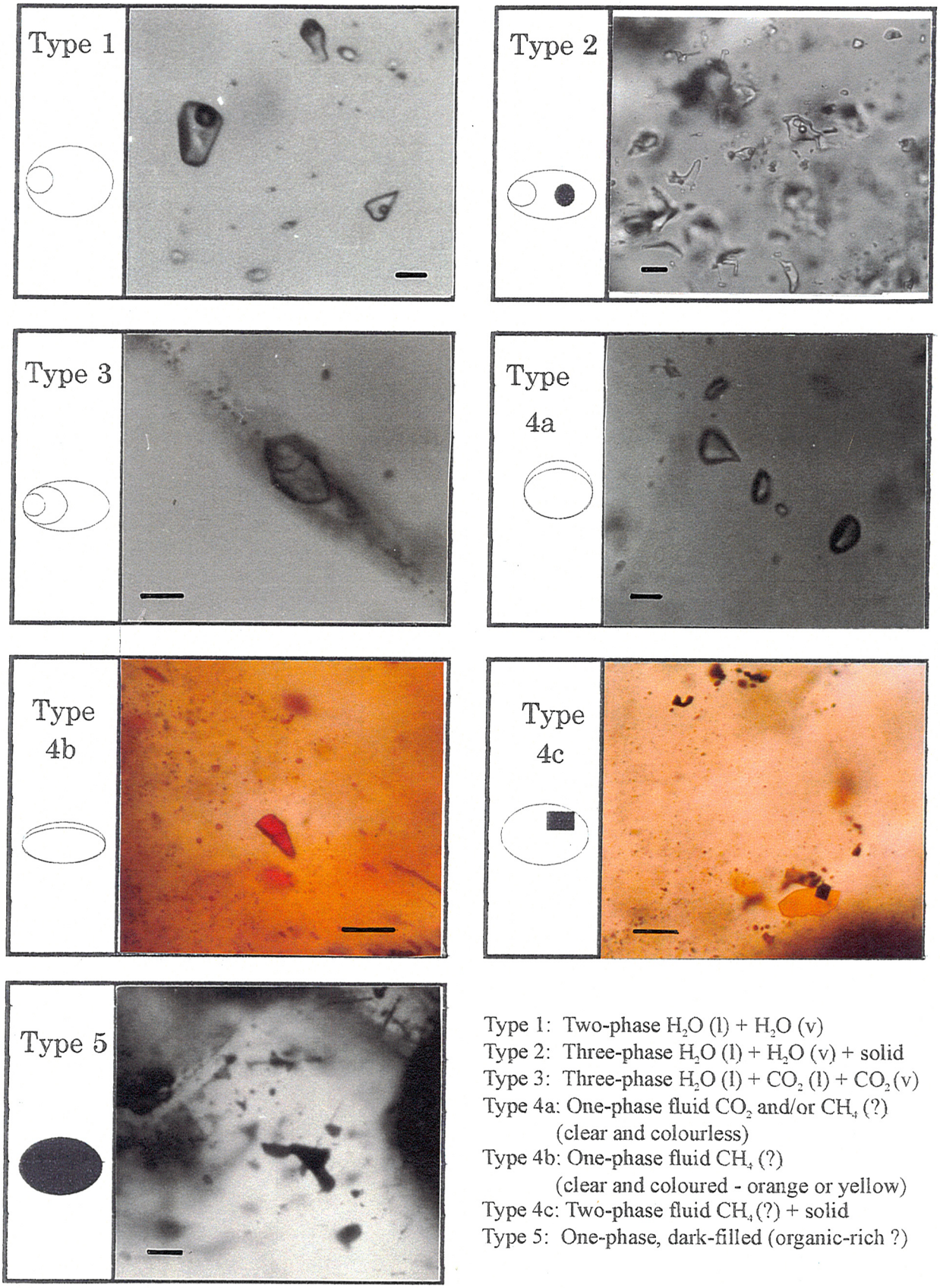

Fig.4-1. Fluid inclusions types illustrated by diagrams (left) and photomicrographs (right) showing phase(s) observed at room temperature. Bar scale equals 10 μm.

halite); **Type 3**, three-phase H_2O (l) ,+ CO_2 (l) + CO_2 (v); **Type 4a**, one-phase fluid CO_2/CH_4 (clear and colourless), **Type 4b**, one-phase fluid CH_4 (?) (clear and coloured - orange or yellow), **Type 4c**, two-phase fluid CH_4 (?) + solid; and **Type 5**, one-phase, dark-filled (organic-rich ?). Fluid inclusions are considered to be primary or pseudosecondary based on three modes of occurrence within a single grain: i) isolated; ii) in 3-D clusters; or, iii) distributed in planes. When the identification was not obvious the inclusions were classed as pseudosecondary/secondary. The distribution of these types is summarized in Table 4-1.

Table 4-1. Summary of inclusion types, deposits and minerals in which they occur. Microthermometry has been conducted in all cases except those underlined, (sphal=sphalerite, dol=dolomite, qtz=quartz, calc=calcite).

Type 1		Type 2
Gayna River - sphal, dol, qtz Cypress - sphal, dol, qtz Econ - sphal, dol, calc, barite Ab - sphal Cab - sphal, dol, qtz Palm - sphal, dol, qtz Bob - sphal Mawer - sphal, dol Joli Green - sphal, dol Bear - sphal, dol, qtz Rev - sphal, dol, qtz		Econ - sphal Cab - qtz
Type 3		Type 4a
Rev - sphalerite		Gayna - sphalerite Econ - sphalerite Ab - sphalerite Cab - sphalerite Palm - dolomite Bob - sphalerite Bear - dolomite, quartz
Type 4b		Type 4c
Bob - sphalerite Joli Green - sphalerite Rev - sphalerite		Rev - sphalerite
Type 5		Decrepitated Inclusions - sphalerite
Cypress - sphalerite Cab - sphalerite Bob - sphalerite		Cypress - sphalerite Bob - sphalerite

MICROTHERMOMETRIC RESULTS FOR TYPE 1

Type 1 fluid inclusions occur in sphalerite, dolomite, quartz, calcite, and barite, and homogenize to a liquid upon heating. Vapour bubbles typically occupy 5-10% by volume of the fluid inclusion. They occur in all deposits as primary, pseudosecondary, and secondary inclusions. Microthermometric results for **Type 1** aqueous fluid inclusions are summarized in Table 3-2. The data are presented in order of age of host rock from oldest (Proterozoic) to youngest (Devonian).

Table 4-2. Summary of microthermometric results of **Type I** aqueous fluid inclusions.

Deposit	Host	Stage	Type	No.	Tn - ice (°C)	Tm - 1st (°C)	Tm - ice (°C)	Salinity (Range)	Salinity (Mean)	No.	Th (°C) (Range)	Th°C (Mean)
Gayna R.	Sphalerite	ore	P/PS	53	-60 to -75°	< -26 to -44°	-11.5 to -28.2°	15.5-26.5	20.2	66	127-216°	169°
	Quartz	syn/post-ore	P/PS	44	-51 to -70°	< -26 to -43°	-10.0 to -23.4°	13.9-24.5	18.4	44	132-228°	176°
Cypress	Sphalerite	ore	P/PS	20	-51.6 to -69.5°	< -30 to -45°	-5.6 to -21.0°	8.6-23.0	12.9	12	140-169°	157°
	Sphalerite	ore	PS/S	45	-42 to -50.6°	< -30 to -45°	-2.0 to -4.4°	3.3-6.8	4.8	33	140-227	187°
	Dolomite	syn/post-ore	P/PS	9	-46.9 to -71.5°	< -30 to -40°	-2.3 to -22.5°	3.9-24.0	12.8	17	144-246°	180°
	Quartz	syn/post-ore	P/ PS	36	-46.5 to -49.5°	< -23 to -35°	-2.0 to -3.7°	3.4-6.0	4.6	44	172-242°	209°
Econ	Sphalerite(2)	ore	PS	17	-61.0 to -65.4°	< -30 to -47°	-11.7 to -12.8°	15.7-16.7	16.2	9	112-138°	124°
	Sphalerite(2)	ore	PS/S	35	-42.3 to -52.0°	< -11 to -35°	(-4.9 to -11.5°)	(4-15.5)	(6.4)**	60	116-147°	132°
	Dolomite	syn/post-ore	P/PS							1		149°
	Sphalerite(2)	ore	PS/S	2	-46.1 to -47.3°			4-7	(5)**	11	113-145°	130°
	Dolomite	syn/post-ore	P/PS	1	-51.2°		-4.2°		6.7	1		153°
	Calcite	post-ore	P/PS	20		< -22 to -35°	-2.4 to -8.5°	4.1-12.3	9.0	18	127-146°	137°
	Barite	post-ore	PS/S	8	-46.0 to -55.9°	<-26 to -33°	-2.9 to -6.6°	4.8-9.9	8.0	16	107-142°	124°
Cab	Dolomite(1)	pre-ore	P/PS	6	-64.0 to -79.9°	< -42°	-12.4 to -15.2°	16.3-18.8	17.8	12	147-199°	176°
	Sphalerite(1)	ore	P/PS	5	-54.9 to -69.1°	< -45°	(-12.6 to -17.9°)	(16.5-20.5)	(18.9)	12	147-199°	153°
	Dolomite(2)	syn-ore	P/PS	3	-61.3 to -81.9°	< -46°	-9.8 to -17.7°	13.7-20.7	17.6	17	169-249°	213°
	Quartz(2)	syn-ore	P/PS	20	-54.7 to -71.2°	< -35 to -50°	-8.0 to -20.6°	11.7-22.8	19.1	42	172-269°	222°
	Sphalerite(2)	ore	P/PS	36	-67.9 to -84.9°	-36.2 to -56.2°	-15.8 to -25.3°	19.3-24.5	22.4	31	88-123°	104°

Deposit	Host	Stage	Type	No.	Tn - ice (°C)	Tm - 1st (°C)	Tm - ice (°C)	Salinity (Range)	Salinity (Mean)	No.	Th (°C) (Range)	Th°C (Mean)
Ab	Sphalerite(1)	ore	P/PS	6	-50.5 to -78.9°	< -47°	(-9 to -20.5°)	(12.8-22.7)	(15.6)	11	102-122°	111°
	Sphalerite(2)	ore	P/PS	2	-79.4 to -81.8°	< -45°	-21.1 to -21.3°	23.1-23.2	23.1	28	91-122°	109°
Bob	Sphalerite	ore	PS/S	3	-40 to -45°	< -27°	-5.3 to -6.8°	8.2-10.2	9.4	5	96-137°	122°
	Dolomite	pre/syn-ore			No fluid inclusions found							
Palm	Dolomite	pre/syn-ore	P/PS	5	-71.4 to -79°		-14.4 to -21.7°	18.1-23.6	21.5	32	171-203°	189°
	Sphalerite	ore	P	8	-59 to -72.6°	< -40 to -48°	-13.2 to -18.7°	16.9-21.5	19.0	11	134-153°	145°
	Quartz	post-ore	PS/S	2	-36.6 to -37.7°		-1.9 to -2.2°	3.2-3.7	3.5	2	178-188°	183°
Joli Green	Dolomite	pre-ore	P/PS	11	-74.6 to -84.7°	~-53 to ~-56°	-26.3 to -27.9°	25.5-26.3	26.1	14	191-236°	211°
	Sphalerite	ore	P/PS	9	-88.1 to -93.2°	-50 to ~-55°	-25.9 to -28.2°	25.5-26.3	25.6	10	105-168°	130°
	Sphalerite	ore	PS/S	4	-69.7 to -77.6°	< -50°	-12.5 to -19.5°	16.4-21.3	19.1	11	178-247°	209°
Mawer	Sphalerite	ore	P/PS	10	1) -59.8 to -65.5° 2) -69.0 to -71.8°	< -40 to ~-45°	-15.4 to -17.6°	18.9-20.7	19.8	10	151-190°	171°
	Dolomite	post-ore	P	17	-68.2 to -94.4°	~-58 to -60.3°	-26.0 to -35.3°	25.5-27.0	26.3	25	175-227°	208°
Bear	Dolomite	pre/syn-ore	P/PS	19	-34.9 to -86.4°	~-44 to ~-49°	-17.6 to -25.3°	20.7-25.0	23.8	42	161-248°	210°
	Quartz	pre/syn-ore	P/PS	8	-63.7 to -82.4°	~-45 to -49°	-21.2 to -24.2°	23.2-25.0	24.3	5	216-255°	235°
	Sphalerite	ore	P	1	-75.5°	~ -43°	-22.9°		25	1		203°
	Sphalerite	ore	PS	71	-58.1 to -67.8°	~-45 to -50°	-10.3 to -16.0°	14.2-19.4	16.9	84	142-213°	188°
	Sphalerite	ore	S	14	-42.6 to -47.8°				low	14	94-124°	118°
	Quartz	syn-ore	PS/S	16	-46.4 to ~-69°	~-41 to -52°	-10.4 to -16.4°	14.4-19.8	16.6	18	158-227°	204°
	Quartz	post-ore	S	11	-44.6 to -48.3°	~-35 to -45°	-0.4 to -5.1°	0.7-8.0	4.1	12	220-254°	236°

Deposit	Host	Stage	Type	No.	Tn - ice (°C)	Tm - 1st (°C)	Tm - ice (°C)	Salinity (Range)	Salinity (Mean)	No.	Th (°C) (Range)	Th°C (Mean)
Rev	Sphalerite	ore	P/PS	9	-57.6 to -79.4°	< -45 to -59°	-21.2 to -28.7°	23.2-26.3	25.2	20	146-218°	175°
	Sphalerite	ore	PS/S	4	-64.3 to -69.8°	~-50 to -55°	-12.4 to -15.1°	16.3-18.7	17.6	9	140-225°	192°
	Sphalerite	ore	S	2			-4.1 to -4.4°	6.6-7.0	6.8	7	131-213°	177°
	Sphalerite -all data	ore	P/PS/ S	19			-1.9 to -28.7°	3.23-26.3	20.5	59	108-225°	160°
	Dolomite	syn-ore	P/PS	49	-60.7 to -88.2°	~-55 to ~ -76°	-20.9 to -30.5°	22.9-26.3	25.0	71	140-236°	204°

Locations of deposits are shown in Figure 1-1. Host=mineral containing the fluid inclusions, Stage=pre-ore, ore, syn-ore, post-ore, Type= P for primary, PS for pseudosecondary, and S for secondary, No.= number of inclusions for which the data has been summarized, Tn-ice(°C)=temperature of nucleation of the ice, Tm-1st(°C)= first melting temperature i.e. an approximation of eutectic temperature (Te) the values given represent the temperatures at which melting processes started to be observable and the actual Te could be lower than the temperature observed, Tm-ice(°C)=temperature at which the ice melted, salinity=equivalent wt. % NaCl, Th (°C)=homogenization temperature. Blank spaces means that no data was collected usually because phase changes were too subtle to see. Temperatures in brackets are based on limited observations. **Salinity data derived from Tn - ice because no Tm - ice could be observed. Based on the premise that, in general, the lower the temperature of freezing (Tn - ice) the more dissolved salt the inclusion contains (Roedder, 1984).

MICROTHERMOMETRIC RESULTS FOR **TYPES 2 TO 5**

Type 2, three-phase H_2O (l) + H_2O (v) + solid, fluid inclusions occur in sphalerite and quartz, and homogenize to a liquid upon heating. Vapour bubbles occupy 5-10% by volume of the fluid inclusion. The melting temperature of the solid was not determined. This type has limited occurrence, found only at Econ as primary/pseudosecondary inclusions in sphalerite and as pseudosecondary/secondary inclusions at Cab in quartz.

Type 3, three-phase H_2O (l) + CO_2 (l) + CO_2 (v), fluid inclusions were found only at Rev as secondary inclusions in sphalerite. The CO_2(v) phase (i.e. the inner bubble) homogenized to a liquid between 28.7° and 31.1°C. The CO_2(l) phase homogenized before decrepitating in those inclusions near critical density. The probability of such inclusions decrepitating before final homogenization is high and commonly occurs unless the inclusion has a near critical density. Of 13 CO_2-H_2O inclusions in sphalerite, five inclusions decrepitated between 217° and 267°C. The remaining eight were then subjected to numerous freezing runs where the temperature of nucleation of CO_2 and the melting temperature indicated the presence of pure CO_2. Microthermometric results for six of the eight **Type 3** inclusions are given in Table 4-3 below.

Table 4-3. **Type 3** Rev CO_2-H_2O inclusions in sphalerite.

Rev SP5504(2) Chip #9	Tmin (°C)	Th (°C)	Tm(ice) (°C)	Tn(ice) (°C)	Tm (°C) clathrate	Tm(CO_2) (°C)	Tm(CO_2) corrected	Tn(CO_2) (°C)	Th (CO_2)	Td (°C)
No. 0.	-127.2°		-7.4°	-41.8°	0.1°	-59.2°	**-56.2°**	-100.5°	29.9°	391°
4.										225°
5.	-125.2°		1.1°	-36.3°	5.7°	-59.3°	**-56.3°**	-89.8°	30.5°	313°
7.	-121.7°	336°	-0.7°	-42.4	2.1°	-59.3°	**-56.3°**	-98.5°	29.5°	282°
8.									29.9°	
12.										217°
13.			-5.2°	<-47°	(-0.7°)	-59.2°	**-56.2°**	-99.6°	30.3°	346°
14.	-121.4°									254°
15.	-120.2°	>350°	0.7°		2.2°	-59.2°	**-56.2°**	-100.8°	30.4°	
16.										255°
17.										267°

No.= number of inclusion for which the data was collected, Tmin=lowest temperature to which inclusion was subjected, Th=homogenization temperature, Tm-ice(°C)=temperature at which the ice melted, Tn-ice(°C)=temperature of nucleation of the ice, Tm-clathrate=temperature at which solid CO_2-hydrate melted, Tm(CO_2)C°=temperature at which the CO_2(l) melted, Tm(CO_2) corrected=temperature corrected from the calibration curve, Tn(CO_2)°C=temperature of nucleation of the$_2$ CO (l), Th(CO_2)=homogenization temperature of CO_2(v), Td=temperature of decrepitation.

Type 4a, one-phase fluid CO_2/CH_4 inclusions, occur in sparse quantities in most deposits, as noted below. One-phase fluid CO_2 (clear and colourless) inclusions, at room temperature, at greater than critical density, nucleated a vapour bubble upon cooling before the temperature reached 0°C. Other characteristic behaviour included the fact that ice nucleated upon cooling at around -103°C, and melted between -58.7° and -60.4°. CO_2 homogenized between 2.6° and 13.8°C. The "low" melting temperature of CO_2 indicates the presence of additional volatile phases, probably CH_4 (Roedder, 1984).

Gayna River - CO_2 and CH_4 confirmed in sphalerite sample SP3408B by quadrupole mass spectrometric analysis - crush-leach method (see Fig. 4-2 for graph and analysis). The analysis showed the presence of significant CH_4 and CO_2 contained in either one-phase inclusions, such as those noted in sphalerite, or possibly in the vapour bubble phase of primary/pseudosecondary, modified, Type 1 inclusions. Note that **Type I** inclusions were not defined as containing vapour other than H_2O because this has only been suspected, but has not been confirmed. The fact that many Type 1 fluid inclusions take longer, and a higher temperature, to homogenize than would be expected considering the size of the vapour bubble is often noted, and this effect could be caused by the presence of CO_2/CH_4 in the vapour bubble (Roedder, pers. comm., 1994).

Econ - CH_4-rich pseudosecondary/secondary inclusions were confirmed in sphalerite; low temperature microthermometry showed vapour bubbles forming at -185°C which then homogenized between -82° and -92°C. This low temperature behaviour distinguished these inclusions from aqueous inclusions (Fig. 4-3).

Ab - CO_2 and/or CH_4 pseudosecondary/secondary inclusions occur in sphalerite. In an attempt to identify the fluid in these inclusions, they were examined under UV (ultraviolet) light (50 watt arc lamp) at Carleton University, Ottawa under the direction of Dr. George Dix. As none of the inclusions fluoresced, two interpretations are plausible: i) no hydrocarbon is present; or, ii) the inclusions could be filled with "dead oil", that is to say, over-mature hydrocarbon, which does not fluoresce (Gize,1993; Burruss, 1981; Roedder, 1984).

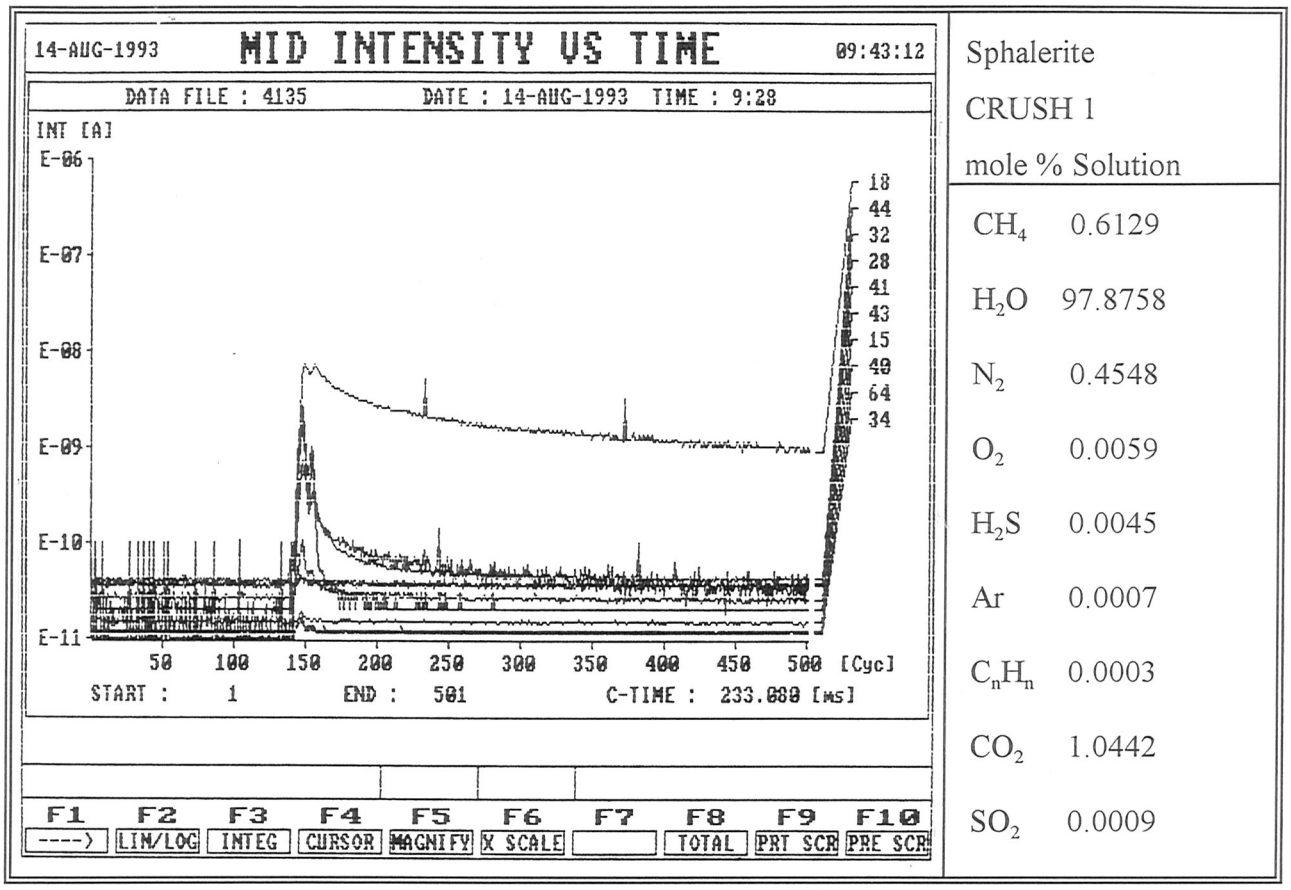

Fig. 4-2. Graph and analysis of CO_2/CH_4 confirmed in sphalerite Gayna River sample SP3408B by quadrupole mass spectrometric analysis, conducted at New Mexico Institute of Mining and Technology (D.I. Norman, pers. comm., 1993).

Fig. 4-3. Photomicrographs showing the location and mode of occurrence of confirmed CH_4 inclusions in sphalerite from sample Econ-1C Chip #11. The one-phase inclusions pictured above developed a vapour bubble on cooling to -185°C, and homogenized between -82° and -92°C. This low temperature behaviour distinguished them from aqueous inclusions. Width of view of photo on left equals 1.4 mm, and on the right equals 0.1 mm.

Type 4a

Cab - CO_2-rich pseudosecondary/secondary inclusions were confirmed in sphalerite by their low temperature behaviour.

Palm - unconfirmed CO_2 and/or CH_4 in dolomite.

Bob - unconfirmed CO_2 and/or CH_4 pseudosecondary/secondary inclusions in sphalerite.

Joli Green - unconfirmed CO_2 and/or CH_4 primary/pseudosecondary inclusions in sphalerite.

Bear - CO_2-rich pseudosecondary/secondary inclusions confirmed in dolomite and quartz (see Carrière and Sangster, 1996). Microthermometric results for **Type 4a** one-phase fluid CO_2 inclusions (clear and colourless) in dolomite and quartz from Bear deposit are recorded in Table 4-4 below.

Sample I.D. Number	Host	No.	Tm CO_2	Th CO_2	Tn °C
SP5487 Chip #11	dolomite	6	-60.2 to -60.4°	4.8° to 6.9°	-101 to 103.9°
SP5489(1) Chip #16	quartz	8	-60.4°	2.6 to 11.3°	-101 to -103.9°
SP5489(2) Chip #7	quartz	7	-58.7 to -58.9°	4.0 to 13.8°	-100.4 to -102.9°

Table 4-4. **Type 4a** CO_2 inclusions in dolomite and quartz from the Bear deposit. Sample identification number, No.=number of inclusions, melting (Tm) and homogenization (Th) temperatures, temperature of nucleation (Tn).

Rev - unconfirmed CO_2 and/or CH_4 pseudosecondary/secondary inclusions in sphalerite.

Type 4b, one-phase fluid CH_4 (?) (clear and coloured - orange or yellow), inclusions showed no phase changes during heating and freezing runs. Limited occurrence, only observed in three deposits as listed below:

Bob - unconfirmed CH_4 in pseudosecondary/secondary inclusions in sphalerite.

Joli Green - unconfirmed CH_4, limited occurrence in pseudosecondary/secondary inclusions in sphalerite.

Rev - unconfirmed CH_4, very abundant as primary(?), pseudosecondary/secondary inclusions in sphalerite.

Type 4c, two-phase fluid CH_4 (?) + solid, inclusions show no phase changes taking place during heating and freezing runs. Very limited occurrence, only found in Rev sphalerite.

Type 5, one-phase, dark (organic-rich ?), inclusions showed no phase changes during heating and freezing runs. Limited occurrence, only observed in the following deposits:

Cypress - abundant in sphalerite, but could be very dark Type 1 inclusions in some cases.

Cab - some sphalerite grains contain thousands of one-phase dark inclusions which are tiny near the outer edge of the grain and larger towards the core of the grain.

Bob - abundant in sphalerite.

VARIABILITY OF DATA - EXPLANATION AND SIGNIFICANCE

Attempts were made to collect enough data from various sizes and shapes of inclusions within a single FIA to represent the full range of variability. Data variability within a FIA suggests that immiscibility, reequilibration, or necking may have adversely affected inclusions within the FIA. Immiscibility involves the separation of CO_2- and/or CH_4-rich fluids from H_2O-rich fluids. It is well known that brines in the subsurface contain significant dissolved methane and, therefore, it is reasonable that some aqueous inclusions should contain methane, mainly partitioned into the bubble. Some inclusions in the study have been shown to contain detectable CH_4 through cooling runs and quadrupole mass spectrometer analysis. One-phase CO_2-rich and CH_4-rich fluid inclusions are present in several deposits and indicate either immiscibility during inclusion entrapment or post-entrapment volume changes, i.e. necking. According to Hanor (1980) if there is methane or some other compressed gas present, then Th of the inclusions should be interpreted with caution. The presence of methane complicates the interpretation of inclusion behaviour and could yield homogenization and apparent entrapment temperatures (Tt) that are erroneously high (possibly in excess of 30°C). The effects of CH_4 on Tm ice are relatively minor.

Stretching is the nonelastic deformation of fluid inclusion walls in response to an increase in internal pressure as the temperature is raised (Bodnar and Bethke, 1984) or by expansion of ice due to freezing (Lawler and Crawford, 1983) which produces a volume increase and a concomitant increase in the fluid inclusion Th in subsequent heating tests, without loss of the inclusion contents. Stretching or necking of inclusions is commonly the result of overpressuring from natural heating and results in reequilibration. Sources of natural heating include burial and the presence of nearby igneous intrusions. There is a strong and positive relationship between a mineral's ability to withstand high fluid inclusion internal pressure and its hardness. Moreover, easily cleavable minerals, such as sphalerite, deform more

readily than those without cleavage. Minerals such as calcite and quartz tend towards plastic deformation while dolomite is more prone to brittle deformation. Each inclusion within a FIA may behave differently during overheating. Some inclusions will reequilibrate easily and repeatedly, and other inclusions may not reequilibrate at all. The variables that control whether or not reequilibration takes place include strength of the enclosing crystal, amount of overheating, confining pressure, other stresses, P-V-T properties, composition of the fluid, and the shape, size, and orientation of the inclusion, and the inclusion position relative to dislocations or discontinuities in the crystal. Each of these variables could exert an effect on a population of overheated fluid inclusions to cause significant variability in the Th data. The amount of overheating required to initiate stretching of inclusions in sphalerite ranges from <8°C for an inclusion several hundred micrometres in diameter to >75°C for a 10-μm-diameter inclusion. Regularly shaped inclusions are less likely to stretch than irregularly shaped inclusions in all minerals; smoothly rounded to subhedral inclusions are more resistant to stretching than are angular or negative crystal-shaped inclusions. Inclusions of different sizes and shapes, therefore, respond differently to processes of thermal reequilibration, and will yield a range of data if such a process occurred. The degree of stretching will determine the new temperature of homogenization (Th). The exact temperature to which a fluid inclusion has been subjected is not the new Th. The new Th is higher than the original temperature of entrapment (Tt), but less than that to which the mineral was heated. Only under extreme conditions is complete reequilibrium to the new conditions ever attained. For example, a burial depth of greater than 5 km would be required to completely reequilibrate all inclusions.

VARIABILITY OF DATA - THIS STUDY

Table 4-5 lists the data variation for sphalerite from 12 deposits. Table 4-6 lists the data variation for other minerals associated with sphalerite - dolomite, quartz, calcite, and barite, for nine deposits. When the data from this study are examined a moderate variability in the Th data is observed for most of the deposits, i.e. moderate variability occurs when inclusions of variable size and shape measured in a single FIA do not have 90% of the Th data within a 10-15°C interval. Goldstein and Reynolds (1994) state that data of moderate variability are geologically reasonable and a significant proportion of FIAs data from fluid inclusions in sedimentary systems yield such moderately variable data. Moderately variable Th data for individual FIAs may be due to thermal reequilibrium, undetectable necking down, or may represent unaltered fluid inclusions collected from FIAs with real

variability; that is, FIAs that formed over a range of P-T-X conditions with time (particularly likely for inclusions in dolomite). Perhaps the original formation conditions may never be determined from the microthermometic data; however, these data do yield useful information about mineralizing fluids (Goldstein and Reynolds, 1994). In this study, inclusions in the FIAs measured have experienced processes that have caused some degree of thermal reequilibration and, therefore, the Th's are likely higher than the actual temperature of homogenization/entrapment due to one or all of the reasons stated above.

Table 4-5. Data Variation for Sphalerite.

Property	Size range per FIA* (length) and\or (length x width)	Shapes# per FIA (1-5)	No.	Th range(°C) per FIA	Maximum Variation 100% (90%)
Gayna River	1) (approx. 5 to 9 µm)	2	5	127-141°	14°
	2) 7.5 to 20x10 µm	3,4,5	6	139-169°	30° (14°)
	3) 7 to 12.5 µm	2,3,5	6	141-180°	39° (29°)
	4) 5 to 9 µm	2,3,5	4	166-172°	6°
	5) 9x5 to 29x7.5 µm	2,3,5	7	168-199°	31° (23°)
	6) 7.5 to 12 µm	2,5	7	153-216°	63° (43°)
	7) 2 to 12.5 µm	2,5	4	142-153°	11°
	8) 7.5 to 17.5 µm	2,5	3	175-181°	6°
	9) no data	2,5	4	149-191°	42° (28°)
Cypress	1) 4.5 to 10.5 µm	4,5	4	140-169°	29° (20°)
	2) 4.5 to 15 µm	1,2	6	140-163° 150-	23° (17°)
	3) 4.5 to 6 µm	2,4	5	167°	17° (13°)
	4) 6 to 16.5 µm	4,5	5	216-227°	11°
	5) 4.5 to 6 µm	4,5	4	161-213°	52° (27°)
	6) 6 to 12 µm	2,4	5	204-236°	32° (24°)
	7) 12 to 33 µm	3,5	4	145-182°	37° (20°)
Bob	1) 4 to 4.5 µm	3,5	2	137-141°	4°
Ab	1) 6x9 to 12x15 µm	1,2	5	91-116°	25° (17°)
	2) 9x9 to 18x36 µm	2,5	4	91-114°	23° (20°)
	3) 12x12 to 15x15 µm	2,3	4	104-119°	15°
	4) 6x9 to 9x18 µm	2,5	4	114-122°	8°
	5) 3x12 to 15x15 µm	2,4	5	114-122°	8°
	6) 4x6 to 5x15 µm	2,3,5	4	101-106°	5°
	7) 6x10 to 15x18 µm	2,5	4	100-111°	11°
	8) 6x12 to 12x45 µm	5	5	115-118°	3°
Econ	1) 4.5 to 16.5 µm	1,2,3,4	9**	130-132°	2°
	2) 2.5 to 4 µm	2,5	5**	116-127°	11°
	3) 9 to 18 µm	2,5	4**	116-123°	7°
	4) 12 to 30 µm	2,5	4**	121-125°	4°
	5) 9 to 22 µm	2,5	5**	126-133°	7°
	6) 6 to 15 µm	2,5	8**	125-130°	5°
	7) 4 to 6 µm	2,5	4	111-121°	10°
	8) (approx. 5 to 15 µm)	5	3**	124-130°	6°

Table 4-5. Data Variation for Sphalerite (con't):

Property	Size range per FIA* (length) and\or (width x length)	Shapes# per FIA (1-5)	No.	Th range(°C) per FIA	Maximum Variation 100% (90%)
Bear	1) 4 to 7 µm	1,2	9	200-203°	3°
	2) 7.5 to 12 µm	2,5	5	173-196°	23° (20°)
	3) 4 to 11 µm	2,5	8	188-197°	9°
	4) 6 to 21 µm	2,5	6	176-183°	7°
	5) 5 to 13 µm	2	6	176-186°	10°
	6) 4 to 25 µm	2,5	14	195-204°	9°
	7) 4 to 10x6 µm	2,5	4	146-154°	8°
	8) 6 to 18 µm	1,2	7	168-190°	22° (15°)
	9) 3 to 15 µm	1,2,5	7	177-199°	22° (7°)
	10) 3.5 to 5 µm	1,2	5	185-193°	8°
	11) 2x4 to 10x12 µm	2,5	8**	116-124°	8°
Palm	1) 4.5 to 12 µm	1,2	5	139-153°	14°
	2) 5x7 to 12x14 µm	1,5	3	134-153°	19° (10°)
Joli Green	1) 5 to 10 µm	4,5	7	105-129°	24° (18°)
	2) 3 to 8 µm	2,4	3	159-168°	9°
	3) 4 to 8 µm	2,4	3	194-216°	22° (17°)
	4) 2.5 to 5 µm	2,3	4	202-247°	45° (33°)
Cab(SPLR 2)	1) 6x6 to 30 µm	2,3,5	6	101-106° 88-	5°
	2) 9x9 to 15x30 µm	2,3	6	101°	13°
	3) 6x9 to 15x18 µm	1,2,3,4,5	7	100-112°	12°
	4) 4 to 18 µm	1,2,3,4,5	5	101-123°	22° (15°)
Cab(SPLR 1)	5) (approx. 4 to 8 µm)	2,5	6	130-166°	36° (25°)
Mawer	1) 5 to 12x10 µm	1,2	4	170-182°	12°
	2) 4 to 6 µm	2	5	151-177°	26° (19°)
Rev	1) 5x1.5 to 5x4 µm	1,2,3,	4	146-181°	39° (19°)
	2) 4x3 to 6x4.5 µm	1,4,5	3	154-175°	21° (11°)
	3) 3x3 to 7x4 µm	1,2,3,4,5	10	163-225°	62° (30°)
	4) 3x2 to 6x3 µm	1,2	5	147-172°	25° (22°)
	5) 4x3 to 5x4.5 µm	1,2,5	8	150-181°	31° (17°)
	6) 3x2 to 10x8 µm	1,3	6	134-174°	40° (35°)
	7) 4x3 to 13x6 µm	1,2,5	10	178-207°	29° (20°)

* FIA - Fluid Inclusion Assemblage is a group of fluid inclusions that resulted from the same most finely discernable event of fluid inclusion entrapment. Data have been collected from primary inclusions in individual growth zones or pseudosecondary inclusions in individual planes of different sizes and shapes. Some FIA's of secondary inclusions are included. No. = Number of inclusions in the FIA

** Low salinity inclusions Tm=<-5°C and Salinity =< 8 equiv. wt. % NaCl

*** Moderate salinity inclusions Tm= or >-5 and = or < -6.7°C and Salinity = 8 to 10 equiv. wt. % NaCl

#Shapes: 1=round, 2=oval or oblong, 3=square or rectangle, 4=triangular, 5=irregular

Table 4-6. Data variation for dolomite, quartz, calcite, and barite.

Property	Size range per FIA* (length) and/or (length x width)	Shapes# per FIA (1-5)	No.	Th range(°C) per FIA	Maximum Variation 100% (90%)
Gayna River (Quartz)	1) 5 to 35 μm	2,5	7	141-202°	61° (49°)
	2) 5 to 15 μm	2,5	6	140-201°	61° (30°)
	3) 12 to 15 μm	2,5	5	170-239°	69° (58°)
	4) 4 to 12 μm	3,5	4	170-215°	45° (15°)
	5) 7 to 20 μm	2,3,5	9	150-200°	50° (16°)
	6) 9 to 25 μm	2,3,5	5	152-226°	74° (49°)
	7) 9 to 15 μm	2,5	7	144-202°	58° (27°)
	8) 9 to 15 μm	2,3	5	132-145°	13°
	9) no data		5	191-205°	14°
Cypress (Quartz)	1) 7.5 to 12 μm	2,5	6**	181-236°	55° (45°)
	2) 4.5 to 21 μm	2,5	5**	198-225°	27° (21°)
	3) 6 to 36 μm	2,5	6**	175-226°	51° (39°)
	4) 6 to 12 μm	2,5	8**	206-236°	30° (25°)
	5) 4.5 to 6 μm	2,5	4**	172-222°	50° (45°)
	6) 4.5 to 36 μm	2,5	10**	193-243°	50° (39°)
(Dolomite	1) 4.5 to 9 μm	3	4	157-197°	40° (21°)
	2) 5 to 7.5 μm	3	3	144-175°	31° (6°)
	3) 4.5 to 6 μm	3	3	162-179°	17°
Bear (Dolomite)	1) 3 to 6 μm	2,3,5	6	231-244°	13°
	2) 2 to 7 μm	2,3,5	6	161-241°	80° (50°)
	3) 3x2.5 to 6 μm	3,5	6	191-249°	58° (33°)
	4) 2x2 to 5 μm	2,3,5	6	166-189°	23° (20°)
	5) 2x2 to 5 μm	2,3,5	3	206-244°	38° (35°)
	6) 3 to 5 μm	2,3	3	176-183°	7°
	7) 4 to 6 μm	3,5	3	187-207°	20° (14°)
(Quartz)	1) 4x5 to 5x7 μm	2,3,5	5	222-227°	5°
	2) 5 to 20 μm	2,5	4	189-236°	47° (24°)
	3) 1.5x5 to 3x13 μm	2,3,5	6**	217-265°	48° (22°)
	4) 3x6 to 5x6(3x7)μm	(2,5)	5	192-227°	35° (21°)
	5) 3 to 6 μm	2,3,5	6	172-189°	17° (13°)
Palm (Dolomite)	1) 2 to 5 μm	3,5	7	188-197°	9°
	2) 2 to 4 μm	3,5	5	174-197°	23° (18°)
	3) 2 to 4 μm	3,5	4	192-194°	2°
	4) 2x2 to 2x3 μm	3,5	6	174-203°	29° (15°)
	5) 1.5x1.5 to 3x4 μm	3,4	4	172-180°	8°
	1) 1.5x3 to 2.5x6 μm	3	2**	169-179°	10°
Joli Green (Dolomite)	1) 1.5x2 to 3x3 μm	2,3	5	210-236°	26° (19°)
	2) 1.5x1.5 to 5x5 μm	2,3	4	187-207°	20° (16°)
	3) 1x3 to 3x10 μm	2,3	5	203-220°	17° (15°)

Econ (Calcite)	1) 6 to 12 µm	2,5	5***	124-131°	7°
	2) 9 to 27 µm	2,5	4***	137-142°	5°
	3) 4.5 to 15 µm	2,5	6***	123-140°	17° (9°)
(Barite)	1) 6 to 16.5 µm	5	6**	106-124°	18° (12°)
Cab (Saddle DLMT)	1) 3 to 5 µm	2,3,5	5	198-238°	40° (33°)
	2) (approx. 3 to 5 µm)	2,3,5	5	237-252°	15°
	3) 4 to 5 µm	3,5	4	182-195°	13°
Hydrothermal DLMT	1) 2 to 5 µm	2,3,5	5	169-194°	25° (19°)
	2) 4 to 5 µm	2,3,5	5	170-199°	29° (24°)
	3) 1.5x2 to 4 µm	3,5	3	147-163°	16°
Cab (Quartz)	1) 6 to 17 µm	2,5	8	182-242°	60° (39°)
	2) (10 to 30 µm)	2,5	5	219-244°	25° (11°)
	3) (10 to 30 µm)	2,5	6	209-246°	37° (23°)
	4) 4x7 to 8x21 µm	2,3,5	9	172-236°	64° (47°)
	5) 6 to 36 µm	2,3,5	8	207-240°	33° (29°)
Mawer	1) 3x1 to 4x2 µm	3,4,5	6	175-227°	52° (45°)
	2) 2x3 to 20x8 µm	2,5	11	177-219°	42° (17°)
	3) 3 to 6 µm	3	6	201-225°	24° (10°)
	4) 4to 6 µm	3,5	3	181-201°	20° (11°)
Rev	1) 4 to 8 µm	3,5	8	179-214°	35° (29°)
	2) 2x2 to 10x2 µm	3,5	7	178-231°	53° (25°)
	3) 3x1 to 7x4 µm	3,5	8	193-236°	43° (31°)
	4) 2x2 to 6x4 µm	3,5	7	140-192°	52° (40°)
	5) 3x2 to 8x5 µm	2,5	5	160-207°	47° (31°)
	6) 3x1 to 9x4 µm	2,3	8	186-236°	50° (16°)
	7) 2x2 to 5.5x3 µm	3,5	10	186-228°	42° (34°)
	8) 3x2 to 8x5 µm	3,5	7	183-235°	52° (36°)
	9) 3x2 to 5.5x3 µm	2,3,5	7	166-213°	47° (33°)

CHARACTERIZATION OF FLUIDS

This study has concentrated on deposits aligned along the shale-carbonate boundary which marks the change from deep water of the Misty Creek Embayment, an extension of the Selwyn Basin, and the shallower water covering the carbonate platform from Late Proterozoic to Late Cretaceous. This paper presents results of fluid inclusion studies of ancient fluid regimes likely originating from the Selwyn Basin. Fluid regimes can be defined by their salinity and temperature characteristics. When the fluid inclusion data for Type 1 inclusions were plotted as salinity versus homogenization temperature for each deposit, four distinct groups, and two sub-groups, became apparent. The confining limits of total salinity range versus the range of mean homogenization temperature (Th) for each group or fluid type are shown in Figure 4-4. They are identified as Fluid Ia, highest Th and salinity, to Fluid IV, lowest Th with low salinity.

The characteristics of the four distinct mineralizing fluids, with two sub-types, identified in the present study have been summarized in Table 4-7. **Fluid Ia** was found in primary and/or pseudosecondary inclusions primarily in dolomite, with a few representative primary and/or pseudosecondary inclusions in sphalerite and quartz, and has mean characteristics of >20 eq. wt.% NaCl at a mean T_{min} 175°C. **Fluid Ib** was found in primary and/or pseudosecondary inclusions primarily in sphalerite, with a good representation of primary and/or pseudosecondary (some secondary) in quartz, and only a few primary and/or pseudosecondary inclusions in dolomite. Fluid Ib is less saline, ranging from 12.8-20.2 eq. wt.% NaCl and mean T_{min}153°C, and could represent an evolved version of Ia, or one resulting from mixing with a cooler less saline fluid. **Fluid II** was found only in primary and/or pseudosecondary inclusions from sphalerite. **Fluid IIa** has a mean salinity >22 eq. wt.% NaCl and a T_{min} 104°C. **Fluid IIb** has mean salinity ranging between 15 and 20 eq. wt.% NaCl, and mean T_{min} 111°C. **Fluid III** was represented in pseudosecondary and/or secondary inclusions from sphalerite and primary/pseudosecondary/secondary inclusions in quartz, but not in dolomite. The mean salinity of Fluid III ranges from 3.5-6.8 eq. wt.% NaCl and mean T_{min} 177°C. **Fluid IV** was found only in pseudosecondary and/or secondary inclusions from sphalerite and primary/pseudosecondary/secondary inclusions in calcite and barite. Fluid IV mean salinity ranges from 5-9.4 eq. wt.% NaCl and mean T_{min} 118°C. The characterization of the fluids was further refined by examining the 1st melting temperatures (Tm - 1st), which approximate eutectic temperatures. **Fluids I** and **II** have approximate eutectic temperatures ranging from -26 to -60°C which suggests these fluids belong to the $NaCl-CaCl_2-MgCl_2-H_2O$ system (Goldstein and Reynolds, 1994, p. 99).

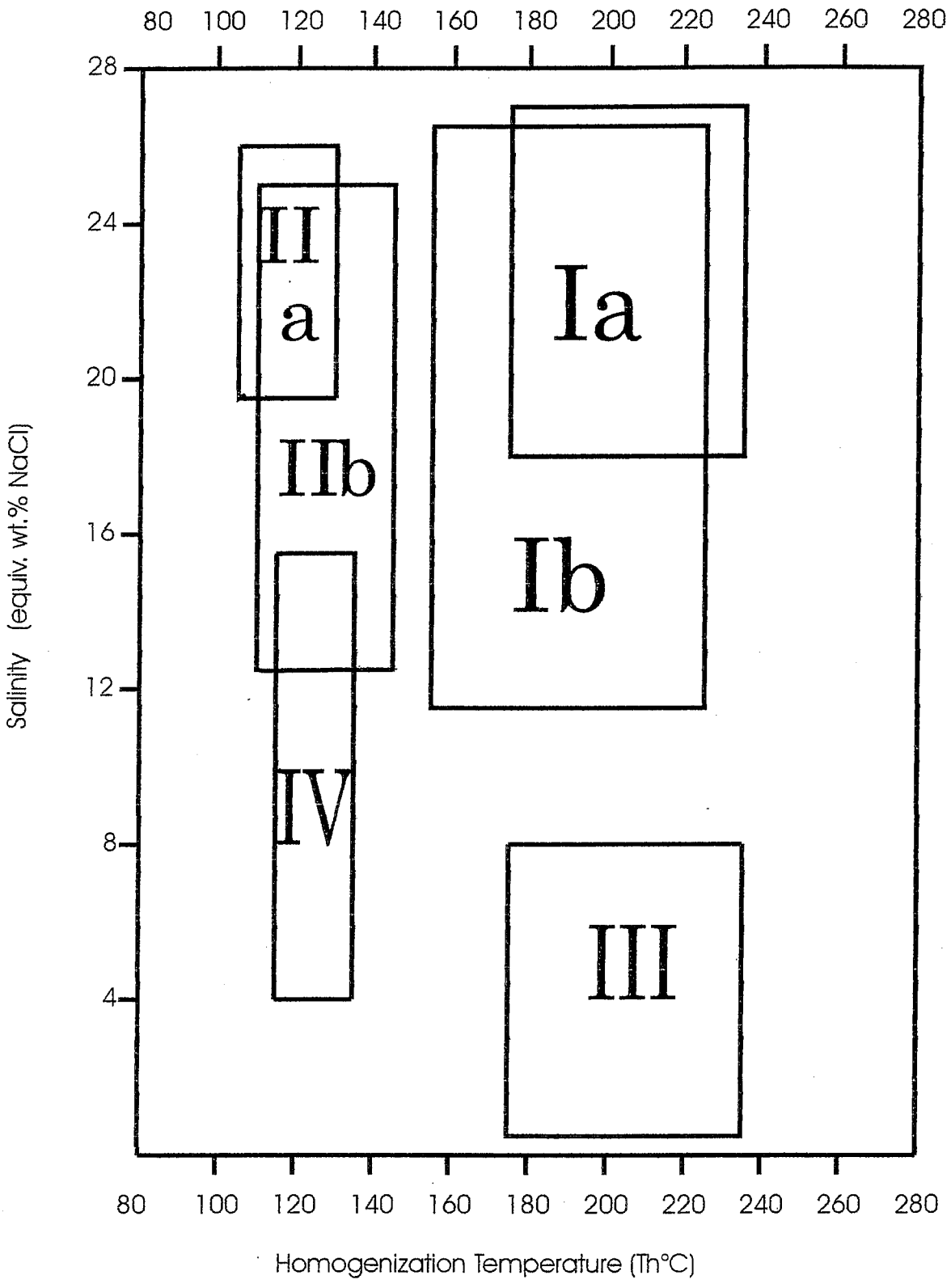

Figure 4-4. Plot of total salinity ranges versus ranges of the mean homogenization temperatures defining fluid types I to IV from data gathered from Type 1 inclusions. and summarized in Table 4-7.

Fluids III and **IV**, on the other hand, have approximate eutectic temperatures ranging from -11 to -45°C which place them in a different system, likely the NaCl-$MgCl_2$-H_2O System. Temperature of nucleation of ice (Tn) has been used as another defining characteristic as it appears to be directly related to the salinity. Note that even though these deposits would have been subjected to repeated cooling to temperatures as low as -40°C in the Arctic climate in which they are now found, it can be seen that very few inclusions would have nucleated ice under these conditions.

Table 4-7. Summary of the characteristics of each fluid from data contained in Table 4-2.

Fluid	Tn Range (°C)	Tm - 1st (°C)	Tm - ice (°C)	Salinity Range (equiv. wt.% NaCl)	Range of Mean Salinities (equiv. wt.% NaCl)	Range of Mean Th(°C)
Fluid Ia	-57.6 to -94.4°	~-43 to 60.3°	-14.4 to -35.3°	18.1-27.0	21.5-26.3	175-235°
Fluid Ib	-46.4 to -79.9°	< -26 to -55°	-8.0 to -28.2°	11.7-26.5	12.8-20.2	153-222°
Fluid IIa	-67.9 to -93.2°	-36.2 to -56.2°	-15.8 to -28.2°	19.3-26.3	22.4-25.6	104-130°
Fluid IIb	-50.5 to 78.9°	<-28 to -48°	-9 to -26°	12.8-25.0	15.6-19.9	111-145°
Fluid III	-36.6 to -50.6°	< -23 to -45°	-0.4 to -5.1°	0.7-8.0	3.5-6.8	177-236°
Fluid IV	-40 to -55.9°	<-11 to -35°	-2.4 to -11.5°	4-15.5	5-9.4	118-137°

Work by Nesbitt and Muehlenbachs (1993) identified two major fluid events in the southern Canadian Rockies and showed that fluids closely associated with Laramide deformation (Cretaceous to Early Tertiary) are geochemically distinct from fluids involved in a pre-Laramide (post-Middle to Late Devonian) event. They describe Event 1 (pre-Laramide) fluids from Phanerozoic units (>20 eq. wt.% NaCl, Mg-Ca rich brines at a T_{min} of 175°C) as representing a post-Devonian, pre-thrusting, west to east migration from a Paleozoic shale basin into carbonates of the Western Canadian Sedimentary Basin (WCSB). They state that this fluid was responsible for the late dolomitization throughout the WCSB and MVT mineralization at Pine Point. They conclude that one implication of this work is that MVT deposits in WCSB are not a product of gravity driven flow associated with Laramide uplift of the Rockies. In Nesbitt and Muehlenbachs (1994) they refine the timing of the pre-Laramide orogenic fluid event to sometime after Middle to Late Devonian. This conclusion is supported by the Late Devonian Rb-Sr age for Pine Point mineralization obtained by Nakai et al.(1993). Note that there are paleomagnetic ages for Pine Point

mineralization which do not agree with this conclusion (e.g. Qing, 1991 and Symons et al., 1993). An episode of Late Devonian-Early Mississippian convergence, known regionally as the Antler orogeny, which affected much of the western margin of North America (Dorobek, 1995), could have been the triggering mechanism for Event 1 fluid. Large scale fluid movements could have been related to the tectonic compression and sedimentary loading which occurred during the Antler orogeny. Event 2 fluids of Nesbitt and Muehlenbachs (1993) represent post-deformation infiltration of meteoric water (<10 eq. wt.% NaCl at T_{min} of 130°C).

Results of the present study suggest that there were two, or more, fluid events in the northern Canadian Rockies. Multiple periods of sulphide mineralization is a common characteristic of MVT deposits. In this preliminary study all possibilities have not been discovered; for example, in Hewton (1982) it is stated that Gayna has experienced at least three periods of sulphide mineralization, whereas our data reveals only one period of mineralization represented by Fluid Ib. Gibson (1975) states that he recognized at least five distinct paragenetic stages of mineralization in the Econ deposit, and our data picked up two stages of mineralization represented by Fluids IIa and IV.

The areal and stratigraphic extent of one mineralizing event is indicated by the fact that Fluid I was found in the deposits: Gayna River, Cypress, Cab, Palm, Bear, Rev, Mawer, and Joli Green. These deposits occur from one end of the study area to the other and are found in rocks of ages from Mesoproterozoic to Ordovician-Silurian. Table 4-8 list the deposits by fluid type for easy reference.

Table 4-8. Deposits by fluid type (F.I.=fluid inclusion).

FLUID TYPE	DEPOSITS	HOST MINERAL	F.I. TYPE	NO. of F.I.s	STAGE
Ia	Palm	dolomite	P/PS	32	pre-ore/syn-ore
	Bear	sphalerite	P	1	ore
		dolomite	P/PS	42	pre-ore/syn-ore
		quartz	P/PS	8	pre-ore/syn-ore
	Rev	sphalerite	P/PS	20	ore
		dolomite	P/PS	71	syn-ore
	Mawer	dolomite	P/PS	25	syn-ore/post-ore
	Joli Green	dolomite	P/PS	14	pre-ore
Ib	Gayna River	sphalerite	P/PS	66	ore
		quartz	P/PS	44	syn-ore/post-ore
	Cypress	sphalerite	P/PS	20	ore
		dolomite	P/PS	17	syn-ore/post-ore
	Cab	sphalerite(1)	P/PS	12	ore
		dolomite(1)	P/PS	12	pre-ore
		dolomite(2)	P/PS	17	syn-ore
		quartz(2)	P/PS	42	syn-ore
	Joli Green	sphalerite	PS/S	11	ore
	Mawer	sphalerite	P/PS	10	ore
	Bear	sphalerite	PS	84	ore
		quartz	PS/S	18	syn-ore
	Rev	sphalerite	PS/S	9	ore
IIa	Econ	sphalerite(2)	PS	17	ore
	Ab	sphalerite(1)	P/PS	11	ore
	Palm	sphalerite	P	11	ore
IIb	Cab	sphalerite(2)	P/PS	36	ore
	Ab	sphalerite(2)	P/PS	28	ore
	Joli Green	sphalerite	P/PS	10	ore
III	Cypress	sphalerite	PS/S	45	ore
		quartz	P/PS	44	syn-ore/post-ore
	Palm	quartz	PS/S	2	post-ore
	Bear	quartz	S	12	post-ore
	Rev	sphalerite	S	7	ore
IV	Econ	sphalerite(2)	PS	60	ore
		sphalerite(2)	PS/S	11	ore
		calcite	P/PS	20	post-ore
		barite	PS/S	16	post-ore
	Bob	sphalerite	PS/S	5	ore
	Bear	sphalerite	S	14	ore

5. CARBONATE GEOCHEMISTRY

ELECTRON MICROPROBE STUDIES

Methods

Electron microprobe analyses for Ca, Mg, Mn, Fe, Ba, Sr, and Zn were carried out on the host dolomite and dolomite cement using a Cameca SX50 instrument. The microprobe was operated at 15 kV, with a beam current of 10 to 30 nA depending on the element, sample stability, and size. Minimum detection limits were calculated (J. Stirling, Mineralogy Section, Geological Survey of Canada, pers. comm., 1997). These detection limits were adjusted for the mole % end member values, and only those values above the detection limits were used for plotting purposes. Detection limits for wt% end members are shown in brackets following the value for mole % end members. The minimum detection limits for mole % end members are 0.10 (0.11) for $CaCO_3$, 0.06 (0.07) for $MgCO_3$, 0.14 (0.18) for $MnCO_3$, 0.20 (0.25) for $FeCO_3$, 0.11 (0.20) for $BaCO_3$, 0.08 (0.12) for $SrCO_3$, and 0.34 (0.38) for $ZnCO_3$. The location of all microprobe runs were marked on CL view photomicrographs which can be obtained upon request from the first author.

Results

The electron microprobe analyses were based on the dolomite types identified by petrography and cathodoluminescence (CL) work. The dolomite cement has been divided into two dolomite groups based on grain size. Finer grained dolomite cement [or dolomite cement(1) in the paragenesis] is defined as ranging in grain size from 60-2000 μm (mean 515 μm) and includes replacive saddle dolomite. Coarse-grained saddle dolomite ranges in grain size from 200-6600 μm (mean 1570 μm).

Electron microprobe studies of cathodoluminescent, zoned dolomite cement and host dolomite revealed that one group of deposits, including Ab, Cab, Bob, Econ, Palm, Ice, and Arn (hosted in Lower Cambrian Sekwi Formation), Tic (hosted in atypical Sekwi Formation), Cypress (hosted in Late Hadrynian Sheepbed (?) Formation), and Gayna (hosted in Helikian Little Dal Group) had higher Fe and slightly lower Mn content than the second group (Table 5-1). The latter group, hosted in carbonate rocks younger than Middle Cambrian, includes Bear, Rev, Rain-Snow, Joli Green, Mawer, and Snobird. The dolomite in all these deposits contains insignificant amounts of Fe (i.e. >60% of values under detection limit), and all but Bear and Rev contain insignificant amounts of Mn (Table 5-1). Bear and Rev dolomite have elevated levels of Mn.

Table 5-1. Summary of microprobe analyses of host dolomite and dolomite gangue for 15 deposits analyzed from the Mackenzie Platform (see Fig. 5-16 for number af analyses).

Age of Host	Older than Middle Cambrian			Late Cambrian and younger		
Rock Type	Range of Means	Overall Mean	% of values >m.d.l.	Range of Means	Overall Mean	% of values >m.d.l.
Dolomite gangue mol% $FeCO_3$	0.8-3.9	2.31	87%	0.2-0.4	0.36	23%
Host Dolomite mol% $FeCO_3$	0.5-3.77	2.01	84%	0.26-0.42	0.35	36%
Dolomite gangue mol% $MnCO_3$	0.21-0.48	0.28	59%	0.17-0.46	0.33	21%
Host Dolomite mol% $MnCO_3$	0.19-0.26	0.23	54%	0.15-0.51	0.39	22%

m.d.l.= minimum detection limit. Only values above the minimum detection limit were used to calculate means.

Mole fraction compositions (mole % carbonate) of the host dolomite, finer grained dolomite cement and coarse grained saddle dolomite have been plotted in Fig. 5-1 to 5-15 to illustrate the details. The $ZnCO_3$ data were not available for every deposit. It is not known if the $ZnCO_3$ values are real or if there are submicroscopic inclusions of sphalerite.

The data shows that in most deposits the geochemistry is similar for all three dolomite types. The obvious exception is Bob host dolomite which has very low $FeCO_3$ and $MnCO_3$ versus the finer grained dolomite cement which has significantly higher $FeCO_3$ and $MnCO_3$. Econ shows a similar pattern, although the difference is not as striking. Cypress and Palm are the only two deposits that show a compositional difference between the coarse grained saddle dolomite and the other types. Cypress saddle dolomite contains noticably less $FeCO_3$ than the finer grained dolomite or the host dolomite. In Palm saddle dolomite the $FeCO_3$ values are higher and more erratic than the finer grained dolomite or the host dolomite. Some basic groupings of deposits can be made by using the Fe content (see Table 5-2).

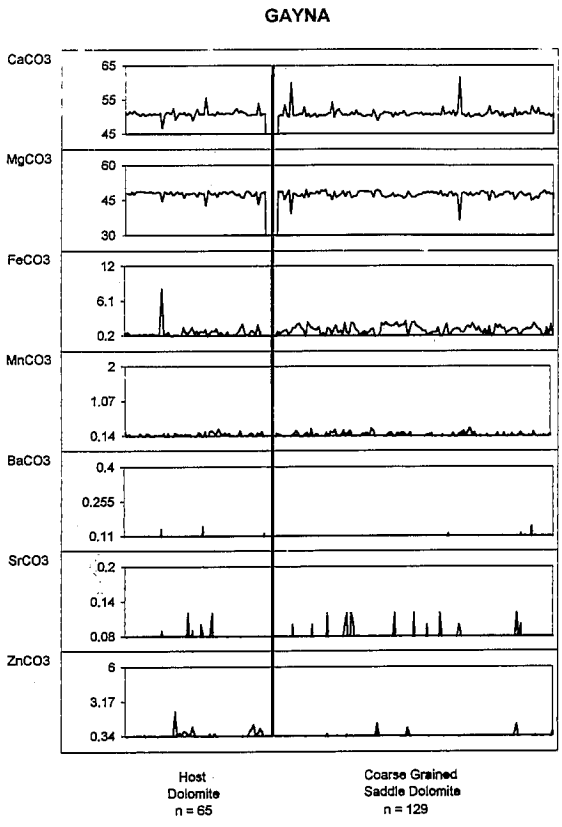

FIG 5-1. **Mole fraction composition (mole % carbonate) of host dolomite and dolomite cements.**

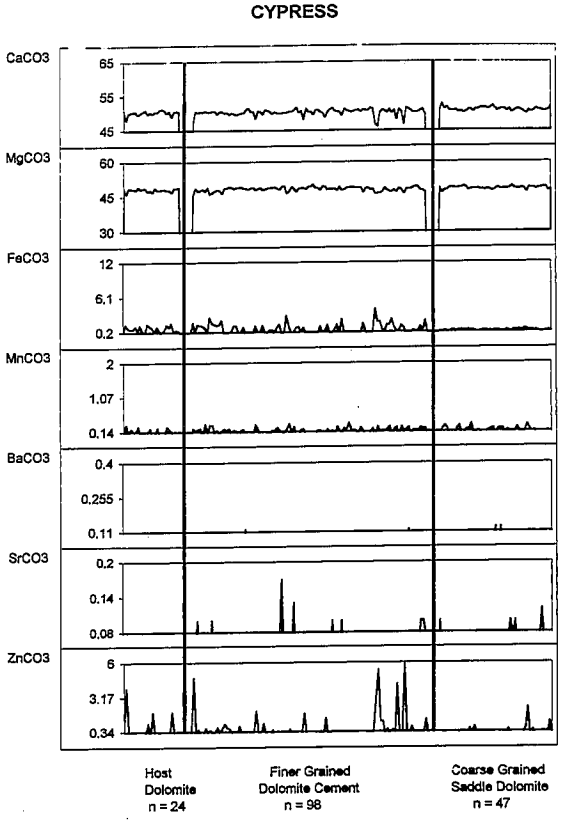

FIG 5-2. **Mole fraction composition (mole % carbonate) of host dolomite and dolomite cements.**

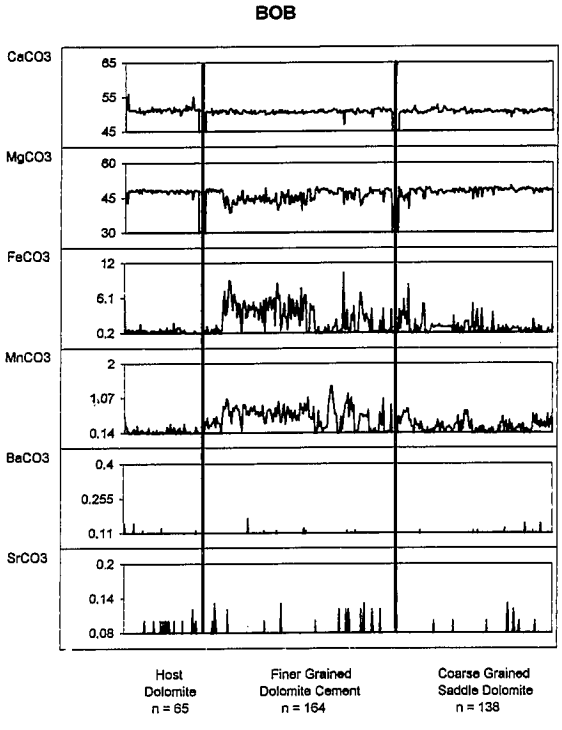

FIG 5-3. **Mole fraction composition (mole % carbonate) of host dolomite and dolomite cements.**

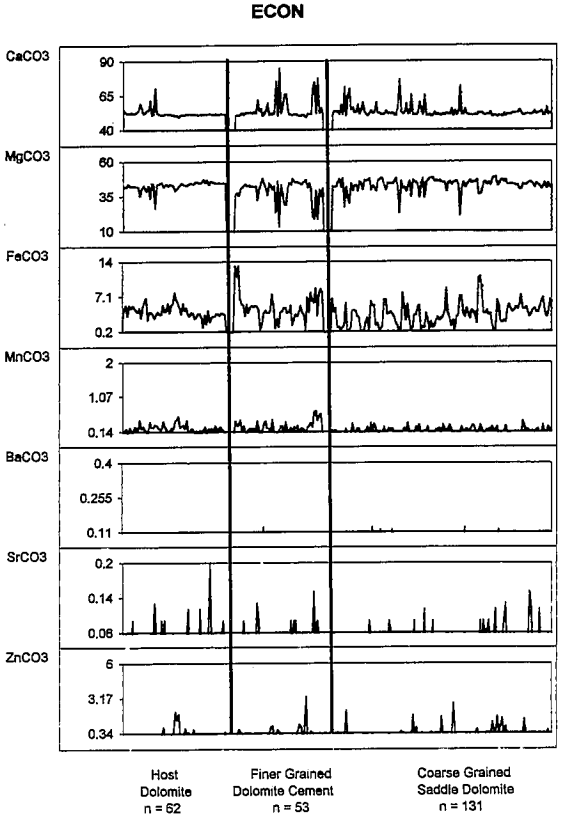

FIG 5-4. **Mole fraction composition (mole % carbonate) of host dolomite and dolomite cements.**

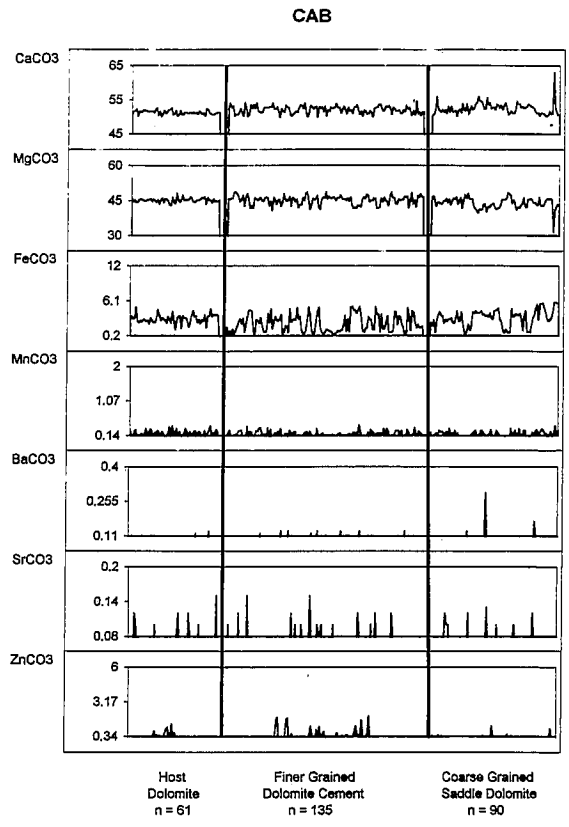

FIG 5-5. Mole fraction composition (mole % carbonate) of host dolomite and dolomite cements.

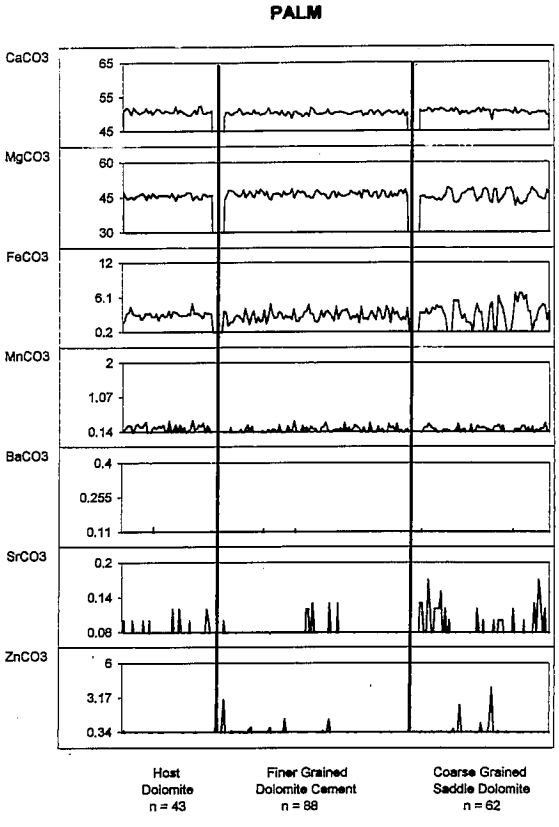

FIG 5-6. Mole fraction composition (mole % carbonate) of host dolomite and dolomite cements.

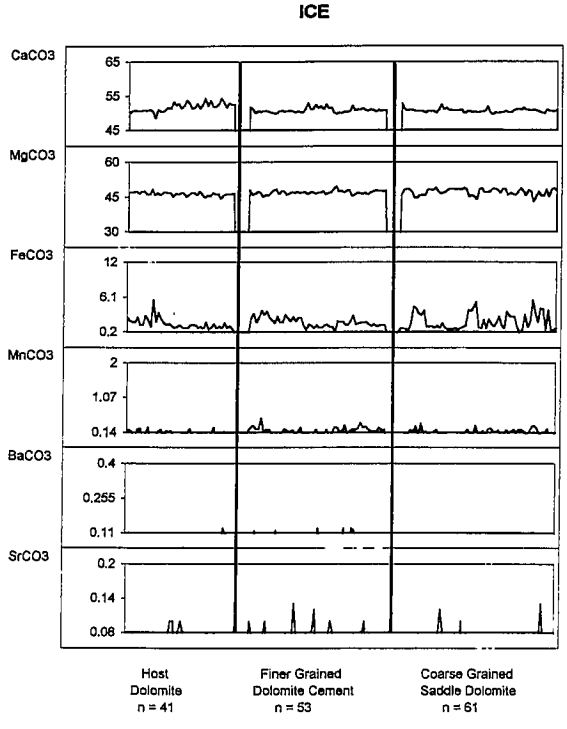

FIG 5-7. Mole fraction composition (mole % carbonate) of host dolomite and dolomite cements.

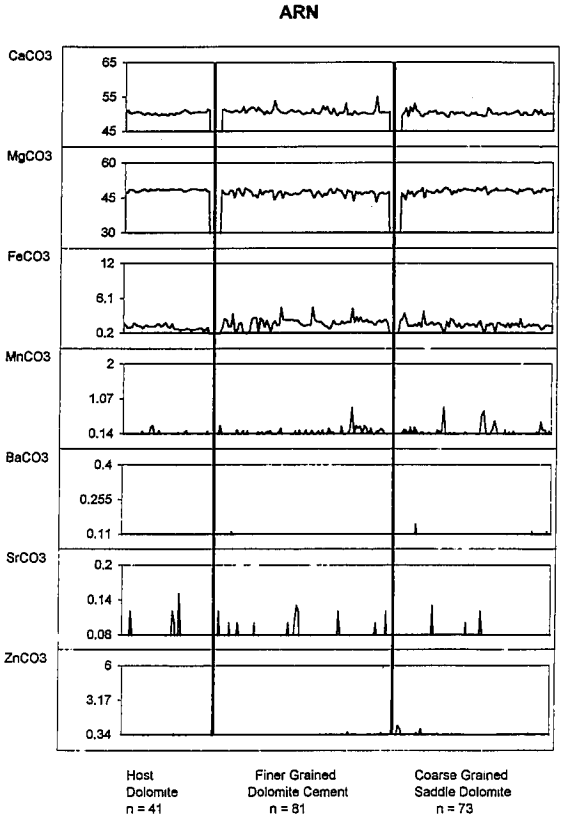

FIG 5-8. Mole fraction composition (mole % carbonate) of host dolomite and dolomite cements.

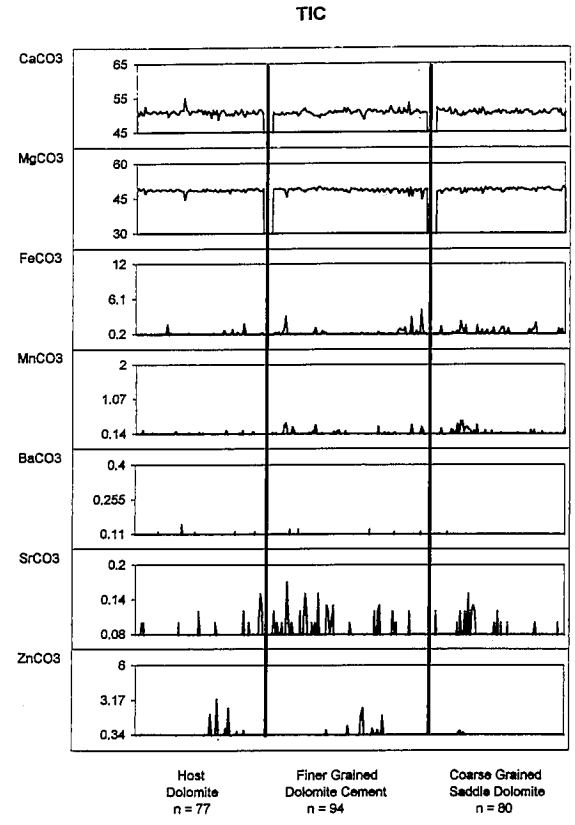

FIG 5-9. **Mole fraction composition (mole % carbonate) of host dolomite and dolomite cements.**

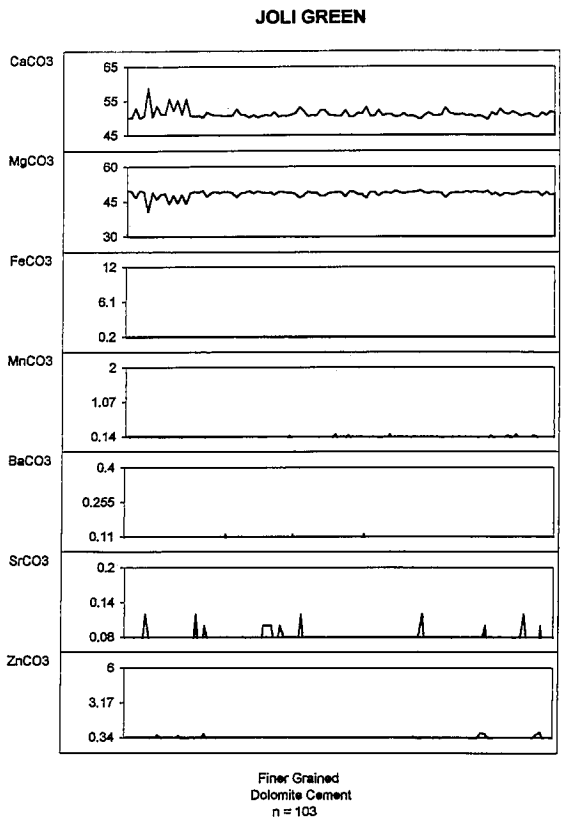

FIG 5-10. **Mole fraction composition (mole % carbonate) of host dolomite and dolomite cements.**

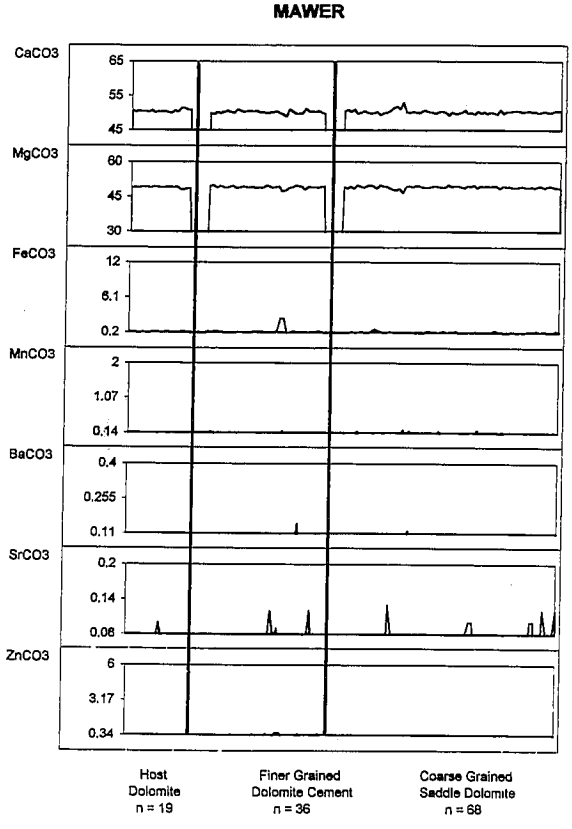

FIG 5-11. **Mole fraction composition (mole % carbonate) of host dolomite and dolomite cements.**

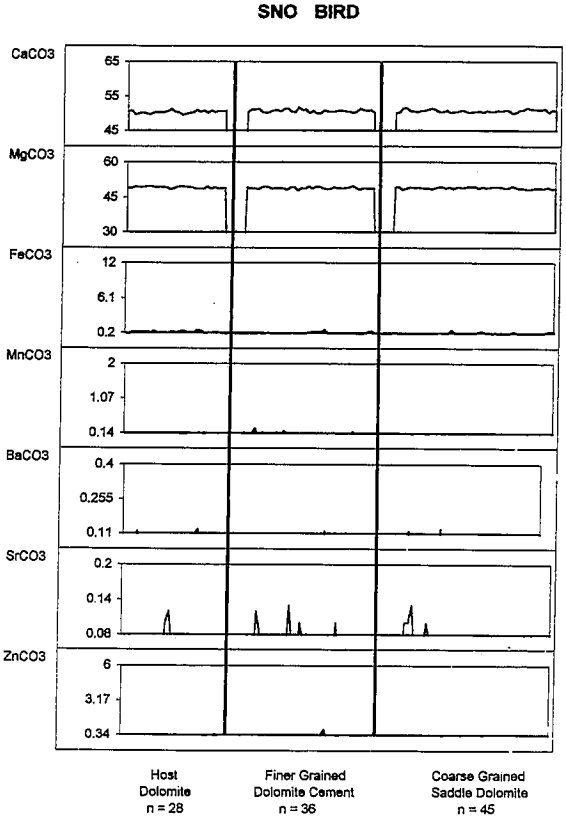

FIG 5-12. **Mole fraction composition (mole % carbonate) of host dolomite and dolomite cements.**

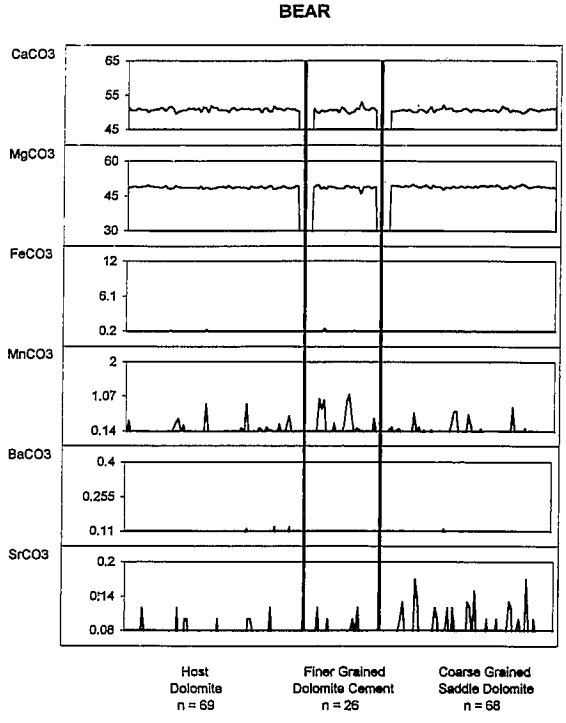

FIG 5-13. Mole fraction composition (mole % carbonate) of host dolomite and dolomite cements.

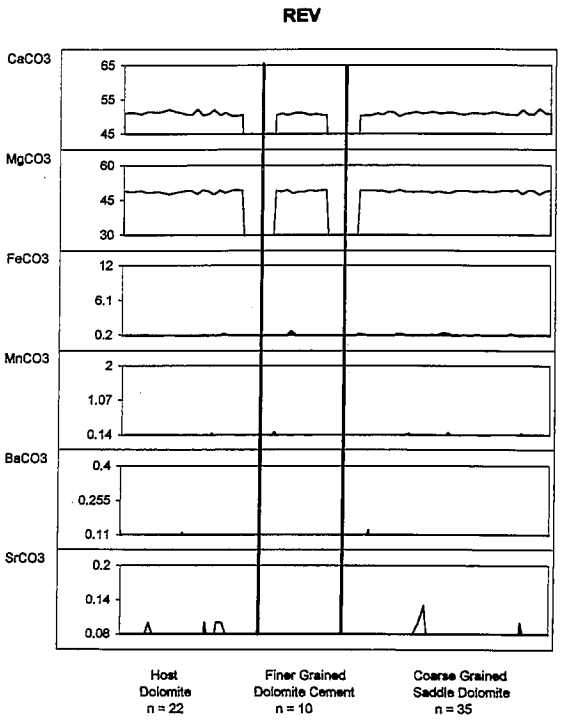

FIG 5-14. Mole fraction composition (mole % carbonate) of host dolomite and dolomite cements.

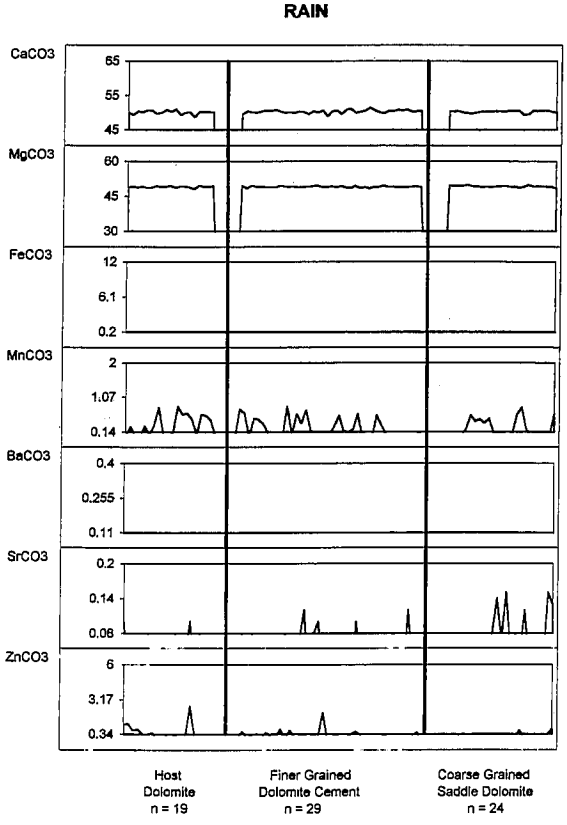

FIG 5-15. Mole fraction composition (mole % carbonate) of host dolomite and dolomite cements.

Table 5-2. Deposit groupings based on Mole % composition of $FeCO_3$.

Deposit	$FeCO_3$ Mole % value	Other elements and /or Comments
Bob Econ	High	Fe minor in host dolomite Fe lower in host dolomite
Cab Palm Arn Ice	Medium	Sr significant in all four deposits
Gayna Cypress Tic	Minor	Sr significant, Zn less so Sr significant, Zn very significant Sr very significant, Zn less so
Mawer Joli Green Snobird Rev	very low to negligible	Sr significant in all four deposits
Bear Rain	very low to negligible	Mn, Sr significant Mn significant, Sr, Zn less so

Ternary plots of the 2821 analyses of carbonate minerals show end-member compositions for all dolomite types (Fig. 5-16). Deposits which contain little or no luminescent dolomite including Tet-Rap, Birkland, Keg, Art, Scat, Rio, Aj, and Big Red are commonly hosted in limestone rather than dolomite, and contain more abundant quartz and calcite. No analyses are available for these deposits.

All dolomite analyses are included in the appendix, on diskette, in Microsoft Excel spreadsheets in .xls format. There is a README file describing the data.

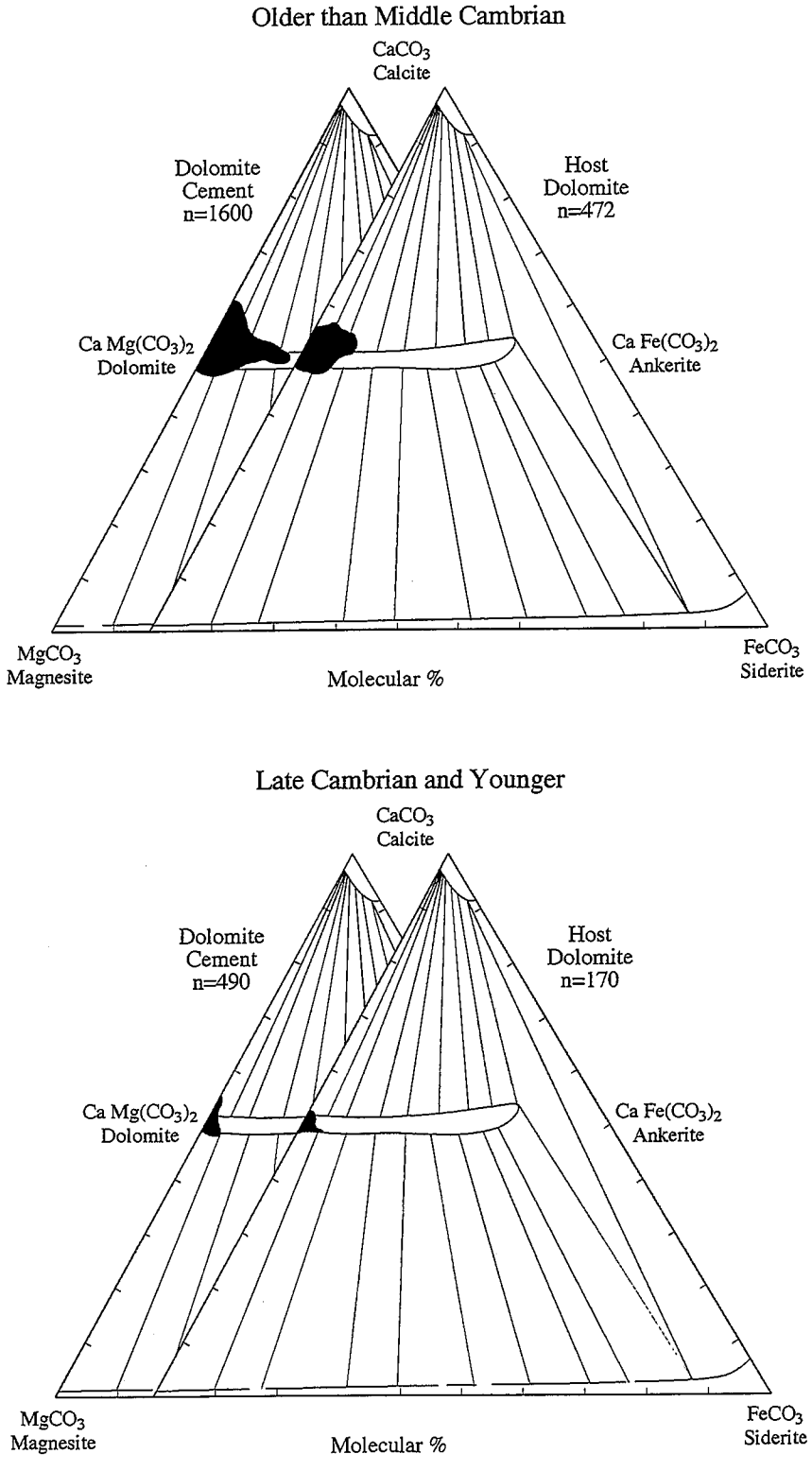

Fig. 5-16. Ternary plots showing composition of host dolomite and dolomite cement (black fields) for deposits hosted in rocks older and younger than Middle Cambrian (Adapted from Anovitz and Essence,1987)

6. SPHALERITE GEOCHEMISTRY

ELECTRON MICROPROBE STUDIES

Methods

Mississippi Valley-type ore deposits contain significant quantities of minor elements, which are present partly in the form of separate mineral phases and partly in solid solution in the major sulphide phases (Hagni, 1983). In this study the sphalerite from eight deposits has been analyzed by electron microprobe for major and minor elements contained in solid solution. According to Hagni (1983) the most abundant minor elements in Mississippi Valley-type sphalerite crystals are cadmium, iron, silver, germanium, gallium, indium, thallium, cobalt, nickel, and mercury. Table 6-1 lists the elements detected by electron microprobe in this study.

The analyses were performed at the Geological Survey of Canada, with a Cameca SX50 electron microprobe which has four wavelength dispersive spectrometres. The raw counts (with a GSC modified dead time calculation) were corrected to elemental concentrations using the Camecea PAP program (Pouchou and Pichoir, 1985). The standards were mostly metals or simple compounds, e.g., pyrite for S. The operating conditions were 30 Kv, 10 nA and 10 sec peak counts for the major elements, and 100 nA and 100 sec peak counts for the traces.

Results

The most abundant minor elements found in the eight deposits analysed (Gayna, Cypress, Econ, Palm, Cab, Joli Green, Bear, and Rev) were cadmium, iron, indium, cobalt, and in addition, copper, bismuth, arsenic and selenium. Silver and gallium contents were insignificant except for silver in Econ and gallium in Gayna. Germanium was significant in only one deposit (Econ). McLaren and Godwin (1979b) analyzed sphalerite from 48 deposits and found concentrations of silver, cadmium, cobalt, copper, iron, manganese, nickel, lead, and mercury. In this study nickel and mercury were not analysed. They discovered that sphalerite in carbonate rocks of the Northern Cordillera is generally enriched in copper, lead, and mercury, and depleted in iron, relative to other carbonate-hosted zinc-lead districts in North America. Minor element variations within single deposits are small relative to those between deposits; therefore, each deposit is characterized by the minor element assemblage of its sphalerite. Figure 6-1 shows a graphic presentation of the analyses for eight deposits with only values above the detection limit plotted (i.e. the base line of the graph for each element is the detection limit).

Table 6-1. Summary of major and minor element analyses for eight deposits shown in Figure 6-1.

Element	Range (wt.%)	Mean (wt.%)	detection limit	% of values above m.d.l.*	Std. Dev.
Zn	59.594-67.258	65.013	0.058	100%	1.560
S	31.705-33.8	32.808	0.056	100%	0.291
Pb	0.014-0.146	0.0076	0.014	6%	0.210
Fe	0.043-2.209	0.426	0.043	74%	0.624
Cd	0.017-0.515	0.162	0.017	99%	0.085
Cu	0.011-0.309	0.026	0.003	100%	0.06
Mn	0.003-0.01	0.003	0.003	31%	0.002
Co	0.003-0.006	0.003	0.003	75%	0.001
Ge	0.024-0.095	0.007	0.024	16%	0.019
Ga	0.002-0.021	0.003	0.002	4%	0.002
Ag	0.02-0.058		0.02	1%	n/a
Bi	0.016-0.034	0.022	0.016	91%	0.005
As	0.006-0.034	0.019	0.006	100%	0.005
Se	0.021-0.034	0.029	0.009	100%	0.003
In	0.006-0.016	0.01	0.006	99%	0.002

* detection limit, Std. Dev.= Standard Deviation, Number of analyses=158

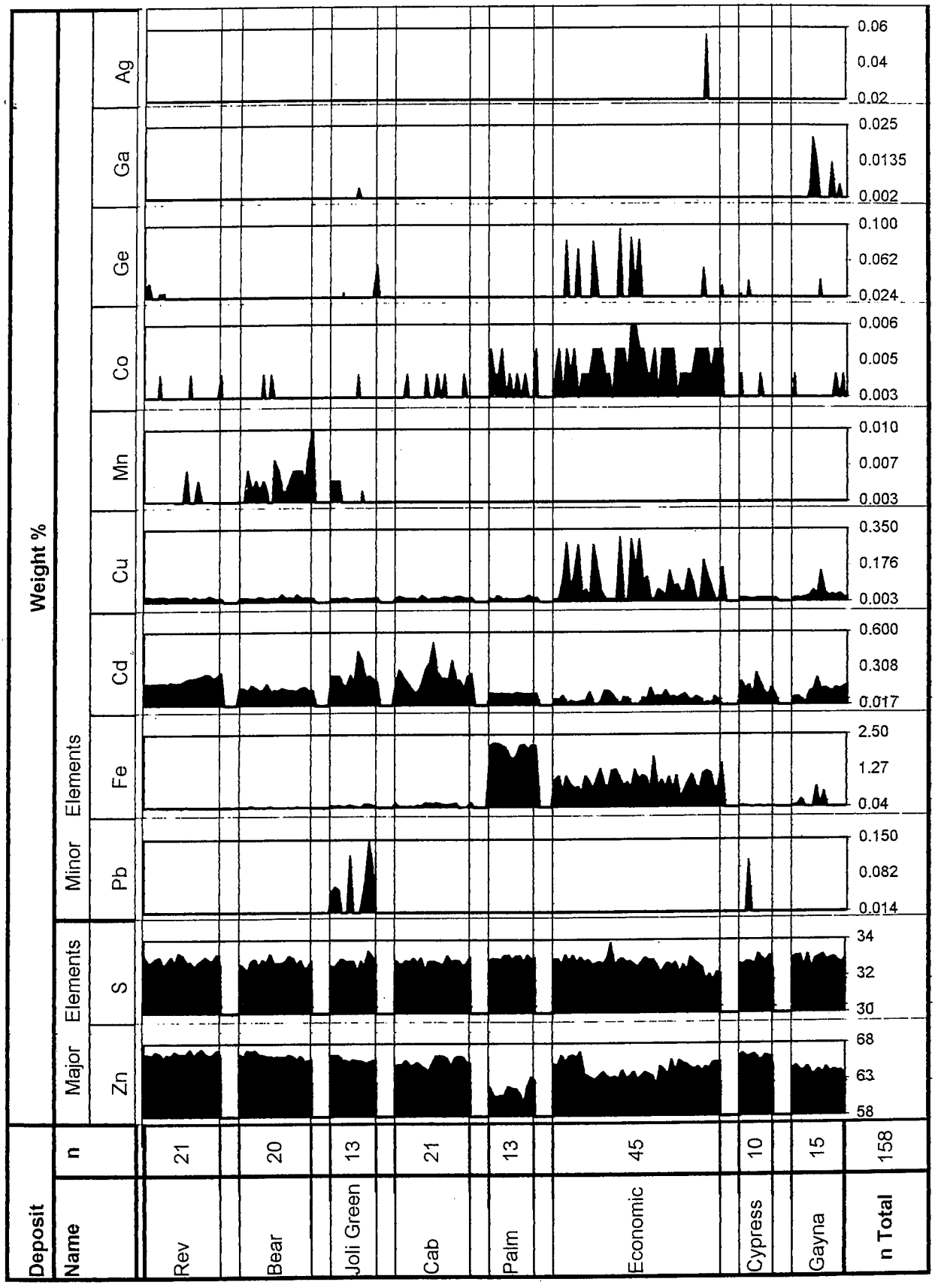

Fig. 6-1. Wt.% values of major and minor elements analyzed in sphalerite from eight deposits (n=number of analyses, base line for each graph for the minor elements is the minimum detection limit for that paricular element).

A description of the occurrence of each of the elements analyzed follows:

Major Elements

Zinc

The concentration of Zn in sphalerite (see Fig. 6-1) shows little variance in six deposits ranging from 63.14 to 67.26 wt.%.

Exceptions are the Palm deposit, where the Zn content is noticeably less ranging from 59.59 to 63.32, and in the Economic (Econ) deposit, where Zn content fluctuates more than in the other deposits, ranging from 62.05 to 66.77 wt.%.

Sulphur

The concentration of S in sphalerite appears very consistent between deposits except for an obvious peak in Econ (max=33.8), ranging from 31.71 to 33.41 wt.%.

Minor Elements

Lead

The concentration of Pb in sphalerite as shown in Figure 6-1. Only 6% of the values are above the detection limit, with only significant levels in the Joli Green deposit and possibly Cypress.

Iron

The concentration of Fe in sphalerite is very similar for six of the eight deposits studied, and the only significant variation is in the Palm and Econ deposits. Iron levels range from 0 to 0.72 wt.% in the six similar deposits, from 0.27 to 1.74 wt.% in Econ, and from 1.65 to 2.21 wt.% in Palm sphalerite with 75% of the values are above the detection limit.

Cadmium

Cadmium was detected in all sphalerite grains analyzed, ranging from 0.039 to 0.515 wt.%, with 99% of the values above the detection limit. Only Palm sphalerite, ranging from 0.102 to 0.116 wt.%, and Econ sphalerite, ranging from <0.017 to 0.148 wt.%, contain somewhat less than the other deposits.

Copper

Copper was also detected in all sphalerites analyzed, with values ranging from 0.011 to 0.145 wt.%; all values were above the detection limit. Copper is particularly significant in the Econ deposit, and ranges from 0.012 to 0.309 wt.%.

Manganese

Only 31% of the values analyzed in sphalerite are above the detection limit, and were detected in only three deposits. These values are particularly significant in Bear deposit, ranging from <0.003 to 0.01 wt.%. A few peaks in Rev range from <0.003 to 0.006 wt.%, and in Joli Green sphalerite ranges from <0.003 to 0.005 wt.%.

Cobalt

Cobalt was detected in all sphalerites, with 75% of values above the detection limit. Cobalt is particularly significant in Econ sphalerite, ranging from 0.003 to 0.006 wt.%, and Palm sphalerite, ranging from 0.003 to 0.005 wt.%. Values in the other six deposits range from <0.003 to 0.004 wt.%.

Germanium

Germanium was detected in sphalerite grains from five deposits, but is significant only in the Econ deposit, ranging from <0.024 to 0.095 wt.%. A few values out of the 16% above detection limit occur in the sphalerite of Rev, Joli Green, Cypress and Gayna deposits.

Gallium

Gallium was detected in sphalerite grains from two deposits, and is only significant in Gayna, ranging from <0.002 to 0.021 wt.%. One value, out of the 4% above the detection limit, was detected in Joli Green sphalerite.

Silver

Concentrations of Ag were not detected in any of the deposits other than in three values at Economic deposit ranging from <0.02 to 0.056 wt.%.

Bismuth, Arsenic, Selenium, and Indium

The levels of Bi, As, Se, and In were relatively constant within and between samples in all eight deposits, and therefore were not included in fig. 6-1. These elements were detected in all sphalerite grains analyzed, with 91, 100, 100, and 99% of the values above detection limit respectively.

The limited data for minor elements in sphalerite from the study area support the divisions of deposits by fluid type. Fluid I, discussed in the Microthermometric Section, formed the sphalerite in the Gayna, Cypress, Joli Green, Bear, and Rev deposits. The minor element contents of

sphalerites from these deposits are similar in most respects. The differences could perhaps be explained by the fact that the host rocks, through which the fluids flowed, are different for many of these deposits. The Econ (Economic) deposit stands out as being completely different because of its high and varied minor element content of sphalerite, which was formed from Fluid IV. Palm sphalerite, formed from Fluid II, is also different in that it contains significantly more Fe than any other deposit.

All sphalerite analyses, in weight per cent, are included in the appendix, on diskette, in Microsoft Excel spreadsheet entitled "Sphalerite.xls".

7. Burial History of Mackenzie Platform

INTRODUCTION

Palinspastic reconstructions for this area are not available other than the restored stratigraphic section shown in Fig. 7-1 (Abbott et al., 1986, Figure 2) which overlaps the study area. These authors state that the thickest part of the prism comprising Lower Cambrian to Devonian shelf dolomites and limestone is 6.5 km. From Fig. 7-1 it can be inferred, by measuring, that the burial depth for the Ordovician Whittaker Fm, *for example*, would have been from 2 to 5 km depending on the assumed thickness of the Mississippian to Triassic strata. There is an unconformity shown between the upper Devonian and younger strata which could further increase the estimated burial depth. At some time in their history, Zn-Pb deposits in the Mackenzie Platform have been buried to significant depths, as supported by the following: 1) host dolomite textures and the presence of saddle dolomite, 2) the fluid inclusion data, and 3) post-mineralization effects (Table 3-4).

Burial history models have been developed recently by Feinstein et al., (1996) for the Mackenzie Plain which lies directly east of the study area. They state that Phanerozoic strata of the Mackenzie Plain region record a complex, multi-phase history of burial, exhumation and deformation which resulted in the development of several major unconformities. Abbott et al. (1986) also describe unconformities in their tectonic interpretation of the study area. They state that continued, intermittent crustal extension in the northern Cordillera is indicated by late Cambrian development of the Misty Creek Embayment, Middle(?) Ordovician development of Meilleur River Embayment, and Root Basin. Considering the similar tectonic histories, it would seem reasonable, therefore, that the conclusions reached by Feinstein et al. (1996) could be extrapolated to the nearby study area. Major unconformities in the Mackenzie Plain region were characterized by Feinstein et al. (1996) using paleothermometric and paleobarometric methods. Their studies implied that the maximum pre-erosion thickness of Cretaceous-Tertiary strata was about 3 km. The major maturity discontinuity that exists between Cretaceous and Devonian strata in the Paleozoic Root Basin portion of their study area indicated about 0.5 to 2 km of erosion at this unconformity, and high geothermal gradients (about 55-65°C/km), sometime prior to mid-Cretaceous time.

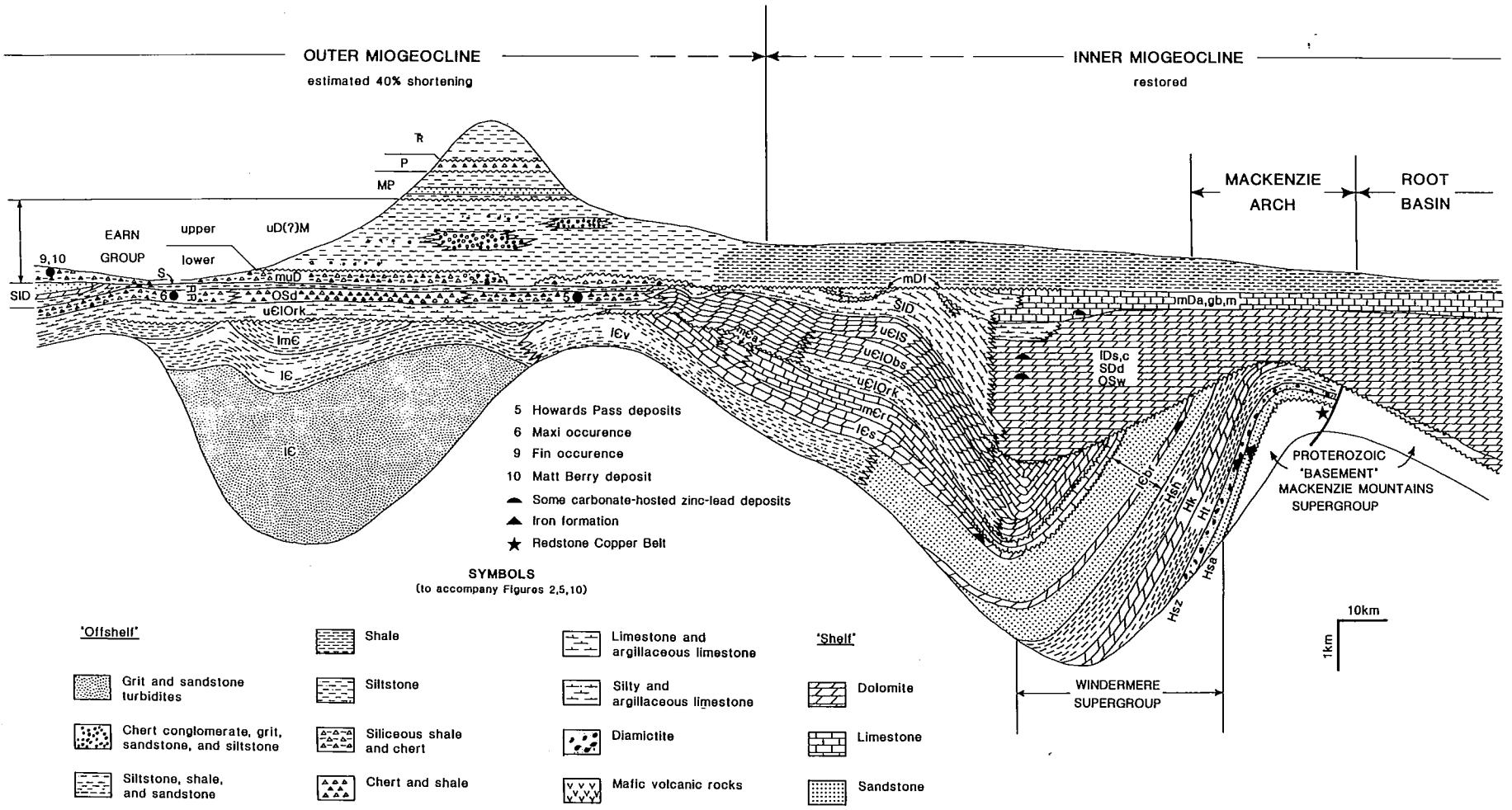

FIGURE 2. Restored stratigraphic section across the Cordilleran miogeocline in Yukon and Northwest Territories, modified from Gordey (1981b, 1982). Location shown in Figure 1. Hsa - Sayunei Fm, Hsz - Shezal Fm., Ht - Twitya Fm, Hk - Keele Fm, Hsh - Sheepbed Fm, lCbr - Backbone Ranges Fm, lCs - Sekwi Fm, lCv - Vampire Fm, mCr - Rockslide Fm, lCObs - Broken Skull Fm, uCOrk - Rabbitkettle Fm, OSd - Duo Lakes Fm, OSw - Whittaker Fm, SDd - Delorme Fm, - lDs - Sombre Fm, lDc - Camsell Fm, mDa - Arnica Fm, mDgb - Grizzlie Bear Fm, mDm - Manetoe Fm, mDln - Nahanni Fm, nDh - Headless Fm, mDl - Landry Fm, mDf - Funeral Fm, mDna - Natla Fm.

Fig. 7-1. Restored stratigraphic section across the Cordilleran miogeocline in Yukon and Northwest Territories (Abbott et al., 1986, Fig. 2).

CONODONT COLOUR ALTERATION INDEX

Conodonts are distributed worldwide in marine rocks of diverse composition and age (Cambrian to Triassic) but are most easily extracted from carbonate rocks, which makes them very useful for MVT deposit studies. Conodonts undergo sequential colour changes with increasing temperature (Table 7-1) and this is used to estimate the temperature and thus burial depth of the host rocks. The colour changes are produced by progressive carbonization and eventual distillation of organic matter sealed within the layers of individual conodont elements.

The colour changes (CAI) in the conodonts reflects changes in the organic matter. Rocks of Late Cambrian age and younger, contain conodonts, termed euconodonts, which are composed of individual layers. The organic matter within these layers is contained in a sealed system and reacts predictably to thermal stress. In older rocks protoconodonts occur which have a different structure and the organic matter contained in these conodonts does not change as systematically under thermal stress, and, therefore, are not as reliable as a thermal maturation indicator. In this study most CAI readings are from euconodonts.

Table 7-1. Correlation of Conodont Colour Alteration Index Values and Temperatures (after Epstein et al., 1977, and Rejebain et al., 1987).

Index	Temperature Range (°C)
1	<50-80
1.5	50-90
2	60-140
3	110-200
3.5	155-250
4	190-300
5	300-480
6	360-550
6.5	440-610

In addition to recording thermal effect, colour alteration index (CAI) values are also logarithmically time-dependent (see Ahrrenius plot, Fig. 9, Epstein et al., 1977) . Conodonts subjected to low temperatures for long periods of time can yield higher colour alteration index values than

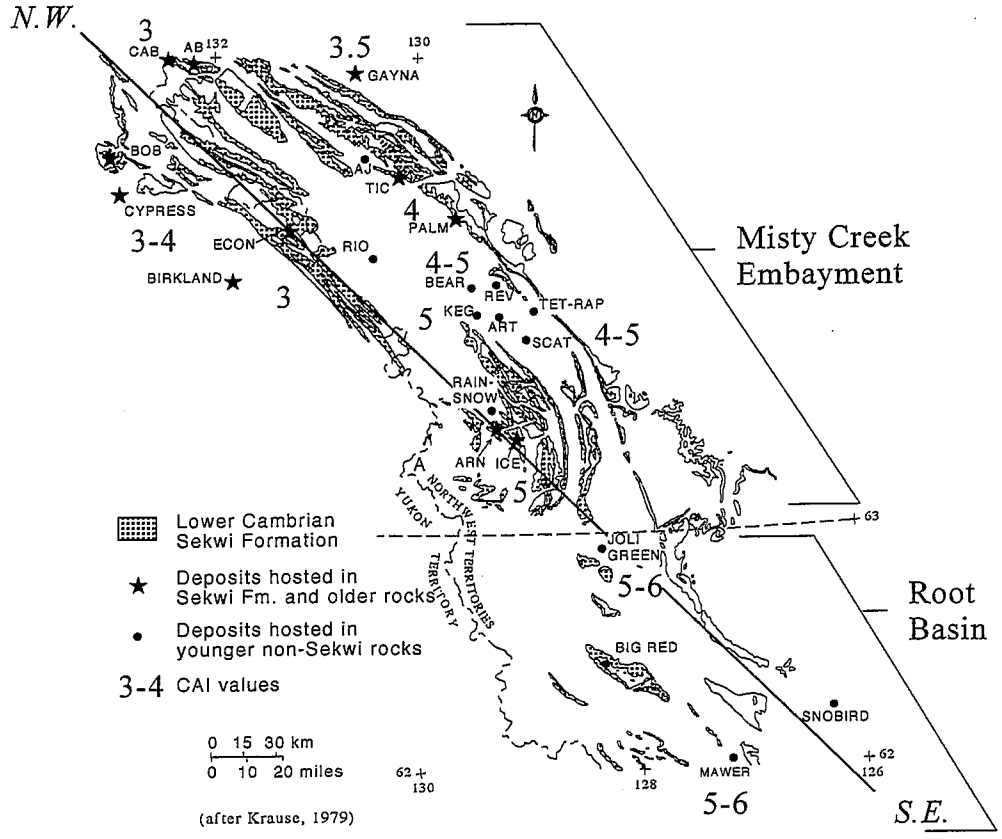

Fig. 7-2. CAI values, compiled from Read et al.,(1991a), Dougherty et al., (1991), and Read et al., (1991b).

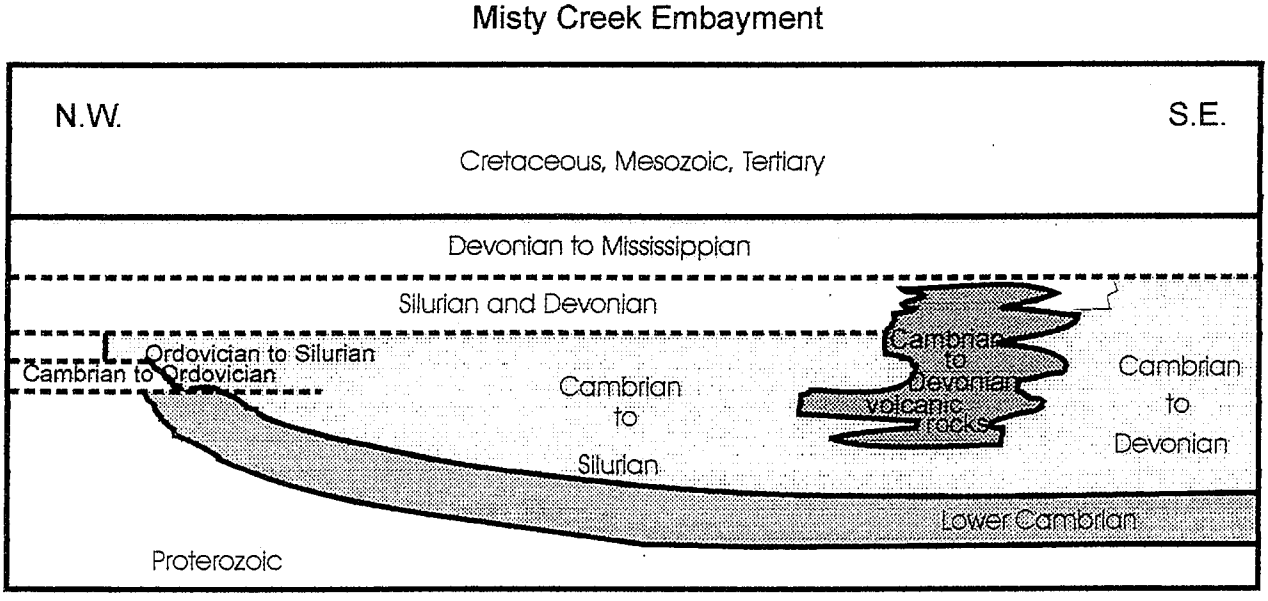

Fig. 7-3. Schematic stratigraphic relationship for the Misty Creek Embayment from 63° to 65°N (after Cecile, 1982, Figure 1). Unconformity.....

conodonts subjected to high temperatures over short periods (Helsen, 1995). CAI values are plotted in Figure 7-2. Note that the Misty Creek Embayment becomes progressively hotter (Fig. 7-2) and deeper to the southeast as shown in Fig. 7-3. The trend continues into the Root Basin where the Joli Green and Mawer deposits are located. The conodonts, for example, from the Mount Kindle/Whittaker Fm. are of Ordovician to Silurian age, and have a CAI of 4 (Read et al., 1991a) correlating with a temperature range of 190° to 300°C (Table 7-1). Conodonts from the Mount Kindle/Whittaker Formation and adjacent formations were not from an area near any deposit, and, therefore, likely attained their temperature history through burial rather than through contact with mineralizing fluids. In addition, the period of time during which mineralizing fluids might have passed would likely be relatively short compared to the long period of burial (Rowan and Goldhaber, 1995). The maximum possible time span for burial of these rocks is from the Ordovician-Silurian boundary to the end of the Cretaceous which is approximately 335 m.y., at which time unloading had begun. This length of time would reduce the temperature required to yield the indicated CAI.

These data would suggest that CAI values obtained for Mackenzie Platform host rocks may have resulted from other factors such as high geothermal gradient (55°-65°C/km) and length of time of burial, making the original estimate of burial depth of 2-5 km possible.

THERMAL MATURATIION

Thermal maturation is a process which occurs upon burial when organic matter in sedimentary rocks undergoes numerous compositional changes that are dictated initially by microbial agencies and later by thermal stress (Horsfield and Rulkötter, 1994). Vitrinite reflectance (R_o) is one method used to measure thermal maturation. Vitrinite reflectance data can be expected from Devonian and younger rocks only because vitrinite is formed from land plants which did not exist in pre-Devonian time. There are four levels of thermal maturity: Immature ($R_o < 0.5\%$), Mature ($0.5\% < R_o < 1.5\%$), Overmature ($1.5\% < R_o < 3.0\%$), and Supermature ($3.0\% < R_o < 4.0\%$). Correlation of organic maturation indices for all four levels are given in Table 7-2.

Table 7-2. Correlation of organic maturation indicies: Vitrinite Reflectance (%Ro), Thermal Alteration Index (TAI), Conodont Alteration Index (CAI) and Tmax (after Dougherty, et al., 1991, Dougherty, 1995, and Horsfield and Rullkötter, 1994).

%Ro	TAI	CAI	Tmax (°C)	Level of Thermal Maturity	Thermal Maturation Processes
	1	1.0			
				Immature	Diagenesis
0.3	1+		425		
0.4					
	2-				
			430	**Marginally Mature**	
0.5		1.5			
0.6	2				
0.9	2+				
		2.0		**Mature**	
1.0				peak of oil formation	Catagenesis
1.2	3-				
1.35		2.5	450		
	3	3.0			
				Marginally Overmature	
1.5		3.5	475		
	3+				
		4.0			
2.0	4-		500	**Overmature**	
2.2		4.5			
3.0	4				
					Metagenesis
	4+	5			
				Supermature	
4.0	5				
		6.0			

BEHAVIOUR AND SIGNIFICANCE OF ORGANIC MATTER

Organic matter, the major global precursor of petroleum, consists of selectively preserved, resistant, cellular organic materials (algal, pollen, spores, and leaf cuticle - or precursor organisms such as plankton and algae) and the degraded residues of less resistant biological matter (amorphous material) in variable proportions. With increasing maturation the organic matter fractionates into bitumens and nonbitumens. As a soluble fraction, the bitumen is able to migrate into traps. The non-soluble pyrobitumens (including the kerogen fraction) does not migrate away from the source rock. The Mature level of thermal maturity constitutes the principal stage of oil formation. As thermal maturation continues the Overmature level (CAI 3.5 to 4.5) is reached in which only methane, hydrogen, and highly carbonized solid organic material are stable. Once the CAI reading reaches 4.5 or greater, the Supermature level, everything has been cooked and all that remains is inert, fixed carbon.

Maximum burial of 6 km is thought to have occurred in Late Cretaceous-early Tertiary time (Feinstein et al., 1996). Their burial models also indicate that significant burial occurred in mid-Mesozoic time when temperatures from 100° to 300°C are indicated. As burial proceeds, organic matter, derived from the degradation products of marine microorganisms and indigenous to the host rocks (Gize and Hoering, 1980), undergoes chemical reactions and products such as CO_2, H_2S CH_4, N_2 etc. are formed. CO_2 and CH_4 have been identified in Mackenzie Platform ore and gangue minerals (this study). Bacterial and thermochemical sulphate reduction reactions also occur and Machel et al. (1995) point out that the major products and by-products from these two reactions are identical, even though they take place in mutually exclusive thermal regimes. Products include altered and oxidized hydrocarbons, hydrogen sulphide, base and transition metal sulphides, elemental sulphur, and carbonates (mainly calcite and dolomite).

The Palaeozoic rocks of the study area appear to be overmature with respect to liquid hydrocarbon generation. The conodont data indicate CAI values range from 3 in the northwest to a maximum of 6 in the southeast (Fig. 7-2). This trend correlates with increasing burial depth of the Misty Creek Embayment (Fig. 7-3).

THERMAL COMPARISON USING FLUID INCLUSIONS

Following on the studies of Sangster et al. (1994) a thermal comparison of the MVT deposits of the Mackenzie Platform and their host rocks was made using fluid inclusion data gathered in the present study and conodont colour alteration index data from recent publications covering the study area (e.g.

Pohler and Orchard, 1990). The comparison for Group 1 deposits (ore temperature=host rock temperature; Sangster et al., 1994) is shown in Fig. 7-4a, and includes Gayna, Cypress, Ab, Cab, and Econ. The comparison for Group 3 deposits (ore temperature<host rock temperature) is shown in Fig. 7-4b, and includes Palm, Mawer, Joli Green, Bear, and Rev.

The fluid inclusion data from sphalerite and gangue minerals for Gayna, Cypress, Ab, Cab, and Econ deposits give minimum values from 88° to 150°C and maximum values from 122° to 252°C with mean values ranging from 110° to 197°C. The CAI temperature range for rocks hosting or overlying these deposits is 3 to 3.5 representing a temperature range of 110° to 250°C. These deposits, therefore, fit the criteria for Group 1 deposits as defined by Sangster et al., (1994). Host rocks were heated at burial depths indicated by the colour alteration index values, then ore was deposited from fluids in thermal equilibrium with the host rocks at this depth of burial.

In contrast, fluid inclusion data from sphalerite and dolomite cement for Palm, Mawer, Joli Green, Bear, and Rev deposits give minimum values from 94° to 175°C and maximum values from 153° to 256°C with mean values ranging from 145° to 210°C. The CAI temperature range for rocks hosting or overlying these deposits is 4 to 6 representing a temperature range of 190° to 550°C. Since the temperatures indicated by the fluid inclusion data are less than those indicated by the CAI data from host rocks, these deposits fit the criteria for Group 3 deposits (Sangster et al, 1994).

At a geothermal gradient of 50°C/km and a surface temperature of 20°C, a temperature of 550°C suggests 10.6 km of burial. As discussed earlier, the burial depth could be less if the geothermal gradient (55°-65°C/km) suggested by Feinstein et al. (1996) is accepted and if the burial time is extended to approximately 335 Ma. A higher geothermal gradient is considered plausible due to the presence of nearby Paleozoic igneous rocks (Fig. 7-5). There is some overlap of temperatures at the CAI 4 value. For Group 3 deposits scenario no. 3 from Sangster et al. (1994) explains the data best if a mineralization age of Late Devonian to Late Carboniferous is accepted (see later discussion). Mineralization occurred at an early stage in host-rock diagenesis (e.g. pre-Mesozoic), and post-ore heating, by continued burial (or possible igneous influence from the Cambrian to Lower Devonian Marmot volcanic intrusions), raised host rock temperatures higher than the temperature of mineralization, but only the host rock recorded higher temperatures. The conodonts in the host rocks record the temperature induced by the burial depth and accompanying factors, and reflect more closely the true maximum temperature. The fluid inclusions in the ore and gangue minerals are sealed systems and were not affected by the burial depth to the same extent. The fluid inclusions from deposits in Group 3 show some indication of reequilibration (see discussion in Microthermometry section) and

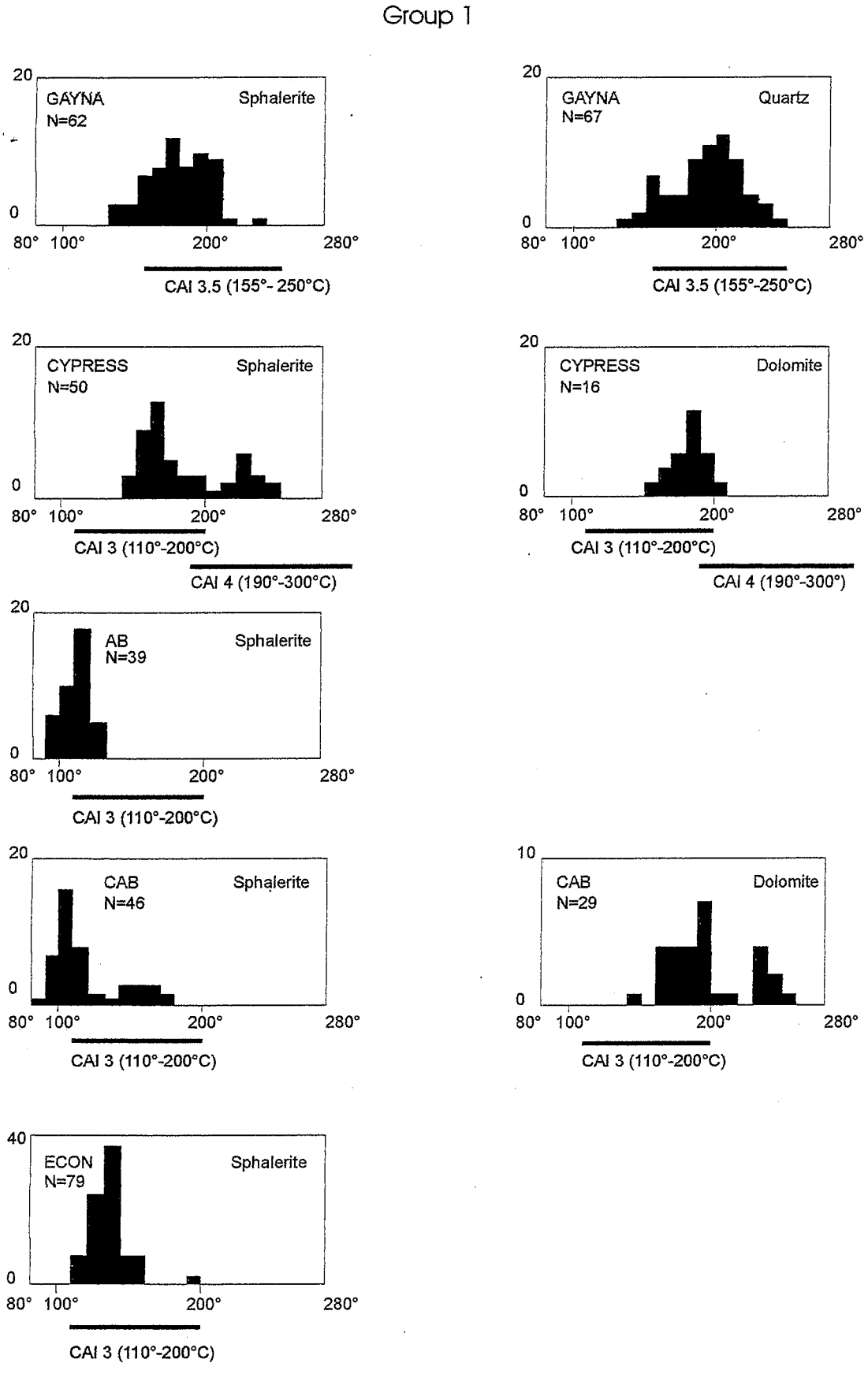

Fig. 7-4a. Homogenization temperatures (histograms) for sphalerite and gangue quartz and dolomite for Group 1 deposits (after Sangster et al., 1994) compared with the temperature range for conodont colour alteration index (CAI - bar graphs) from the Phanerozoic formations hosting or overlying these deposits. N = number of analyses.

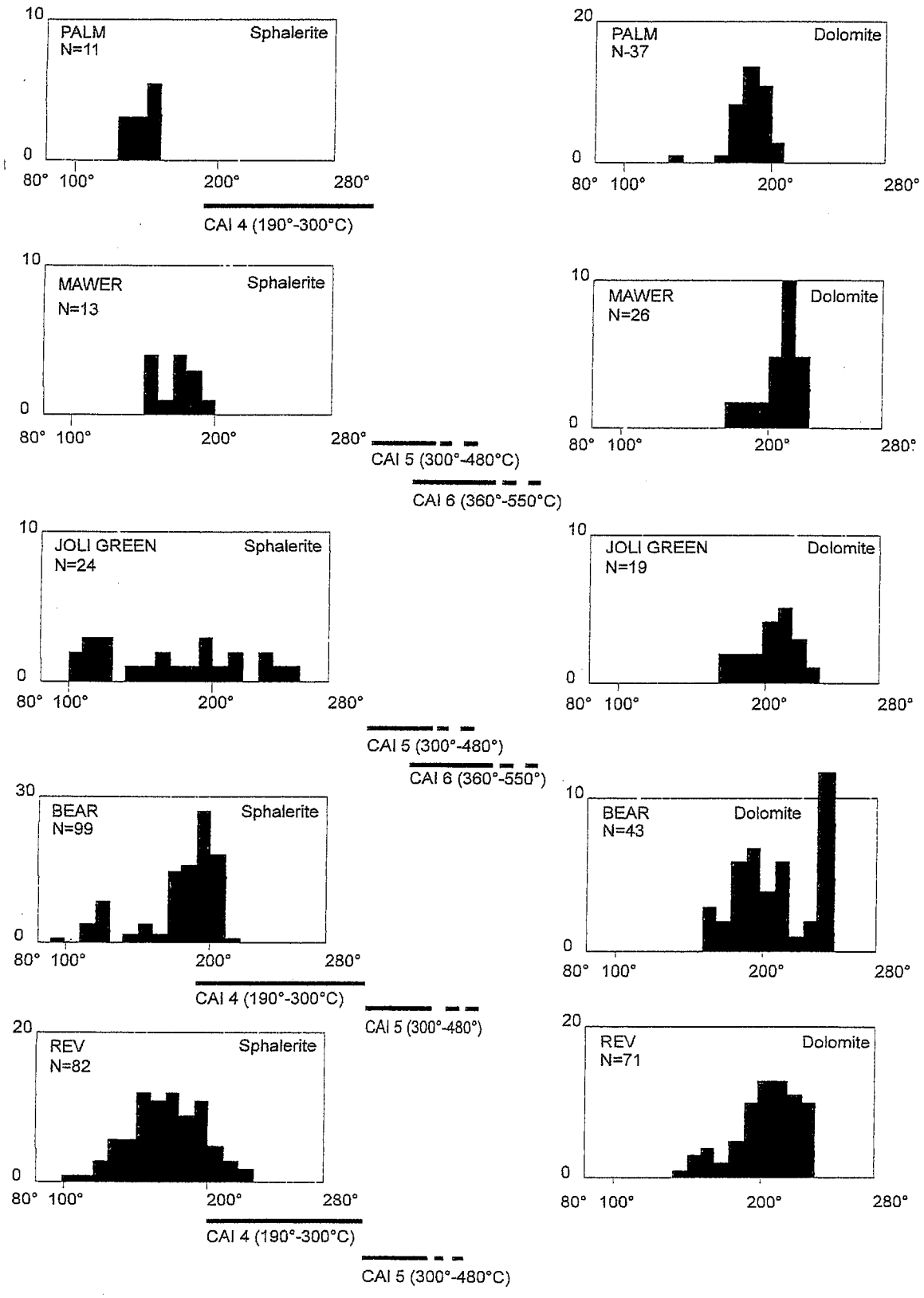

Fig. 7-4b. Homogenization temperatures (histograms) for sphalerite and gangue dolomite for Group 3 deposits (after Sangster et al., 1994) compared with the temperature range for conodont colour alteration index (CAI - bar graphs) from the Phanerozoic formations hosting or overlying these deposits. N = number of analyses.

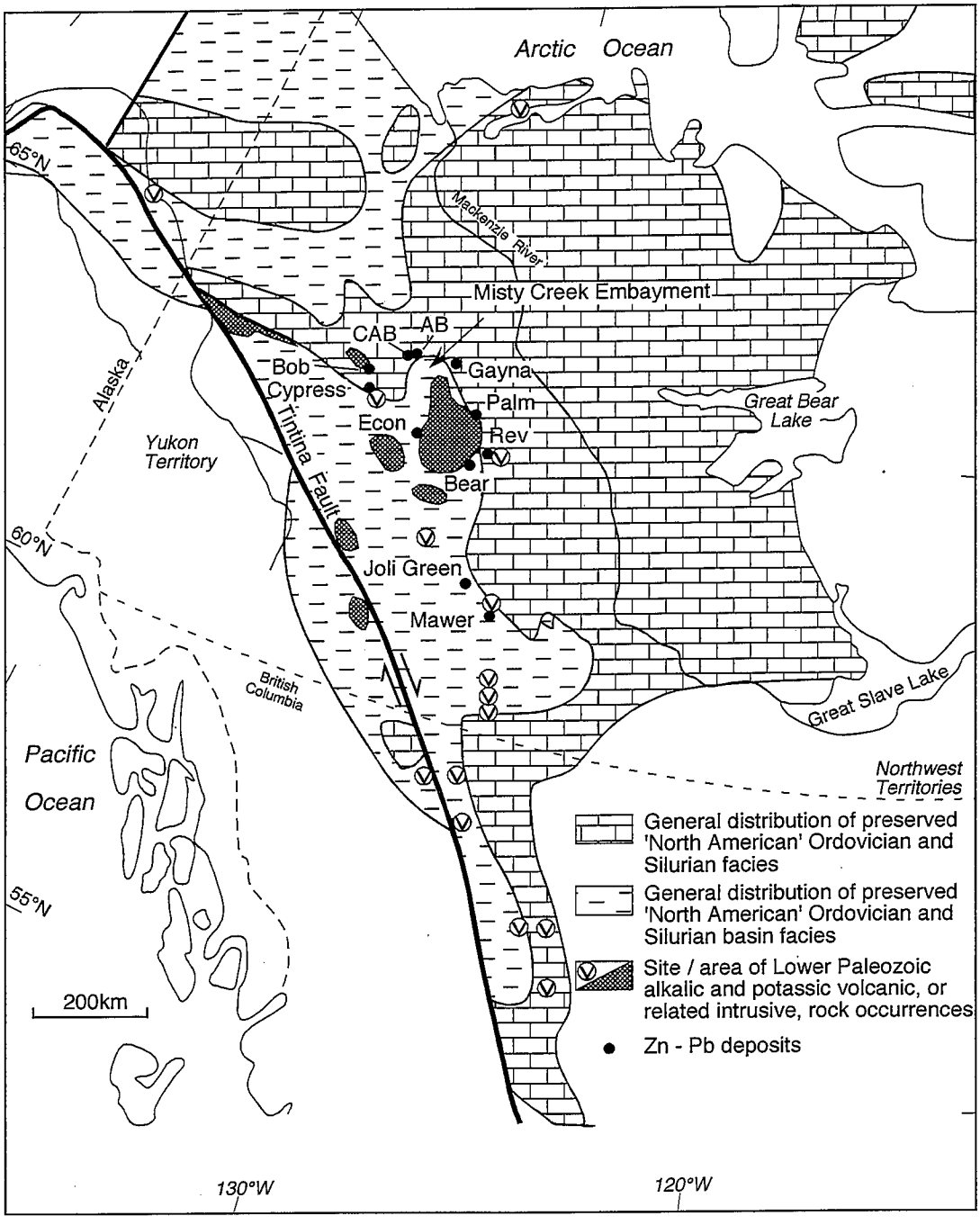

Fig. 7-5. Map showing location of Misty Creek Embayment, occurrences of alkalic and potassic Lower Paleozoic rocks, and the location of deposits for which there are some fluid inclusion data (after Cecile et al., 1997).

likely reflect temperatures greater than ore deposition but less than those indicated by the conodont colour alteration index. Group 3 deposits which are located toward the S.E. end of the Misty Creek Embayment and into the adjacent Root Basin may have been deposited at a greater depth than Group 1(Fig. 7-3); and, with the additional post-ore heating the fluid inclusions in these deposits were more likely to have undergone some reequilibration.

8. SUMMARY

The study involves the integration of petrography, microthermometry, cathodoluminescence microscopy, and electron microprobe analyses. The results of our study are noted here as follows:

1. The deposits of the study area are located in strata older than Late Devonian. The deposits follow the trend of Lower Paleozoic strata, which marks the shale to carbonate facies change, for 360 km along the Mackenzie Fold Belt, and appear to be of classic Mississippi Valley-type (Dawson, 1975). Zinc commonly predominates over lead by at least 10:1 (Gibbins, 1983). Zinc-lead occurrences and deposits occur in platform carbonates surrounding the Misty Creek Embayment, an outlier of the Selwyn Basin within the "Mackenzie Platform". The embayment is a northwest-trending depositional feature defined by the change from Upper Cambrian-Lower Ordovician, and from Upper Ordovician-Lower Silurian platform carbonate, into correlative transition and deeper water limestone, shale and chert; and by Middle Cambrian and Middle Ordovician basin shale and transition units (Cecile,1982). The embayment is best defined by the transition from platform to basin facies because these strata are extensively preserved within and around the embayment. Cecile et al., (1997).

2. The mineralogy of the sixteen deposits studied in detail includes dolomite cement, pyrite, sphalerite, galena, quartz, calcite, and occasionally barite. Secondary minerals include bitumen, smithsonite, hydrozincite, and cerussite. Mineralization commonly occurs in collapse breccias, as open space filling of vugs, fractures and veins, and as replacement of sedimentary structures and disseminations along bedding planes. Channelways in favourable host dolomite units are controlled, in part, by jointing, fracturing and faulting.

3. The dolomite cement was divided into two dolomite groups based on grain size. Finer grained dolomite cement [or dolomite cement(1) in the paragenesis] was defined as ranging in grain size from 60-2000 μm (mean 515 μm) and includes replacive saddle dolomite. Coarse-grained saddle dolomite ranges in grain size from 200-6600 μm (mean 1570 μm).

4. The cathodoluminescence (CL) work showed that in all examples the saddle dolomite cement is paragenetically associated with sulphide mineralization. The dolomite cement, generally coarse-grained saddle dolomite and/or the finer grained dolomite cement, which can be replacive saddle dolomite, is commonly intergrown with the sulphides and is either co-genetic or deposition of dolomite is closely alternating with the sulphide minerals (in space and time).

5. Ternary plots of the 2821 analyses of carbonate minerals show end-member dolomite

compositions for all dolomite types. Deposits which contain little or no luminescent dolomite including Tet-Rap, Birkland, Keg, Art, Scat, Rio, Aj, and Big Red are commonly hosted in limestone rather than dolomite, and contain more abundant quartz and calcite.

6. The observed paragenetic sequence is generally similar in all sixteen deposits studied which have predominent dolomite cement. The most obvious difference between the sixteen deposits is in the host dolomite which, in some cases, contains disseminated pyrite. The host dolomite is, for the most part, nonplanar dolomite, which develops in excess of 50°C in the burial environment (1km or greater) by dolomitization of limestone or neomorphic recrystallization of preexisting dolomite. The average grain size of host dolomite ranges from 42 to 215 μm. Dolomite cement(1) is finer grained dolomite cement defined as ranging in grain size from 60-2000 μm (mean 515 μm) and includes replacive saddle dolomite. Dolomite cement(2) is coarse-grained saddle dolomite and ranges in grain size from 200-6600 μm (mean 1570 μm). In most cases dolomite cements(1) and (2) formed from the same fluid as suggested by the carbonate geochemistry. Possible exceptions could be Palm, Cypress, Bob, and Econ. One of the factors determining grain size was possibly the size of the cavity in which the cement grew.

Pyrite occurs as sparse to abundant euhedral to subhedral disseminations in the host dolomite of deposits Ab, Cab, Bob, Palm, Mawer, Bear, Snobird, and Rev. Deposits in which host dolomite does not contain pyrite include Econ, Ice, Arn, Rain, Cypress, Tic, and Joli Green. Pyrite occurs as an ore stage mineral in deposits Tic, Ice, Arn, Tet-Rap, Birkeland, Keg, Aj, and Big Red, and is particularly abundant at Bob deposit.

Sphalerite(1), where present, is disseminated in the host dolomite and commonly replaces the disseminated pyrite. Sphalerite(2) is coarse grained and fills open spaces.

Quartz occurs as detrital grains in some host dolomite such as Cab, and in varying amounts as authigenic quartz in ore- and post-ore stages of the paragenesis. Ab, Cab, Cypress, Tic, Palm, Mawer, Bear, and Snobird contain quartz as an ore stage mineral. Econ, Ice, Arn, and Rain have no ore stage quartz. In the Joli Green deposit the ore stage quartz is a mélange of quartz and calcite.

7. Post-mineralization effects observed in deposits hosted in rocks older than Middle Cambrian include twinned sphalerite and fluid inclusions in sphalerite aligned along former cleavage fractures in Gayna deposit, decrepitated inclusions in sphalerite from Cypress and Bob deposits, bent cleavage planes in sphalerite from Bob deposit, and undulatory extinction in quartz from Bob deposit. Post-mineralization effects observed in deposits hosted in rocks younger than Middle

Cambrian include healed fractures in sphalerite and wispy texture created by many fluid inclusion trails criss-crossing the quartz grain from the Bear deposit, dolomite host rock cut by stylolites, and dolomite cement veins cutting dolomite host rock, offset by stylolites, and bent cleavage planes and disrupted extinction in sphalerite from Rev deposit.

8. Five types of fluid inclusions were identified although not all five were present in any one deposit. They are defined as follows: **Type 1**, two-phase H_2O (l) + H_2O (v); **Type 2**, three-phase H_2O (l) + H_2O (v) + solid (rounded or disc shaped - not halite); **Type 3**, three-phase H_2O (l) + CO_2 (l) + CO_2 (v); **Type 4a**, one-phase fluid CO_2/CH_4 (clear and colourless), **Type 4b**, one-phase fluid CH_4 (?) (clear and coloured - orange or yellow), **Type 4c**, two-phase fluid CH_4 (?) + solid; and **Type 5**, one-phase, dark-filled (organic-rich ?).

9. Type 4 inclusions containing CO_2/CH_4 were shown to occur in sparse quantities in most deposits, and have been confirmed in the following deposits: Gayna, Econ, Ab, Cab, Rev and Bear.

Note: **Type I** inclusions were not defined as containing vapour other than H_2O because this has only been suspected, but has not been confirmed. The fact that many Type 1 fluid inclusions take longer, and a higher temperature, to homogenize than would be expected considering the size of the vapour bubble is often noted, and this effect could be caused by the presence of CO_2/CH_4 in the vapour bubble (Roedder, pers. comm., 1994).

10. Microthermometric data for **Type 1** inclusions display moderate variability. Variability was not assessed for the other inclusion types because not enough data was collected. Moderate variability occurs when inclusions of variable size and shape measured in a single FIA do not have 90% of the Th data within a 10-15°C interval.

11. Four distinct mineralizing fluids, with two sub-types, have been identified. Fluid Ia has mean characteristics of >20 eq. wt.% NaCl at a mean T_{min} 175°C. Fluid Ib is less saline, ranging from 12.8-20.2 eq. wt.% NaCl and mean T_{min}153°C. Fluid IIa has a mean salinity >22 eq. wt.% NaCl and a T_{min} 104°C. Fluid IIb has mean salinity ranging between 15 and 20 eq. wt.% NaCl, and mean T_{min} 111°C. The mean salinity of Fluid III ranges from 3.5-6.8 eq. wt.% NaCl and mean T_{min} 177°C. Fluid IV mean salinity ranges from 5-9.4 eq. wt.% NaCl and mean T_{min} 118°C.

12. Electron microprobe studies of cathodoluminescent, zoned dolomite cement and host dolomite revealed that one group of deposits, including Ab, Cab, Bob, Econ, Palm, Ice, and Arn (hosted in Lower Cambrian Sekwi Formation), Tic (hosted in atypical Sekwi Formation), Cypress (hosted in Late Hadrynian Sheepbed (?) Formation), and Gayna (hosted in Helikian Little Dal Group) had

higher Fe and slightly lower Mn content than the second group (Table 5-1). The latter group, hosted in carbonate rocks younger than Middle Cambrian, includes Bear, Rev, Rain-Snow, Joli Green, Mawer, and Snobird. The dolomite in all these deposits contains insignificant amounts of Fe (i.e. >60% of values under detection limit), and all but Bear and Rev contain insignificant amounts of Mn (Table 5-1). Bear and Rev dolomite have elevated levels of Mn.

13. The limited data for minor elements (Pb, Fe, Cd, Cu, Mn, Co, Ge, Ga, Ag, Bi, As, Se, and In) in sphalerite support the divisions of deposits by fluid type. Fluid I formed the sphalerite in the Gayna, Cypress, Joli Green, Bear, and Rev deposits. The minor element contents of sphalerites from these deposits are similar in most respects. The differences in minor element content of sphalerites in these deposits could perhaps be explained by the fact that the host rocks, through which the fluids flowed, are different for many of these deposits. The Economic (Econ) deposit stands out as being completely different because of its high and varied minor element content of sphalerite, which was formed from Fluid IV. Palm sphalerite, formed from Fluid II, is also different in that it contains significantly more Fe than any other deposit.

14. The following characteristics of the dolomite were observed (i) the majority of the dolomite hosting Zn-Pb deposits is made up of nonplanar dolomite, (ii) all sixteen deposits hosted in dolomite contain saddle dolomite, (iii) fluid inclusion data for saddle dolomite from seven of these deposits indicate that the dolomite formed at temperatures greater than 150°C from highly saline, Na-Ca-Mg-Cl type, brines. Although both planar and non-planar dolomite types are present, a majority of host dolomite and dolomite cement display nonplanar texture.

15. Microthermometric data indicated two groups of deposits as per Sangster et al., (1994). Group 1 (ore temperature=host rock temperature) and Group 3 (ore temperature< host rock temperature). Deposits meeting the criteria of Group 2 (Sangster et al., 1994) were not found in this study.

16. Fluid I is found in deposits hosted in Proterozoic rocks (Gayna River, Cypress), Cambrian rocks (Cab, Palm), Late Cambrian-Early Ordovician (Joli Green), Middle Ordovician (Mawer), and Ordovician-Silurian rocks (Bear, Rev). The areal and stratigraphic extent of this mineralizing event is indicated by the fact that Fluid I was found in these deposits which are located from one end of the study area to the other and occur in rocks of ages from Mesoproterozoic to Ordovician-Silurian.

17. Solid pyrobitumen, post-sulphide, occurs in the centres of vugs lined with dolomite cement in deposits such as Bob.

9. DISCUSSION AND CONCLUSIONS

CHARACTERISTICS OF DEPOSITS

Deposits occur in platform carbonates surrounding the Misty Creek Embayment, an outlier of Selwyn Basin within the "Mackenzie Platform". Cecile et al., (1997) discuss evidence for three extensional events following initial rifting and breakup in parts of the Canadian Cordillera: 1) Early Cambrian; 2) Middle Ordovician; and 3) Late Silurian to Early Devonian. The Middle Ordovician event was accompanied by widespread alkalic and potassic volcanism and igneous activity; the Late Silurian-Early Devonian event also resulted in alkalic volcanism (Goodfellow et. al., 1995). Gabrielse et al., (1991) recognized five tectonic events through time. The extensional events which possibly could have initiated fluid flow are as follows: 1) Early to Middle Cambrian time, the opening of Misty Creek Embayment, preceding the opening of contiguous Selwyn Basin in Cambro-Ordovician time; 2) Middle Cambrian rifting in the northern Rocky and Selwyn mountains; 3) Early to Middle Ordovician time, the development of the Meilleur River Embayment and Root Basin; 4) Cambro-Ordovician and Devonian rifting in the Rocky Mountains and Selwyn Basin; and the most likely event, 5) Late Devonian to Early Mississippian time, the southward progradation of a clastic wedge following block uplift, granitoid plutonism, and alkalic volcanism accompanying a major Cordilleran rifting event.

Mineralogy is simple and consists of pyrite, sphalerite, galena, dolomite, quartz and calcite. Texture of ore is predominately open-space filling of secondary porosity with some replacement of breccia fragments and host rock. Sulphides and carbonates constitute the cement between breccia fragments composed of host dolomite. Both ore and gangue minerals are coarse grained (200-6600 μm).

There is a possibility of a remote association with igneous rocks (Fig. 7-4). Deposits occur in area of mild deformation expressed as structures dominated by open folds and zones of complex folding and thrusting regionally, as well as deformation features on a microscopic scale. Fluid inclusions in sphalerite, dolomite, and quartz contain, saline, aqueous brines. Total dissolved salts range from 12 to 27 equiv. wt. % and are predominantly sodium, calcium, and magnesium chlorides. It was concluded that Fluids I and II belong to the $NaCl\text{-}CaCl_2\text{-}MgCl_2\text{-}H_2O$ system. Fluids III and IV have been placed in a different system, likely the $NaCl\text{-}MgCl_2\text{-}H_2O$ system.

SETTING OF MINERALIZATION

The stratigraphic, petrographic, geochemical, CL, conodont, and fluid inclusion microthermometry data presented here suggest dolomitization by hot brines, in a burial setting. Dolomites are considered to be burial dolomites that have formed at depths greater than 1 km. Inclusions in the FIAs measured have experienced processes that have caused some degree of thermal reequilibration and, therefore, the Th's are likely higher than the actual temperature of homogenization/entrapment. Only under extreme conditions is complete reequilibrium to the new conditions ever attained. For example, a burial depth of greater than 5 km would be required to completely reequilibrate all inclusions.

Data discussed suggests that higher than normal geothermal gradients and length of time of burial were factors which contributed to the high CAI values for Mackenzie Platform host rocks. The higher geothermal gradient of 55-65°C/km (Feinstein et al., 1996) is supported by the presence of nearby Paleozoic igneous rocks. If the burial time is extended to approximately 335 Ma the original estimate of burial depth 2-5 km is possible.

Given the problems in generating large volumes of magnesium required to dolomitize limestone, most burial dolomites are probably restricted to the margins of carbonate platforms in direct contact with the dewatering basinal sediments (e.g. Selwyn Basin) or to aquifiers carrying these fluids (Warren, 1989). The deposits of the study area occur in platform carbonates surrounding the Misty Creek Embayment, an outlier of the Selwyn Basin, and the Root Basin within the "Mackenzie Platform". The deposits follow the trend of Lower Paleozoic strata, which marks the shale to carbonate facies change, for 360 km along the Mackenzie Fold Belt. Although the facies change boundary between the shale and carbonate shifted over time, the belt of rocks which has been mineralized hugs close to this boundary over the length of 360 km.

To further investigate possible settings, the deposits for which there is microthermometric data have been divided into two groups depending on the temperature of mineralization as compared to the temperature of the host rock (Sangster et al., 1994). For Group 1 (Gayna, Cypress, Ab, Cab, Econ deposits) based on Sangster et al. (1994) one possible setting senerio to explain the findings would be, host rocks were heated at temperatures indicated by the colour alteration index values, then ore was deposited from fluids in thermal equilibrium with the host rocks. For Group 3 (Palm, Mawer, Joli Green, Bear, and Rev deposits) based on Sangster et al. (1994) mineralization could have occurred at an early stage in host-rock diagenesis (e.g. pre-Mesozoic), and post-ore heating, by

continued burial (or possible igneous influence from the Cambrian to Lower Devonian Marmot volcanic intrusions), raised host rock temperatures higher than the temperature of mineralization, but only the host rock recorded higher temperatures. The conodonts in the host rocks record the temperature induced by the burial depth and accompanying factors, and reflect more closely the true maximum temperature. The fluid inclusions in the ore and gangue minerals are sealed systems and were not affected by the burial depth to the same extent.

Group 3 deposits which are located toward the S.E. end of the Misty Creek Embayment and into the adjacent Root Basin may have been deposited at a greater depth than Group 1; and, with the additional post-ore heating the fluid inclusions in these deposits were more likely to have undergone some reequilibration. Deposits in these two groups are not mutually exclusive as far as genesis of the mineralization because it has been shown that Fluid 1 was identified in deposits from both groups.

AGE OF MINERALIZATION

McLaren and Godwin (1979b) proposed that two independent processes of mineralization (metallogenic events) were responsible for carbonate-hosted zinc-lead deposits in the region. One during Middle to Late Cambrian responsible for the mineralization at Gayna, Birkeland, Cypress, Palm, Econ, and Tic deposits, hosted in rocks of Lower Cambrian and older, and another during Late Devonian or later responsible for the mineralization at Bear, Rev, Rain-Snow, Art, and Aj deposits hosted in rocks younger than Middle Cambrian. They suggest a karstic model for the former group and a basin dewatering model for the latter group. Continuing the research, Godwin et al., (1982) reported Pb-isotope data for 34 carbonate-hosted deposits and demonstrated two groups of deposits, those with $^{206}Pb/^{204}Pb$ = 16.27 to 19.66 [~0.52 Ma (Early Cambrian)] and another with $^{206}Pb/^{204}Pb$ = 18.17 to 20.26 [~ 0.37 Ma (Early Carboniferous)] which supported the earlier proposal of two independent metallogenic events and two different sources of Pb. Interestingly, Pb isotope data for eight of the 34 deposits included in Godwin et al. (1982) divide the deposits into somewhat different groupings; one (Econ) falls in the "karstic" group, whereas seven [Palm, Birkeland, Rev, Tegart (Tic), Backbone (Art), Weather (Rain-Snow), and Twitya (Bear-Twit)] are in the "basin dewatering" group.

Timing of mineralization can be inferred when several factors are considered: 1) fluid inclusion data suggest that some reequilibration has occurred which requires the fluid inclusions to

have been subjected to overheating, likely due to post-ore burial, 2) presence of deformation textures in sulphide minerals suggest that burial continued and/or some tectonic activity occurred after ore formation, 3) Fluid I is found in deposits hosted in Proterozoic rocks (Gayna River, Cypress), Cambrian rocks (Cab), and Silurian/Lower Devonian rocks (Bear, Rev) which means mineralization resulting from Fluid I occurred after the Lower Devonian rocks were lithified, and 4) solid pyrobitumen occurs in the centres of vugs lined with dolomite cement in deposits such as Bob which attests to the former presence of oil, at least locally. According to Morrow and Aulstead (1995) oil maturation and migration into the Manetoe Dolomite reservoirs, which are located just to the south-east of the study area, occurred during Carboniferous time, before the host carbonate sediments were deeply buried. The Manetoe Dolomite represents a diagenetic facies superimposed on pre-existing limestones and dolostones of the Lower Devonian Landry Formation within lower Paleozoic Mackenzie Shelf carbonate sequence of the Mackenzie mountains and the Interior Plains. They state that petrographic and textural observations indicate that emplacement of the coarsely crystalline "saddle" dolomite cements of the Manetoe Dolomite predate the emplacement of bitumen.

The dolomitization of the host rock and the formation of dolomite cement in the study area also appears to be a diagenetic facies superimposed on various formations. This conclusion is supported by the similarity in the geochemical data derived from electron microprobe analyses between the host and the dolomite cement (see Carbonate Geochemistry). The Manetoe Dolomite is present in the study area and extends beyond it to the southeast. The maximum depth to which the Manetoe Dolomite could have been buried is 5000 m in Late Cretaceous-Tertiary time (Morrow and Aulstead, 1995). The deposits studied microthermometrically are all in formations located stratigraphically below the Landry/Arnica Formations, and, therefore, predate the emplacement of bitumen. If organic matter played a role in the formation of the Zn-Pb deposits (see Spirakis and Heyl, 1993, 1994 and 1995) of the Mackenzie Platform then the deposits must have formed before the time of maximum burial to take advantage of the presence of CO_2, H_2S, CH_4, N_2 etc. After maximum burial all that remained was inert fixed carbon which means that there would be no organic matter or derived gases available in the host rocks to react with the ore forming fluids. If a similar timing for oil maturation and migration can be extrapolated to the study area, then, the above factors (1 to 4) suggest that mineralization associated with coarse crystalline "saddle" dolomite documented in the study area and associated with Fluid I took place sometime between Late

Devonian to Carboniferous time.

Several deposits in northern Canada have been dated. The Late Devonian to Carboniferous age for mineralization is supported by the Late Devonian Rb-Sr age for Pine Point mineralization obtained by Nakai et al.(1993). Note that there are ages for Pine Point mineralization which do not agree with this conclusion. Qing, (1991) and Symons et al, (1993) conclude a Laramide (Cretaceous to Early Tertiary) age for Pine Point mineralization based on the systematic decrease of $^{87}Sr/^{86}Sr$ ratios and homogenization temperatures with corresponding increasing delta ^{18} O values of saddle dolomite, and paleomagnetism. Two other deposits in the Canadian Cordillera have been dated using paleomagnetic methods. Both Robb Lake and Kicking Horse have been assigned a Laramide age of mineralization (Symons et al., 1998, Smithurst et al., in press), which is much younger than the age of mineralization suggested for the study area i.e. Late Devonian to Carboniferous time. Work by Nesbitt and Muehlenbachs (1993) identified two major fluid events in the southern Canadian Rockies and showed that fluids closely associated with Laramide deformation are geochemically distinct from fluids involved in a pre-Laramide (post-Middle to Late Devonian) event. They describe Event 1 fluids from Phanerozoic units (>20 eq. wt.% NaCl, Mg-Ca rich brines at a T_{min} of 175°C) as representing a post-Devonian, pre-thrusting, west to east migration from a Paleozoic shale basin into carbonates of the Western Canadian Sedimentary Basin (WCSB). They state that this fluid was responsible for the late dolomitization throughout the WCSB and MVT mineralization at Pine Point. They conclude that one implication of these studies is that MVT deposits in WCSB are not a product of gravity driven flow associated with Laramide uplift of the Rockies.

Age dating of ore-stage minerals in MVT deposits has aided in providing a test for the temporal relation between hypothesized cause and effect which has furthered the evolution of genetic models for MVT deposits. Ideas have evolved from a model in which one orogeny formed all MVT deposits in the United States (Nakai et al., 1990), to a model in which MVT deposits formed during various orogenies at different times in Earth's history (Pan et al., 1990, Nakai et al., 1993; Chesley et al., 1994), to a model that infers MVT's can also form in a rifting environment (Christensen et al., 1995; Brannon et al., 1996).

GEOCHEMICAL MODELS

The sulphate reduction model is favoured over the mixing model and the reduced sulphur

model (Sverjensky, 1986) as a means of precipitating sulphides because several criteria found in this study point to this model. These critera include the presence of organic matter in the host rocks, CO_2 and/or CH_4 in sphalerite, microthermometric data, and distinctive habits (euhedral to subhedral) of the pyrite and dolomite cement.

Studies of burial history and dolomite textures were initiated to define the thermal regime in which the host rocks, and possibly the mineralization, formed. Maximum burial is thought to have occurred in Late Cretaceous-early Tertiary time (Feinstein et al., 1996). The burial models of Feinstein et al. (1996) also indicate that significant burial occurred in mid-Mesozoic time when temperatures from 100° to 300°C are indicated. Organic matter, derived from the degradation products of marine microorganisms and indigenous to the host rocks (Gize and Hoering, 1980), undergoes chemical reactions as burial proceeds. Products such as CO_2, H_2S CH_4, N_2 etc. are formed. Bacterial and thermochemical sulphate reduction reactions also occur. Machel et al. (1995) point out that the major reaction products and by-products from these two reactions are identical, even though they take place in mutually exclusive thermal regimes, and include altered and oxidized hydrocarbons, hydrogen sulphide, base and transition metal sulphides, elemental sulphur, and carbonates (mainly calcite and dolomite). CO_2 and CH_4 have been identified in Mackenzie Platform ore and gangue minerals (this study).

Thermochemical sulphate reduction (TSR) is considered as a possible reaction involved in the precipitation of the Mackenzie Platform deposits because of several distinguishing criteria. In the dolomite cement, according to Machel et al. (1995), these critera include: i) the fact that fluid inclusions are large enough to yield microthermometric results, ii) homogenization temperatures exceeding 150°C, and iii) the distinctive habit of the coarse-crystalline saddle dolomite cements. Pyrite formed as a by-product of TSR tends to be cubic or prismatic in habit. All these critera have been met in this study. The carbon isotopes of carbonates and sulfur isotopes of elemental sulfur and sulfides are also discriminating criteria (Machel et al., 1995), but were beyond the scope of this study.

According to Spirakis and Heyl (1993), the key to localization of Mississippi Valley-type ore is the presence of organic matter at the site of deposition. They proposed that the ores were localised where a hot (80°-220°C) brine bearing thiosulphate ($S_2O_3^{2-}$) and metals interacted with organic matter. A series of reactions is suggested involving organic matter that may account for the major aspects of MVT mineralization and alteration, such as the oscillation between the precipitation

and dissolution of sulphides and carbonates.

The behaviour and significance of organic matter has been discussed in Section 7. The principal feature of the thermal maturation of organic material in host rocks is the evolution of hydrocarbon gases such as CH_4, CO_2, and C_2H_6 which, if trapped, provide a reservoir of reductant for sulphate, either present locally [according to Brock (1976) the Lower and Middle Devonian carbonate strata are characterized by widespread evaporitic sequences, ...] or dissolved in the mineralizing fluid itself (Anderson, 1991). The presence of either CH_4 or CO_2, present in minerals in several deposits in the study area, could be used as indirect evidence to support the presence of organic matter. The products produced (CO_2, H_2S, CH_4, N_2 etc) from chemical reactions as burial proceeds act as a reductant, a source of organic acid, a source of CO_2, and a substrate for bacterial metabolism, and thereby played a critical role in each stage of the paragenesis of Mississippi Valley-type deposits. Spirakis and Heyl (1993) explain how the reduction by organic matter of dissolved partly oxidized sulphur species, such as thiosulphate, at the sites of mineralization presents an alternative mechanism to precipitate sulphide minerals. Other mechanisms include: 1) transport of sulphur as sulphate along with dissolved metals and reduction of sulphate to sulphide by organic matter at the sites of mineralization, and 2) mixing of sulphide-bearing and metal-bearing solutions at the sites of mineralization.

Two processes are likely to form thiosulphate in basins. One involves the remobilization of sulphur in diagenetic pyrite. The other possible process involves the slow reduction of sulphate by hydrocarbons at temperatures of 150° to 200°C. Most Mackenzie Platform host dolomites contain abundant diagenetic pyrite (see Section 4). Pyrite is stable in a wide range of chemical environments, but is susceptible to oxidation. Sediments buried 2-5 km are removed from the influence of atmospheric oxygen, and oxidants are scarce. One oxidizing agent that remains is ferric iron. Much of the ferric iron is initially incorporated in smectite. With increasing depth of burial in sedimentary basins and subsequent heating to about 80°, smectite slowly converts to illite and releases ferric iron, which is then available to participate in redox reactions (Choquette and James, 1990). The almost ubiquitous occurrence of this reaction in terrigenous sedimentary basins worldwide would suggest that the Selwyn Basin-Mackenzie Platform rocks would yield a similar conversion (Hillier et al., 1995). Although the Selwyn Basin-Mackenzie Platform is not a terrigenous basin as such, the "Platform" has been defined as being an area with thick-bedded dolostone and/or limestone with minor terrigenous clastics by Cecile et al., (1997), interpreted to

have been of shallow water origin. Experiments have shown that ferric iron is capable of oxidizing sulphur in pyrite. If the amount of ferric iron is limited, sulphur is liberated from pyrite in the form of thiosulphate (Spirakis and Heyl, 1993). In conclusion they stated a sequence of reactions that address the entire paragenesis, as follows:

-Organic matter acted as a reductant and reduced thiosulphate to produce sulphide sulphur to form galena, sphalerite, and other sulphides, and produced -1 valent sulphur to form disulphides.

-Thermal degradation of organic matter produced organic acids and carbon dioxide, which, depending on their relative proportions, either dissolved or precipitated carbonate minerals.

-In the cool waning stages of mineralization, organic matter acted as a substrate for bacterial metabolism of thiosulphate to produce oxidized and reduced sulphur species along with carbon dioxide. These precipitated as the late-stage barite along with disulphides and calcite.

GENETIC MODELS

Although MVT deposits are related by common features (Sangster, 1996), genetic mechanisms may have been extremely varied between individual deposits and mining districts. Godwin et al., (1982) suggest a karstic model for the deposits hosted in rocks older than Middle Cambrian and a basin dewatering model for the deposits hosted in rocks younger than Middle Cambrian. The stratigraphic framework presented by McLaren and Godwin (1979a) is used to illustrate the relative positions of the zinc-lead deposits in this study. As discussed previously, two major groups of sedimentary rocks hosting zinc-lead deposits in the northern Canadian Cordillera can be identified on the basis of depositional tectonics: i) a Proterozoic to Lower Cambrian succession of carbonates and clastics; and ii) an Upper Cambrian to Devonian basinal shale and laterally equivalent platformal carbonate sequence. This grouping is reinforced by bimodal minor element distributions in sphalerite (McLaren and Godwin, 1979b). The deposit population with lower or 'depleted' minor element content in sphalerite is consistently centred on, and extends beyond the limits of, the Ordovician, Silurian and Devonian host rock distribution, whereas the 'enriched' population of minor elements in sphalerite exists mainly in the "older" group and rarely extends into the area of the younger hosts. This pattern suggested to McLaren and Godwin (1979a) that an event leading to mineralization in Ordovician to Devonian age rocks was concentrated in these units, but extended into adjacent Proterozoic and Lower Cambrian units which had been tilted by earlier tectonic events and were positioned in the path of the basinal brines (e.g. Gayna River and

Cypress deposits). This interpretation agrees with the fact that Fluid I formed deposits hosted in rocks from Proterozic to Devonian age. Conversely, a mineralizing episode affecting the Proterozoic and Lower Cambrian rocks was restricted to these older units, and was regarded by these authors as a separate event which took place prior to deposition of the younger rocks.

Genesis of the MVT deposits of the Mackenzie Platform could be related to geopressure zones and/or convection cells. The proximal geopressure zone model of origin for Pb-Zn deposits as discussed by Fowler (1994) points out that geopressure zones are large masses of impermeable undercompacted sediment that have fluid pressures in excess of hydrostatic. Due to the insulating effects of surrounding rocks such as shales, geopressure zones may trap heat and therefore also become geothermal zones. The geopressure zone is a source of hot mineralizing fluid formed directly subjacent to host rocks for mineralization. Mineralizing fluids could have been derived from the deeper water outer detrital belt within the Sekwi Formation (W. Fritz, pers. comm., 1995). Alternately, geopressure zones located in the Misty Creek Embayment may have forced metal-bearing brines within the basin to flow upward east and northeast into the adjoining rocks of the Mackenzie Platform. The Misty Creek Embayment is filled with black, organic-rich, pyritiferous shales and basic volcanics which provide an excellent source of metal (Cecile and Morrow, 1978). The fluids had relatively short distances to flow because, although the facies change boundary between the shale and carbonate shifted over time, the belt of rocks which has been mineralized hugs close to this boundary over a length of 360 km.

Fluids, driven by free convection in the subsurface, perhaps activated by local tectonic events, could have circulated through local faults and deposited minerals wherever organic matter existed. Free convection is driven by buoyancy forces related to temperature and salinity variations (Morrow, 1998). High heat flow, possibly the result of rifting, drove fluids from below (thermal buoyancy), up into the faults created by the tectonic movement and into the awaiting porous, freshly consolidated host rocks. The very high salinities of fluid inclusions found both in the dolomite cements and sphalerite indicates that there was little or no admixture of fresh meteoric water during precipitation of these minerals. Convection may have been initiated by high heat flow in the late Paleozoic time, possibly coinciding with times of rifting, which affected large areas of northwestern Canada (Feinstein et al., 1996, Dorobek, 1995). The mineralization associated with coarse crystalline "saddle" dolomite documented in the study area and associated with Fluid I took place sometime between Late Devonian to Carboniferous time. A major Cordillera rifting event took

place in Late Devonian to Early Mississippi time, and an episode of Late Devonian-Early Mississippian convergence, known regionally as the Antler orogeny, which affected much of the western margin of North America (Dorobek, 1995), could have been the triggering mechanism for Event 1 fluids. Large scale fluid movements could have been related to the tectonic compression and sedimentary loading which occurred during the Antler orogeny or could have resulted from the rifting event.

Paleozoic time in general may have been favourable for the development of convection systems because of the prevalence of broad, low relief or shallow water carbonate shelves (Morrow, 1998). Estimated late Paleozoic geothermal gradients in nearby areas of over 50°C/km (Feinstein et al., 1996) favour the initiation of convection in subhorizontal strata. Evidence of the circulation of fluids in a regional convection system is seen as a visible imprint on the host strata in the form of breccia masses cemented by saddle dolomite.

REFERENCES

Abbott, J.G., Gordey, S.P. and Tempelman-Kluit, D.J.
1986:
Setting of stratiform, sediment-hosted lead-zinc deposits in Yukon and northeastern British Columbia; in Mineral Deposits of Northern Cordillera, The Canadian Institute of Mining and Metallurgy, Special Volume 37, p. 1-18.

Anderson, G.M.
1991:
Organic maturation and ore precipitation in southeast Missouri; Economic Geology, v.86, p. 909-926.

Anderson, R.G.
1988:
An overview of some Mesozoic and Tertiary plutonic suites and their associated mineralization in the northern Canadian Cordillera; in Recent Advances in the Geology of Granite-related Mineral Deposits, R.P. Taylor and D.F. Strong eds., Canadian Institute of Mining and Metallurgy, Special Volume 39, p. 96-113.

Anovitz, L.M. and Essence, E.J.
1987:
Phase equilibria in the system $CaCO_3$ - $MgCO_3$ - $FeCO_3$. Journal of Petrology, v. 28, p. 389-415.

Bodnar, R.J. and Bethke, P.M.
1984:
Systematics of stretching of fluid inclusions; fluorite and sphalerite at 1 atmosphere confining pressure; Economic Geology, v. 79, p. 141-161.

Brannon, J.C., Cole, S.C., Podosek, F.A., Ragan, V.M., Coveney Jr., R.M., Wallace, M.W. and Bradley, A.J.
1996:
Th-Pb and U-Pb dating of ore-stage calcite and Paleozoic fluid flow; Science, v. 271, p. 491-493.

Brock, J.S.
1974:
Arctic Red Venture: Preliminary geological report and proposed exploration on the Ab minerals claims, Mackenzie Mining District, Northwest Territories, Canada; Welcome North Mines Ltd. (N.P.L.), Appendix B, 7 p.

Brock, J.S.
1976:
Recent developments in the Selwyn-Mackenzie Zinc-Lead Province Yukon and Northwest Territories; Western Miner, March, p. 9-16.

Burruss, R.C.
1981:
Hydrocarbon fluid inclusions in studies of sedimentary diagenesis; in Fluid Inclusions: Applications to Petrology, Mineralogical Association of Canada Short Course, Calgary, May 1981, L.S. Hollister and M.L. Crawford eds., 304 p.

Carrière, J.J. and Sangster, D.F.
1992:
Preliminary studies of fluid inclusions in sphalerite, quartz, and dolomite from Gayna River MVT deposit, Northwest Territories; in Current Research, Part A; Geological Survey of Canada, Paper 92-1A, p. 47-53.

Carrière, J.J. and Sangster, D.F.
1996:
A progress report on Mississippi Valley-type deposits of the Mackenzie Platform: fluid inclusion studies in sphalerite, quartz, and dolomite from the Bear deposit, Northwest Territories; in Current Research 1996-E, Geological Survey of Canada, p. 87-96.

Cecile, M.P.
1982:
The Lower Paleozoic Misty Creek Embayment, Selwyn Basin, Yukon and Northwest Territories; Geological Survey of Canada, Bulletin 335, 78p.

Cecile, M.P. and Morrow, D.M.
1978:
Galena-sphalerite mineralization near Palmer Lake, Northwest Territories, Scientific and Tecnichal Notes, in Current Research, Part A, Geological Survey of Canada, Paper 78-1A, p. 474-474.

Cecile, M.P., Morrow, D.W., and Williams, G.K.
1997:
Early Paleozoic (Cambrian to Early Devonian) tectonic framework, Canadian Cordillera; Bulletin of Canadian Petroleum Geology, v. 45, no. 1, p. 54-74.

Chesley, J.T., Halliday, A.N., Kyser, T.K., and Spry, P.G.
1994:
Direct dating of Mississippi Valley-type mineralization: Use of Sm-Nd in fluorite; Economic Geology, v. 89, p. 1192-1199.

Choquette, P.W. and James, N.P.
1990:
Limestones - The Burial Diagenetic Environment; in Diagenesis, Geoscience Canada, Reprint Series No. 4, I.A. McIlreath and D.W. Morrow eds., p. 75-111.

Christensen, J.N., Halliday, A.N., Vearncombe, J.R., and Kesler, S.E.
1995:
Testing models of large-scale crustal fluid flow using direct dating of sulfides: Rb-Sr evidence for early dewatering and formation of Mississippi Valley-type deposits, Canning Basin, Australia; Economic Geology, v. 90, p. 877-884.

Dawson, K.M.
1975:
Carbonate-hosted zinc-lead deposits of the Northern Canadian Cordillera; in Report of Activities, Part A, Geological Survey of Canada, Paper 75-1A, p. 239-241.

Dawson, K.M., Panteleyev, A., Sutherland Brown, A., and Woodsworth, G.J.
1991:
Regional metallogeny, Chapter 19 in Geology of the Cordilleran Orogen in Canada, H. Gabrielse and C.J. Yorath eds.; Geological Survey of Canada, Geology of Canada, no. 4, p. 707-768.

Dorobek, S.L.
1995:
Synorogenic carbonate platforms and reefs in foreland basins: Controls on stratigraphic evolution and platform/reef morphology; in Stratigraphic Evolution of Foreland Basins. SEPM Special Publication no. 52, S.L. Dorobek and G.M. Ross eds., Society for Sedimentary Geology, p. 127-147.

Dougherty, B.J.
1995:
Time-slice thermal maturation data for mainland Yukon and Northwest Territories; Geological Survey of Canada, Open File 3058, Proceedings of the Oil and Gas Forum '95, Energy from Sediments, J.S. Bell, T.D. Bird, T.L. Hillier, and P.L. Greener eds., p. 183-185.

Dougherty, B.J., Abercrombie, H.J., Achab, A., Bertrand, R., Goodarzi, F., Snowdon, L.R., and Utting, J.
1991:
Correlation of thermal maturity indicators for the Tenlen A-73, Crossley Lake South K-60, and Kugaluk N-02 wells in the northern District of Mackenzie, Northwest Territories; in Current Research, Part E, Geological Survey of Canada, Paper 91-1E, p. 197-202.

Ebers, M.L. and Kopp, O.C.
1979:
Cathodoluminescent microstratigraphy in gangue dolomite, the Mascot-Jefferson City district, Tennessee; Economic Geology, v. 74, p. 908-918.

Epstein, A.G., Epstein, J.B., and Harris, L.D.
1977:
Conodont Color Alteration - an index to organic metamorphism; U.S. Geological Survey Professional Paper 995, 27 p.

Feinstein, S., Issler, D.R., Snowdon,L.R., and Williams, G.K.
1996:
Characterization of major unconformities by paleothermometric and paleobarometric methods: application to the Mackenzie Plain, Northwest Territories, Canada; Bulletin of Canadian Petroleum Geology, v. 44, no. 1, p. 55-71.

Fowler, A.D.
1994:
The role of geopressure zones in the formation of hydrothermal Pb-Zn Mississippi Valley-type

mineralization in sedimentary basins; in Geofluids: Origin, Migration and Evolution of Fluids in Sedimentary Basins, Geological Society Special Publication, no. 78, J. Parnell ed., p. 293-300.

Fritz, W.H.
1972:
Lower Cambrian trilobites from the Sekwi Mountain map-area, Yukon Territory and District of Mackenzie; Geological Survey of Canada, Buulletin 212, 90 p.

Fritz, W.H., Cecile, M.P., Norford, B.S., Morrow, D., and Geldsetzer, H. H. J.
1991:
Cambrian to Middle Devonian assemblages; in Chapter 7 of Geology of the Cordilleran Orogen in Canada, H. Gabrielse and C.J. Yorath eds.; Geological Survey of Canada, Geology of Canada, no. 4, p. 151-218.

Gabrielse, H. and Campbell, R.B.
1991:
Upper Proterozoic assemblages, Chapter 6 in Geology of the Cordilleran Orogen in Canada, H. Gabrielse and C.J. Yorath eds.; Geological Survey of Canada, Geology of Canada, no. 4, p. 125-150.

Gabrielse, H., Monger, J.W.H., Wheeler, J.O., and Yorath, C.J.
1991:
Part A. Morphogeological belts, tectonic assemblages, and terranes; in Chapter 2 of Geology of the Cordilleran Orogen in Canada, H. Gabrielse and C.J. Yorath eds.; Geological Survey of Canada, Geology of Canada, no. 4, p. 15-28.

Garvin, G. and Freeze, R.A.
1984a:
Theoretical analysis of the role of groundwater flow in the genesis of stratabound ore deposits; 1, Mathematical and numerical model; American Journal of Science, v. 284, no. 10, p. 1085-1124.

Garvin, G. and Freeze, R.A.
1984b:
Theoretical analysis of the role of groundwater flow in the genesis of stratabound ore deposits; 2, Quantitative results; American Journal of Science, v. 284, no. 10, p. 1125-1174.

Gibbins, W.A.
1983:
Mississippi Valley Type lead-zinc district of northern Canada; in International Conference on Mississippi Valley-type lead-zinc deposits, Proceedings Volume, University of Missouri-Rolla, Rolla, Missouri, p. 403-414.

Gibson, G.
1975:
Economic geology of the Econ claim group, Bonnet Plume area, eastern Yukon Territory; B.Sc. Thesis, University of British Columbia, 59 p.

Gize, A.P.
1993:
The analysis of organic matter in ore deposits; in Bitumens in Ore Deposits, J. Parnell, H. Kucha, and P. Landais eds., Springer-Verlag, 517 p.

Gize, A.P. and Barnes, H.L.
1994:
Organic contributions to Mississippi Valley-type Lead-Zinc genesis - A critical assessment; in Sediment-Hosted Zn-Pb Ores, Spec. Publ. No. 10, Soc. Applied to Mineral Deposits, Fontboté and Boni eds., p. 13-26.

Gize, A.P. and Hoering, T.C.
1980:
The organic matter in Mississippi Valley-type deposits; Carnegie Inst. Washington Year Book, 79, p. 384-388.Gize, A.P. and Manning, D.C., 1993. Aspects of the organic geochemistry and petrology of metalliferous ores; in Organic Geochemistry, eds. M.H. Engel and S.A. Macko. Plenum Press, New York, p. 565-580.

Godwin, C.I., Sinclair, A.J., and Ryan, B.J.
1982:
Lead isotope models for the genesis of carbonate-hosted Zn-Pb, shale-hosted Ba-Zn-Pb, and silver-rich deposits in the northern Canadian Cordillera; Econ. Geol., Vol. 77, p. 82-94.

Goldstein, R.H. and Reynolds, T.J.
1994:
Systematics of fluid inclusions in diagenetic minerals; SEPM Short Course 31, Society for Sedimentary Geology, 199 p.

Goodfellow, W.D., Cecile, M.P., and Leybourne, M.I.
1995:
Geochemistry, petrogenesis and tectonic setting of Lower Paleozoic alkalic and potassic volcanic rocks, northern Canadian Cordilleran Miogeocline; Canadian Journal of Earth Sciences, v. 32, p. 1236-1254.

Gordey, S.P. and Anderson, R.G.
1993:
Evolution of the northern Cordilleran miogeocline, Nahanni Map Area (105I), Yukon and Northwest Territories; Geological Survey of Canada, Memoir 428, 214 p.

Gregg, J.M. and Sibley, D.F.
1984:
Epigenetic dolomitization and the origin of xenotopic dolomite texture; Journal of Sedimentary Petrology, v. 54, p. 908-931.

Hagni, R.D.
1983:
Minor elements in Mississippi Valley-type ore deposits; in Cameron Volume on Unconventional Mineral Deposits, W.C. Shanks, III ed., Society of Economic Geologists, p.71-88.

Hanor, J.S.
1980:
Dissolved methane in sedimentary brines; potential effect on the PVT properties of fluid inclusions; Economic Geology, v. 75, p. 603-609.

Helsen, S.
1995:
Burial history of Paleozoic strata in Belgium as revealed by conodont color alteration data and thickness distribution; Geol Rundsch, v.84, p. 738-747.

Hewton, R.S.
1982:
Gayna River: A Proterozoic Mississippi Valley-type Zinc-Lead deposit; in Precambrian Sulphide Deposits, H.S. Robinson Memorial Volume, R.W. Hutchinson, C.D. Spence, and J.M. Franklin eds., Geological Association of Canada, Special Paper 25, p. 667-700.

Hillier, S., Matyas, J., Matter, A., and Vasseur, G.
1995:
Illite/smectite diagenesis and its variable correlation with vitrinite reflectance in the Pannonian Basin; Clays and Clay Minerals, v. 43, p. 174-183.

Horsfield, B. and Rullkötter, J.
1994:
Diageneis, catagenesis,and metagenesis of organic matter; in The Petroleum System - From Source to Trap, AAPG Memoir 60, Magoon and Dow eds., p. 189-199.

Krause, F.F.
1979:
Sedimentology and stratigraphy of a continental terrace wedge: the Lower Cambrian Sekwi and June Lake Formations (Godlin River Group), Mackenzie Mountains, Northwest Territories, Canada; Unpubl. Ph.D. thesis, University of Calgary, 252 p.

Lawler, J.P. and Crawford, M.L.
1983:
Stretching of fluid inclusions resulting from a low-temperature microthermometric technique; Economic Geology, v. 78, p. 527-529.

Leach, D.L. and Rowan, E.L.
1986:
Genetic link between Ouachita foldbelt tectonism and the Mississippi Valley-type lead-zinc deposits of the Ozarks; Geology, v.14, no. 11, p. 931-935.

Machel, H.G., Krouse, H.R., and Sassen, R.
1995:
Products and distinguishing criteria of bacterial and thermochemical sulfate reduction; Applied Geochemistry, v. 10, p. 373-389.

Macqueen, R.W.
1976:
Sediments, zinc and lead, Rocky Mountain Belt, Canadian Cordillera; Geoscience Canada, v. 3, p. 71-81.

Mazzullo, S.J.
1992:
Geochemical and neomorphic alteration of dolomite: a review; Carbonates and Evaporites, v. 7, no. 1, p. 21-37.

McArthur, G.F. and McArthur, M.L.
1976:
Geological and Geochemical report on the Cab mineral claims (Arctic Red Project); Welcome North Mines Ltd. (N.P.L.).

McLaren, G.P.
1978:
Minor elements in sphalerite and their implications for metallogenesis of carbonate-hosted zinc-lead deposits of the Yukon Territory and adjaacent District of Mackenzie; unpub. M.Sc. Thesis, University of British Columbia, 236 p.

McLaren, G.P. and Godwin, C.I.
1979a:
Stratigraphic framework of lead-zinc deposits in the northern Cordillera northeast of the Tintina Trench; Can. Jour. Earth Sci., Vol. 16, No. 2, p.380- 386.

McLaren, G.P. and Godwin, C.I.
1979b:
Minor elements in sphalerite from carbonate-hosted zinc-lead deposits, Yukon Territory and adjacent district of Mackenzie, Northwest Territories; Mineral Industry Report, 1977, Econ. Geol. Survey 1978-79, p. 5-21.

Morrow, D.
1998:
Regional subsurface dolomitization: Models and constraints; Geoscience Canada, v. 25, no. 2, p. 57-70.

Morrow, D.W. and Aulstead, K.L.
1995:
The Manetoe Dolomite; a Cretaceous-Tertiary or a Paleozoic event? Fluid inclusion and isotopic evidence; Bulletin of Canadian Petroleum Geology, v. 43, no. 3, p. 267-280.

Nakai, S., Halliday, A.N., Kesler, S.E., Jones, H.D.
1990:
Rb-Sr dating of sphalerites from Tennessee and the genesis of Mississippe Valley type ore deposits; Nature, v. 346, p. 354-357.

Nakai, S., Halliday, A.N., Kesler, S.E., Jones, H.D., Kyle, J.R., and Lane, T.E.
1993:
Rb-Sr dating of sphalerites from Mississippi Valley-type (MVT) ore deposits; Geochimica et Cosmochimica Acta, v. 57. P. 417-427.

Nesbitt, B.E. and Muehlenbachs, K.
1993:
Crustal hydrogeology of the Rockies: Implications to the origins of brines and Pb-Zn mineralization in the Western Canadian Sedimentary Basin; Geological Association of Canada Annual Meeting Programme with Abstracts, v. 18, p. A-76.

Nesbitt, B.E. and Muehlenbachs, K.
1994:
Paleohydrogeology of the Canadian Rockies and origins of brines, Pb-Zn deposits and dolomitization in the Western Canada Sedimentary Basin; Geology, v. 22, p. 243-246.

Padgham, W.A., Seaton, J.B., Laporte, P.J. and Murphy, J.D.
1976:
Mineral Industry Report, 1973, Northwest Territories, Indian and Northern Affairs, Canada, EGS 1976-9, 211 p.

Pan, H., Symons, D.T.A., and Sangster, D.F.
1990:
Paleomagnetism of the Mississippi Valley-type ores and host rocks in the northern Arkansas and Tri-State districts; Canadian Journal of Earth Sciences, v. 27, p. 923-931.

Paradis, S., Nelson, J.L., and Zantvoort, W.
1999:
A new look at the Robb Lake carbonate-hosted lead-zinc deposit, northeastern British Columbia; in Current Research 1999-A; Geological Survey of Canada, p. 61-70.

Pohler, S.M.L. and Orchard, M.J.
1990:
Ordovician conodont biostratigraphy, western Canadian Cordillera; Geological Survey of Canada, Paper 90-15, 37 p.

Pouchou, J.L. and Pichoir, F.
1985:
"PAP" o(pz) procedure for improved quantitative microanalysis; Microbeam Analysis, v. 20, p. 104-106.

Qing, H.
1991:
Diagenesis of Middle Devonian Presqu'ile Dolomite, Pine Point, NWT and adjacent subsurface; Ph.D. Thesis, McGill University, 287 p.

Radke, B.M. and Mathis, R.L.
1980:
On the formation and occurrence of saddle dolomite; Journal of Sedimentary Petrology, v. 50, p. 1149-1168.

Read, P.B., Psutka, J.F., and Fillipone, J.
1991a:
Organic maturity data for the Canadian Cordillera; Geological Survey of Canada, Open File 2341, 140 p.

Read, P.B., Woodsworth, G.J., Greenwood, H.J., Ghent, E.D., and Evenchick, C.A.
1991b:
Metamorphic Map of the Canadian Cordillera; Geological Survey of Canada, Map 1714A, scale 1:2 000 000

Rejebian, V.A., Harris, A.G., and Huebner, J.S.
1987:
Conodont color and textural alteration: An index to regional metamorphism, contact metamorphism, and hydrothermal alteration; Geological Society of America Bulletin, v. 99, no. 4, p. 471-479.

Roedder, E.
1984:
Fluid Inclusions; Reviews in Mineralogy, v. 12, Mineralogical Society of America, 646p.

Rowan,E.L. and Goldhaber, M.B.
1995:
Duration of mineralization and fluid-flow history of the Upper Mississippi Valley zinc-lead district; Geology, v. 23, no. 7, p. 609-612.

Sangster, D.F.
1996:
Mississippi Valley-type lead-zinc; in Geology of Canadian Mineral Deposit Types, O.R. Eckstrand, W.D. Sinclair, and R.I. Thorpe, eds., Geological Survey of Canada, Geology of Canada, no. 8, p. 253-261.

Sangster, D.F. and Carrière, J.J.
1991:
Preliminary studies of fluid inclusions in sphalerite from Robb Lake Mississippi Valley-type deposit, British Columbia; in Current Research, Part E; Geological Survey of Canada, Paper 91-1E, p. 25-32.

Sangster, D.F. and Lancaster, R.D.
1976:
Geology of Canadian leadand zinc deposits; in Report of Activities, Part A, Geological Survey of Canada, Paper 76-1A, p.301-310.

Sangster, D.F., Nowlan, G.S., and McCracken, A.D.
1994:

Thermal comparison of Mississippi Valley-type lead-zinc deposits and their host rocks using fluid inclusion and conodont color alteration index data; Economic Geology, v.89, p. 493-514.

Sibley, D.F. and Gregg, J.M.
1987:
Classification of dolomite rock textures; Journal of Sedimentary Petrology, v. 57, p. 967-975.

Sinclair, W.D., Morin, J.A., Craig, D.B. and Marchand, M.
1976:
Mineral Industry Report, 1975, Yukon Territory; Indian and Northern Affairs, Canada, EGS 1976-15, 210 p.

Smithurst, M.T., Symons, D.T.A., Sangster, D.F., and Lewchuk, M.T.
in press
Paleomagnetic age for Zn-Pb mineralization at Robb Lake, northeastern British Columbia; Canadian Petroleum Geology Bulletin.

Spirakis, C.S. and Heyl, A.V.
1993:
Organic matter (bitumen and other forms) as the key to localization of Mississippi Valley-ores; in Bitumens in Ore Deposits, Parnell, J., Kucha, H., and Landais, P., eds., Springer-Verlag, New York, p. 381-398.

Spirakis, C.S. and Heyl, A.V.
1994:
Precipitation of Mississippi Valley-type ores: The importance of organic matter and thiosulphate; in Sediment-Hosted Zn-Pb Ores, Soc. Geol. Applied to Mineral Deposits, Spec. Publ. No. 10, eds. Fontboté and Boni, p. 27-41.

Spirakis, C.S. and Heyl, A.V.
1995:
Interaction between thermally convecting basinal brines and organic matter in genesis of Upper Mississippi Valley zinc-lead district; Trans. Institution of Mining and Metallurgy (Section B: Applied Earth Science), v. 104, p. B37-B45.

Sverjensky, D.A.
1986:
Genesis of Mississippi Valley-type lead-zinc deposits; Annual Review of Earth and Planetary Sciences, v. 14, p. 177-199.

Symons, D.T.A., Pan, H., Sangster, D.F, and Jowett, E.C.
1993:
Paleomagnetism of the Pine Point Zn-Pb deposits; Canadian Journal of Earth Sciences, v. 30, p. 1028-1036.

Symons, D.T.A., Lewchuk, M.T., and Sangster, D.F.
1998:
Laramide orogenic fluid flow into the Western Canada Sedimentary Basin: Evidence from paleomagnetic dating of the Kicking Horse Mississippi Valley-type ore deposit; Economic Geology, v. 93, p. 68-83.

Warren, J.K.
1989:
Evaporite Sedimentology: Importance in Hydrocarbon Accumulation; Chapter 5, Dolomites and Dolomitization, Prentice Hall, Englewood Cliffs, New Jersey, p. 164-205.

Woody, R.E., Gregg, J.M., and Koederitz, L.F.
1996:
Effect of texture on petrophysical properties of dolomite: evidence from the Cambro-Ordovician of southeastern Missouri; AAPG Bulletin, v.80, p. 119-132.

Zenger, D.H.
1983:
Burial dolomitization in the Lost Burro Formation (Devonian), east-central California, and the significance of late diagenetic dolomitization; Geology, v. 11, p. 519-522.

Appendix I: List of deposits and corresponding sample numbers.

Deposit Name(s)/ N.T.S.	Numbers of Samples available from GSC* collection in Ottawa	Samples used for Electron Microprobe	Samples used for Microthermometry	Samples used for Cathodoluminescence
Tet-Rap 106A/1	KQ-73-282 - KQ-73-284	None	None	KQ-73-283
Gayna (Gayna River) 106B/15	SP3389 - SP3399 SP3400 - SP3409 SP5371 - SP5378	SP3400	SP3389, SP3389A SP3406, SP3408 SP3409, SP3409B	SP3400 SP3408A SP3409A
Birkeland 106B/4	SP5484,SP5485	None	None	SP5485
Cypress (Mt. Tillicom) 106C/7	SP3264 - SP3268 SP3272, SP3275 SP5405 - SP5408	SP3264 SP3266 SP3267	SP3266(1) SP3266(2) SP3267, SP3268	SP3264, SP3266 SP3267, SP3275
Ab	SP4172 - SP4174 SP5466 - SP5470	None	SP4172 SP4174	None
Cab 106C/16	SP3296 - SP3301 SP4197, SP4199 SP5461 - SP5465	SP5462a, SP5462b	SP3296, SP3300 SP3300A, SP4197 SP4199	SP5462a, SP5462b SP3280, SP3296 - SP3301
Bob 106C/10	SP5394 - SP5399 SP5400 - SP5402	SP5494, SP5495 SP5496	SP5399(1) SP5399(2)	SP5494, SP5495 SP5496
Palm 106A/5	PMCM 8003 PMCM 8004 Palms Claims(1) Palms Claims(2)	Palms Claims(1) Palms Claims(2)	Palms Claims(1)	Palms Claims(1) Palms Claims(2)
Econ (Economic) 106B/6	SP4200, SP4203 SP4205, Econ-1 8002A, SE-Veins SP5490 - SP5496	Econ-1A 8002A SE-Veins	SP4200-1, 8002B Econ-1B, Econ-1C SE-Veins B-1 SE-Veins B-2	Econ-1A 8002A SE-Veins
Tic (Tegart) 106 B/9	SP4212 - SP4216	SP4213 SP4215 SP4215(1)	None	SP4212, SP4213 SP4214B, SP4215 SP4215(1), SP4216
Ice 105P/11	SP4242, KQ-73-285 SP5445 - SP5453	SP4242, KQ-73-285 SP5452, SP5453	None	SP4242, SP5452 SP5453, KQ-73-285
Arn 105P/11	SP4237 SP5422 - SP5433	SP4237, SP5430 SP5431	None	SP4237, SP5430 SP5431
Joli Green 105I/16	SP5412 - SP5418 sample 105I/16	SP5413	SP5413	SP5412, SP5413 sample 105I/16
Mawer (Ma) 95L/3	SP5403 SP5404	SP5403	SP5403	SP5403

Property Name	Numbers of Samples available from GSC* collection in Ottawa	Samples used for Electron Microprobe	Samples used for Microthermometry	Samples used for Cathodoluminescence
Keg 105P/14	KQ-73-273	None	None	KQ-73-273
Bear-Twit (Twitya) 106A/3	SP5486 - SP5489 BEAR	SP5487, SP5489	SP5487, BEAR SP5489(1) SP5489(2)	SP5487 SP5489
Snobird 95L/1	SP3413 - SP3421	SP3417A	None	SP3415, SP3417A SP3417B, SP3419 SP3422
Rev	SP5497 - SP5499, SP5500 - SP5507	SP5501 SP5506	SP5501, SP5504(2) SP5505, SP5506	SP5501 SP5506
Rain-Snow (Weather) 105P/14	SP5479 Rain 3	Rain 3	None	Rain 3
Art (Backbone) 105P/14	SP5480, SP5481 SP5482, SP5483	None	None	SP5482
Scat 105P/14,15	SCAT	None	None	SCAT
Rio 106B/1	SP5476 SP5477	None	None	SP5477
Aj (Essau) 106B/15,16	SP5420 SP5421	None	None	SP5420
Big Red 105I/8	SP5441, SP5442 SP5443, SP5444	None	None	SP5441 SP5443

* Geological Survey of Canada
Natural Resources Canada
Earth Science Sector
Mineral Resources Division
601 Booth St.
Ottawa, Ontario
K1A 0E8

APPENDIX II: (on diskette)

Microsoft Excel 97 spreadsheets in .xls format by deposit name
README file in WordPerfect 6.0 describing data
Microsoft Excel 97 spreadsheet entitled "Sphalerite.xls"

Included on this diskette are all the original data spreadsheets for Electron Microprobe Analyses performed by John Sterling (GSC, Mineralogy Section). The analyses include data for dolomite and sphalerite. The results are saved in .xls format from Microsoft Excel 97.

Dolomite data is divided among several spreadsheets entitled "p9449x01.xls" to "p9449x14.xls". Each such spreadsheet represents results from a shuttle holding three thin sections. Only analyses for which the Weight % End Members totalled between 97% and 103% where included. Analyses indicating calcite composition were eliminated.

The legend for the column entitled "type" in the dolomite spreadsheets is:

H: host dolomite
F: finer grained dolomite cement
C: coarse grained saddle dolomite cement

All sphalerite data is included in the spreadsheet entitled "Sphalerite.xls"